TU Delft

Delft University of Technology

Transport Processes in Hydrating Cementitious Coating Systems

Dong, Hua

DOI
10.4233/uuid:a8ff1ebb-0a67-42b2-a611-0c4d930421f1

Publication date
2018

Document Version
Final published version

Citation (APA)
Dong, H. (2018). *Transport Processes in Hydrating Cementitious Coating Systems*. [Dissertation (TU Delft), Delft University of Technology]. https://doi.org/10.4233/uuid:a8ff1ebb-0a67-42b2-a611-0c4d930421f1

Important note
To cite this publication, please use the final published version (if applicable).
Please check the document version above.

Copyright
Other than for strictly personal use, it is not permitted to download, forward or distribute the text or part of it, without the consent of the author(s) and/or copyright holder(s), unless the work is under an open content license such as Creative Commons.

Takedown policy
Please contact us and provide details if you believe this document breaches copyrights.
We will remove access to the work immediately and investigate your claim.

This work is downloaded from Delft University of Technology.
For technical reasons the number of authors shown on this cover page is limited to a maximum of 10.

Transport Processes
in Hydrating Cementitious Coating Systems

Proefschrift

ter verkrijging van de graad van doctor
aan de Technische Universiteit Delft,
op gezag van de Rector Magnificus prof.dr.ir. T.H.J.J. van der Hagen;

voorzitter van het College voor Promoties,
in het openbaar te verdedigen op
maandag 11 juni, 2018 om 12:30 uur

door

Hua DONG

Master of Science in Materialogy, Southeast University, P.R. China
geboren te Taizhou, P.R. China

Dit proefschrift is goedgekeurd door de promotoren:

Prof. dr. ir. K. van Breugel
Dr. G. Ye

Samenstelling promotiecommissie:

Rector Magnificus,	voorzitter
Prof. dr. ir. K. van Breugel,	Technische Universiteit Delft, promotor
Dr. G. Ye,	Technische Universiteit Delft, promotor

Onafhankelijke leden:

Prof. Dr. F. Benboudjema	Ecole Normale Supérieure de Cachan, Frankrijk
Prof. dr. ir. E. Schlangen	Technische Universiteit Delft
Prof. dr. ir. R. B. Polder	Technische Universiteit Delft
Dr. Ravi A. Patel	Paul Scherrer Institute, Switzerland
Prof. dr. ir. L. J. Sluys	Technische Universiteit Delft, reservelid

Overig lid:

Prof. Dr. C. Qian,	Southeast University, China

ISBN: 978-94-6186-934-0

Keywords: cementitious coating, simulation, moisture transport, hydration, chloride transport, service life assessment.

Printing: Gildeprint Drukkerijen

Cover design: Hua Dong

Copyright © 2018 by Hua Dong

All rights reserved. No part of the material protected by this copyright notice may be reproduced or utilized in any form or by any means, electronic or mechanical, including photocopying, recording or by any information storage and retrieval system, without written consent from the author.

Printed in the Netherlands.

Acknowledgements

Life is a series of journeys. I am so grateful for that the beautiful city of Delft has bestowed upon me the marvellous journey since 2011. In the past few years I have experienced and gained a lot, not only in PhD research, but also in life. I treasure in my heart the memory of this unforgettable journey. For all that have happened to me in these years I want to express my appreciation:

My promotor Prof. dr. ir. Klaas van Breugel. My PhD thesis is greatly attributable to your patient guidance and constructive advice. My thesis would not have been done without your great support. I appreciate this more than you will ever know.

My promotor Dr. Guang Ye. You have been my daily supervisor of the PhD study and given me so much encouragement during these years. I would like to extend my heartfelt thanks to you for all your help.

Prof. Chunxiang Qian. You were my supervisor for master study. You inspired me to pursue PhD study in Delft University of Technology. The inspiration is so important to me and I will be forever grateful.

Technologiestichting STW financially supported my PhD research project and is greatly acknowledged.

I also would like to give many thanks to all other committee members of the defence of my PhD thesis. They are Prof. dr. ir. Erik Schlangen, Prof. dr. ir. Rob. B. Polder, Prof. Dr. Farid Benboudjema, Prof. dr. ir. L. J. (Bert) Sluys, Dr. Ravi Ajitbhai Patel. Thanks a lot for your careful reading and valuable feedback on my thesis.

Claire, Iris, Nynke, Claudia and Melanie. You helped me with the documents for my legal stay in the Netherlands. Dr. Dessi Koleva, Dr. Henk Jonkers, Dr. Oguzhan Copuroglu, Dr Yun Huang, Prof. Dr. Jiangxiong Wei and Professor. Dr. Yingzi Yang. Your meticulous attitude towards academic research inspired me a lot. Gerrit, Arjan, John and Maiko are also helpful to me. Peter and Tim were so kind to help me with the translation of summary and propositions into Dutch language. I want to give my great thanks to all of you.

Zhaochuan Fan, Philips, Liyuan Fan, Xiaoqian Lv and Yong Wang. We got to know each other and became friends in the first year when I settled down in Delft. I still remember how free we were like a fish in the swimming pool. I would never forget how impressive it was in the islands of Spain and Greece. Later Mingzhi Dong, Chaoran Fan and Yong Cui came to the Netherlands, and joined us for board games and sunshine on the beach. You have brought me so much joy. Every time I look back upon these memories, I am always reminded of how grateful I am to have you in my life!

Peng Gao, Zhuqing Yu, Tianshi Lu and Hongzhi Zhang. You have been so generous to share your lives with me in these years. We talked about research, enjoyed nice foods and played games. You brightened my day and lifted my spirits. The friendship between us means so much to me. Many thanks for all you have done for me.

Yinglin Cao. We went to the breath-taking Niagara Falls in the US and travelled through the archipelago (Thousand Islands) that straddles the Canada-US border. We went ice-skating with other friends and enjoyed a lot even though we were all beginners. Those were special experiences of me. I can't thank you enough.

Zhiwei Qian, Hao Huang (Niha), Jiayi Chen, Wenqin Shi, Xuliang Hou (Ying Yang), Bei Wu, Xu Ma, Yibing Zuo and Shizhe Zhang. We took a cruise ship tour with roaring waves in Marsseile; we were involved in the vast expanse of lavender in Provence; we enjoyed the stunning view of the Mediterranean Sea in Nice; we stayed in the cosy chalet and wondered in the "fairyland" in Austria. Those days we were overwhelmed with joy and happiness. I thank you from the bottom of my heart.

Mladena and Branko. You are always diligent and helpful. I am so proud of you! Thanks for the nice discussions and the help over research. Most importantly, thanks for having invited me to Serbia. I enjoyed a lot in your homeland.

Marija and Patrick. Thank you so much for joining me for a visit to the Hans Christian Andersen House in Denmark. The trip was as beautiful as a fairy tale and unforgettable. Also many thanks to you for helping me practise Dutch language.

Jie Zhao, Senot, Farhad, Kai Zhang, Natalie, Balqis, Damian, Eirini, Mohammad, Xiaowei Ouyang, Yun Zhang and Zainab. We used to share one office room. I really enjoyed your company and thank you so much.

Qi Zhang, Ying Wang, Virginie, Quantao Liu, Yuwei Ma, Jie Hu, Mingzhong Zhang, Lupita, Chunping Gu, Haoliang Huang, Jiahua Liu, Yong Zhang, Agus, Jeanette, Renee, Zhipei Chen, Leyang Lu, Stefan, Shi Xu, Wenjuan LYU, Zhenming Li, Claudia, Yading Xu, Albina, Boyu Chen and Yidong Gan. We are members in such a nice group of microlab. I cannot stay warm in Delft without you. I will always be indebted to you.

Last but not least, my parents. You gave me birth and raised me up. I could not express my gratitude with words. I deeply wish you health and happiness!

Hua Dong
Delft, March 2018

Table of contents

List of figures xi
List of tables xix
List of symbols xxi
List of abbreviations xxvii

Part I Introduction

Chapter 1 1
General introduction
1.1 Research background 1
1.2 Aim, objectives and scope of this study 3
1.3 Research strategy of this study 4
1.4 Outline of this research 5

Chapter 2 7
General literature review
2.1 Introduction 7
2.2 Surface protections for concrete structures 8
2.2.1 Impregnations into the surface layer of concrete 9
2.2.2 Coatings for concrete structures 9
2.2.3 Selection of coatings 11
2.2.4 Failure of coating systems 12
2.3 An important concern - moisture transport in cementitious coating systems 13
2.3.1 Simulation of moisture transport in cement-based materials 15
2.3.2 Simulation of moisture transport in cementitious overlay systems 16
2.4 Long-term performance of cementitious coating system - chloride ingress 17
2.4.1 General introduction of chloride transport in concrete structures 17
2.4.2 Simulation of chloride transport in concrete structures 17
2.4.3 Simulation of chloride transport in coating systems 17
2.5 Problem definition 18
2.5.1 Moisture transport in cementitious coating systems and parameter study 18
2.5.2 Chloride transport in cementitious coating systems and service life assessment 19
2.6 Conclusions 19

Part II Moisture transport in hydrating cementitious coating systems

Chapter 3 21
Mechanisms of moisture transport in hydrating cementitious coating systems
3.1 Introduction 21
3.2 Mechanisms of moisture transport in cementitious materials 22
3.2.1 Moisture transport in saturated cementitious material 22
3.2.2 Moisture transport in partially saturated cementitious material 22
3.2.3 Equation describing moisture transport in partially saturated cementitious materials 26
3.3 Moisture-Hydration model for simulating moisture transport in hydrating coating systems 27
3.3.1 Factors considered for simulating moisture transport in hydrating cementitious coating systems 27
3.3.2 Liquid water transport in a hydrating cementitious material 28
3.3.3 Water consumed by hydration of cementitious materials with arbitrary water content 30
3.3.4 Water vapour diffusion in the pore system of cementitious materials 32
3.3.5 Liquid water - vapour phase transition 34
3.3.6 Water transfer/vapour diffusion across the coating-substrate interface 36
3.3.7 Water evaporation from the surface of a coating system 38
3.3.8 Flow chart of the Moisture-Hydration model 40
3.4 Summary 42

Chapter 4 43
Quantification of transport properties and parameters for simulation of moisture transport
4.1 Introduction 43
4.2 Intrinsic permeability $K(\alpha)$ $[m^2]$ 48
4.2.1 Outline of the quantification of intrinsic permeability of hydrating cementitious materials 48
4.2.2 Method to determine intrinsic permeability of cementitious materials at early ages - Lattice Boltzmann Method 49
4.2.3 Method to determine intrinsic permeability of cementitious materials at later ages 50
4.2.4 Example calculation of intrinsic permeability of a hydrating cement paste 51
4.3 Moisture isotherm (for determining parameters in the Van Genuchten model) 53
4.3.1 Outline of the quantification of moisture isotherm of hydrating cementitious materials 53

4.3.2 Method to determine moisture isotherms of cementitious materials at early ages - Level Set Method 55
4.3.3 Method to determine moisture isotherm of cementitious materials at later ages 56
4.3.4 Example calculation of moisture isotherm of a hydrating cement paste 57
4.4 Rate of hydration $\dot{\alpha}(\alpha, s_{cap})$ 60
4.4.1 Method to determine rate of hydration $\dot{\alpha}(\alpha, s_{cap})$ 60
4.4.2 Example calculation of rate of hydration $\dot{\alpha}(\alpha, s_{cap})$ of a cement paste 63
4.5 Capillary porosity ϕ_{cap}, gel porosity ϕ_{gel} and total porosity ϕ 64
4.5.1 Method to determine capillary porosity ϕ_{cap} 64
4.5.2 Method to determine gel porosity ϕ_{gel} 65
4.5.3 Example calculation of capillary porosity ϕ_{cap}, gel porosity ϕ_{gel} and total porosity ϕ of a hydrating cement paste 67
4.6 Summary 67

Chapter 5 69
Simulation of moisture transport in hydrating cementitious coating systems and evaluation of drying shrinkage-induced cracking of coatings
5.1 Introduction 69
5.2 Moisture change and hydration of a reference cement paste (sealed curing) 70
5.2.1 Materials of the reference cement paste 70
5.2.2 Moisture content and degree of hydration of the reference cement paste 71
5.3 Materials of coating systems for the simulation of moisture transport 72
5.3.1 Coating-mixture composition 72
5.3.2 Substrate 72
5.4 Exposure scenarios of the coating systems and parameters to be evaluated 72
5.5 Simulation results and discussion 74
5.5.1 Effect of coating thickness (6, 10 and 20 mm) on moisture transport in the coating system and on the hydration of the coatings 74
5.5.2 Effect of curing regime on moist transport in the coating system and on the hydration of the 10 mm-thick coatings 77
5.5.3 Effect of substrate type (substrate OC and substrate HPC) on moisture transport in coating systems and on the hydration of 10 mm-thick coatings 83
5.5.4 Investigation of water loss of the coating materials 86
5.5.5 Overview of the simulated DOH of the coatings at 14 days 89
5.6 Probability of drying shrinkage-induced cracking 91
5.6.1 Calculation of mechanical properties of the coating 92
5.6.2 Case study of drying shrinkage-induced cracking 93
5.7 Conclusion 96

Part III Chloride transport in hydrating cementitious coating systems

Chapter 6 99
Numerical study on chloride ingress in cementitious coating systems and evaluation of effectiveness of coatings
6.1 Introduction 99
6.2 Mechanisms of chloride ingress in hydrating coating systems 101
6.2.1 Chloride transport in hydrating cementitious materials 101
6.2.2 Chloride transport in the crack of the materials 103
6.2.3 Chloride transport across the coating-substrate interface 103
6.3 Quantification of material properties for the simulation 105
6.3.1 Chloride diffusivity 105
6.3.2 Chloride binding isotherm 106
6.4 Validation of the simulation of chloride ingress in the coating system 108
6.5 Simulation of chloride transport in coating systems 109
6.5.1 Materials of coating systems 110
6.5.2 Exposure scenario for the coating systems and parameters to be evaluated 112
6.5.3 Surface chloride and initial chloride 117
6.5.4 Critical chloride concentration and cover thickness 117
6.6 Simulation results and discussion 117
6.7 Conclusion 132

Part IV Conclusions and summary

Chapter 7 135
Retrospection, Conclusions, Recommendations and Future work
7.1 Retrospection 135
7.2 Conclusions 137
7.3 Recommendations for the design and the application of cementitious coating material 138
7.4 Contributions of this study 139
7.5 Future work 140

Summary 141
Samenvatting 143

Appendix A 147
Evaluation of equations commonly used for simulating moisture transport in partially saturated cementitious materials
A.1 Introduction 147
A.2 Equations describing moisture transport in partially saturated cementitious materials 147
A.2.1. Relative humidity as a variable 147
A.2.2. Water content as a variable 148
A.3 Case study of moisture transport in cementitious materials for evaluating the equations 148
A.4 Summary 151

Appendix B 153
Boundary condition for simulating moisture transport in cementitious materials
B.1 Introduction 153
B.2 Calibration of the boundary condition - cement paste hydrating under 90% RH 154
B.3 Validation of the boundary condition- drying of hardened concrete substrate 156
B.4 Summary 157

Appendix C 159
Methodology of Lattice Boltzmann Method
C.1 Introduction 159
C.2 Basic equations of Lattice Boltzmann Method 159

References 163

List of figures

Fig. 1.1 Schematic illustration of a concrete substrate and a coating system. 1
Fig. 1.2 Schematic chloride profiles in a coating system. Solid black line is chloride profile in an old concrete substrate. The red dashed line shows the chloride profile after redistribution of chloride in the coating system. 3
Fig. 1.3 Outline of this thesis. 6

Fig. 2.1 Cracking and interface delamination of an overlay system due to differential shrinkage [19]. 8
Fig. 2.2 Factors affecting durability of concrete repairs ([46]). 12
Fig. 2.3 Schematic illustration of moisture transport in a coating system. Basically, moisture transport takes place in 4 forms: 1. water evaporation to the environment, 2. water uptake from the environment, 3. absorption by the substrate, and 4. water uptake from the substrate. This figure shows the water loss of the coating due to water evaporation to the environment and water absorption by the substrate. 14
Fig. 2.4 Boundary condition on exposed surface. 16

Fig. 3.1 Structure of the study of moisture transport in hydrating cementitious coating systems. 21
Fig. 3.2 Schematic illustration of factors affecting moisture transport in a hydrating cementitious coating system. 22
Fig. 3.3 Moisture transport mechanisms and the definition of pore size classes (after Klopfer [101]). 23
Fig. 3.4 Moisture transport in a capillary pore with a continuous liquid water phase. 25
Fig. 3.5 Moisture transport in a capillary pore with a discontinuous liquid water phase. 25
Fig. 3.6 Water distribution in a drying cement paste. (a) 2D schematic microstructure of a water-saturated cement paste (b) drying takes place in capillary pores, remaining water are available for both hydration and drying (c) drying takes place in gel pores (RH $\leq$ 80%), remaining water is only available for drying, no hydration is considered. 31
Fig. 3.7 Schematic illustration of the volume changes of water, unhydrated cement, hydration products and pores in a hydrating cement paste under sealed condition. α is the degree of hydration and v is the volume. 32
Fig. 3.8 Explanation of the water-filled capillary porosity in cement paste. 32
Fig. 3.9 Correlation between relative humidity and pore size of the largest water-filled pore in the material, according to Kelvin equation (Eq. 3.31) (atmospheric pressure, $T = 293$ K). 35
Fig. 3.10 Schematic illustration of moisture distribution in a coating system. This figure is typical for a coating with a pore structure coarser than the substrate. w_v is water content in the gas, and s is water saturation level in the coating or the substrate. The red lines show the initial moisture profiles in the coating system. The nodes are numbered incrementally from 0 to n. $c0$ and $s0$ represent the interface nodes of the coating and the substrate, respectively. 37
Fig. 3.11 Schematic illustration of moisture at the interface between the ambient air and the porous material. The dimension of the porous material is 100×100 μm^2. The top surface of the material

is exposed to the ambient air. Other surfaces are sealed. 39
Fig. 3.12 Flowchart for the simulation of moisture transport in a hydrating cementitious coating system. t and T are the time after application of the coating and the target time, respectively. 41

Fig. 4.1 Structure of the study of moisture transport in hydrating cementitious coating systems. 43
Fig. 4.2 Schematic illustration of factors affecting moisture transport in a hydrating cementitious coating system. c0 and s0 represent the interface nodes of the coating and the substrate, respectively. cn represents the node of the coating at coating-environment interface. 44
Fig. 4.3 Transport properties and parameters used for simulating moisture transport in hydrating cenmentitious coating systems. 46
Fig. 4.4 Schematic illustration of the relationship between intrinsic permeability and degree of hydration of a cement paste (w/c = 0.3). The intrinsic permeability of the cement paste is determined by LBM simulation when $\alpha \leq 15\%$, and by empirical relation when $\alpha \geq 50\%$. For $15\% < \alpha < 50\%$, the intrinsic permeability of cement paste is obtained by interpolation. 49
Fig. 4.5 Schematic illustration of water flow in a porous material under hydraulic pressure. 49
Fig. 4.6 Relative changes in permeability ($k_r = \ln(k_t/k_{28})$) due to hydration, compiled from the data in [124]. hcp represents cement paste. The specimens are cured under saturated condition. k_{28} can be determined by permeability measurements. 50
Fig. 4.7. Streamline of water flow in the microstructure of a fresh cement paste (w/c = 0.3), the microstructure is generated by HYMOSTRUC3D. 51
Fig. 4.8. Intrinsic permeability versus capillary porosity. Red triangles represent the results in this study. The microstructures of a cement paste (w/c = 0.3) were generated by HYMOSTRUC3D. Results represented by dots were derived from Zalzale [133], based on virtual cement pastes generated by μic model (w/c = 0.3, 0.4, 0.5, 0.6 and 0.7, digital resolution = 1 $\mu m/voxel$). 52
Fig. 4.9 Intrinsic permeability of a cement paste (w/c = 0.3). The calculated intrinsic permeability is obtained by LBM simulation when $\alpha \leq 15\%$, and by using empirical model when $\alpha \geq 50\%$. The intrinsic permeability is obtained by spline curve fitting when $15\% < \alpha < 50\%$. 53
Fig. 4.10 Schematic illustration of the relationship between water saturation level and capillary pressure in a cement paste. This curve can be obtained either from Level Set simulations ($\alpha \leq 15\%$) or experiments ($\alpha \geq 52\%$). 54
Fig. 4.11 Displacement of water by air in a porous material. The porous material is initially water saturated. Air intrudes from one surface of the material. 55
Fig. 4.12. Air-water-solid interface during the desorption of an initial saturated fresh cement paste (w/c =0.3, degree of hydration α = 0%). The air intrudes from the left surface of the microstructure. The solid phase is not illustrated in this figure, but it can be referred to Fig. 4.7a. 57
Fig. 4.13 Relationship between water saturation level and capillary pressure in a cement paste (w/c = 0.3). Results (dots) are determined by Level Set simulation of water desorption. Fitted curve by the Van Genuchten model is according to Eq. (3.12). 58
Fig. 4.14 Relationship between water saturation and capillary pressure in a cement paste (w/c = 0.3, after 7-day saturated curing). Results (dotted) are determined by an empirical model for water

adsorption isotherm (Eq. (4.12)). Fitted curve by VG model is according to Eq. (3.12). 59
Fig. 4.15 Evolution of Van Genuchten parameters of a cement paste (w/c = 0.3). The Van Genucthen parameters, a and m, are determined from the capillary pressure - water saturation level curves. The capillary pressure - water saturation level curves are determined by by Level Set simulation when $\alpha \leq 15\%$, and by using empirical model when $\alpha \geq 52\%$. The Van Genucthen parameters, a and m, are determined by spline curve fitting when $15\% < \alpha < 52\%$. 59
Fig. 4.16 Basic principles of HYMOSTRUC3D and formation of hydration products (by van Breugel [8]). 61
Fig. 4.17 Schematic illustration of water in a capillary pore of a cement paste. 61
Fig. 4.18 Schematic illustration of the composition of a cement paste..... 62
Fig. 4.19 DOH of cement pastes (w/c = 0.3). Hydration takes place under a sealed or a saturated condition. Experimental data were derived from [147]. 63
Fig. 4.20 Influence of water saturation level in capillary pores on the rate of hydration α of the cement particles in a cement paste with w/c = 0.3..... 64
Fig. 4.21 Evolution of capillary, gel and total porosity of a cement paste (w/c = 0.3). 67

Fig. 5.1 Structure of the study of moisture transport in hydrating cementitious coating systems. 69
Fig. 5.2 A typical scenario of moisture transport in a coating system. 70
Fig. 5.3 Evolution of calculated degree of hydration, porosity, water saturation level and water content of a reference cement paste (w/c = 0.3, Portland cement CEM I 42.5N is used). The reference cement paste is cured under sealed curing condition (20 °C). 71
Fig. 5.4 Illustration of different curing regimes (T = 20 °C). The coating is applied on the substrate at $t = 0$. In the 1D simulation, the top surface of the coating system is subjected to various curing regimes, while the bottom surface of the substrate is always sealed (Fig. 5.2). One wet-dry cycle consists of 3 days moist curing and 3 days curing at 50% RH. 73
Fig. 5.5 Calculated moisture profiles in the coating system C10-OC(s=50%)-Moist1d (Table 5.2). A 10 mm-thick coating (w/c = 0.3) is applied on substrate OC. One day moist curing is applied, followed by exposure to 50% RH until 14 days. 74
Fig. 5.6 Calculated water content and calculated degree of hydration of the coatings (w/c = 0.3) with different thicknesses (6, 10 and 20 mm). The coatings are applied on substrate OC (s = 50%). One day moist curing is applied, followed by exposure to 50% RH until 14 days. The reference cement paste (w/c = 0.3, no substrate) is cured under sealed condition. 76
Fig. 5.7 Calculated average degree of hydration at 14 days of the coatings (w/c = 0.3) with different thicknesses (6, 10 and 20 mm). The coatings are applied on substrate OC (s = 50%). One day moist curing is applied, followed by exposure to 50% RH until 14 days. The reference cement paste (w/c = 0.3) is cured under sealed condition. 76
Fig. 5.8 Calculated moisture profiles in the coating system C10-OC(s=50%)-Moist3d (Table 5.2). A 10 mm-thick coating (w/c = 0.3) is applied on substrate OC ($s = 50\%$). Three days moist curing is applied, followed by exposure to 50% RH until 14 days. 78
Fig. 5.9 Calculated moisture profiles in the coating system C10-OC(s=50%)-Sealed3d (Table 5.2). A 10 mm-thick coating (w/c = 0.3) is applied on substrate OC ($s = 50\%$). Three days sealed curing

is applied, followed by exposure to 50% RH until 14 days. 78
Fig. 5.10 Calculated moisture profiles in the coating system C10-OC(s=50%)-WetDry (Table 5.2). A 10 mm-thick coating (w/c = 0.3) is applied on substrate OC (s = 50%). Two wet-dry cycles are applied, followed by exposure to RH = 50% until 14 days. One wet-dry cycle consists of 3 days moist curing and 3 days curing at 50% RH. 79
Fig. 5.11 Calculated water content and calculated degree of hydration of the 10 mm-thick coatings (w/c = 0.3) applied on substrate OC (s = 50%), and exposed to different curing regimes (1, 3 or 7 days moist curing, followed by exposure to RH = 50% until 14 days). The reference cement paste (w/c = 0.3) is cured under sealed condition. 81
Fig. 5.12 Calculated water content and calculated degree of hydration of the 10 mm-thick coatings (w/c = 0.3) applied on substrate OC (s = 50%), and exposed to different curing regimes (1, 3 or 7 days sealed curing, followed by exposure to RH = 50% until 14 days). The reference cement paste (w/c = 0.3) is cured under sealed condition. 81
Fig. 5.13 Calculated water content and calculated degree of hydration of the 10 mm-thick coating (w/c = 0.3) applied on substrate OC (s = 50%), and cured under 2 wet-dry cycles. One wet-dry cycle consists of 3 days moist curing and 3 days curing at 50% RH. The reference cement paste (w/c = 0.3) is cured under sealed condition. 82
Fig. 5.14 Calculated average degree of hydration of the 10 mm-thick coatings (w/c = 0.3) at 14 days. The coatings are applied on substrate OC (s = 50%). The top surfaces of the coatings are sealed or subjected to moist curing for 1, 3 or 7 days, followed by exposure to RH = 50% until 14 days. In addition, the DOH of a coating cured under 2 wet-dry cycles is also presented (green column). The reference cement paste (w/c = 0.3) is cured under sealed condition all the time. 82
Fig. 5.15 Calculated evolution of water content (a) and degree of hydration (b) of the 10 mm-thick coatings (w/c = 0.3). The coatings are applied on substrate OC (s = 50%, or s = 100%). Moist curing (1, 3 or 7 days) is applied, followed by exposure to RH = 50% until 14 days. The reference cement paste (w/c = 0.3, no substrate) is cured under sealed condition. 84
Fig. 5.16 Calculated evolution of water content (a) and degree of hydration (b) of the coatings. The coatings (10 mm-thick, w/c = 0.3) are applied on substrate OC (s = 50%) or substrate HPC (s = 77%). The coatings are moist-cured for 1, 3 or 7 days, followed by exposure to RH = 50% until 14 days. 85
Fig. 5.17 Calculated evolution of water content (a) and degree of hydration (b) of the coatings. The coatings (10 mm-thick, w/c = 0.3) are applied on substrate OC (s = 50%) or substrate HPC (s = 77%). The coatings are sealed-cured for 1, 3 or 7 days, followed by exposure to RH = 50% until 14 days. 85
Fig. 5.18 Calculated average degree of hydration at 14 days of the 10 mm-thick coatings (w/c = 0.3) applied on different substrates (OC with s = 50%, OC with s = 100% and HPC with s = 77%). The coatings are moist/sealed cured for 1, 3 or 7 days, followed by exposure to RH = 50% until 14 days. The reference cement paste (w/c = 0.3, no substrate) is cured under sealed condition. . 86
Fig. 5.19 Calculated average water saturation level of the coating material in C10-OC(s=50%)-Moist3d. A 10 mm-thick coating (w/c = 0.3) is applied on substrate

OC(s=50%). Three days moist curing is applied, followed by exposure to RH = 50% until 14 days. 87
Fig. 5.20 Calculated evolution of porosity and water content of the coating in C10-OC(s=50%)-Moist3d. A 10 mm-thick coating (w/c = 0.3) is applied on substrate OC. Three days moist curing is applied, followed by exposure to RH = 50% until 14 days. 88
Fig. 5.21 Calculated water loss of the coatings applied on different substrates. The 10 mm-thick coatings are applied on ordinary concrete (substrate OC) or a high performance concrete (substrate HPC). Three days moist curing is applied, followed by an exposure to RH = 50% until 14 days. 89
Fig. 5.22 Schematic illustration of the development of tensile strength $f_t(t)$ and drying shrinkage-induced stress $\sigma(t)$ of the coating material. $f_t(t)$ and $\sigma(t)$ have a Gaussian distribution with a standard deviation of $0.08 \cdot f_t(t)$ and $0.08 \cdot \sigma_t(t)$, respectively. 91
Fig. 5.23 Evolution of the calculated DOH and the calculated water saturation level of the coatings. The 10 mm-thick coatings (w/c = 0.3) are applied on substrate OC (s = 50%), and moist-cured for 3 or 7 days, followed by exposure to 50% RH until 56 days. 94
Fig. 5.24 Calculated shrinkage-induced stress in the coatings. The 10 mm-thick coatings (w/c = 0.3) are applied on substrate OC (s = 50%), and moist-cured for 3 or 7 days, followed by exposure to 50% RH until 56 days. 94
Fig. 5.25 Calculated index of drying shrinkage-induced cracking of the coatings. The 10 mm-thick coatings (w/c = 0.3) are applied on substrate OC (s = 50%), and moist-cured for 3 or 7 days, followed by exposure to 50% RH until 14 days. The probability of cracking is caculated based on the curves presented in Fig. 5.24. 95
Fig. 5.26 Calculated shrinkage-induced stress in the coatings. The 10 mm-thick coatings (w/c = 0.3) are applied on substrate OC (s = 50%), and moist-cured for 3 or 7 days, followed by exposure to 50% RH until 56 days. This figure compares the tensile stress induced by drying with the tensile strength. The tensile strength is calculated assuming that the coating material is fully sealed or saturated. 96

Fig. 6.1 Schematic illustration of chloride ingress into a cementitious coating system. The coating is applied on a cracked concrete substrate. 99
Fig. 6.2 Schematic illustration of chloride profiles in a coating-substrate system. 102
Fig. 6.3 Schematic illustration of chloride diffusion through the interface between two materials. .. 103
Fig. 6.4 1D schematic illustration of the free chloride profile in a coating system. The red lines show the initial state. The nodes are numbered incrementally from $c0$ to cn in the coating, and $s0$ to sn in the substrate. $c0$ and $s0$ represent the interface nodes in the coating and the substrate, respectively. 104
Fig. 6.5 Schematic presentation of chemical reactions in a Portland cement paste. The hydration products of interest are C-S-H and AFm, which bind the chlorides. Schematic chloride binding of each product is shown. 107
Fig. 6.6 Schematic illustration of two hardened cement pastes that are cemented by a cement slurry. 108

Fig. 6.7 Comparison of simulated and measured ([6]) profiles of free chloride in two specimens. The two specimens (90 days old) are cemented together by a fresh cement slurry. After another 225 days, free chloride profile is determined. In the experiments ([6]), the solutions expressed from the discs of specimens were analysed for the Cl^- content by means of a spectrophotometric technique..... 109
Fig. 6.8 Evolution of degree of hydration and the amounts of hydrates ([g per cm^3 of cement paste]). (a) coating (w/c = 0.3), (b) substrate (w/c = 0.48). The coating and the substrate are cured under saturated condition.....111
Fig. 6.9 Chloride binding capacity ($\partial Cf/\partial Ct$) of the coating (w/c = 0.3) and the substrate (w/c = 0.48) at different degree of hydration. $\partial Cf/\partial Ct$ is calculated with Eq. (6.14)-(6.18). 111
Fig. 6.10 Illustration of the dimension of the coating system (coating and substrate).....112
Fig. 6.11 Schematic illustration of a coating system exposed in a tidal and splash zone (modified based on [180]). 113
Fig. 6.12 Substrate and coating systems. Coatings with different w/c ratios and thicknesses are applied on young substrates. 114
Fig. 6.13 Coating failure in the coating system. Coatings are applied on young substrates. After t (5, 10 or 20) years, the coating fails due to cracking or de-bonding.....114
Fig. 6.14 Concrete substrate with a late application of the coating. Before applying the coatings, the substrates have been exposed to the chloride environment for 5, 10 or 20 years.....115
Fig. 6.15 Cracked substrates with coatings. The surface crack has a size of 0.4×10 mm^2, 0.4×15 mm^2 or 0.4×20 mm^2. Before applying the coatings, the cracked substrates have been exposed to the chloride environment for 10 years.....115
Fig. 6.16 Profiles of free chloride in the uncoated substrate (Sub in Table 6.5) after 50-year exposure to the chloride environment. Chloride transport is simulated with and without considering chloride binding of the substrate.....118
Fig. 6.17 Evolution of concentration of free chloride at the steel surface and predicted time until initiation of reinforcement corrosion in the uncoated substrates (Sub in Table 6.5). Chloride transport is simulated with and without considering chloride binding of the substrate.....118
Fig. 6.18 Profiles of free chloride in the uncoated substrate and the coating systems with 10 mm-thick coatings after 50-year exposure to the chloride environment. The 10 mm-thick coatings with different w/c ratios (i.e. 0.3, 0.4 or 0.5) are applied on young substrates (age = 7 days). 120
Fig. 6.19 Evolution of concentration of free chloride at the steel surface (a) and predicted time until initiation of reinforcement corrosion in the concrete substrates (b). The 10 mm-thick coatings with different w/c ratios are applied on young substrates (age = 7 days)..... 120
Fig. 6.20 Profiles of free chloride in the uncoated substrate and the coating systems after 50-year exposure to the chloride environment. The coatings (w/c = 0.3) with different thicknesses (i.e. 3, 6 or 10 mm) are applied on young substrates (age = 7 days). 121
Fig. 6.21 Evolution of concentration of free chloride at the steel surface (a) and predicted time until initiation of reinforcement corrosion in the concrete substrates (b). The coatings (w/c = 0.3) with different thicknesses (i.e. 3, 6 or 10 mm) are applied on young substrates (age = 7 days). 122

Fig. 6.22 Chloride profiles in the uncoated substrate and the coating system. This figure shows the chloride profile in the uncoated substrate after 10-year exposure to the chloride environment. Then a 10 mm-thick coating (w/c = 0.3) is applied on the 10-year old substrate. The chloride profiles in the coating system (C10(wc0.3)-S10y) at 10.1, 11 and 15 years are presented. 123
Fig. 6.23 Chloride profiles in the uncoated substrate and the coating systems after 50-year exposure to the chloride environment. The 10 mm-thick coatings (w/c = 0.3) are applied on old substrates. Before application of the coatings, the substrates have been exposed to chloride environment for 0, 5, 10 or 20 years. Magnified illustration of the chloride profiles at the steel surface is also shown. 123
Fig. 6.24 Evolution of concentration of free chloride at the steel surface (a) and predicted time until initiation of reinforcement corrosion in the concrete substrates (b). The 10 mm-thick coatings (w/c = 0.3) are applied on old substrates. Before application of the coatings, the substrates have been exposed to chloride environment for 0, 5, 10 or 20 years. 124
Fig. 6.25 Profiles of free chloride in the uncoated substrate and the coating system. In the coating system, a 10-mm thick coating (w/c = 0.3) is applied on a young substrate (age = 7 days). The free chloride profile in the coating system at 20 years (dotted red line) is presented. After 20 years, the coating fails and no protection of the substrate is considered. The chloride profile in the coating system at 50 years (red line) is compared to that in the uncoated substrate (black line). 126
Fig. 6.26 Evolution of concentration of free chloride at the steel surface (a) and predicted time until initiation of reinforcement corrosion in the concrete substrates (b). The 10 mm-thick coatings (w/c = 0.3) are applied on young substrates (age = 7 days). The time of coating failure is assumed to be 5, 10 or 20 years, respectively. 126
Fig. 6.27 Chloride transport in the substrate (Sub-Crack15mm). A surface crack is located at half height of the substrate. The crack has a size of $0.4 \times 15\ mm^2$. (a) cracked concrete structure (b) free chloride profile after 10 years exposure (c) free chloride profile after 50 years exposure.. 127
Fig. 6.28 Chloride transport in the coating system ("C10-Old Sub-Crack15mm"). The crack has a size of $0.4 \times 15\ mm^2$. (a) a 10 mm-thick coating is applied on a cracked concrete substrate that has been exposed to chloride environment for 10 years (b) free chloride profile after 10.1 years exposure (c) free chloride profile after 50 years exposure. 128
Fig. 6.29 Evolution of concentration of free chloride at the steel surface in the uncoated substrates (see Fig. 6.27a). The substrates have a surface crack with a depth of 15 mm and different widths (i.e. 0,1, 0,2 and 0.4 mm). The thickness of concrete cover is 30 mm. 128
Fig. 6.30 Evolution of concentration of free chloride at the steel surface (a) and the predicted time until initiation of reinforcement corrosion in the cracked substrates (b). The coatings (10 mm-thick, w/c = 0.3) are applied on 10 year-old cracked substrates. Before application of the coating, the cracked substrates have been exposed to chloride environment for 10 years. The surface crack in the substrate has a width of 0.4 mm, and a depth of 10, 15 or 20 mm. The original thickness of concrete cover is 30 mm. 130

Fig. A.1 Schematic illustration of moisture transport in two identical concrete samples. Sample A is water saturated, and sample B is partially saturated. The surfaces of the bonded samples are sealed. Moisture is only allowed to transfer within the two samples. 149
Fig. A.2 Moisture profiles in the bonded concrete samples (A and B). Sample A and B have an initial water saturation level of 100% and 27%, respectively. The samples are bonded together (Fig. A.1a). Moisture is allowed to transfer within the samples. The moisture profiles in the bonded concretes in equlibrated state are calculated by Eq. (A.3) and Eq. (A.2), respectively. Note that Eq. (A.3) gives a proper description of moisture transport process in concrete, while Eq. (A.2) does not. 150
Fig. A.3 Water saturation level versus relative humidity of the concrete samples. The desorption isotherm of the concrete (1-year old, w/c = 0.48) is derived from [60]. The initial moisture state of sample A and sample B are shown in this figure. The two sample s are bonded together and sealed. Moisture is only allowed to transfer within in the samples. E2 and E3 show the moisture states of the bonded samples (A and B) in equilibrated state, calculated by Eq. (A.2) and Eq. (A.3), respectively. Note that Eq. (A.3) gives a proper description of moisture transport process in concrete, while Eq. (A.2) does not. 150

Fig. B.1 Schematic illustration of a setup for relative humidity measurement above the concrete surface, reproduced based on [183]. The concrete specimen is placed in a glass container. Only the top surface of the container is open. The top surface of the specimen is exposed, and other surfaces are sealed. 154
Fig. B.2 Schematic illustration of a cement paste (w/c = 0.3) hydrating in a glove box [184]..... 154
Fig. B.3 Schematic illustration of a cement paste (w/c = 0.3) hydrating under RH = 90%. The boundary condition is applied at a distance x (x = 30, 60 or 100 mm) from the surfaces of the specimen. 155
Fig. B.4 Comparison of experimental ([184]) and simulation results of the DOH of a 1.6 mm-thick cement paste. The cement paste is moist-cured for 6 hours, followed by exposure to RH = 50%. In the simulation, the boundary condition (RH = 90%) is applied at a distance x (x = 30, 60 or 100 mm) from the exposed surfaces of the cement paste. 155
Fig. B.5 Schematic illustration of the concrete substrate under drying. 156
Fig. B.6 Drying of 1-year old concrete. The concrete has a w/c of 0.48 (see Table. 5.1). The top surface of the concrete is exposed to a 50% relative humidity at 20 °C, with other surfaces sealed. Experimental results are derived from [60]. In the simulation, the boundary condition (RH = 50%) is applied at a distance x = 60 mm from the exposed surface of the concrete..... 156

Fig. C.1 Lattice velocity directions of two Lattice Boltzmann models..... 159

List of tables

Table 2.1 Surface treatments of concrete structures (EN 1504-2 [21]). 8
Table 2.2 Properties of cement-based coatings and polymer-based coatings, with advantages marked by "+" and disadvantages marked by "−". 10
Table 2.3 Factors to be considered in coating selection ([38, 39]). 11
Table 2.4 Causes and modes of repair failure [48]. 12

Table 4.1 Dependency of different parameters of a coating material. 46
Table 4.2 Mineral composition of Portland cement ([8]) 51
Table 4.3 Values of constants in Eq. (4.23) for the hydration of individual clincker in cement pastes [150]. 66
Table 4.4 Parameters for determining the mass of C-S-H gel in a cement paste [149]. 66

Table 5.1 Water-to-cement ratios and properties of the concrete substrates [60]. 72
Table 5.2 Description of the reference cement paste and the coating-substrate systems. 73
Table 5.3 Calculated degree of hydration and calculated capillary porosity of the coating materials at 14 days after application 90

Table 6.1 Factors considered in the numerical simulation. 100
Table 6.2 Parameters for determining the mass of AFm in a cement paste [149]. 108
Table 6.3 Materials used in the coating systems. 110
Table 6.4 Dimension of the substrates and size of the cracks. 112
Table 6.5 Abbreviated designations of the concrete substrate and the coating systems (the coatings and the substrates are saturated). 116
Table 6.6 Parameters for simulating chloride transport in the coating systems. 117
Table 6.7 Parameters for predicting the time until initiation of reinforcement corrosion in concrete structures. 117
Table 6.8 Overview of the predicted time until initiation of reinforcement corrosion in the concrete structures[years] 131

Table A.1 Water saturation level and relative humidtity in two identical concrete samples (w/c = 0.48, the relation between s and RH is described by the desorption isotherm derived from [60]). 148

List of symbols

Roman lower case letters

a	[−]	Parameter in Van Genuchten (VG) model
c_s^2	[−]	Lattice speed of sound
e_i	[−]	Microscopic velocity vector
f	[−]	Convection coefficient
f_c	[MPa]	Compressive strength of cementitious material
f_i	[−]	Non-equilibrium distribution function
f_i^{eq}	[−]	Equilibrium distribution function
f_t	[MPa]	Tensile strength of cementitious material
g	[m/s^2]	Acceleration of gravity
g_{agg}	[−]	Volume fraction of the aggregates
i	[−]	Lattice directions around the node
k	[m/s]	Water permeability of the porous material
$k(s)$	[−]	Relative water permeability of non-saturated material
k_0	[−]	Basic rate factor of the boundary reaction
k_i	[−]	Ratio of the DOH of clinker i to the total DOH of cement
k_1	[−]	Empirical constant for calculating the DOH of clinkers
k_2	[−]	Empirical constant for calculating the DOH of clinkers
k_3	[−]	Empirical constant for calculating the DOH of clinkers
k_c	[m^{-1}s^{-1}]	Conversion coefficient
k_{lb}	[−]	Permeability of porous material
k_r	[−]	Ratio of water permeability of concrete to the 28 day-value
k_t	[m/s]	Water permeability of material at a particular curing age
k_w	[m/s]	Water permeability
k_{28}	[m/s]	Water permeability of material at 28 days
k'	[m^{-1}]	Mean curvature of the vapour-liquid interface
k''	[−]	Parameter for calculating moisture isotherm
m	[−]	Parameter in Van Genuchten (VG) model
m_{cem}	[kg]	Amount of cement particles in a unit volume of cement paste
$\vec{n}$	[−]	Outward normal of the interface
n'	[−]	Parameter for calculating moisture isotherm
p	[Pa]	Capillary pressure
p_{sat}	[Pa]	Saturated vapour pressure
p_v	[Pa]	Vapour pressure
q	$[m/s]$	Flux of water

r	[m]	Radius of the capillary pore
s	[−]	Water saturation level
s_{cap}	[−]	Water saturation level in capillary pores
s_e	[−]	Locally equilibrated water saturation level in the material
s_{sd}	[−]	Standard deviation of tensile strength
u	[−]	Velocity
v_a	[m^3]	Unit volume of air
v_p	[−]	Poisson's ratio
v_v	[m/s]	Velocity of water vapour
w_i	[−]	Weight factor in the ith direction
w_{sat}	[kg]	Mass of saturated water vapour in a unit volume of air
w_v	[kg/m^3]	Vapour content in a unit volume of material
w_{ve}	[kg]	Locally equilibrated vapour content in the gas
t	[s]	Time
x	[m]	Distance from the surfaces
$\vec{x}$	[−]	Motion of a particle
x_s	[m]	Coordinate of the exposed surface of the materials

Roman capital case letters

AH_v	[kg/m^3]	Absolute humidity
AH_{sat}	[kg/m^3]	Absolute humidity in a space saturated with water vapour
A_{por}	[μm^2]	Total surface area of capillary pores
A_{wat}	[μm^2]	Surface area of water-filled capillary pores
C	[−]	Parameter for calculating moisture isotherm
C_0	[mol/L]	Initial concentration of free chloride in the materials
C_b	[kg/m^3]	Bound chloride per m^3 of material.
C_c	[kg/m^3]	Free chloride content per m^3 of material
C_{b-AFm}	[mol/mol]	Bound chloride per mole of AFm
C_{b-CSH}	[mmol/g]	Bound chloride per gram of C-S-H
C'_{b-AFm}	[mol/g]	Bound chloride per gram of AFm
C'_{b-CSH}	[mol/g]	Bound chloride per gram of C-S-H
C_f	[mol/L]	Concentration of free chloride per liter of pore solution
$C_{f_{co}}$	[mol/L]	Concentration of free chlorides at the interface
$C_{f_{so}}$	[mol/L]	Concentration of free chlorides at the interface
C_s	[mol/L]	Surface chloride concentration
C_r	[mol/L]	Critical concentration of free chloride at rebar surface
C_t	[kg/m^3]	Total chloride content per m^3 of material.
D_0	[m^2/s]	Chloride diffusivity in free water

D_0	[−]	Empirically fitted constant
D_{agg}	[cm^2/s]	Chloride diffusivity of aggregate
D_{Cl}	[m^2/s]	Chloride diffusivity
D_{Cl-c}	[m^2/s]	Chloride diffusivity of coating
D_{Cl-s}	[m^2/s]	Chloride diffusivity of substrate
D_{Cl-cr}	[m^2/s]	Chloride diffusivity in the solution in the cracks
D_l	[m^2/s]	Moisture diffusivity
D_{RH}	[m^2/s]	Effective diffusivity
D'_{RH}	[m^2/s]	Effective diffusivity
D_v	[m^2/s]	Vapour diffusivity
D_θ	[m^2/s]	Hydraulic diffusivity
E_p	[MPa]	Elastic modulus of coating material
F	[−]	Resistance factor
F_0	[m^{-1}]	Speed of a moving interface
F_1	[−]	'Net' temperature function in HYMOSTRU3D
F_2	[−]	Temperature function in HYMOSTRU3D
F_i	[−]	External forcing term
F_v	[kg·m/s]	Flux of water vapour in a clear fluid
L_c	[m]	Concrete cover thickness
J_a	[kg·m^{-2}·s^{-1}]	Moisture flux in the gas
J_{Cl-int}	[mol·m/s]	Flux of free chloride across coating-substrate interface
J_s	[kg·m/s]	Liquid water flux
J_v	[kg·m/s]	Vapour flux in a material
K	[m^2]	Intrinsic permeability of porous material
K_p	[MPa]	Bulk modulus of coating
K_s	[MPa]	Bulk modulus of the solid material in the coating
M_{AFm}	[kg]	Amount of monosulphate per m^3 of cementitious material
M_{Cl}	[g/mol]	Molar mass of chloride
M_{CSH}	[kg]	Total mass of C-S-H in a unit volume of cement paste
M_{HD}	[kg]	Mass of HD C-S-H in a unit volume of cement paste
M_{LD}	[kg]	Mass of LD C-S-H in a unit volume of cement paste
M_r	[−]	Ratio of the mass of LD C-S-H to the total mass of C-S-H
N_{ct}	[−]	Parameter for calculating moisture isotherm
Q	[−]	Number of microscopic velocity vectors connected to node i
R	[J·mol^{-1}·K^{-1}]	Universal gas constant
RH	[−]	Relative humidity
RH_{am}	[−]	Environmental relative humidity
RH_s	[−]	Relative humidity at the drying surface
T	[K]	Temperature
$T_{corrosion}$	[−]	Time until initiation of reinforcement corrosion

V_{cp}	[m^3]	Unit volume of cement paste
V_{ct}	[−]	Parameter for calculating moisture isotherm
V_m	[N/m]	Molar volume of water
$V_m{}'$	[−]	Parameter for calculating moisture isotherm
V_{w-0}	[−]	Volumetric mixing water
W	[kg]	Amount of adsorbed water per m^3 of material
W_{hyd}	[−]	Sink term accounting for hydration
$W_{l\rightarrow v}$	[−]	Transformation of water from liquid phase to vapour phase

Greek letters

α	[−]	Degree of hydration
α_i	[−]	Degree of hydration of clinker i
$\dot{\alpha}$	[s^{-1}]	Rate of hydration
γ	[N/m]	Surface tension of water
δ_x	[−]	Length of lattice
δ_{x-phy}	[−]	Length in physical field
δ_{tr}	[μm]	Transition thickness
$\delta_{x,j}$	[μm]	Thickness of the product layer
Δt_{j+1}	[s]	Time step for simulating hydration of cement
$\Delta\delta_{in,x,j+1}$	[μm]	Increase of the penetration depth
ε	[−]	Free drying shrinkage strain
θ	[−]	Volumetric water content
θ_{cap}	[kg]	Amount of capillary water
θ_r	[kg]	Residual water content
θ_s	[kg]	Water content in saturated condition
λ	[−]	Factor depending on rate controlling mechanism
μ	[Pa·s]	Viscosity of fluid
ρ	[−]	Macroscopic density
ρ_{cem}	[kg/m^3]	Density of cement particles
ρ_g	[kg/m^3]	Density of the gas
ρ_w	[kg/m^3]	Density of water
σ	[MPa]	Shrinkage-induced stress
τ	[−]	Relaxation time
υ	[−]	Lattice kinematic shear viscosity of the fluid
ϕ	[−]	Porosity of porous material
ϕ_{cap}	[−]	Capillary porosity
ϕ_g	[−]	Volume fraction of gas-filled pores
ϕ_{gel}	[−]	Gel porosity

ϕ'_{cap}	[−]	Percolation threshold of capillary pores
ϕ_{cap-w}	[−]	Water-filled capillary porosity
ϕ_s	[−]	Porosity of substrate
ϕ_w	[−]	Water-filled porosity
Φ	[−]	Probability of cracking of coating
ω	[−]	Water-to-cement ratio
ω_v	[−]	Mass fraction of water vapour in gas
Ω_1	[−]	Reduction factor
Ω_2	[−]	Reduction factor
Ω_3	[−]	Reduction factor

List of abbreviations

1D	One-dimensional
2D	Two-dimensional
AFm	Monosulphate
BET	Brunauer-Emmett-Teller
C-S-H	Calcium silicate hydrate
C_2S	Dicalcium silicate $2CaO \cdot SiO_2$
C_3S	Tricalcium silicate $3CaO \cdot SiO_2$
C_3A	Tricalcium aluminate $3CaO \cdot Al_2O_3$
C_4AF	Calcium ferroaluminate $4CaO \cdot Al_2O_3 \cdot Fe_2O_3$
$C\bar{S}H_2$	Gypsum
CT scan	X-ray computed tomography
DOH	Degree of hydration
H	Water
HD C-S-H	High density calcium silicate hydrate
HPC	High performance concrete
ITZ	Interfacial transition zone
LD C-S-H	Low density calcium silicate hydrate
LBM	Lattice Boltzmann Method
NMR	Nuclear magnetic resonance
w/c	Water-to-cement ratio
OC	Ordinary concrete
RH	Relative humidity
ROH	Rate of hydration

Chapter 1

General introduction

1.1 Research background

Concrete is the most widely used material in the construction field. Long-term performance of concrete has to be guaranteed for concrete structures to reach the designed service life. However, the initial scatter in the quality of concrete is commonly seen in practice, possibly resulting from improper design, poor construction practices and improper curing. Areas of concrete with poor quality may become a path for aggressive substances to penetrate into the concrete, like CO_2 and chloride ions, resulting in premature deterioration of the concrete and/or corrosion of the reinforcing steel. Repair is a measure to bring the deteriorated concrete structure back to the desired performance. For concrete structures with slightly unsatisfactory surface areas (e.g. voids and pits, or tiny cracks), from either aesthetic or durability point of view, an ideal solution would be applying a cementitious coating. Cementitious coatings act as a physical barrier and can be used to protect the concrete structures against the attack of detrimental substances [1, 2]. The thickness of the coating is often no more than several millimeters. Materials thicker than 10 mm can be classified as repair. A concrete substrate and a coating system are schematically shown in Fig. 1.1. In this thesis, a coating system refers to a system that consists of a coating and a concrete substrate.

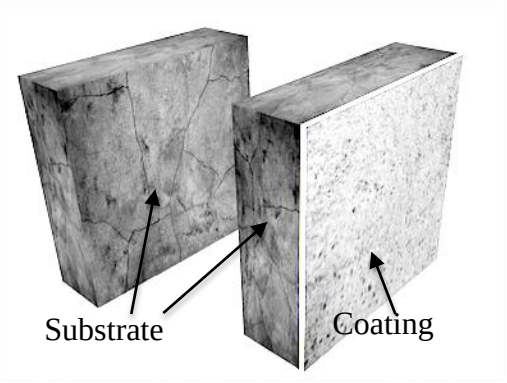

Fig. 1.1 Schematic illustration of a concrete substrate and a coating system.

In order to investigate the performance of concrete repairs, a European project "ConRepNet" has been carried out from 2002 to 2006. It is reported that only 45% of concrete repairs can survive for 10 years after application, and about 10% can survive for 25 years [3]. An analysis of specific repair failures reveals that a minimum set of measures or requirements are needed for ensuring a proper structural repair, such as [4]:

1. Removal of deteriorated concrete layer,
2. Replacement of corroded reinforcement or incorporation of new reinforcement,
3. Matching the physical and chemical properties of repair material to the concrete substrate.

A cementitious coating can be applied directly on concrete substrates without removing the surface layer of the substrate and without replacing the corroded reinforcement. The requirement "matching the physical and chemical properties of repair to the concrete substrate" is dominant. Differential drying shrinkage is one of the major causes of failure of the coating. The drying shrinkage of the coating and the substrate is determined by the moisture gradient and the mechanical properties (e.g. elastic modulus).

Generally, transport and mechanical properties of the concrete substrate are constant in time because the substrate usually has reached a mature state already. However, for a coating applied on the substrate, uncertainties in performance of the coating may arise due to its interaction with the substrate and the environment. Moisture transport in young cementitious coatings may take place simultaneously with hydration of the coatings. The ongoing hydration goes along with the evolution of transport and mechanical properties of the coating material over time. Premature failure of a coating may happen if the drying shrinkage-induced stress exceeds the tensile strength of the coating. As a result, the effectiveness of the coating to improve the performance of concrete structures will be reduced. For a good performance of the coating system, a proper mix design of the coating material, as well as appropriate construction practices, i.e. applying a proper curing regime, are needed.

To provide guidance for the design of the coating material and the construction practice, knowledge on moisture transport in hydrating coating systems is needed. Moisture transport in cementitious materials is determined by their microstructure and moisture content. As the cementitious material hydrates, both the microstructure and the water content change with time. A clear understanding of coupled moisture transport and hydration processes is necessary for further study on the evolution of mechanical properties and the probability of drying shrinkage-induced cracking of a hydrating coating material. Based on an improved understanding of moisture transport in hydrating coating systems, suggestions for the mix design of the coating material and execution procedures can be proposed for achieving a good performance of the coating system.

Long-term performance of coated concrete structures has to be studied for evaluating the effectiveness of the coating. For reinforced concrete structures, the ingress of chemical substances (e.g. Cl^- and SO_4^{2-}) is critical. Chloride diffusion and chloride binding are two important processes during chloride transport process. As hydration of the coating material

proceeds, the chloride diffusivity and the chloride-binding capacity change accordingly. Few numerical studies are known to simulate chloride transport in overlay systems [5-7]. However, the chloride diffusivity and the chloride-binding capacity are usually not related to the hydration process of the overlay material in these simulations. For a proper service life assessment, the chloride ingress and the chloride binding in hydrating cementitious coating systems have to be known in detail. Fig. 1.2 schematically shows the profiles of free chloride in the uncoated and the coated substrates. The profile of free chloride in the concrete substrate is shown with the solid black curve. After application of the coating, redistribution of chloride ions takes place immediately in the coating system, resulting in the profile of free chloride as shown with the dashed red curve.

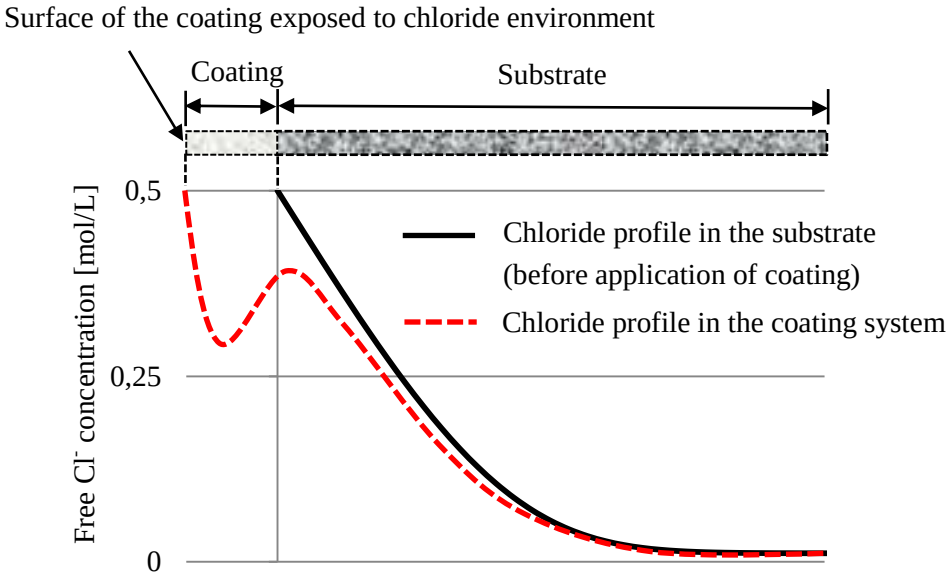

Fig. 1.2 Schematic chloride profiles in a coating system. Solid black line is chloride profile in an old concrete substrate. The red dashed line shows the chloride profile after redistribution of chloride in the coating system.

1.2 Aim, objectives and scope of this study

The aim of this research is to investigate the performance of a protective cementitious coating system (system = substrate + coating). *Moisture transport* in cementitious coating systems (hydrating coating material and mature substrate) will be studied taking into account the hydration process of the coating material. *Chloride transport* in cementitious coating systems (hydrating coating material and hydrating substrate) will be studied taking into account the hydration process of the coating material and the substrate. The objectives of this research are listed as follows, and the scope is specified accordingly:

- To study the mechanisms of coupled hydration and moisture transport processes in cementitious coating systems, and to evaluate the influencing parameters (e.g. coating thickness, curing regime, type of the substrate and initial water content of the substrate) on the moisture profiles in the coating systems. Based on the simulated moisture profiles in the coating systems and the degree of hydration of the coating material, the probability of drying shrinkage-induced cracking of the coating will be evaluated. Recommendations will be proposed for the design and the application of the coating material. The coating material in this research is limited to cement paste.
- To investigate long-term performance of the coating systems. Chloride ingress into uncoated/coated concrete structures is simulated. Based on the simulated chloride profile, the time needed for free chloride to reach a critical concentration at the reinforcing steel of concrete structures is determined. This time, $T_{corrosion}$, also corresponds to the initiation of reinforcement corrosion in concrete structures. The effectiveness of the coatings was indicated by $T_{corrosion}$. When simulating chloride ingress, the coating systems are considered saturated. Parameter studies are conducted with respect to the composition (e.g. water-to-cement ratio) of the coating, the thickness of the coating, early or late application of the coating, time of failure of the coating and the presence of surface cracks in the substrate.

1.3 Research strategy of this study

In order to reach the objectives, the following strategy will be followed:

Moisture transport in the coating systems with various coating materials will be simulated. In the simulation transport of liquid water and transport of water vapour are considered, respectively. Hydration of the coating material is also taken into account, which consumes a certain amount of water during moisture transport. The rate of hydration of the coating material with arbitrary moisture contents is needed in the simulation and will be determined with a numerical hydration model. The transport properties (e.g. intrinsic permeability) of the coating material change with the hydration process and will be described as a function of the degree of hydration.

Chloride ingress into uncoated/coated concrete structures is studied by simulation. Coatings are applied on young/old concrete substrates. The young substrates are 7 days old, while the old substrates have been exposed to chloride environment for a certain period of time (i.e. 5 or 10 years). Hydration of the coating material and the young substrate are taken into account. The chloride diffusivity of the coating and the substrate is determined as function of their microstructures, while the chloride binding capacity is determined by the amounts of hydration products in the coating and the substrate.

1.4 Outline of this research

This thesis includes 7 chapters. The flow chart is shown in Fig. 1.3.

In chapter 2 a literature survey is given regarding moisture transport in hydrating cementitious materials, and chloride-based service life assessment of concrete structures.

In chapter 3 a Moisture-Hydration model is proposed that takes into account liquid water transport, water vapour transport and hydration of the coating material. To run this model, the rate of hydration of the coating material with arbitrary water contents will be determined. Besides, time-dependent transport properties (i.e. intrinsic permeability and moisture diffusivity) of cementitious materials need to be characterized.

In chapter 4 the rate of hydration of the coating material (e.g. a cement paste) with arbitrary water contents is determined using the HYMOSTRUC3D model [8-10]. Time-dependent transport properties (i.e. intrinsic permeability and moisture diffusivity) of the coating material are quantified and described as a function of the degree of hydration.

In chapter 5 *moisture transport* in hydrating cementitious coating systems is simulated with the model proposed in chapter 3. Several parameters are considered, including coating thickness, curing regime and initial water content of the substrate. The simulated moisture profile and degree of hydration of the coating are presented and discussed. The preliminary study on the probability of drying shrinkage-induced cracking of the coating is conducted. Based on the simulation results, the influencing factors are discussed. Some suggestions (e.g. a proper curing regime) are made for a better performance of the coating system.

In chapter 6 *chloride transport* in hydrating cementitious coating systems is simulated. Several parameters are considered in the simulation, i.e. the composition (e.g. water-to-cement ratio) of the coating material, the thickness of the coating, early or late application of the coating, time of failure of the coating and the presence of cracks in the substrate. With the simulated free chloride profile, the time needed for the free chloride to reach a critical concentration (assumed to be 0.2 mol/L) at the reinforcing steel of concrete structures is determined. This time, $T_{corrosion}$, also corresponds to the initiation of reinforcement corrosion in concrete structures. The effectiveness of the coatings is indicated by the extended time for initiation of reinforcement corrosion in the concrete structures.

In chapter 7 conclusions are drawn and prospects are described. Some remarks on future research are presented for a proper application of a cementitious coating.

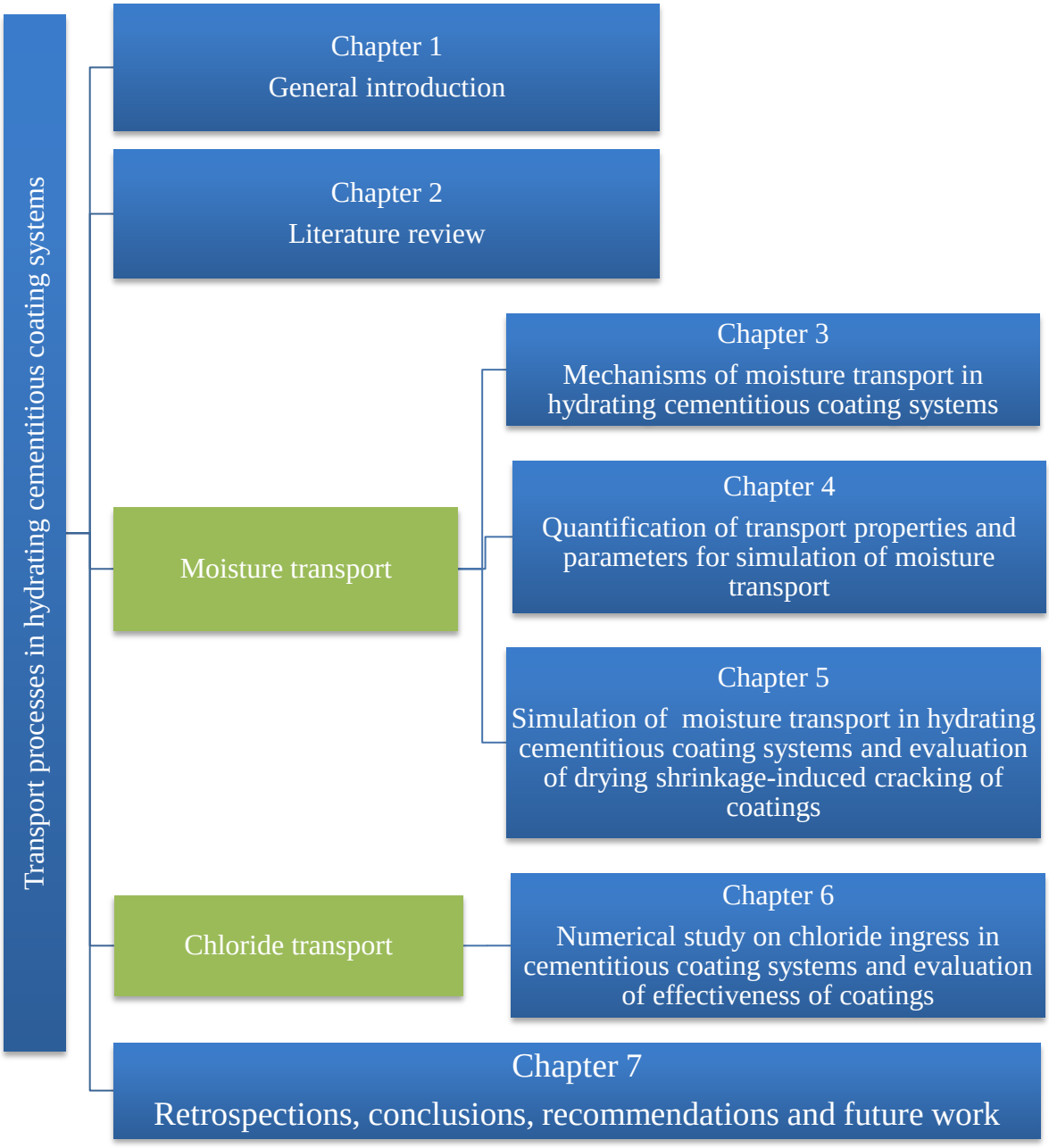

Fig. 1.3 Outline of this thesis.

Chapter 2

General literature review

2.1 Introduction

Concrete is the most commonly used material in the construction industry. It has a good behavior under compressive loads, but it is weak in tension. To carry tensile loads, steel reinforcement is widely used. First application dates back to the time when reinforced concrete was used for a rowboat by Joseph Louis Lambot on the occasion of the Paris Exposition in 1854 [11]. With the development of concrete science, more and more attention has been given to the durability of concrete structures [12, 13]. Amongst the durability related issues, chloride-induced corrosion of reinforced concrete is one of the major forms of deterioration. Corrosion of the reinforcement may weaken the bond between reinforcement and concrete, and further deteriorate the whole concrete structure by reducing the cross section of the reinforcement. Concrete, as a porous material, cannot completely avoid the ingress of potentially harmful agents into the material. It is only a matter of time for such harmful chemicals to penetrate. Furthermore, micro-cracks and micro-pores will appear either due to improper mix design or poor workmanship. Concrete structures with such defects are even more likely to suffer from deterioration. The protection of steel reinforcement by the concrete cover is highly dependent on the cover thickness and the properties of the concrete. Besides the concrete cover, an additional thin coating could be applied to act as an extra "barrier" and cut off the transportation path of external chemicals into concrete [14].

A number of cement-based and polymer-based coatings have been proposed to enhance the performance of concrete structures [3, 15-17]. Among all types of coatings, cement-based coatings are in some cases preferable for concrete substrates due to their good compatibility with the substrate and color similarity. However, some other problems arise, especially for coatings with a thickness of no more than several millimeters. For instance, the hydration process of the coating material may be affected by the water absorption by the substrate and water evaporation. Such moisture loss can cause differential volume changes and may result in cracking and de-bonding of the coating [18]. The presence of cracks may have a major impact on the durability of the whole system by facilitating ingress of chemicals and promoting corrosion. In turn, corrosion causes enlargement of cracks and aggravate the deterioration. When the coating material is reinforced by polymer fibers, micro-cracking of the coating material may take place under tension. These cracks can be beneficial to the performance of the coating system, because they can accommodate the differential volume change of coating and substrate and reduce the risk of de-bonding from two ends of the coating (Fig. 2.1) [19].

Moreover, further hydration of cement in the coating material will promote intrinsic self-healing of the cracks and increase the effectiveness of the coating material [20].

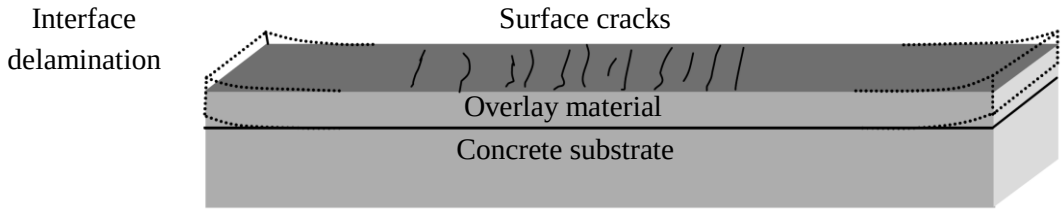

Fig. 2.1 Cracking and interface delamination of an overlay system due to differential shrinkage [19].

In this chapter a literature survey is presented regarding the surface protection of concrete structures and the failure modes of the overlay materials. As stated above, moisture loss from the coating material is a great concern with regard to the hydration of the coating and the drying shrinkage-induced cracking of the coating. The effectiveness of the coating to extend the service life of concrete structures is another and main issue to be studied in this thesis. Moisture transport and chloride transport in overlay systems are reviewed, respectively.

2.2 Surface protections for concrete structures

Several protective measures have been adopted to improve the performance of concrete structures including: use of protective concrete surface coatings, pretreatment of the steel reinforcement and incorporation of corrosion inhibitors. In this thesis, concrete surface protections are concerned. Different surface treatments have been applied on concrete structures to extend the service life (Table 2.1). These treatments are used for both new concrete and for existing structures.

Table 2.1 Surface treatments of concrete structures (EN 1504-2 [21]).

	Definition	Description
Hydrophobic impregnation	A treatment of concrete to create a water-repellent surface.	The pores and capillaries are internally coated, but they are not filled.
Impregnation	A treatment of concrete to reduce the surface porosity and to strengthen the surface.	The pores and capillaries are partially or totally filled.
Coating	A treatment to produce a continuous protective layer on the surface of concrete.	The thickness is typically of 0.1-5.0 mm. Particular applications may require a thickness greater than 5 mm. Coating materials may be organic polymers, organic polymers with cement as a filler or hydraulic cement modified with polymer dispersion.

2.2.1 Impregnations into the surface layer of concrete

Concrete is a hydrophilic material, with a wide range of pore sizes from nanometers to microns. Aggressive ions (e.g. Cl^-) are considered detrimental to reinforced concrete structures. Water absorption by partially saturated concrete promotes chloride ingress [22]. It is, therefore, preferable to make the concrete surface hydrophobic, or densify the exposed surface, in order to reduce water adsorption and ensure its durability [23]. For this, an emulsion enriched with a hydrophobic agent (e.g. polymethyl-hydrogen siloxane oil) can be applied on the surface of concrete to make it water-repellent [24]. Besides, a concrete densifier (e.g. colloidal silica) can be applied to a concrete surface in order to fill pores and increase the surface density, which can reduce the permeability of concrete to liquids [25]. Impregnations are suitable for concrete structures where the concrete surface will not be damaged by abrasion or by the formation of cracks, etc.

2.2.2 Coatings for concrete structures

Surface coatings for concrete structures are classified into two groups, i.e. polymer coatings and cement-based coatings.

2.2.2.1 Polymer coating

There are several types of polymer-based coatings widely used for the protection of concrete structures, such as epoxy resin, polyurethane resin, acrylic resin, and silane/siloxane [26]. These types of polymer coatings differ in terms of price, performance and method of application [27]. Among the existing polymer coatings, acrylic resins and epoxy resins are the most used ones [28].

Adhesion between the polymer coating and the substrate plays an important role in the performance of the polymer coating-substrate system. The adhesion is determined by the properties of both the coating and the concrete substrate. A dry concrete substrate at the time of application is considered preferable for the adhesion [29]. However, a good adhesion is not always beneficial for the performance of coating systems. According to Seneviratne et al. [30], a modest adhesion is beneficial to prevent the coating system from de-bonding. Already a modest adhesion can tolerate de-bonding stresses associated with movements in the concrete.

2.2.2.2 Cement-based coating

Cement-based coatings have been used as they are considered safe from the viewpoint of preserving the alkaline nature of the concrete pore solution [2]. They are also used because of their similar appearance and color of the concrete substrates. Cement-based coatings are usually modified with polymers, in order to obtain a proper adhesion and crack-bridging ability [2]. Twofold effects of the polymers can be ascribed to the protection of coatings, namely reducing coating porosity and increasing surface hydrophobicity [16]. Besides

polymer, other supplementary materials can be incorporated into the cement-based coatings, such as fibers, for a better crack-bridging capacity [31], and rice husk ash for a higher bond strength due to the chemical reaction between the rice husk ash and calcium hydroxide in the cement matrix [32]. Extensive tests have proven the effectiveness of cement-based coating to protect the underlying concrete substrates against chemical attack [1, 33].

2.2.2.3 Comparison of various coatings

Polymer-based and cement-based coatings have a different hardening process. Polymer as a binder determines the performance of polymer-based coatings. Due to a fast polymerization process, less time is needed for hardening. This is one of the biggest advantages compared to cement-based repairs/coatings [34]. Comparisons between polymer coatings and cement-based coatings are reported in the literature [15, 27, 35]. Polymer coatings (e.g. acrylic and polyurethane coatings) have a lower diffusion coefficient than cementitious coatings. The polymer coatings are reported to have a higher resistance against chemical attack [15, 27]. However, the effectiveness of polymer coatings doesn't necessarily have to be higher, because the thickness of polymer coatings is usually much smaller than that of cement-based coatings (e.g. hundreds of microns versus several millimeters) [35].

Table 2.2 shows the properties of cement-based and polymer-based coatings, where cement-based coatings refer to both pure cementitious coatings and cement-based polymer-modified coatings.

Table 2.2 Properties of cement-based coatings and polymer-based coatings, with advantages marked by "+" and disadvantages marked by "–".

	Cement-based coating (1)	Polymer-based coating
Setting (required time, temperature)	–	+
Influence of moisture in substrate (2)	+	–
Thermal deformation	+	–
Shrinkage	–	+
Tensile, adhesive, sheer bond strength	–	+
Crack bridging	–	+
Permeability/Chemical resistance	–	+
Maximum service temperature	+	–
Aging (Ozone/ultra violet light, etc.)	+	–
Cost	+	–

(1) Pure cementitious coating or polymer-modified coating.

(2) A high moisture content in the substrate gives chance to osmotic blistering of the coating [36].

2.2.3 Selection of coatings

A proper selection of adequate coatings depends on many factors. Factors to be considered in coating selection are summarized in Table 2.3. For each specific case, several different properties of the coating are required. However, it is believed that in any given structure these requirements may not be met by one single material [37]. Selection of a coating material, therefore, becomes more difficult.

Table 2.3 Factors to be considered in coating selection ([38, 39]).

Type and condition of concrete substrate	*Nature of concrete protection needed*	*Coating*
New/old concrete Rough/smooth Contamination Water saturation	Abrasion Chemical attack Alkali-aggregate reaction Freezing and thawing Salt scaling Water absorption	Adhesion strength Crack bridging Chemical/water resistance Abrasion resistance Color retention UV resistance Aesthetic appearance

Exposure environment	*Application of coating*	*Overall cost*
Atmospheric, buried or marine	Application method Ease of overcoating Curing regime	Material cost Labor cost Maintenance cost

For good performance of a coating system, "compatibility" between coating material and substrate is crucial. According to Emmons and Vaysburd [40], the general definition of compatibility in concrete repair systems is defined as "*the balance of physical, chemical, and electrochemical properties and deformations between the repair and the existing substrate that ensures that the composite repair system withstands all stresses induced by all loads, chemical and electrochemical effects and deterioration over a designed period of time*" [41]. Obviously, compatibility between repair and substrate is a basic requirement, and it should be recognized during the design of concrete repairs [19, 42, 43]. It is emphasized that compatibility between the repair material and the substrate is a "global" issue and related to many factors (Fig. 2.2). Compatibility in several aspects (chemical, electrochemical, permeability and dimensional) is essential for achieving a durable concrete repair. Detailed discussion on compatibility issues can be found in [44, 45]. Among these compatibilities, the dimensional compatibility is believed to be one of the most vexatious problems of concrete repairs [45]. To obtain a proper dimensional compatibility, "*an ideal overlay material would be volumetrically stable, i.e. it would undergo neither shrinkage nor expansion once installed and would display similar modulus of elasticity and thermal expansion characteristics to the substrate concrete. Unfortunately, despite the best efforts of product formulators such products do not appear to exist"* [45].

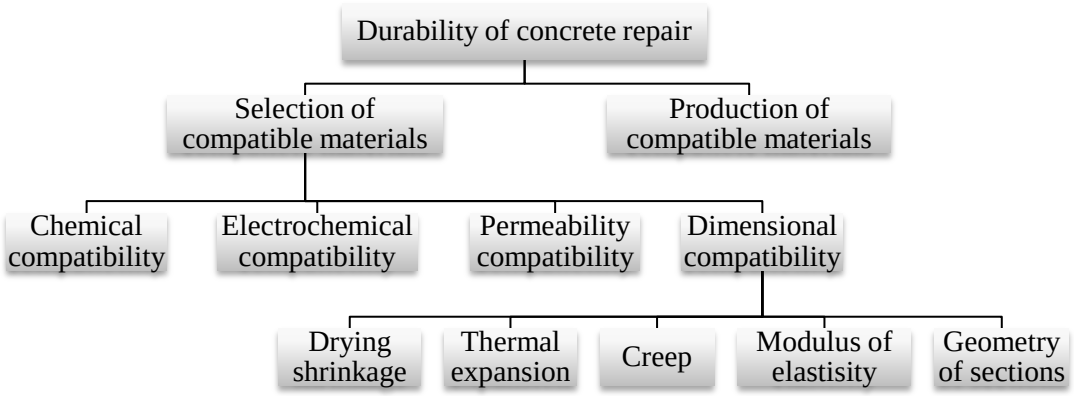

Fig. 2.2 Factors affecting durability of concrete repairs ([46]).

2.2.4 Failure of coating systems

The causes of failure of polymer-based coatings and cement-based coatings are different. The polymer coatings usually fail due to cracking and/or debonding, caused by mechanical stresses, chemical attack, weathering stress and osmotic blistering [47]. The causes of cement-based coating failure and the failure modes can be referred to the report from a European project "ConRepNet" (Table 2.4). Continued corrosion of the reinforcement in the substrate and cracking of the repair material are two main modes of the repair failure. Note that coatings are preventive measures for concrete structures, while repairs are measures for damaged concrete structures, e.g. cracking and spalling of concrete due to corrosion.

Table 2.4 Causes and modes of repair failure [48].

Causes of repair failure	Wrong diagnosis of the cause of initial damage/deterioration of the structure	16%
	Inappropriate design of intervention works	38%
	Inappropriate specification or choice of the materials used	15%
	Poor workmanship	19%
	Other factors	12%
Modes of repair failure	Continued corrosion	37%
	Cracking	36%
	Debonding	6%
	Alkali-aggregate reaction	4%
	Other modes	17%

2.3 An important concern - moisture transport in cementitious coating systems

Cementitious coating material, characterized by a small thickness (no more than 10 mm), is very susceptible to water loss. The water loss will cause a poor dimensional compatibility between the coating and the substrate, which impairs the effectiveness of the coating [49]. The dimensional incompatibility of the coating material caused by the water loss involves the following stages:

1. The coating material loses its water in the hardening phase due to water absorption by substrate and water evaporation to the environment.
2. The water loss of the coating material affects the hydration process and results in a moisture gradient in the coating system.
3. The moisture gradient in the coating system causes differential shrinkage of the coating and the substrate, and induces cracking and/or debonding of the coating material.

The cracking of the coating material poses negative effects on the performance of the coating system by allowing for rapid ingress of ions (e.g. chlorides, oxygen, alkali and sulphate) [19]. To study the probability of drying shrinkage-induced cracking of the coating, a clear understanding of moisture transport in the coating system is necessary.

The moisture content in the coating material changes due to the moisture exchange between the coating and the substrate, between the coating and the environment, and/or the water consumption by hydration. Fig. 2.3 schematically shows the water loss of the coating due to water evaporation to the environment and water absorption by the substrate. Two experimental techniques are commonly used to trace the moisture transport in cementitious overlay systems, viz. nuclear magnetic resonance (NMR) [50-52] and X-ray computed tomography (CT scan) [53, 54]. Brocken et al. [50] investigated moisture transport in a two-layer system (fresh mortar applied on bricks) by using NMR techniques. They found that the water extraction process was slowed down only if the bricks were almost fully saturated. Faure et al. [51] and Kazemi-Kamyab et al. [52] recorded the magnetic resonance imaging profiles of a hydrating overlay system. It was found that water in the fresh material was first absorbed by the substrate, and transferred back to the fresh material after setting [52]. Bentz et al. [53] applied CT scan technique to trace moisture transport in two fresh cement pastes with different w/c ratios. Water was found to move from the less dense to the more dense paste. Lukovic et al. [54] studied moisture transport in a repair system. It was found that water loss from the repair material to the substrate reduced the effective w/c ratio and resulted in a lower degree of hydration of the repair material at 3 days compared to a repair material (no substrate is used) cured under sealed condition.

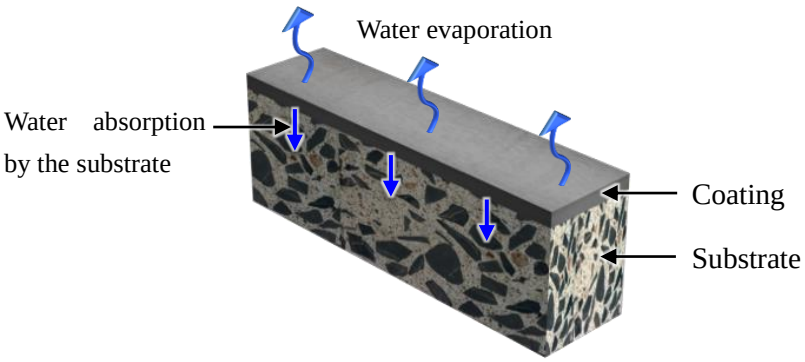

Fig. 2.3 Schematic illustration of moisture transport in a coating system. Basically, moisture transport takes place in 4 forms: 1. water evaporation to the environment, 2. water uptake from the environment, 3. absorption by the substrate, and 4. water uptake from the substrate. This figure shows the water loss of the coating due to water evaporation to the environment and water absorption by the substrate.

Both the overlay material and the substrate play an important role in moisture transport in the overlay system. Pre-wetting of the concrete substrate is commonly used in practice. However, biased views about the effectiveness of pre-wetting are found in literature. For instance, Júlio [55] found that 24-hour pre-wetting of substrate was not important to bond strength. However, a lower bond strength was found between the saturated concrete substrate (water saturation = 99%) and the cementitious repair, compared to a dry substrate (water saturation = 14.4%). This phenomenon was attributed to a wall effect at the interface, where the local w/c ratio was higher than that in the bulk repair material [18]. The higher local w/c ratio at the interface will create a porous interface with low bond strength, causing a "sliding layer" for the repair material. The porous interface has a negative effect on volume stability of the overlay system, in the sense that delamination of the overlay material will be promoted when differential shrinkage takes place in the overlay system [56]. However, according to Courard [57], a higher water absorption by the concrete substrate will allow for a better development of mechanical and chemical bond between the overlay material and the substrate, because of a large interaction area. Lukovic et al. [54] found that a large amount of air voids was introduced into the repair-substrate interface when a dry substrate was used. The air voids at the interface may reduce the adhesion at the interface. More specifically, water saturation levels from 50% to 90% were found to be beneficial to promote the adhesion between cementitious repair and concrete substrate [58]. Usually, problems of adhesion occur when the surface is too dry [45]. Regarding the pretreatment of concrete substrate, it is recommended that the substrate is neither completely dry nor completely wet.

2.3.1 Simulation of moisture transport in cement-based materials

2.3.1.1 Moisture transport in hardened cement-based materials

Numerical simulations of moisture transport in cement-based materials help to figure out the most influencing factors. Moisture transport in hardened cement-based materials has been simulated decades ago [59-62]. The moisture diffusivity can be expressed as a function of relative humidity [63-70], water content [50, 71] or water saturation level of the material [60]. When simulating moisture transport in a material, relative humidity is preferably used as a variable, because the relative humidity is easy to be determined by experiments for verifying the simulation results.

2.3.1.2 Moisture transport in hydrating cement-based materials

Simulation of moisture transport in hydrating cement-based materials can also be found [61, 65, 67, 68]. To account for the effect of hydration on the moisture transport process, various methods have been adopted. For instance, Kim et al. [65] assumed that the variation of relative humidity due to self-desiccation in drying specimens was the same as that in sealed specimens. The drop of relative humidity as a function of time due to hydration under sealed curing condition was obtained from experiments and directly incorporated in the equations to account for the hydration of materials. Bakhshi et al. [61] assumed the amount of water consumption by hydration to be proportional to the amount of free water left in the material. Others [67, 72, 73] described the drop of relative humidity due to hydration as a function of the degree of hydration. Besides, water consumed by hydration of materials subjected to drying has also been analyzed with numerical cement hydration models, e.g. HYMOSTRUC model [74] and CEMHYD3D [75]. In general, a clear correlation between moisture diffusivity and degree of hydration (DOH) is still lacking, which is needed for a proper simulation of moisture transport in a hydrating cement-based material.

2.3.1.3 Boundary condition

The boundary condition at the exposed surface is another important issue in the simulation of moisture transport in porous materials. An additional boundary layer with a thickness of about 1 mm was added on the surface of concrete for simulating moisture transport. The interface between the additional boundary layer and the environment was considered perfectly transmitting (Fig. 2.4a) [61, 76]. More realistically, convective boundary conditions are commonly specified, by introducing a convection coefficient f [65, 69, 77]. With the convection coefficient, moisture flux (described in relative humidity) across the exposed surface is determined (Fig. 2.4b). The convection coefficient f depends mainly on the ambient temperature, the wind speed and the surface texture of the materials. Akita et al. [78] and Wong et al. [77] reported that the convection coefficient changes with the w/c ratio of cementitious materials. For a hydrating cementitious material, determination of the convection coefficient is challenging because the microstructure changes continuously.

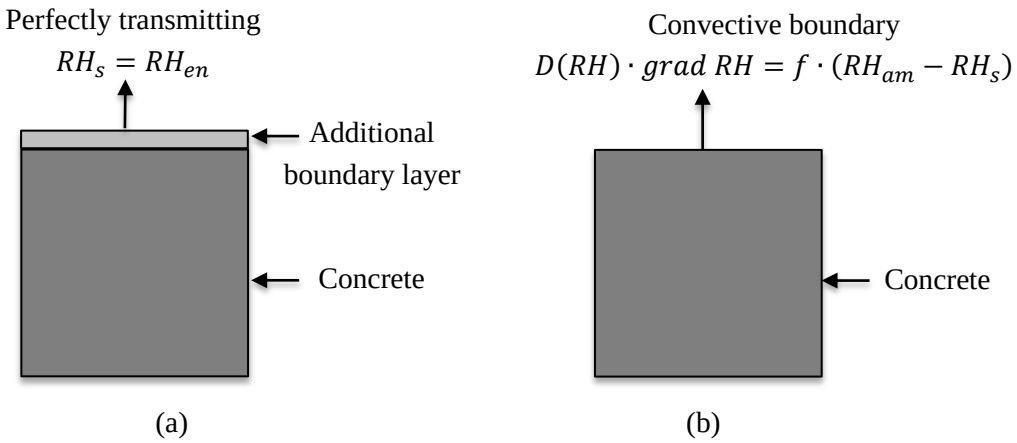

Fig. 2.4 Boundary condition on exposed surface.

(a) Additional layer of concrete is added to original concrete. The new surface of this layer is considered perfectly transmitting. Therefore, the relative humidity at the drying surface (RH_s) equals the ambient relative humidity (RH_{am}) [76].

(b) Convective boundary condition is considered. D(RH) is the moisture diffusivity, and f is the convection coefficient [65, 69].

2.3.2 Simulation of moisture transport in cementitious overlay systems

Efforts have been made to simulate moisture transport in cementitious overlay systems. Brocken et al. [50] simulated water extraction from fresh mortar by bricks by assuming a constant diffusivity of the mortar. A uniform moisture distribution was found in the mortar, while the moisture distribution in the bricks showed a significant gradient. This was because the bricks had lower moisture diffusivity compared to fresh mortars. In their work, only mortars in fresh state were studied. The effect of hydration of mortars was not considered. Åhs [79] calculated the ultimate relative humidity in sealed screed-concrete overlays, without considering time-dependent parameters (e.g. moisture diffusivity and rate of hydration). Lukovic et al. [70] simulated moisture transport in a cementitious repair system to evaluate the risk of drying shrinkage-induced damage. Time-dependent moisture profiles in the repair system were presented. The work was limited to a hardened cementitious repair. Martinola et al. [80, 81] took into consideration endogenous drying due to hydration, and simulated moisture transport in a repair system. However, detailed description of moisture diffusivity and rate of hydration were not mentioned.

2.4 Long-term performance of cementitious coating system - chloride ingress

2.4.1 General introduction of chloride transport in concrete structures

Long-term performance of coating systems (e.g. resistance to ingress of chlorides and CO_2) affects the service life [48, 82]. In concrete structures, reinforcement is commonly used to take up tensile forces. Generally, reinforcement is passivated due to high alkalinity in concrete. However, depassivation of the reinforcement (or initiation of reinforcement corrosion) takes place when the chloride content reaches a critical value or when the alkalinity decreases. Three stages of corrosion-induced damage in reinforced concrete structures can be distinguished: 1. the cracking stage (due to tensile loads, or restrained shrinkage (if any)); 2. the initiation of reinforcement corrosion stage; 3. the propagation stage. With time, each stage develops into higher levels of damage [83]. An early intervention is considered beneficial to increase the service life of concrete structures [84].

The initiation of reinforcement corrosion depends on several factors, such as concrete mix proportions, temperature, relative humidity, steel surface conditions and exposure environments [85]. The critical chloride content has been identified to be one of the most decisive parameters for predicting the service life of concrete structures [86]. The critical chloride content is commonly expressed as total chloride content relative to the weight of the cement [87], as the free Cl^- concentration [88] or as the molar ratio of Cl^-/OH^- [89]. It is believed that only the free chloride in the pore solution is responsible for initiation of the reinforcement corrosion process [90]. The published critical free Cl^- concentration (laboratory conditions) has a wide range from 0.045 to 3.22 mol/L of pore solution [91].

2.4.2 Simulation of chloride transport in concrete structures

To simulate chloride ingress in concrete structures, a simple error function solution is widely used, with a time-dependent diffusivity [92]. However, there are some limitations to apply this solution [93], e.g. the material should be homogeneous and the chloride binding isotherm is linear. However, the coating material and the substrate are usually two distinct materials, and the chloride binding isotherms are not necessarily linear. Beside the error function solution, Fick's 2^{nd} law of diffusion with a sink term is used to obtain the free chloride profile in concrete structures, taking into account the chloride diffusion process and the chloride binding process [93-95].

2.4.3 Simulation of chloride transport in coating systems

Numerical studies of chloride transport in coating systems are scarce. Zhang et al. [7] calculated chloride profiles in surface coated concretes, where a constant diffusivity of each material was specified. No binding of chlorides was considered. Song et al. [5] simulated

chloride penetration into repaired concrete. Chloride binding behavior was also not considered in their simulation. Time until initiation of reinforcement corrosion in repaired concrete structures was predicted. They found that the extended service life depended on a number of factors, such as the quality of the repair materials, the concrete cover thickness and the age of concrete for repair.

In fact, chloride binding takes place during chloride transport in cementitious materials. For a hydrating cementitious material, both the chloride diffusivity and the chloride binding isotherms change over time. The chloride diffusivity can be related to the pore structure of the material [96], and the chloride binding capacity to the amount of hydrates in cementitious materials (e.g. calcium silicate hydrate (C-S-H) and monosulphate hydrate) [97, 98]. It is believed that the chloride binding by monosulfate hydrate is attributed to the formation of Friedel's salt, while the chloride-binding isotherm of C-S-H follows a Langmuir-type adsorption curve [97, 98].

According to Perez et al. [99], chloride binding behavior has a substantial influence on the chloride transport in cementitious materials. Therefore, chloride binding should be taken into consideration for a proper simulation of chloride transport in a cementitious coating system.

2.5 Problem definition

2.5.1 Moisture transport in cementitious coating systems and parameter study

To achieve a good performance of the coating system, the coating material should undergo a proper hydration process. As stated in section 2.3, water loss of the coating material may affect the hydration process and result in shrinkage-induced cracking of the coating or debonding between the coating and the substrate. To investigate the influence of water loss on the hydration process of the coating material, study of moisture transport in hydrating coating systems is needed.

Several factors play a role in the hydration process of the coating material and the moisture transport process in the coating system. The factors include the curing conditions (e.g. moist curing, sealed curing or exposed to drying condition), the type of substrate and the initial water content of the substrate.

With the simulated degree of hydration of the coating material, the mechanical properties (e.g. elastic modulus and tensile strength) can be determined. Preliminary study of shrinkage-induced cracking of the coating material will be performed.

2.5.2 Chloride transport in cementitious coating systems and service life assessment

Long-term performance of coating systems will be studied, in order to assess the service life of coated concrete structures and to evaluate the effectiveness of a coating. Numerical simulations of chloride ingress in the coating systems will be conducted taking into account the diffusion process and the chloride binding process. Parameter studies of several factors will be carried out, viz. the water-to-cement ratio and the thickness of the coating material, early or late application of the coating material, early failure of the coating material and the presence of surface cracks in the substrates. With the parameter study, the most influencing factors that determine the effectiveness of the coating material will be figured out. Suggestions regarding selection of cementitious coatings will be given for a proper protection of reinforced concrete structures.

2.6 Conclusions

This chapter provided a brief literature survey regarding the performance of various coatings, criteria for coating selection, causes and modes of coating failure. Problems of cementitious coating systems are defined. Some conclusions can be drawn:

- In practice, various coatings systems are currently used, including polymer-based coating systems and cement-based ones. The performance of these systems differs a lot. When selecting cementitious coatings, a large number of factors need to be considered. However, for any given concrete structure, these requirements cannot be fully met by one single coating material.
- The causes and modes of failure in cementitious coatings are reviewed. Failure of coating systems can be caused by wrong diagnosis of the cause of initial damage of the substrate, or improper specification/application of overlay materials. Failure modes of repairs include continuous corrosion of reinforcement in the substrate, cracking and debonding of coatings, etc.
- Water loss of the coating material may affect the hydration process and cause shrinkage-induced cracking in the coating material. Parameter studies of the influencing factors of moisture transport should be performed to give guidance to the design and the application of the coating materials.
- Chloride ingress in cementitious materials is critical for the service life. A numerical study of chloride transport in the coating systems will be conducted considering coupling the chloride diffusion process and the chloride binding process. Suggestions regarding the coating material will be made for a proper protection of the reinforced concrete structures.

Chapter 3

Mechanisms of moisture transport in hydrating cementitious coating systems

3.1 Introduction

As stated in section 2.3, moisture transport in cementitious coating systems may affect the hydration process of the coating material. The moisture loss and the disturbed hydration process of the coating material will lead to impaired performance of the coating system, e.g. drying shrinkage-induced cracking of the coating material. Efforts have been made to simulate moisture transport in hydrating cementitious materials [61, 65, 67, 68]. However, the coupling of moisture transport and hydration processes is often not adequate. Moreover, mass conservation of water in the coating-substrate interface has to be ensured but is often overlooked [100]. In this chapter the mechanisms of moisture transport in hydrating cementitious coating systems are studied. Based on the mechanisms, a "Moisture-Hydration model" is proposed. Fig. 3.1 shows the position of chapter 3 in the structure of the study of moisture transport in hydrating cementitious coating systems.

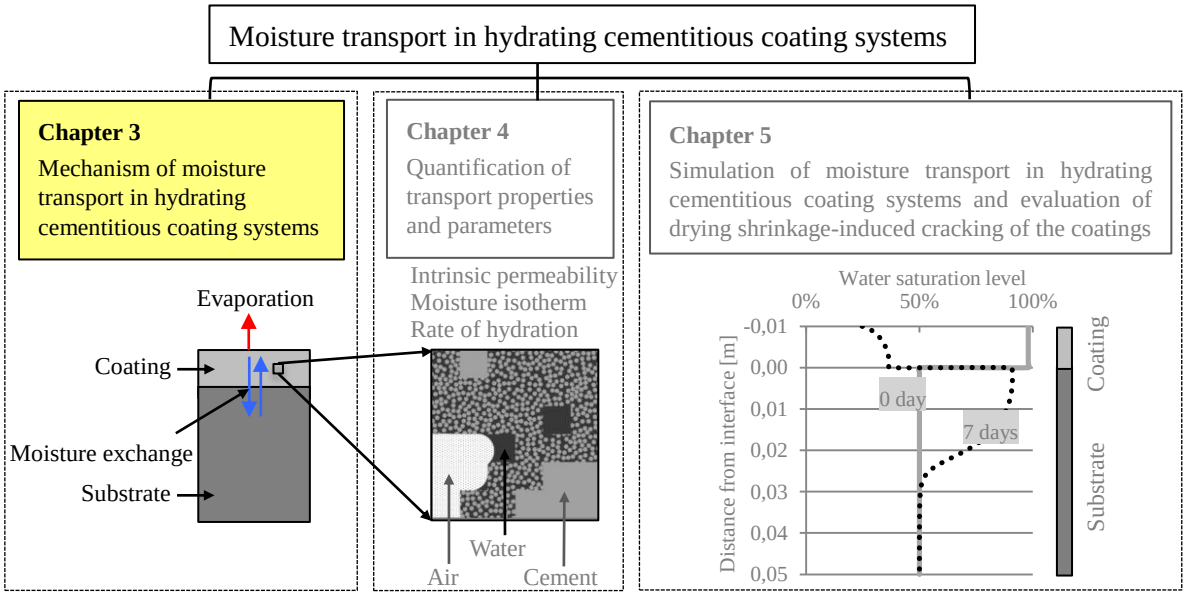

Fig. 3.1 Structure of the study of moisture transport in hydrating cementitious coating systems.

3.2 Mechanisms of moisture transport in cementitious materials

3.2.1 Moisture transport in saturated cementitious material

In saturated cementitious materials, the water flow is driven by a pressure gradient and can be described by Darcy's law:

$$q = \frac{K}{\mu} \cdot \frac{\partial p}{\partial x} \tag{3.1}$$

Where q is the flux $[m/s]$, K is the intrinsic permeability of the porous material [m^2], μ is the viscosity of fluid $[Pa \cdot s]$, and $\partial p / \partial x$ is the pressure gradient vector $[Pa/m]$.

3.2.2 Moisture transport in partially saturated cementitious material

3.2.2.1 Dominant mechanisms of moisture transport in partially saturated cementitious material

In case of moisture transport in hydrating cementitious coating systems (Fig. 3.2), Eq. (3.1) is not applicable, because the coating and the substrate are usually unsaturated. After application of the coating, the water content in the coating material may change due to the following factors:

a) Moisture exchange between the coating and the substrate
b) Moisture exchange between the coating and the environment
c) Water consumption by the hydration process of the coating

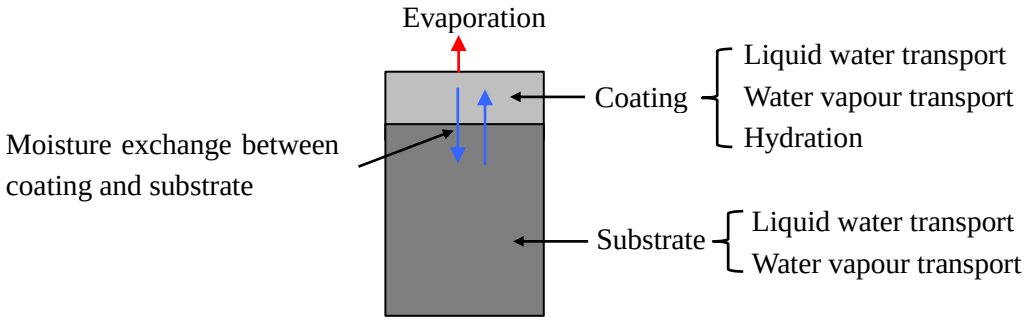

Fig. 3.2 Schematic illustration of factors affecting moisture transport in a hydrating cementitious coating system.

Investigation of the above-mentioned factors requires understanding of the following mechanisms:

1) Moisture transport in cementitious materials (i.e. the coating and the substrate).
2) Moisture transport across the coating-substrate interface and the coating-environment interface.
3) Hydration process of the coating with arbitrary water contents.

In this section, moisture transport in cementitious materials is studied. Moisture transport across the coating-substrate interface and the coating-environment interface, and the effect of hydration of the coating on moisture transport will be studied in section 3.3.

There are two different forms of moisture in porous materials, namely liquid water and water vapour. The movement of liquid water is driven by the gradient of capillary pressure, while the movement of water vapour by the gradient of vapour pressure. The dominant mechanism of moisture transport in porous material depends on pore sizes [101] (see Fig. 3.3). For micro pores, i.e. pores with diameter $d < 0.1\ \mu m$, capillary condensation/evaporation will take place at varying relative humidity (RH). For capillary pores, i.e. $0.1\ \mu m < d < 1000\ \mu m$, capillarity is predominant. For macro pores, i.e. $d > 1000\ \mu m$, fluid flow governs the moisture transport. However, it has to be pointed that, besides the main mechanisms shown in Fig. 3.3, other mechanisms may also apply, depending on the situations. For instance, in addition to capillarity, fluid flow can also happen in capillary pores when external pressure is applied on the material (e.g. water permeability tests on cementitious materials).

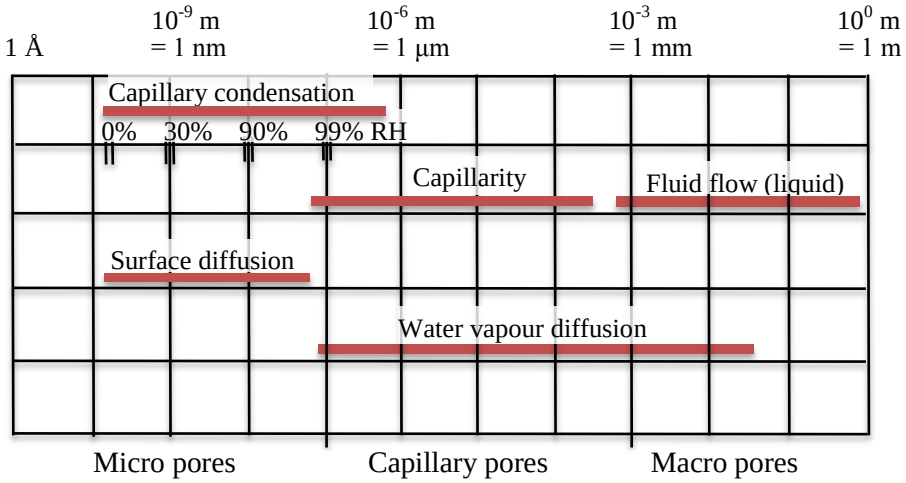

Fig. 3.3 Moisture transport mechanisms and the definition of pore size classes (after Klopfer [101]).

In cementitious materials, pores are usually classified into capillary pores (pore size larger than 10 nm) and gel pores (smaller than 10 nm) [102]. This classification is also adopted in this study. Since the pores in cementitious materials are usually smaller than 1 mm, movements of liquid water and water vapour can be described by 3 main mechanisms [103]:

1) Capillary action

Movement of liquid water is considered as a capillary action. At the gas/liquid/solid interface in a porous material, a concave meniscus occurs because water molecules are more strongly attracted to the pore wall than to each other. A meniscus with a smaller radius indicates a higher capillary pressure. The driving force of liquid water movement is the internal capillary pressure gradient.

2) Vapour diffusion

Movement of water vapour is driven by the vapour pressure difference in local pores. Vapour pressure is defined as a pressure exerted by a vapour in thermodynamic equilibrium with its condensed phases (solid or liquid) at a given temperature in a closed system. The movement of water vapour is a diffusion process, which takes place from areas of a high vapour pressure to other areas with a lower vapour pressure. In the pores, Knudsen diffusion occurs when the pore size is comparable to or smaller than the mean free path of the water molecule. Water molecules frequently collide with the pore wall, and the collision provides the main diffusion resistance. Knudsen diffusion in pores with a regular shape (e.g. straight cylindrical pores) is well formulated [104]. However, it becomes more complicated for a cementitious material because of its complex pore structure. In practice, molecule diffusion and Knudsen diffusion are usually considered as one process, and can be calculated from experimental results [105] or predicted by numerical models [106].

3) Surface diffusion

Besides the movements of liquid water and water vapour, a surface diffusion of absorbed water has been postulated. The surface diffusion is schematically illustrated in Fig. 3.5a. It is believed that the surface diffusion is significant only when the humidity in the pores of concrete is very low [107].

According to Xi et al. [107], moisture transport in cementitious materials often includes contributions from multiple mechanisms; accurate prediction of the total moisture diffusivity is, therefore, difficult. In order to clearly demonstrate the moisture transport in cementitious materials, moisture transport is categorized into two cases. In one case, moisture transport takes place in the pores with a continuous liquid water phase. Another case deals with moisture transport in the pores with a discontinuous liquid water.

3.2.2.2 Moisture transport in pores with a continuous liquid water phase

In Fig. 3.4a two pores are presented, namely pore A and pore B. Note that, in reality the pores in cementitious materials are not discrete objects, because at the nanoscale the pore structure is perpetually continuous [108, 109]. In pore B water forms a meniscus with a smaller radius than pore A ($R_2 < R_1$), corresponding to a higher capillary potential and a lower vapour pressure. Thus, the movement of liquid water is driven from pore A towards pore B, resulting in a new meniscus for both pores with a radius of R. The equilibrated moisture distribution is shown in Fig. 3.4b. Simultaneously, a new vapour pressure forms in the pores, either due to condensation in pore B or evaporation in Pore A. Besides the changes in liquid and vapour phases, the thickness of the absorbed layer on the pore walls also changes due to a varying vapour pressure, resulting in a thinner layer in pore A, and a thicker layer in pore B.

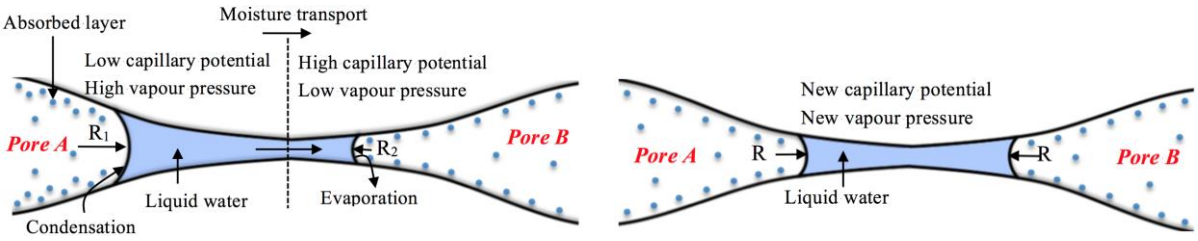

Fig. 3.4 Moisture transport in a capillary pore with a continuous liquid water phase.
(a) Water distribution in a capillary pore (non-steady state), liquid water moves from left to right.
(b) Equilibrated water distribution in a capillary pore.

3.2.2.3 Moisture transport in pores with a discontinuous liquid water phase

When the liquid phase is discontinuous, water vapour diffusion dominates the moisture transport process. In Fig. 3.5a, Pore B has a lower vapour pressure than pore A. Accordingly, water in pore B forms a meniscus with a smaller radius than pore A ($R_2 < R_1$). Therefore moisture transports by vapour diffusion from pore A towards pore B. Consequently, evaporation of water take places in the pore A, and condensation takes place in Pore B. Besides, surface diffusion of absorbed water tends to happen from the region with thicker water layers to the region with thinner ones. Fig. 3.5b shows the equilibrated moisture state in the pores. The vapour diffusion leads to menisci with a new radius (R) in both pores. The pore system has a new capillary potential as well as a new vapour pressure.

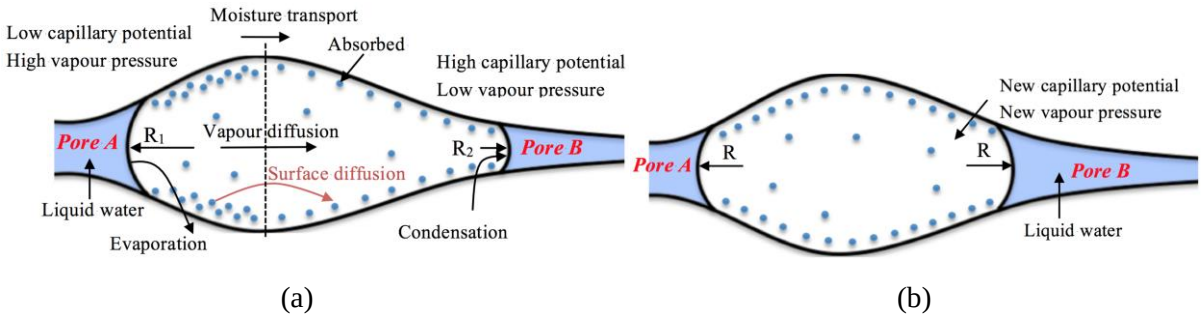

Fig. 3.5 Moisture transport in a capillary pore with a discontinuous liquid water phase.
(a) Water distribution in a capillary pore (non-steady state), water vapour diffuses from left to right.
(b) Equilibrated water distribution in a capillary pore.

3.2.3 Equation describing moisture transport in partially saturated cementitious materials

The moisture transport process in cementitious materials is usually described with nonlinear diffusion equations. Relative humidity as a variable is preferably used to simulate moisture transport in porous material, since its value can be measured in experiments by embedding relative humidity probes in the material. The moisture transport process in cementitious materials can be described by [63]:

$$\frac{\partial \theta}{\partial RH} \cdot \frac{\partial RH}{\partial t} = div(D_{RH} \cdot grad\ RH) \tag{3.2}$$

where RH is the relative humidity, $\partial\theta/\partial RH$ the moisture capacity and D_{RH} the effective diffusivity.

In Eq. (3.2), the moisture capacity $\partial\theta/\partial RH$ can be obtained from the adsorption isotherm of cementitious materials. Determination of adsorption isotherms is presented in [63]. Based on the BET (Brunauer–Emmett–Teller) model [110], a formula has been established to determine the moisture capacity of cementitious materials. In the formula, several parameters are considered, including the type of cement, w/c ratio, temperature and curing time. There are some limitations of this formula. For instance, when the w/c is lower than 0.3, or the curing time is shorter than 5 days, the value of moisture capacity is considered constant. However, the moisture capacity of early-age cementitious materials changes with ongoing hydration, because the microstructure varies a lot due to hydration.

Also Xi et al. [107] proposed an empirical formula to determine the effective diffusivity D_{RH}. In their formula the D_{RH} is a function of the relative humidity, in combination with three empirical coefficients. These three coefficients were calibrated based on test data, and found to be only dependent on the w/c ratio. In fact, the effective diffusivity D_{RH} should also depend on hydration, because hydration changes the microstructure of a cementitious material and further affects its transport properties (e.g. effective diffusivity). However, the dependence of D_{RH} on hydration was not considered in their work. Therefore, practical calculations on moisture transport in cementitious materials based on the proposed parameters remain difficult.

Besides Eq. (3.2), also other equations have been used to simulate moisture transport in cementitious materials. Those equations are introduced in appendix A. A case study of moisture transport in cementitious material is conducted in appendix A to show the validity of those equations.

3.3 Moisture-Hydration model for simulating moisture transport in hydrating coating systems

3.3.1 Factors considered for simulating moisture transport in hydrating coating systems

To simulate moisture transport in a hydrating coating system, a model (Moisture-Hydration model) will be proposed. At early ages, the rate of hydration of the coating strongly depends on the water content. For a proper simulation, the hydration process of the coating material should be coupled with the moisture transport process. Since the mass of water is the physical quantity that needs to be conserved during the moisture transport process, the water saturation level, instead of the relative humidity, will be introduced as a dependent variable in the simulation of moisture transport. By using water saturation level as a dependent variable, water loss due to hydration can be explicitly considered in moisture transport process through a hydrating coating system.

When developing the Moisture-Hydration model for a hydrating coating system, the following aspects will be considered:

1) Water transport process (in liquid form) in the coating system. Water consumed by hydration process of the coating will be considered.

2) Water saturation level dependency of the hydration process. The rate of hydration will be determined for a coating that has a certain degree of hydration and a certain water saturation level.

3) Vapour diffusion process in the coating system.

4) Water - vapour transition in cementitious materials. The phase transition is essential for correlating the water transfer and vapour diffusion processes.

5) Moisture transport (i.e. water transfer and vapour diffusion) across the coating-substrate interface.

6) Water evaporation from the surface of the coating material. The varying microstructure of a hydrating coating material complicates the water evaporation process. Detailed description will be given of the interaction between the coating and the ambient air.

3.3.2 Liquid water transport in a hydrating cementitious material

Unsaturated water flow in porous materials is often described by Richards equation [111].

$$\frac{\partial \theta}{\partial t} = div\big(k \cdot grad\, p(\theta)\big) \tag{3.3}$$

where k is the water permeability of the porous material, and $p(\theta)$ is the capillary pressure.

The Richards equation (Eq. (3.3)) is also widely used for simulating moisture transport in cementitious materials. Since liquid water flow in cementitious materials is dominated by capillary pressure, the effect of gravity is mostly neglected [112]. It is believed that for engineering problems the Richards equation provides a satisfactory description of unsaturated flow [113].

The volumetric water content θ can be substituted by the water saturation level s. By introducing the relative permeability $k(s)$ of the material [114], Eq. (3.3) becomes

$$\frac{\partial(\phi \cdot s)}{\partial t} = div\left(\frac{-K}{\mu} \cdot k(s) \cdot grad\, p(s)\right) \tag{3.4}$$

where ϕ is the porosity of porous material, K is the intrinsic permeability of the porous material, $k(s)$ is relative water permeability of porous material with a water saturation level s and μ is the dynamic viscosity of water.

Water transfer in a hydrating cementitious material is different from that in a porous material with a stable microstructure. In the hydrating cementitious material both the microstructure and the water content change with ongoing hydration, which causes different capillary pressure and moisture gradients in the material. When simulating moisture transport in a cementitious material, the water loss due to hydration is usually linked to the relative humidity [65, 67, 68, 72, 74, 81]. In this study, to account for the hydration of the coating, a sink term "W_{hyd}" will be introduced in Eq. (3.4). Determination of W_{hyd} will be given in section 3.3.3. Water transfer through a hydrating cementitious material can be described by:

$$\frac{\partial(\emptyset \cdot s)}{\partial t} = div\left(\frac{-k}{\mu} \cdot k(s) \cdot grad\, p(s)\right) - W_{hyd} \tag{3.5}$$

Applying the product rule to the left term of Eq. (3.5), it gives:

$$\frac{\partial(\emptyset \cdot s)}{\partial t} = \frac{\emptyset \cdot \partial s}{\partial t} + \frac{s \cdot \partial \emptyset}{\partial t} \tag{3.6}$$

Eq. (3.5) gets a new form:

$$\frac{\emptyset \cdot \partial s}{\partial t} = div\left(\frac{-K}{\mu} \cdot k(s) \cdot grad\, p(s)\right) - W_{hyd} - \frac{s \cdot \partial \emptyset}{\partial t} \tag{3.7}$$

By applying the chain rule, it follows:

$$gradp(s) = \frac{dp(s)}{ds} \cdot grad\, s \tag{3.8}$$

Substituting Eq. (3.8) into Eq. (3.7) gives:

$$\frac{\emptyset \cdot \partial s}{\partial t} = div\left(\frac{-K}{\mu} \cdot k(s) \cdot \frac{dp(s)}{ds} \cdot grad\, s\right) - W_{hyd} - \frac{s \cdot \partial \emptyset}{\partial t} \tag{3.9}$$

The quantities preceding the gradient within the parenthesis can be lumped together to form a single diffusion coefficient (i.e. liquid water diffusivity):

$$D_l(s) = \frac{-K}{\mu} \cdot\ k(s) \cdot \frac{dp(s)}{ds} \tag{3.10}$$

Considering the transformation of water from liquid phase to vapour phase, $W_{l \to v}$, for a one-dimensional case, Eq. (3.9) reads:

$$\frac{\phi \cdot \partial s}{\partial t} = \frac{\partial}{\partial_x} \cdot D_l(s) \cdot \frac{\partial s}{\partial x} - W_{hyd} - \frac{s \cdot \partial \phi}{\partial t} - W_{l \to v} \tag{3.11}$$

In this study, Eq. (3.11) is used to describe the movement of liquid water in the materials under isothermal conditions. The term $D_l(s)$ can be regarded as moisture diffusivity. However, it should be emphasized that the movement of liquid water is driven by capillary pressure. It is not, per se, a diffusive phenomenon.

Solving Eq. (3.11) requires determination of several parameters, viz. intrinsic permeability K, relative permeability $k(s)$, capillary pressure $p(s)$, water loss due to hydration W_{hyd} and total porosity ϕ. All these parameters are time-dependent; they change with the varying microstructure and the remaining water content left after hydration and moisture transport.

To determine the relative permeability $k(s)$ and the capillary pressure $p(s)$, vapour desorption-adsorption isotherms (also known as moisture isotherms) of the materials should be described first. The moisture isotherms show the relationship between the equilibrium water content of the material with the RH at a constant temperature [115]. In a porous material, the RH can be related to the curvature of the smallest water-filled pores by the

Kelvin equation. From the curvature, the capillary pressure $p(s)$ can be calculated based on Young-Laplace equation. The Kelvin equation and the Young-Laplace equation will be presented in section 3.3.5.

The dependency of $k(s)$ and $p(s)$ on the water saturation level is described by the Van Genuchten (VG) model [116].

$$p(s) = a \cdot (s^{-\frac{1}{m}} - 1)^{(1-m)} \tag{3.12}$$

$$k(s) = s^{0.5} \cdot (1 - (1 - s^{1/m})^m)^2 \tag{3.13}$$

where a and m are two fitting parameters, depending on the microstructure of the material. Quantification of these parameters will be carried out in chapter 4 (section 4.6.4).

By substituting Eq. (3.12) into Eq. (3.10), the moisture diffusivity $D_l(s)$ can be written as:

$$D_l(s) = \frac{-K}{\mu} \cdot \frac{a \cdot (m-1)}{m} \cdot (1 - (1 - s^{1/m})^m)^2 \cdot (s^{-\frac{1}{m}} - 1)^{(-m)} \cdot s^{(-\frac{1}{m}-0.5)} \tag{3.14}$$

According to Eq. (3.11), the liquid water flux J_s through a material is proportional to its moisture gradient:

$$J_s = -D_l(s) \cdot grad\ s \tag{3.15}$$

Eq. (3.15) will be used in section 3.3.6 to calculate the liquid water flux through the interface between the coating and the substrate.

3.3.3 Water consumed by hydration of cementitious materials with arbitrary water content

The term W_{hyd} in Eq. (3.11) refers to the water consumption by hydration and has to be formulated for simulating moisture transport in hydrating coating systems. At complete hydration, 1 g of cement chemically binds approximately 0.23 g of water [117]. W_{hyd} can be determined according to Eq. (3.16) and Eq. (3.17).

$$W_{hyd} = \frac{0.23 \cdot m_{cem} \cdot \dot{\alpha}}{\rho_w} \tag{3.16}$$

$$\dot{\alpha} = \frac{d\alpha}{dt} \tag{3.17}$$

where α is the degree of hydration, $\dot{\alpha}$ is the rate of hydration, m_{cem} is the mass of cement in a unit volume of cement paste and ρ_w is the density of liquid water.

For a cement paste with a particular DOH, the rate of hydration $\dot{\alpha}$ depends on, among other things, the water content that is available for hydration, i.e. the capillary water. The distribution of water in a cement paste is schematically shown in Fig. 3.6. Fig. 3.6a presents a water-saturated microstructure. During drying, water in capillary pores is gradually lost, while the remaining water can still be used for further hydration (Fig. 3.6b). After capillary water is used up, either due to drying or continuing hydration, gel pores start to lose water due to continuous drying, while the hydration has almost ceased (Fig. 3.6c).

In the Moisture-Hydration model, the water saturation level s in the total pore space of the materials is used. According to Van Breugel [8], the capillary water content is one of the main factors affecting the rate of hydration $\dot{\alpha}$. To describe the water saturation level dependence of the rate of hydration $\dot{\alpha}$, water saturation level in capillary pores s_{cap} is defined:

$$s_{cap} = \frac{\phi \cdot s - \phi_{gel}}{\phi_{cap}} \tag{3.18}$$

where ϕ is the total porosity, ϕ_{gel} is the gel porosity and ϕ_{cap} is the capillary porosity. Fig. 3.7 schematically illustrates the volume changes of water, unhydrated cement, hydration products and pores in a hydrating cement paste. Explanation of water saturation level in capillary pores s_{cap} is presented in Fig. 3.8.

Given the water saturation level in capillary pores s_{cap}, the rate of hydration $\dot{\alpha}$ of a cementitious material can be determined by using a modified HYMOSTRUC3D model. The HYMOSTRUC3D is a model for simulating hydration, morphology and structure of cement-based materials [8-10]. Detailed information will be given in chapter 4.

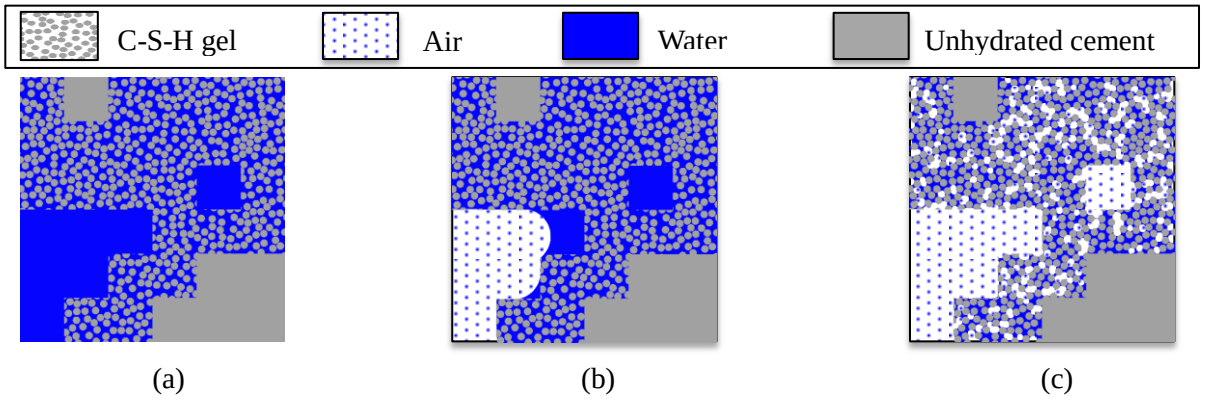

Fig. 3.6 Water distribution in a drying cement paste. (a) 2D schematic microstructure of a water-saturated cement paste (b) drying takes place in capillary pores, remaining water are available for both hydration and drying (c) drying takes place in gel pores (RH $\leq$ 80%), remaining water is only available for drying, no hydration is considered.

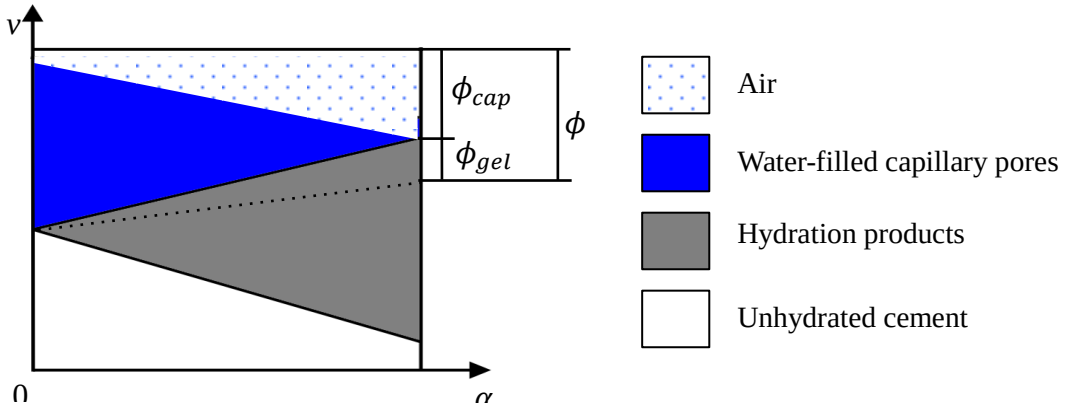

Fig. 3.7 Schematic illustration of the volume changes of water, unhydrated cement, hydration products and pores in a hydrating cement paste under sealed condition. α is the degree of hydration and v is the volume.

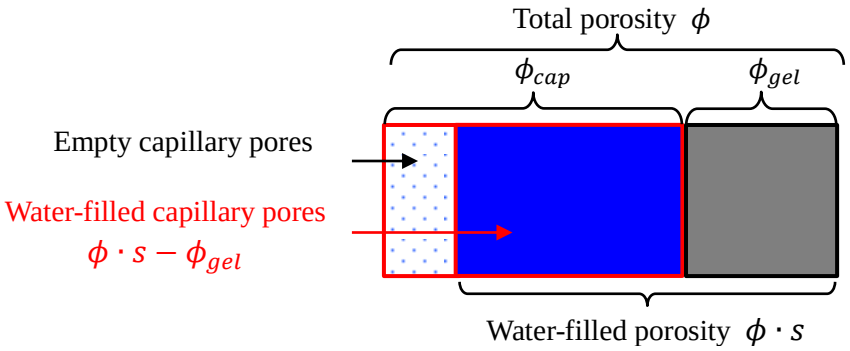

Fig. 3.8 Schematic illustration of the water-filled capillary porosity in cement paste.

3.3.4 Water vapour diffusion in the pore system of cementitious materials

3.3.4.1 Vapour diffusion in a "clear" fluid

According to Ho et al. [118], the flux of water vapour in gas phase can be described as:

$$F_v = -\rho_g \cdot D_{v-g} \cdot grad\ \omega_v \tag{3.19}$$

where ρ_g is the density of the gas, D_{v-g} (m^2/s) is the diffusion coefficient of water vapour in the gas, and ω_v is the mass fraction of water vapour in the gas.

To transform the mass fraction of water vapour in the gas ω_v into the mass of water vapour in a unit volume of gas, the term w_v [kg/m^3] is introduced, with the form of $w_v = \rho_g \cdot \omega_v$. Eq. (3.19) is rewritten as:

$$F_v = -D_{v-g} \cdot grad\ w_v \tag{3.20}$$

In this study the gas pressure in the pore structure is assumed to be equal to the atmospheric pressure [114]. The convection of air in the pore system of the material is neglected. The mass flux of water vapour through a porous material, J_v, can be described as:

$$J_v = \phi_g \cdot v_v = -F(s) \cdot D_{v-g} \cdot grad\, w_v \tag{3.21}$$

where ϕ_g is the volume fraction of gas-filled pores, calculated from the porosity ϕ and the water saturation level s with $\phi_g = \phi \cdot (1 - s)$. v_v is the velocity of water vapour, $F(s)$ is a resistance factor, which depends on the pore structure and water saturation level.

According to Millington et al. [119], the resistance factor $F(s)$ accounts for the tortuosity of the water-filled pore space and is described with an empirical equation:

$$F(s) = \phi^{4/3} \cdot (1 - s)^{10/3} \tag{3.22}$$

3.3.4.2 Vapour diffusion in porous material

For the vapour diffusion through a porous material it holds [118]:

$$\frac{\partial(\phi_g \cdot w_v)}{\partial_t} = div\big(F(s) \cdot D_{v-g} \cdot grad\, w_v\big) \tag{3.23}$$

After rearrangement, Eq. (3.23) becomes:

$$\frac{\phi_g \cdot \partial w_v}{\partial_t} = div\big(F(s) \cdot D_{v-g} \cdot grad\, w_v\big) - \frac{w_v \cdot \partial \phi_g}{\partial_t} \tag{3.24}$$

A single term describing the vapour diffusivity $D_v(s)$ is defined as:

$$D_v(s) = F(s) \cdot D_{v-g} = \phi^{4/3} \cdot (1 - s)^{10/3} \cdot D_{v-g} \tag{3.25}$$

When the liquid-vapour phase transition of water, $W_{l \to v}$, is considered, Eq. (3.24) becomes (see also Eq. (3.11)):

$$\frac{\phi_g \cdot \partial w_v}{\partial_t} = div(D_v(s) \cdot grad\, w_v) - \frac{w_v \cdot \partial \phi_g}{\partial_t} + W_{l \to v} \tag{3.26}$$

The vapour flux of a material J_v in Eq. (3.21) is rewritten:

$$J_v = -D_v(s) \cdot grad\, w_v \tag{3.27}$$

Eq. (3.27) will be used in section 3.3.6 to calculate the vapour flux through the interface between the coating and the substrate.

3.3.5 Liquid water - vapour phase transition

During moisture transport in a cementitious material, transfer of liquid water can be calculated with Eq. (3.9), and transfer of water vapour can be calculated with Eq. (3.23). The liquid water transport and the vapour diffusion will result in different values of RH in the pore space. However, these two processes are not independent. Phase transition between liquid water and water vapour always takes place in the moisture transport process. In the pore space (e.g. Fig. 3.5a), when the relative humidity/vapour pressure drops due to vapour diffusion, evaporation of the liquid water will occur simultaneously in order to maintain the liquid-vapour (isothermal) equilibrium [60]. In cementitious materials, phase transition is assumed to be very fast in the pores, because the pore sizes are mostly below several microns. It is believed that liquid water and water vapour in a small portion of pore space are always in a state of equilibrium [120].

The absolute humidity (AH_v) in the pore space is defined as the mass of water vapour w_v present in a unit volume of air v_a:

$$AH_v = w_v/v_a \tag{3.28}$$

For a pore space saturated with water vapour the absolute humidity is:

$$AH_{sat} = w_{sat}/v_a \tag{3.29}$$

where w_{sat} is the mass of saturated water vapour in a unit volume of air (e.g. about 0.0179 $\mathrm{kg/m^3}$ at 20 °C and 1 atm).

The relative humidity (RH) is calculated with Eq. (3.30):

$$RH = \frac{AH_v}{AH_{sat}} = \frac{w_v}{w_{sat}} \tag{3.30}$$

The relative humidity (RH) can also be defined as the ratio of the vapour pressure p_v to the saturated vapour pressure p_{sat}:

$$RH = p_v/p_{sat} \tag{3.31}$$

The vapour pressure on a curved liquid-vapour interface or meniscus is described with the Kelvin equation:

$$ln\frac{p_v}{p_{sat}} = \frac{2 \cdot \gamma \cdot V_m}{r \cdot R \cdot T} = \frac{2 \cdot \gamma \cdot k^{'} \cdot V_m}{R \cdot T} \tag{3.32}$$

where γ is the surface tension of water, V_m is the molar volume of water, r is the radius of the capillary pore, k' is the mean curvature of the vapour-liquid interface, R is the universal gas constant, and T [K] is the temperature.

Combining Eq. (3.31) and Eq. (3.32) yields the relation between the relative humidity and the pore size of a material (Fig. 3.9), with $\gamma = -0.0728$ [N/m], $V_m = 1.8 \times 10^{-5}$ [m^3/mol], $R = 8.314$ [J·mol^{-1}·K^{-1}] and $T = 293$ [K].

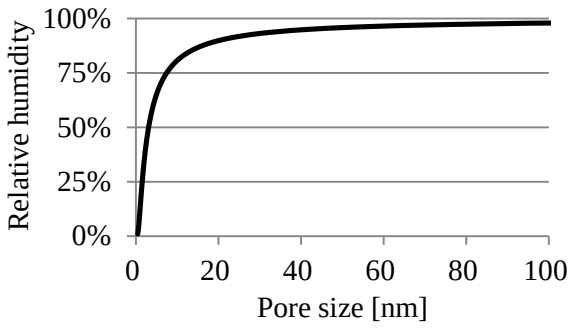

Fig. 3.9 Correlation between relative humidity and pore size of the largest water-filled pore in the material, according to Kelvin equation (Eq. (3.32)) (atmospheric pressure, $T = 293\ K$).

Due to the surface tension of water, there is a pressure differential ΔP across the interface between water and gas. The pressure differential ΔP is known as a capillary pressure p and is related to the shape of the surface (curvature k') by the Young-Laplace equation:

$$p = \Delta P = 2 \cdot \gamma \cdot k^{'} \tag{3.33}$$

In porous material, the capillary pressure $p(s)$ is a function of water saturation level s. Combining Eq. (3.32) and Eq. (3.33), the relative humidity can be calculated:

$$RH = \exp\left(\frac{V_m}{RT} \cdot p(s)\right) \tag{3.34}$$

During a non-steady moisture transport process, the amounts of liquid and vapour phases change over time. The calculated water saturation level s after liquid water transport corresponds to the RH (see Eq. (3.34)). The calculated vapour content w_v after water vapour diffusion corresponds to another RH (see Eq. (3.30)). However, the values of the RH calculated by Eq. (3.34) and Eq. (3.30) can be different, which means that the liquid water and water vapour in the pore space are not in phase equilibrium. In this sense, phase transition (evaporation or condensation of water) will take place between liquid and vapour phases. In the simulation of moisture transport, phase equilibrium is re-established in each time step (detailed description of the implementation of the Moisture-Hydration model is given in section 3.3.8).

Due to evaporation or condensation of water in the pores, the water saturation level changes from s to $s + \Delta s$, with change of the mass of water of $\Delta s \cdot \phi \cdot \rho_w$. In the meantime, vapour content in the gas changes from w_v to $w_v + \Delta w_v$, the change of the mass of water is $\Delta w_v \cdot \phi \cdot (1 - s)$. The amount of water in the evaporation process or condensation process should be conserved. Thus, it follows:

$$\Delta s \cdot \phi \cdot \rho_w = -\Delta w_v \cdot \phi \cdot (1 - s) \tag{3.35}$$

Moreover, after phase transition the relative humidity calculated by Eq. (3.34) and Eq. (3.30) should be equal. The relation holds:

$$\exp\left(\frac{V_m}{RT} \cdot p(s + \Delta s)\right) = \frac{w_v + \Delta w_v}{w_{sat}} \tag{3.36}$$

By solving the equations (i.e. Eq. (3.35) and Eq. (3.36)), the changes of the water saturation level Δs in the material and the vapour content Δw_v in the gas can be determined. Therefore, the locally equilibrated water saturation level ($s_e = s + \Delta s$) and vapour content in the gas ($w_{ve} = w_v + \Delta w_v$) at time $t + \Delta t$ can be calculated.

3.3.6 Water transfer/vapour diffusion across the coating-substrate interface

During moisture transport in a coating system, mass conservation of moisture at the interface between coating and substrate should be dealt with carefully [100, 121]. Usually, the microstructure of the coating material is different from that of the substrate. At the same relative humidity, the coating and the substrate have different water saturation levels. In theory, the relative humidity on both sides of the interface is continuous (Fig. 3.10a), while the water saturation level in the coating and the substrate at the interface are different (Fig. 3.10b). Therefore, attention has to be paid to mass conservation of moisture when computing moisture flux through the boundary.

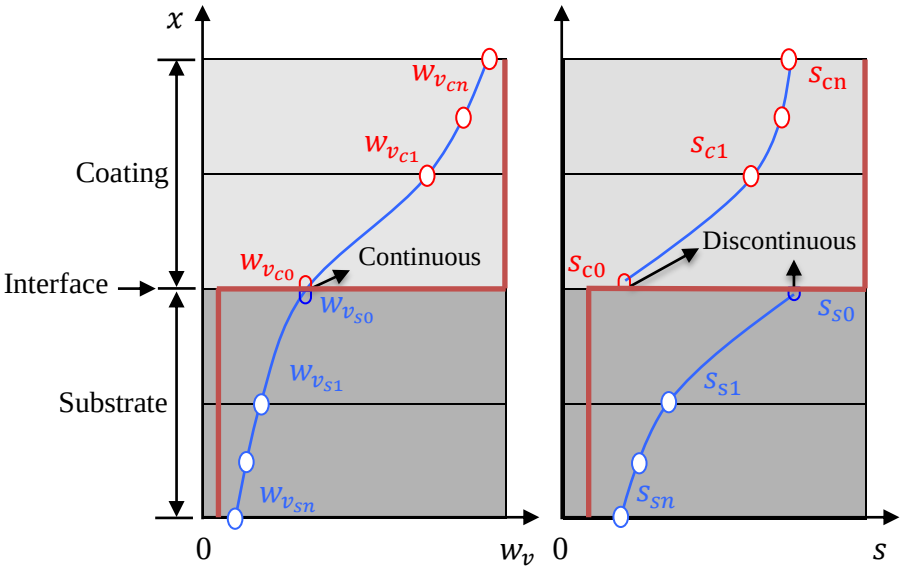

(a) Vapour diffusion (b) Liquid water transfer

Fig. 3.10 Schematic illustration of moisture distribution in a coating system. This figure is typical for a coating with a pore structure coarser than the substrate. w_v is water content in the gas, and s is water saturation level in the coating or the substrate. The red lines show the initial moisture profiles in the coating system. The nodes are numbered incrementally from 0 to n. $c0$ and $s0$ represent the interface nodes of the coating and the substrate, respectively.

c0 and s0 in Fig. 3.10b represent the interface nodes of the coating and the substrate, respectively. During the moisture transport, two conditions are considered for simulating moisture transport across the interface. The first condition is that the capillary pressure $p(s)$ at the interface nodes of the coating and the substrate (i.e. $c0$ and $s0$) should have the same value (Eq. (3.37)):

$$p(s_{c0}) = p(s_{s0}) \tag{3.37}$$

The second condition is that the incoming moisture flux towards one material should be equal to the outgoing flux from the other material. The flux of liquid water at the interface follows Eq. (3.38):

$$J_s(s_{c0}) = J_s(s_{s0}) \tag{3.38}$$

Similarly, the criterion to conserve the vapour phase at the interface (Fig. 3.10a) is described by Eq. (3.39):

$$J_v(w_{v_{c0}}) = J_v(w_{v_{s0}}) \tag{3.39}$$

3.3.7 Water evaporation from the surface of a coating system

Water evaporation is a process by which water is transferred from liquid to gas. A higher temperature or a lower atmospheric pressure will lead to a faster rate of evaporation. It is well know that evaporation is an endothermic process, in which heat is absorbed. In this study, isothermal condition is considered. In air, the driving force of moisture transport is a vapour pressure gradient. In the cement paste, moisture transport is driven both by a gradient of capillary pressure and by a vapour pressure gradient.

When dealing with evaporation, relative humidity is preferably used as a dependent variable, regarding its convenience in verification from experiments. Convective boundary condition is often applied:

$$D(RH) \cdot grad\, RH = f \cdot (RH_{am} - RH_s) \tag{3.40}$$

where RH is the relative humidity in the material, RH_{am} is the relative humidity in ambient air, RH_s is the relative humidity at the drying surface, f is the surface factor or convection coefficient.

Akita et al. [78] proposed a relation between the convection coefficient f and the w/c ratio of cementitious materials based on experimental results. A similar finding is also reported by Wong et al. [77]: the surface factor increases with increasing w/c for cementitious materials. It means that the convection coefficient is dependent on the pore structure of the material. In the case of a hydrating cementitious material, the microstructure changes with hydration, especially during the early ages. Consequently, a significant change of the value of the surface factor will be expected over time. However, to our best knowledge, there is no specific formula describing the surface factor for a hydrating cementitious material.

Therefore, a theoretical moisture flux through material surface is simulated in this study. It allows for conserving the mass of water through the exposed surface of the material. Detailed description of moisture transport between porous media and the environment is given in Fig. 3.11. To account for different curing regimes, boundary condition is applied above the exposed surface.

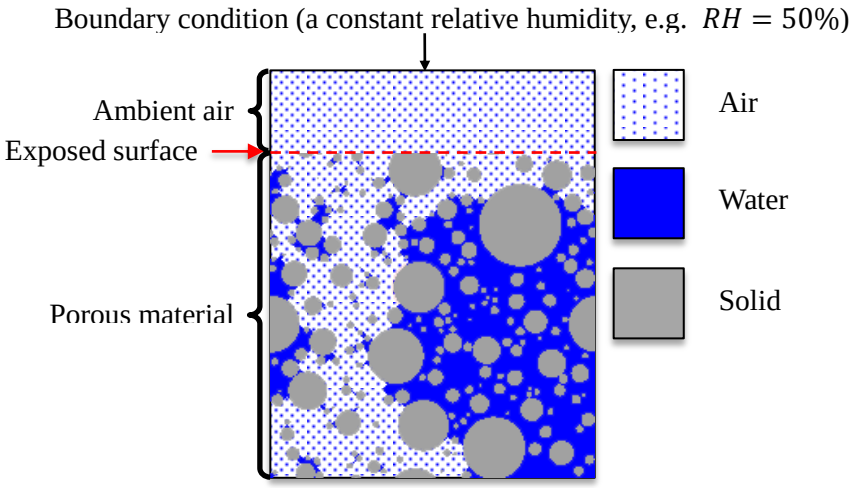

Fig. 3.11 Schematic illustration of moisture at the interface between the ambient air and the porous material. The dimension of the porous material is 100 × 100 μm^2. The top surface of the material is exposed to the ambient air. Other surfaces are sealed.

Under an isothermal condition, water evaporation from the surface of a material is only driven by the gradient of vapour content w_v at the liquid water surface. According to Fick's first law, the moisture flux in the gas J_a [kg m^{-2} s^{-1}] is given by:

$$J_a = -D_{v-g} \cdot grad\, w_v \tag{3.41}$$

From Eq. (3.30), the vapour content in the gas w_v [kg/m^3] can be calculated by:

$$w_v = RH \cdot w_{sat} \tag{3.42}$$

The diffusion coefficient of the water vapour in air, D_{v-g}, can be taken as 2.42×10^{-5} m^2/s at 20 °C and 1 atm, according to Bolz and Tuve [122]. When water evaporation takes place at the surface of the coating, J_s (Eq. (3.15)) or J_a (Eq. (3.41)) can describe the moisture flux at the interface between the coating and the atmosphere. At the interface, it holds:

$$\rho_w \cdot D_l(s_{cn}) \cdot grad\, s = D_{v-g} \cdot grad\, w_v \tag{3.43}$$

where s_{cn} is the water saturation level at exposed surface of the coating.

Eq. (3.43) governs the evaporation process. Therefore, the boundary condition with respect to drying is formulated. Calibration and validation of the boundary condition are given in appendix B.

By assembling all the equations described in section 3.3, a Moisture-Hydration model for simulating moisture transport in a hydrating cementitious coating system is completed.

3.3.8 Flow chart of the Moisture-Hydration model

When simulating moisture transport in a coating system, the hydration process of the substrate is supposed to have ceased. Therefore, only the hydration process of the coating material is considered. The substrate may have different water saturation levels. The Moisture-Hydration model is implemented with Matlab. A flowchart of the simulation of moisture transport in hydrating cementitious coating systems is given in Fig. 3.12.

Initially, the coating has a DOH of 0% and a water saturation level of 98% (with 2% air void by volume). Based on DOH and the water saturation level, the porosity, the intrinsic permeability and the moisture isotherm can be determined. The substrate consists of an old substrate, so no further hydration is considered. With a boundary condition (e.g. exposed condition with RH = 50%), the Moisture-Hydration model can be run. In the step-wise calculation procedure, two processes take place in the coating material, namely the moisture transport and the hydration of the coating. These two processes result in a new DOH of the coating material and a new water saturation level in the coating material. In the substrate, the DOH is constant; only a new water saturation level profile is established. The microstructure of the coating changes with the progress of the hydration process. With the new DOH and water saturation level, the porosity, the rate of hydration, the intrinsic permeability and the moisture isotherm of the coating material can be determined. The simulation continues with the subsequent time step. The coating systems are discretized with a mesh size of 0.002 m. For a stable calculation, the time interval should be sufficiently small. Note that the optimal time interval for the calculation depends on the moisture diffusivity of the coating and the substrate. However, the moisture diffusivity of the coating changes with the progress of hydration process. To ensure a stable calculation, the time interval for the calculation is chosen to be 0.05 second until the target time is reached (e.g. 14 days), based on von Neumann stability analysis. In other words, the solutions presented in this study are independent of mesh and time discretization. The outputs of this simulation are the DOH and porosity of the coating, and the water saturation profile in the coating system (i.e. coating and substrate).

To implement this model, a couple of parameters (e.g. the porosity and the rate of hydration) and properties (i.e. the intrinsic permeability and the moisture isotherm) of the coating material should be quantified first. Detailed description of the quantification will be presented in chapter 4.

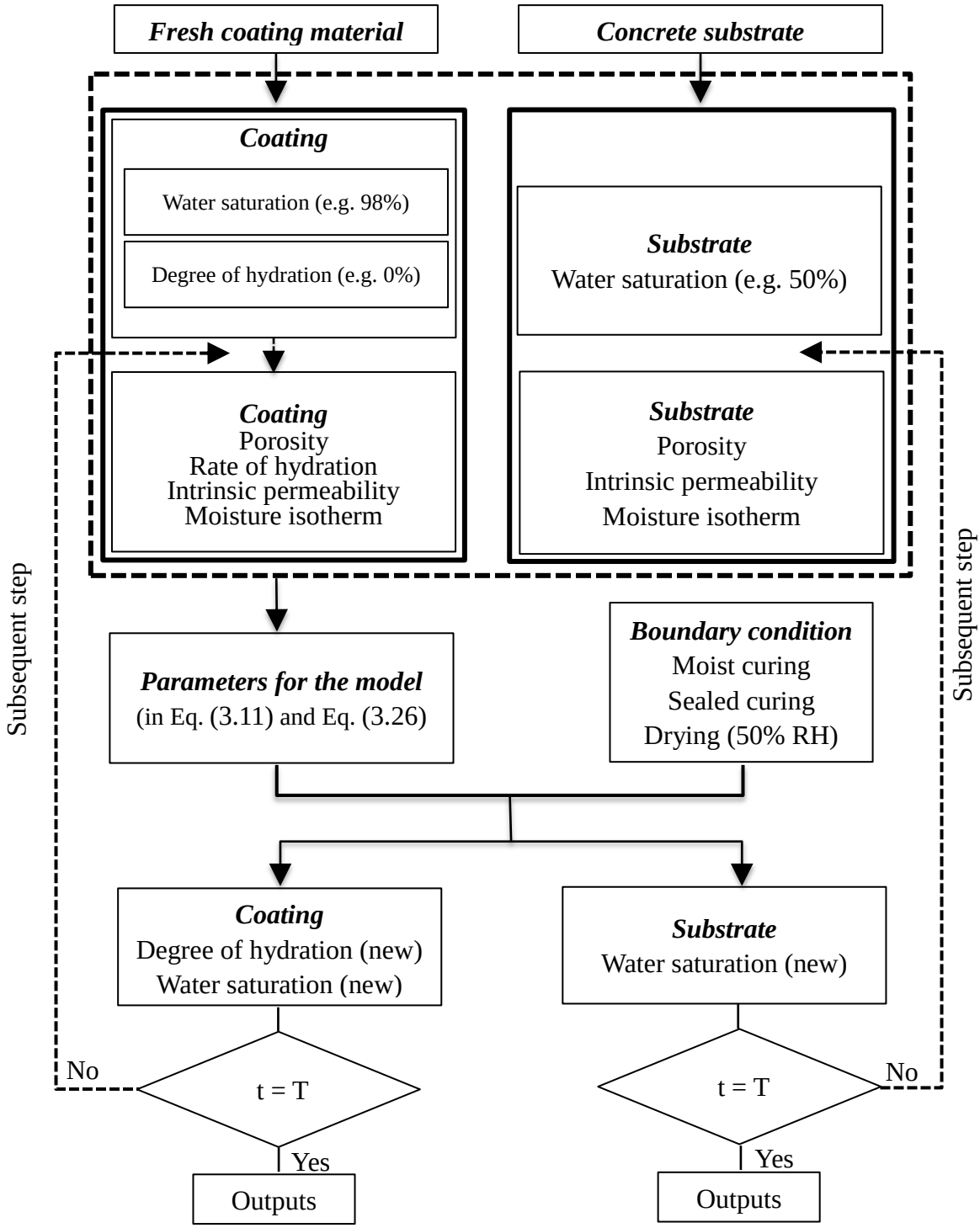

Fig. 3.12 Flowchart for the simulation of moisture transport in a hydrating cementitious coating system. t and T are the time after application of the coating and the target time, respectively.

3.4 Summary

Moisture transport is a process that influences the hydration process of cementitious materials. It plays an important role in the development of the properties (mechanical/durability). The moisture transport in cementititous materials has been comprehensively studied. However, attention on a hydrating overlay system is still insufficient. This Chapter investigated the mechanisms of moisture transport in a hydrating cementitious coating system. A "Moisture-Hydration model" is proposed for simulating moisture transport in the coating system. It can be summarized as:

- Mechanisms were studied regarding the moisture transport in a hydrating cementitious coating system. Proper governing equations were essential to describe moisture transport process through a cementitious material, in the sense of conserving the mass of water.
- Water loss due to hydration was explicitly considered in the Moisture-Hydration model. This consideration enables an appropriate coupling of hydration and moisture transport processes of a hydrating cementitious material.
- Moisture flux through the interface between the coating and the substrate was carefully dealt with. Besides, water evaporation at the exposed surface of the material was also studied in detail. It gives a clear description of the boundary condition for a coating system cured under a particular relative humidity.
- To run the Moisture-Hydration model proposed in this chapter, some parameters and properties of the materials should be quantified, including the rate of hydration, the porosity, the intrinsic permeability and the moisture isotherm of the materials (i.e. coating and substrate). Detailed description of the quantification will be presented in chapter 4.

Chapter 4

Quantification of transport properties and parameters for simulation of moisture transport

4.1 Introduction

In chapter 3, the mechanisms of moisture transport in hydrating cementitious coating systems have been studied. Based on the mechanisms, a Moisture-Hydration model was proposed. In a coating system, the old substrate has a fixed microstructure and constant transport properties, while transport properties of the coating material may change due to ongoing hydration. To run the model, the transport properties of the coating material and parameters for calculating water consumption by hydration of the coating material need to be quantified. The quantification of the transport properties of the coating and the parameters for calculating water consumption by hydration of the coating is the subject of this chapter. Fig. 4.1 shows the position of chapter 4 in the structure of the study of moisture transport in hydrating cementitious coating systems.

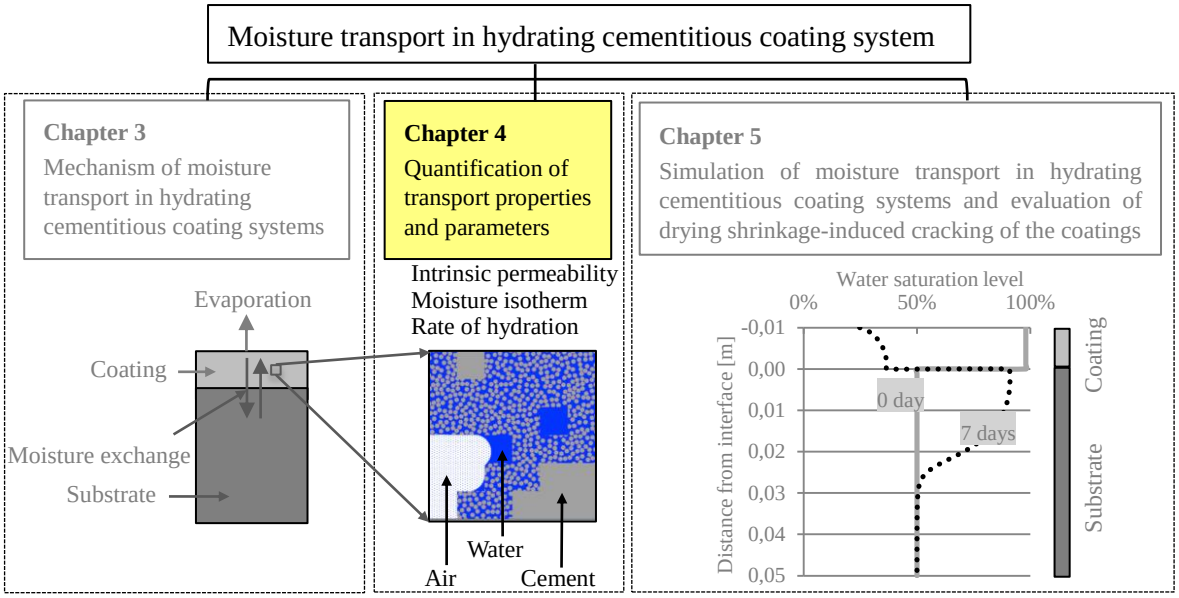

Fig. 4.1 Structure of the study of moisture transport in hydrating cementitious coating systems.

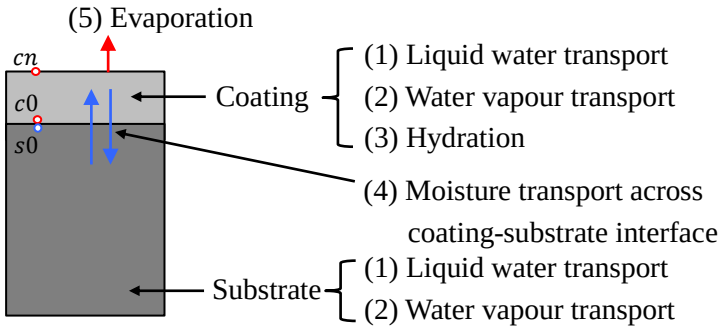

Fig. 4.2 Schematic illustration of factors affecting moisture transport in a hydrating cementitious coating system. Note that $c0$ and $s0$ represent the interface nodes of the coating and the substrate, respectively. cn represents the node of the coating at coating-environment interface.

Fig. 4.2 schematically illustrates the factors affecting moisture transport in hydrating cementitious coating systems, including liquid water transport, water vapour transport, hydration process of the coating and evaporation process (also see section 3.3). The equations describing each process are listed below.

(1) Liquid water transport:
Liquid water transport process in the coating is described by Eq. (4.1), taking into account the hydration of the coating and liquid-vapour phase transition:

$$\frac{\phi \cdot \partial s}{\partial t} = \frac{\partial}{\partial_x} \cdot D_l(s) \cdot \frac{\partial s}{\partial x} - W_{hyd} - \frac{s \cdot \partial \phi}{\partial t} - W_{l \to v} \tag{4.1}$$

where ϕ is the total porosity, t is time, s is the water saturation level, $D_l(s)$ is the liquid water diffusivity, W_{hyd} is a sink term and refers to the water consumption by hydration, $W_{l \to v}$ accounts for liquid-vapour phase transition.

(2) Vapour diffusion:
Vapour diffusion process in the coating is described by Eq. (4.2), taking into account the liquid-vapour phase transition:

$$\frac{\phi_g \cdot \partial w_v}{\partial_t} = div(D_v(s) \cdot grad\, w_v) - \frac{w_v \cdot \partial \phi_g}{\partial_t} + W_{l \to v} \tag{4.2}$$

where ϕ_g is the volume fraction of gas-filled pores, with $\phi_g = \phi \cdot (1 - s)$. w_v is water content in the gas $D_v(s)$ is the vapour diffusivity.

(3) Sink term accounting for hydration:
Sink term, e.g. W_{hyd} in Eq. (4.1), accounting for hydration of the coating, is described by Eq. (4.3). The sink term is a function of the rate of hydration of the coating.

$$W_{hyd} = \frac{0.23 \cdot m_{cem} \cdot \dot{\alpha}}{\rho_w}, \qquad \dot{\alpha} = \frac{d\alpha}{dt} \tag{4.3}$$

where m_{cem} is the mass of cement in a unit volume of cement paste, ρ_w is the density of liquid water, $\dot{\alpha}$ is the rate of hydration and α is the degree of hydration.

(4) Moisture transport across coating-substrate interface:
Three conditions have to be fulfilled for simulating moisture transport across coating-substrate interface. The first one is that the capillary pressure at the interface nodes of the coating and the substrate should be equal:

$$p(s_{s0}) = p(s_{c0}) \tag{4.4}$$

The second one is that the incoming flux and outgoing flux of liquid water through the coating-substrate interface should be equal:

$$D_l(s_{s0}) \cdot grad\ s = D_l(s_{c0}) \cdot grad\ s \tag{4.5}$$

The third one is that the incoming flux and outgoing flux of water vapour through the coating-substrate interface should be equal:

$$D_v(s_{s0}) \cdot grad\ w_v = D_v(s_{c0}) \cdot grad\ w_v \tag{4.6}$$

(5) Water evaporation:
To simulate the water evaporation process, the incoming flux and outgoing flux of moisture through the coating-environment interface should be equal:

$$\rho_w \cdot D_l(s_{cn}) \cdot grad\ s = D_{v-g} \cdot grad\ w_v \tag{4.7}$$

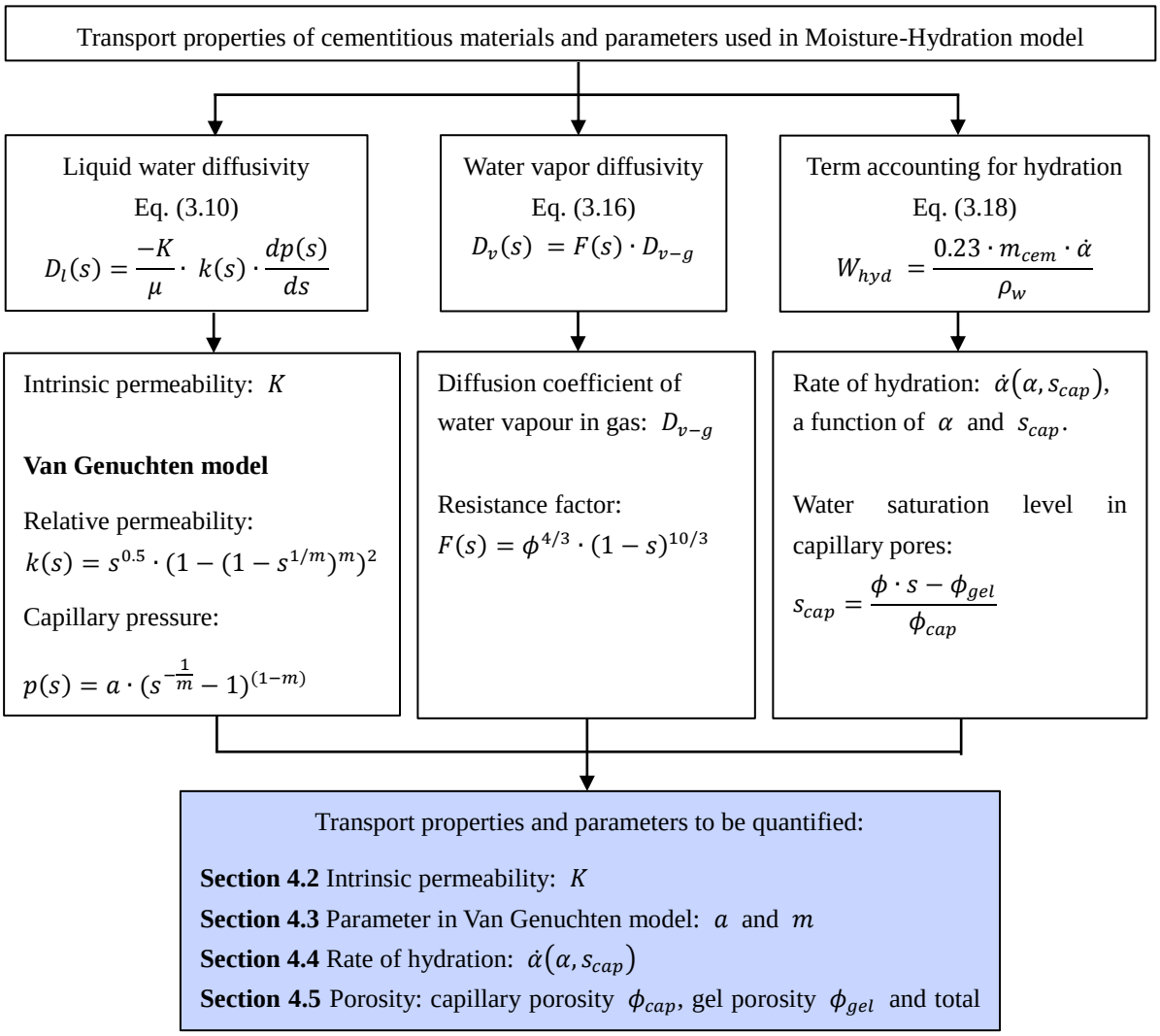

Fig. 4.3 Transport properties and parameters used for simulating moisture transport in hydrating cenmentitious coating systems.

Table 4.1 Dependency of different parameters of a coating material.

	Degree of hydration α	Water saturation level s
Intrinsic permeability K	√	–
Parameters (a and m) in the Van Genuchten	√	–
Rate of hydration $\dot{\alpha}$	√	√
Porosity (ϕ_{cap}, ϕ_{gel} and ϕ)	√	–

* Fitting parameters (a and m) in the Van Genuchten model (Eq. (3.12) and Eq. (3.13)) are obtained from the moisture isotherm of the materials.

Fig. 4.3 shows formulas for the transport properties and parameters of the coating material for running the Moisture-hydration model. The transport properties of the coating material include the liquid water diffusivity and the water vapour diffusivity. The term accounting for water consumption by hydration of the coating material is described as a function of rate of hydration. Detailed description is given as below:

1) Liquid water diffusivity of a partially saturated material $D_l(s)$
   The liquid water diffusivity of a partially saturated material, $D_l(s)$, is expressed as a function of the intrinsic permeability K, the relative humidity $k(s)$ and the capillary pressure $p(s)$. The relative humidity $k(s)$ and the capillary pressure $p(s)$ are calculated according to the Van Genuchten model [116]. There are two fitting parameters, a and m, in the Van Genuchten model, which depend on the microstructure of the material and can be obtained by curve fitting (i.e. water saturation level-capillary pressure curve).

2) Water vapour diffusivity of a partially saturated material $D_v(s)$
   The water vapour diffusivity of a partially saturated material, $D_v(s)$, is expressed as a function of the diffusion coefficient of water vapour in gas D_{v-g} and the resistance factor $F(s)$ of material. The diffusion coefficient of water vapour in gas D_{v-g} is independent on porous material. The resistance factor $F(s)$ is calculated from the total porosity ϕ of the material (see Fig. 4.3).

3) Water consumption by hydration of the material W_{hyd}
   The term accounting for water consumption by hydration of the material, W_{hyd}, is calculated from the rate of hydration $\dot{\alpha}$ (see Fig. 4.3). The rate of hydration $\dot{\alpha}$ is a function of the degree of hydration α and the water saturation level in capillary pores s_{cap}. s_{cap} is calculated from the water saturation level s, the total porosity ϕ, the capillary porosity ϕ_{cap} and the gel porosity ϕ_{gel}.

The parameters included in the Moisture-Hydration model are highlighted in Fig. 4.3 and listed in Table 4.1. Methodologies used for determining each parameter is given in following sections. In each section, example calculation of the parameter of a hydrating cement paste (w/c = 0.3) is presented. This cement paste will be applied as coating on concrete substrate. Moisture transport in the coating system will be simulated in chapter 5.

4.2 Intrinsic permeability $K(\alpha)$ [m^2]

4.2.1 Outline of the quantification of intrinsic permeability of hydrating cementitious materials

In order to simulate the moisture transport in hydrating coating systems, the intrinsic permeability of a hydrating coating material (from casting to hardening) should be determined and described as a function of the degree of hydration.

Permeability of hardened cement pastes has comprehensively been studied experimentally [123-125]. Note that most experimental work focuses on relatively mature cementitious materials (i.e. cement pastes with at least 1 day curing [125]), because the permeability of cementitious materials at very early ages is hard to measure due to the fast hydration process.

Simulation of 3D fluid flow in digital microstructures of cement pastes allows the computation of certain inherent characteristics (i.e. intrinsic permeability K), and thus, may overcome the difficulty in laboratory measurements. Lattice Boltzmann method is a class of computational fluid dynamics methods for the computational modeling of fluid flow problems, originating from the lattice gas automata method [126, 127]. The Lattice Boltzmann method (LBM) has been used for simulating water flow through digital microstructures of cement pastes [128, 129]. The digital microstructures are usually obtained by using imaging techniques (e.g. X ray computed tomography [130]), or numerical cement hydration models (i.e. HYMOSTRUC3D [8], CEMHYD3D [131] or μic [132]).

The intrinsic permeability of hydrating cement pastes is determined by using the following methods:

- At early ages of the cement paste ($\alpha \leq 15\%$), water flow through the cement paste can be simulated using LBM. Then the intrinsic permeability is calculated according to Darcy's law. In LBM simulation, the input microstructure of early-age cement paste is generated by HYMOSTRUC3D.
- At late ages of the cement paste ($\alpha \geq 50\%$), the intrinsic permeability of the cement paste is determined by empirical equations which relate the permeability to the age of cement pastes [124]. The degree of hydration of the cement pastes is calculated from the age using HYMOSTRUC3D. The intrinsic permeability of the cement paste is plotted against the degree of hydration.
- When $15\% < \alpha < 50\%$, the intrinsic permeability of the cement paste is determined by spline interpolation.

Fig. 4.4 shows a schematic illustration of the relation between the intrinsic permeability and the degree of hydration of a cement paste.

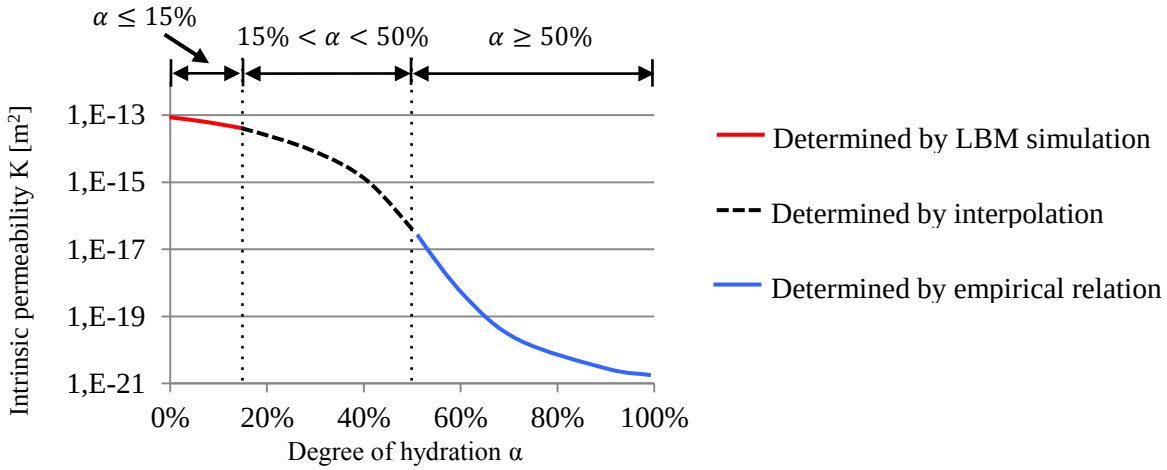

Fig. 4.4 Schematic illustration of the relationship between intrinsic permeability and degree of hydration of a cement paste (w/c = 0.3). The intrinsic permeability of the cement paste is determined by LBM simulation when $\alpha \leq 15\%$, and by empirical relation when $\alpha \geq 50\%$. For $15\% < \alpha < 50\%$, the intrinsic permeability of cement paste is obtained by interpolation.

4.2.2 Method to determine intrinsic permeability of cementitious materials at early ages - Lattice Boltzmann Method

The LBM simulation of water flow is straightforward, because the simulation is directly performed on the digital microstructure. Detailed description of the Lattice Boltzmann method is given in appendix C. Fig. 4.5 shows a schematic illustration of water flow through a porous medium (a body-centered cubic structure).

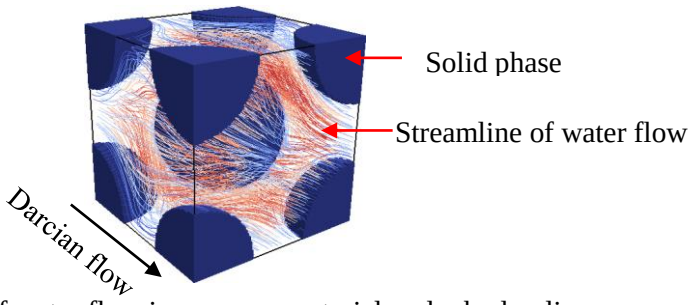

Fig. 4.5 Schematic illustration of water flow in a porous material under hydraulic pressure.

Input microstructure

In general, two possibilities are available to obtain 3D digital microstructure of cement paste, i.e. by reconstruction from CT scans, or from numerical hydration models. In this study, the microstructures are generated by HYMOSTRUC3D (However, due to assumption in the

numerical simulation, gel pores from calcium silicate hydrate (C-S-H) are not involved).

In HYMOSTRUC3D, initially, spherical cement particles are assumed and distributed in a cube ($100 \times 100 \times 100\ \mu m^3$). Under the assumption of spherical growth, formation of the virtual microstructure of a hydrating cement paste can be simulated. The vector-based microstructure consists of unhydrated cement, hydration products and pores. For the LBM simulation of water flow, the vector-based microstructure is digitized to a voxel based one with a digital resolution of $0.5\ \mu m/voxel$. LBM simulation of water flow through an example cement paste is given in section 4.2.4.

4.2.3 Method to determine intrinsic permeability of cementitious materials at later ages

Fig. 4.6 illustrates the relative changes in permeability due to hydration of the materials with respect to the 28-day permeability value [124]. The specimens were cured under saturated conditions. A ratio is defined to describe the relative changes in permeability of specimens at different curing ages [124]:

$$k_r = ln\frac{k_t}{k_{28}} \tag{4.8}$$

For a cementitious material, the water permeability at a particular curing age t (in days), k_t, can be calculated according to Eq. (4.8), given a value of water permeability k_{28}.

In the Moisture-Hydration model, the permeability should be expressed with respect to the DOH α. HYMOSTRUC3D model is used to relate the curing time in Fig. 4.6 to the DOH α. For an Ordinary Portland cement paste with a w/c of 0.3, Fig. 4.6 covers the range of permeability when $50\% \leq \alpha \leq 70\%$.

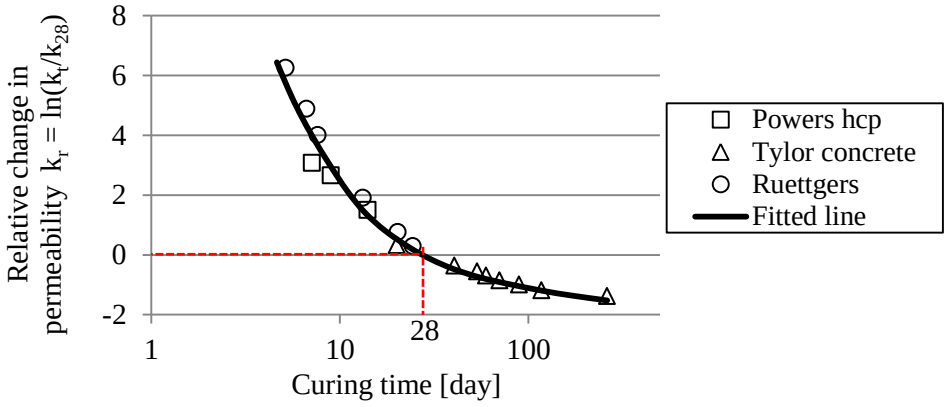

Fig. 4.6 Relative changes in permeability ($k_r = ln(k_t/k_{28})$) due to hydration, compiled from the data in [124]. hcp represents cement paste. The specimens are cured under saturated condition. k_{28} can be determined by permeability measurements.

4.2.4 Example calculation of intrinsic permeability of a hydrating cement paste

Intrinsic permeability of an example cement paste (w/ = 0.3) are calculated using above methods. Portland cement CEM I 42.5N is used. The cement has a continuous particle size distribution ranging from 1 to 50 μm. There are 4 major phases in Portland cement, namely C_3S, C_2S, C_3A and C_4AF. In addition, gypsum ($C\bar{S}H_2$) is added as an inhibitor to prevent flash setting. The mineral composition of the cement used in the example cement paste is listed in Table 4.2, which is derived from [8].

Table 4.2 Mineral composition of Portland cement ([8])

Cement composition	C_3S	C_2S	C_3A	C_4AF	Gypsum
Percentage	53.5%	21%	7.5%	10.7%	6.5%

4.2.4.1 Example calculation of intrinsic permeability of a cement paste at early ages

The initial state of the fresh cement paste ($\alpha = 0\%$) is shown in Fig. 4.7a. Fig. 4.7b illustrates the streamline of water flow in the fresh cement paste. Besides, microstructures corresponding to subsequent DOHs ($\alpha = 15\%$, $\alpha = 30\%$, $\alpha = 45\%$ and $\alpha = 60\%$) are used as inputs for the simulation of the water flow through the paste. The intrinsic permeability determined by LBM simulation is plotted against capillary porosity of the paste in Fig. 4.8. The capillary porosity is calculated from the degree of hydration with Eq. (4.19). For comparison, a series of LBM simulation results from Zalzale [133] are also presented in the figure. In their work, microstructures of cement pastes were generated by μic model.

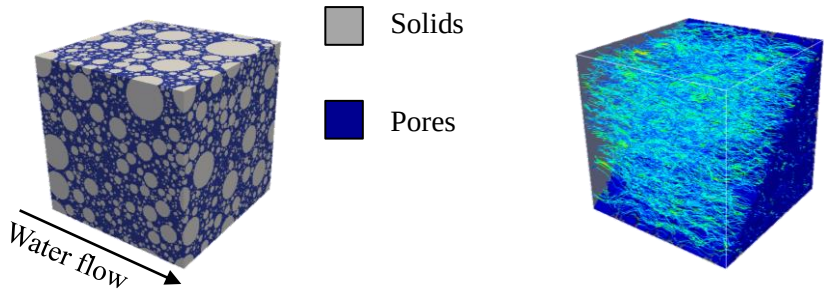

(a) Initial state of a fresh cement paste (b) Streamline of water flow though the cement paste

Fig. 4.7. Streamline of water flow in the microstructure of a fresh cement paste (w/c = 0.3), the microstructure is generated by HYMOSTRUC3D.

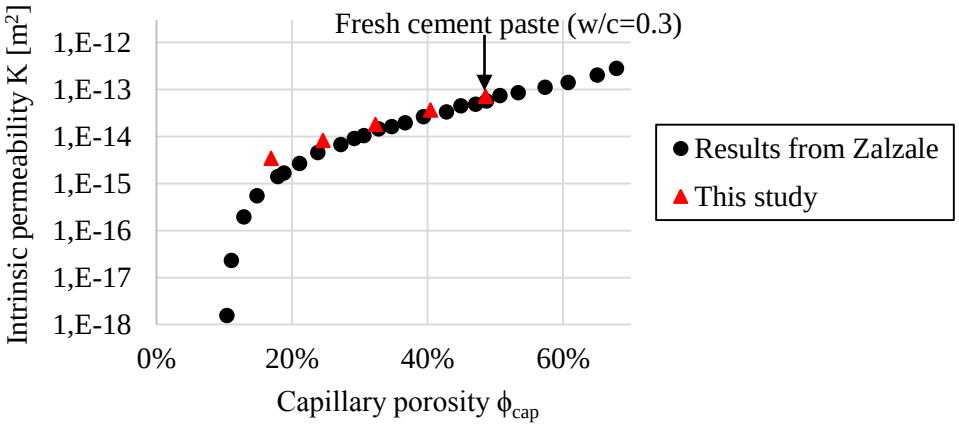

Fig. 4.8. Intrinsic permeability versus capillary porosity. Red triangles represent the results in this study. The microstructures of a cement paste (w/c = 0.3) were generated by HYMOSTRUC3D. Results represented by dots were derived from Zalzale [133], based on virtual cement pastes generated by μic model (w/c = 0.3, 0.4, 0.5, 0.6 and 0.7, digital resolution = 1 $\mu m/voxel$).

From Fig. 4.8, it can be seen that the relation between the intrinsic permeability K and the degree of hydration α obtained in this study is very close to the one obtained by Zalzale [133]. Moreover, the intrinsic permeability ($K = 7.2 \times 10^{-14}\ m^2$) of the fresh cement paste (w/c = 0.3) in this study is close to the experimental result reported by Picandet et al. [134] ($K = 2.9 \times 10^{-14}$ m^2 for a fresh cement paste (w/c = 0.3) made of CEM 32.5R).

As the hydration proceeds, capillary porosity decreases and the pore structure is refined. With respect to hardened cement pastes, reported values of intrinsic permeability vary over several orders of magnitude (typically from 10^{-17} to 10^{-22} m^2) [135-137]. Note that the intrinsic permeability depends on the composition of cement pastes and curing regimes. According to Powers et al. [138], the capillary pores in cement pastes got depercolated when the capillary porosity was lower than about 20%. It means the intrinsic permeability of the cement paste will drastically decrease. However, in the LBM simulation of water flow, when the capillary porosity reaches a low value (e.g. $\phi_{cap} = 17\%$, the corresponding degree of hydration $\alpha = 60\%$), the calculated intrinsic permeability still keeps at a high value at the order of magnitude 10^{-15} m^2. One critical reason can be that the capillary pore structure of virtual cement pastes lacks complexity and fineness compared to the real samples [133]. In this study, values of the intrinsic permeability determined by LBM simulation are adopted only when the degree of hydration $\alpha \leq 15\%$.

4.2.4.2 Example calculation of intrinsic permeability of a cement paste at later ages

For cement pastes at later ages ($\alpha \geq 50\%$.), the water permeability is calculated according to Eq. (4.8). In this equation, the 28-day permeability value of the cement paste with w/c = 0.3 is taken as $k_{28} = 1 \times 10^{-13}$ m/s [139].

In the Moisture-Hydration model, the intrinsic permeability K is considered, instead of water permeability k_w. Therefore, a conversion coefficient is introduced with a form of $k_c = \rho_w g/\mu$, where ρ_w is the water density, g is the acceleration of gravity, and μ is the dynamic viscosity of water. At 20 °C, the conversion coefficient equals to 9.76×10^6 $m^{-1}s^{-1}$. Then the intrinsic permeability is calculated by $K = k_w/k_c$.

The intrinsic permeability of the cement paste (w/c = 0.3) is depicted in Fig. 4.9. In this figure, the permeability of early-age cement paste ($\alpha \leq 15\%$) is determined by LBM simulation of water flow through the paste, while the permeability of hardened cement paste ($\alpha \geq 50\%$) is calculated according to the empirical relation (i.e. Eq. (4.8) that relates the permeability to the 28-day permeability value). A continuous curve describing the evolution of intrinsic permeability as function of the degree of hydration is obtained by spline interpolation. This curve is used in the Moisture-Hydration model to describe the α dependency of the intrinsic permeability of a coating.

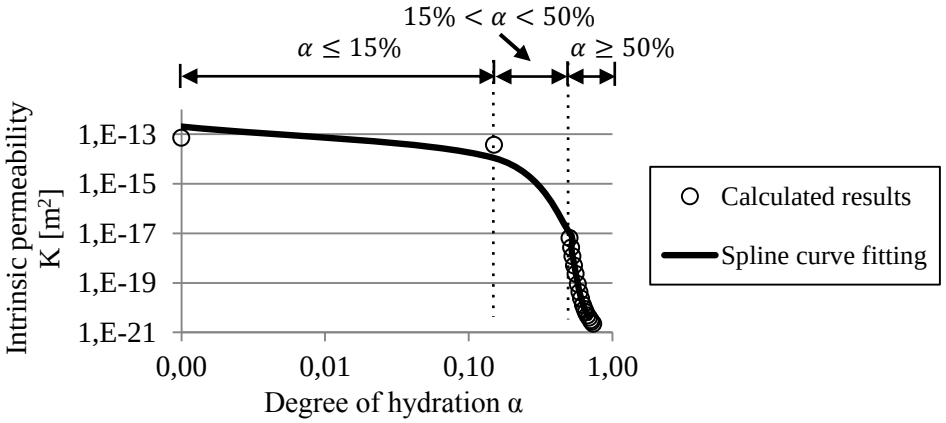

Fig. 4.9 Intrinsic permeability of a cement paste (w/c = 0.3). The calculated intrinsic permeability is obtained by LBM simulation when $\alpha \leq 15\%$, and by using empirical model when $\alpha \geq 50\%$. The intrinsic permeability is obtained by spline curve fitting when $15\% < \alpha < 50\%$.

4.3 Moisture isotherm (for determining parameters in the Van Genuchten model)

4.3.1 Outline of the quantification of moisture isotherm of hydrating cementitious materials

For the simulation of moisture transport in hydrating coating systems, the parameters (i.e. a and m) in the Van Genuchten model have to be determined and described as a function of the degree of hydration. These parameters (i.e. a and m) are obtained from the moisture isotherm of the materials. The moisture isotherm describes the relationship between water content and equilibrium relative humidity of a material at a constant temperature. The moisture isotherms can be classified into two series, namely water vapour desorption and water vapour adsorption

isotherms. Moisture diffusion in the material is a very slow process, because cementitious materials have very complex pore structures with the pore size ranging from nanometers to micrometers. Hence, the determination of the moisture isotherm is usually time-consuming [140]. It means that, once there is a moisture gradient, it will take a long time to reach equilibrium.

Adsorption isotherms of hardened cement pastes (curing age $\geq$ 7 days) are available in literature [115, 141, 142]. Xi et al. [63] proposed an empirical model to predict the adsorption isotherms of hardened cementitious materials. In their model, the age of the materials is more than 5 days. Detailed description of the model will be given in section 4.3.3.

The determination of moisture isotherm becomes difficult for early-age cement pastes, because the microstructures of the cement pastes change with ongoing hydration. A long duration of a test will vitiate the moisture isotherms. Alternatively, numerical models have been proposed to determine moisture isotherms of cementitious materials. Ranaivomanana et al. [106] determined moisture isotherms of cement-based materials by using a pore network model. Based on the Lattice Boltzmann method, Zalzale et al. [133] used a multi-phase algorithm to simulate moisture isotherms of virtual cement pastes generated by a numerical cement hydration model (μic). Prodanović et al. [143] applied a Level Set method to determine capillary pressure-water saturation curves of a porous material. From the curves, the moisture isotherm can be deduced. In terms of computational efficiency, the Level Set method is faster than two-phase LBM methods [144]. The Level Set method is based on the assumption of quasi-static displacement of the water-air interface at a constant capillary pressure and surface tension. The propagation of water-air interface is tracked by solving the level set function. The volume fraction of each phase (i.e. water or air) in a porous material can, therefore, be determined. Moreover, capillary pressure can be correlated to a relative humidity according to Eq. (3.34).

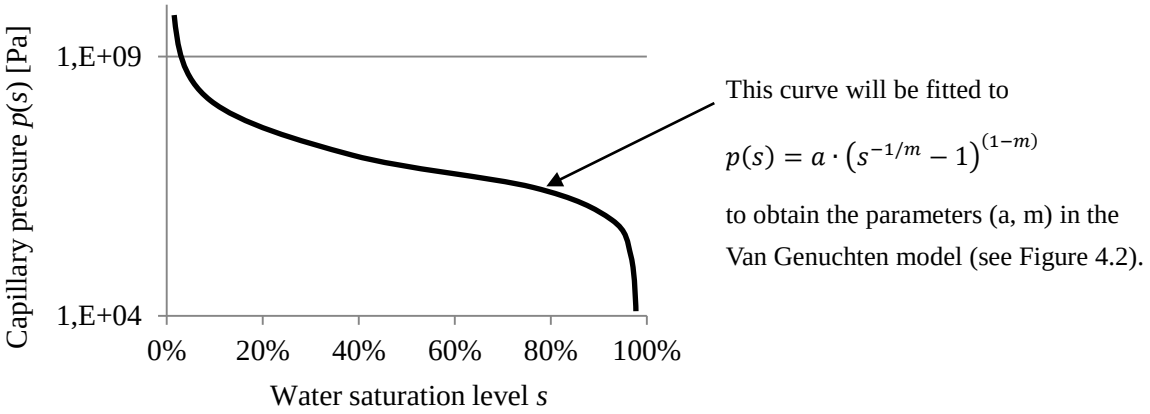

Fig. 4.10 Schematic illustration of the relationship between water saturation level and capillary pressure in a cement paste. This curve can be obtained either from Level Set simulations ($\alpha \leq 15\%$) or experiments ($\alpha \geq 52\%$).

In this chapter, the moisture isotherm of hydrating cement pastes is determined by using thefollowing methods:

- At early ages of the cement paste ($\alpha \leq 15\%$), the displacement of water by air is simulated using a Level Set method [143]. In the simulation, the input microstructures of early-age cement pastes are generated by HYMOSTRUC3D. The capillary pressure - water saturation curves of a cement paste are determined, and the moisture isotherms are deduced.
- At late ages of the cement paste ($\alpha \geq 52\%$), the moisture isotherm of the cement paste is determined by the model proposed by Xi et al. [63].
- The Van Genuchten (VG) parameters "a" and "m" for a cement paste are obtained by curve fitting. The VG parameters (a and m) of a cement paste are plotted against the degree of hydration α. For a cement paste with w/c = 0.3, when $15\% < \alpha < 52\%$, the VG parameters (a and m) of a cement paste is determined by spline interpolation.

4.3.2 Method to determine moisture isotherms of cementitious materials at early ages - Level Set Method

A partially saturated cement paste is a three-phase material consisting of liquid water, gas and solid. The water-air interface forms a meniscus (refer to Fig. 4.17). Capillary pressure represents the pressure difference between water and air (the water-air interface is shown in red), described by Young-Laplace equation (Eq. (3.33)). A Level Set method is applied for determining moisture isotherms of cement pastes generated by HYMOSTRUC3D. Fig. 4.11 shows a schematic illustration of water-air phase displacement in a body-centered cubic structure.

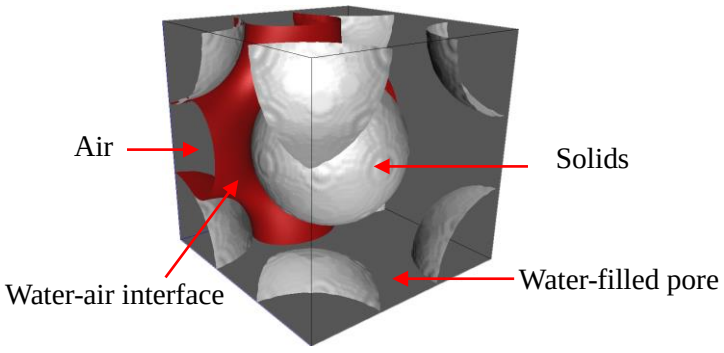

Fig. 4.11 Displacement of water by air in a porous material. The porous material is initially water saturated. Air intrudes from one surface of the material.

Assume an interface that moves at speed F_0, and let this moving surface of interest be embedded as the zero level set of function $\emptyset(\vec{x},t)$ at all times t. The function takes the form:

$$\emptyset(\vec{x}(t),t)=0 \tag{4.9}$$

In order to track the motion of a particle $\vec{x}(t)$ on the interface, the differentiation of Eq. (4.9) with respect to time leads to:

$$\emptyset_t+\nabla\emptyset(\vec{x}(t),t)\cdot\vec{x}'(t)=0 \tag{4.10}$$

Let $\vec{n}=\nabla\emptyset/|\nabla\emptyset|$ be the outward normal of the interface, then $\vec{x}'(t)=F_0\vec{n}$. This yields the governing PDE:

$$\emptyset_t+F_0\cdot|\nabla\emptyset|=0, \text{ given } \emptyset(\vec{x},t=0). \tag{4.11}$$

Eq. (4.11) is solved using LSMPQS programme [143]. The volume of water/gas is recorded with a prescribed mean curvature. Based on the mean curvature, the capillary pressure can be calculated according to Young-Laplace equation (Eq. (3.33)).

4.3.3 Method to determine moisture isotherm of cementitious materials at later ages

Based on the best known isotherm model (Brunauer-Emmett-Teller (BET) model [110]), Xi et al. [63] developed a mathematical model to predict adsorption isotherms of hardened cementitious materials. The adsorption of water in cementitious materials is affected by many parameters, such as type of cement, the water-to-cement ratio w/c, temperature T and curing time t. The amount of adsorbed water W (kg in unit volume of the material) can be calculated according to:

$$W=\frac{V_m{}'\cdot C\cdot k''\cdot RH}{\left(1-k''\cdot RH\right)\cdot\left[1+(C-1)\cdot k''\cdot RH\right]} \tag{4.12}$$

where RH is the relative humidity, and $V_m{}'$, C and k'' stand for:

$$C=exp\left(\frac{855}{T}\right),\qquad k''=\frac{\left(1-\frac{1}{n'}\right)\cdot C-1}{C-1} \tag{4.13}$$

$$V_m{}'=\left(0.068-\frac{0.22}{t}\right)\cdot\left(0.85+-0.45\cdot\frac{w}{c}\right)\cdot V_{ct} \tag{4.14}$$

$$n' = \left(2.5 - \frac{15}{t}\right) \cdot \left(0.33 + 2.2 \cdot \frac{w}{c}\right) \cdot N_{ct} \tag{4.15}$$

The value of V_{ct} and N_{ct} depends on the type of cement. For ordinary Portland cement, V_{ct} and N_{ct} are taken as 0.9 and 1.1, respectively

With the determined parameters (Eq. (4.13) - Eq. (4.15)), the adsorption isotherm of a hardened cement paste can be determined according to Eq. (4.12). Note that this formula deals with cement pastes ($0.3 < w/c < 0.7$) after the age of 5 days. To link the adsorption isotherm to the degree of hydration, the curing time is correlated to the degree of hydration by using HYMOSTRUC3D model. The relative humidity is converted to capillary pressure according to Eq. (3.34).

4.3.4 Example calculation of moisture isotherm of a hydrating cement paste

The moisture isotherms of a hydrating cement paste (w/c = 0.3) are determined using above methods. The mineral composition of the cement used was previously listed in Table 4.2.

4.3.4.1 Example calculation of moisture isotherm of a cement paste at early ages

The initial state of a saturated cement paste was previously shown in Fig. 4.7a. An illustration of air intrusion into the materials is given in Fig. 4.12. In the desorption process, air (in red) is intruded from left surface of the paste. Fig. 4.12a and Fig. 4.12b show the air-water-solid interface in the microstructure, corresponding to different capillary pressures. It can be seen that at a higher capillary pressure more volume of air is intruded into the microstructure.

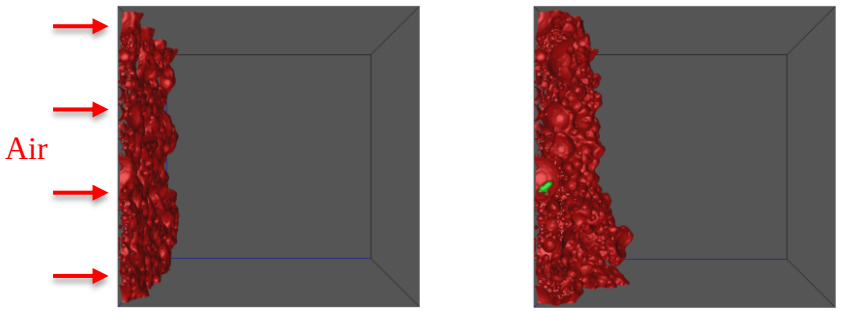

(a) $p_c = 5.7 \times 10^4\ Pa$ (b) $p_c = 1.0 \times 10^5\ Pa$

Fig. 4.12. Air-water-solid interface during the desorption of an initial saturated fresh cement paste (w/c =0.3, degree of hydration α = 0%). The air intrudes from the left surface of the microstructure. The solid phase is not illustrated in this figure, but it can be referred to Fig. 4.7a.

Two curves showing the relation between capillary pressure and water saturation level are plotted in Fig. 4.13, for a fresh cement paste (DOH = 0%) and a young cement paste (DOH = 15%). Note that in this figure the water saturation is the total water saturation s, instead of the capillary water saturation s_{cap}. In the moisture isotherm, the total amount of water is considered. Therefore, the total water saturation s is calculated taking into account gel porosity ϕ_{gel}. It can be seen from the figure that both curves show a very small gradient of capillary pressure when the capillary water saturation ranges from 10% to 90%. Most water in the paste will be lost when the capillary pressure reaches 1 MPa (corresponding relative humidity is 99.89% according to Eq. (3.34)). In contrast, a hardened cement paste (e.g. w/c = 0.34, after 1-year sealed curing) is almost water saturated at this relative humidity [60]. This can be explained by a refined pore structure due to hydration. Water in capillary pores will be gradually lost when the relative humidity drops from 100% to 85%, followed by the water loss in gel pores [145, 146].

In Fig. 4.13, the fitted curves by the Van Genuchten model (Eq. (3.12)) are also depicted. Fitting parameters are used in the Moisture-Hydration model and will be explained in the following part. In theory, desorption or adsorption isotherms should be used for drying or wetting processes, respectively. However, it is believed that the exact values of the adsorption and desorption curves are not as important as the shapes of the curves if one-way drying (no wet-dry cycle) or one-way wetting is concerned. Comparison of experimental results shows that adsorption and desorption curves appear to have the same shape [107]. In this study, a combination of adsorption (Level Set simulation) and desorption isotherms (empirical model-Eq. (4.12)) are used.

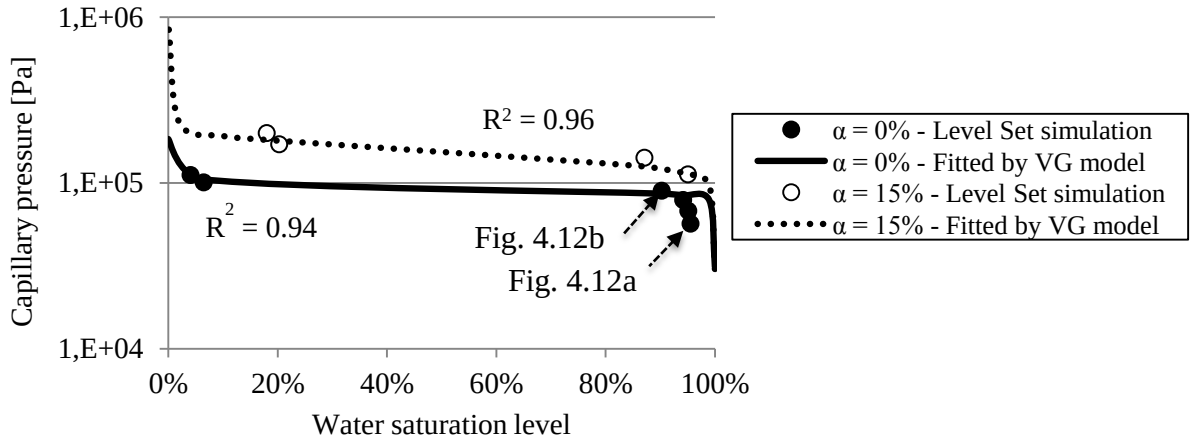

Fig. 4.13 Relationship between water saturation level and capillary pressure in a cement paste (w/c = 0.3). Results (dots) are determined by Level Set simulation of water desorption. Fitted curve by the Van Genuchten model is according to Eq. (3.12).

4.3.4.2 Example calculation of moisture isotherm of a cement paste at later ages

For hardened cement pastes (age ≥ 5 days, degree of hydration ≥ 52%, saturated curing condition), adsorption isotherm is calculated using empirical model (see Eq. (4.12)). Fig. 4.14

shows the relationship between water saturation and capillary pressure for a cement paste with degree of hydration of 55%. The curve fitted by the Van Genuchten model is also presented. It shows that the Van Genuchten model (Eq. (3.12)) has a good fit to the calculated results.

The Van Genuchten (VG) parameters "α" and "m" for a cement paste (w/c = 0.3) are depicted in Fig. 4.15. These two curves describe the α dependency of VG parameters (a and m) of a coating, and will be used for the implementation of Moisture-Hydration model in chapter 5.

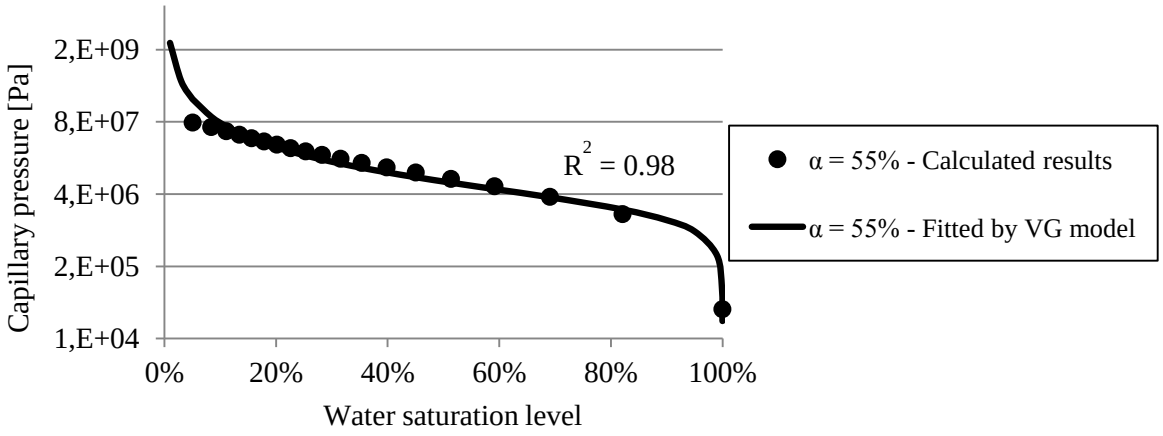

Fig. 4.14 Relationship between water saturation and capillary pressure in a cement paste (w/c = 0.3, after 7-day saturated curing). Results (dotted) are determined by an empirical model for water adsorption isotherm (Eq. (4.12)). Fitted curve by VG model is according to Eq. (3.12).

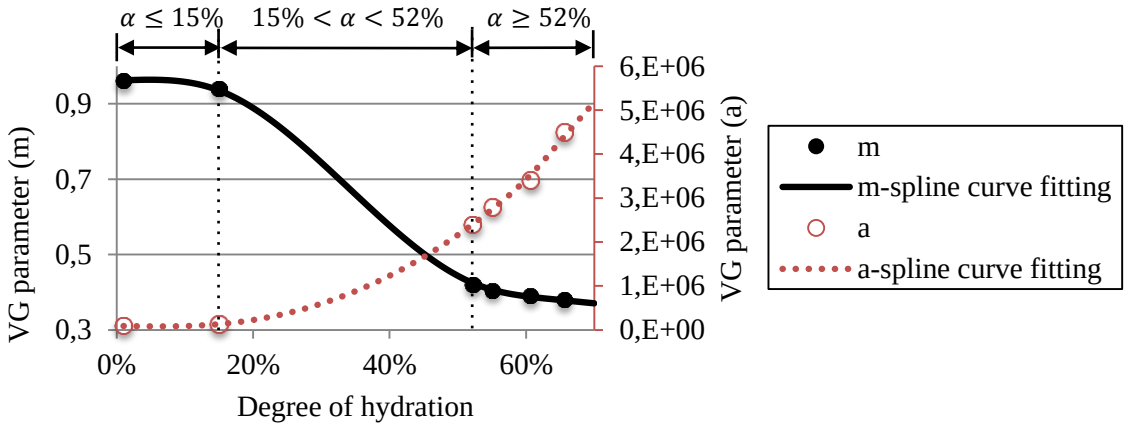

Fig. 4.15 Evolution of Van Genuchten parameters of a cement paste (w/c = 0.3). The Van Genucthen parameters, a and m, are determined from the capillary pressure - water saturation level curves. The capillary pressure - water saturation level curves are determined by by Level Set simulation when $\alpha \leq 15\%$, and by using empirical model when $\alpha \geq 52\%$. The Van Genucthen parameters, a and m, are determined by spline curve fitting when $15\% < \alpha < 52\%$.

4.4 Rate of hydration $\dot{\alpha}(\alpha, s_{cap})$

The rate of hydration (ROH) of a cementitious material is a very important parameter in the simulation of moisture transport, because it determines the amount of water that is consumed by hydration. However, it is not always easy to determine the ROH experimentally. Alternatively, the hydration process influenced by the water content can be calculated using numerical models, e.g. HYMOSTRUC3D [8, 9] or CEMHYD 3D [75]. In these models, the effect of changes in the state of water in the microstructure is explicitly considered so that hydration of cementitious materials can be simulated with arbitrary water contents.

4.4.1 Method to determine rate of hydration $\dot{\alpha}(\alpha, s_{cap})$

In this chapter, the rate of hydration $\dot{\alpha}$ of a cementitious coating material, containing an arbitrary water content, will be studied by using a modified version of HYMOSTRUC3D. This model enables the prediction of hydration curves as a function of the particle size distribution and chemical composition of the cement, the water/cement ratio (w/c) and the actual reaction temperature. A schematic illustration of the basic principles of HYMOSTRUC3D is presented in Fig. 4.16. The original HYMOSTRUC3D simulates the hydration process of cement pastes under a sealed condition. In the hydration process, the rate of penetration of the reaction front at depth x in an individual cement particle at time t_j is given by [8]:

$$\frac{\Delta\delta_{in,x,j+1}}{\Delta t_{j+1}} = k_0(.)\cdot\Omega_1(.)\cdot\Omega_2(.)\cdot\Omega_3(.)\cdot F_1(.)\left[F_2(.)\cdot\left(\frac{\delta_{tr}(.)}{\delta_{x,j}}\right)^{\beta_1}\right]^{\lambda} \tag{4.16}$$

where $\Delta\delta_{in,x,j+1}$ is the increase of the penetration depth in time step Δt_{j+1}, k_0 is the basic rate factor of the boundary reaction. δ_{tr} is the transition thickness [μm], being the thickness of the product layer $\delta_{x,j}$ at time t at which the reaction of the particle in view of changes from the phase boundary reaction into a diffusion controlled reaction. The parameters Ω_i describe the various effects of water on the cement hydration mechanisms and the parameters F_1 and F_2 take into account the influence of temperature on the hydration process. λ is the factor depending on rate controlling mechanism.

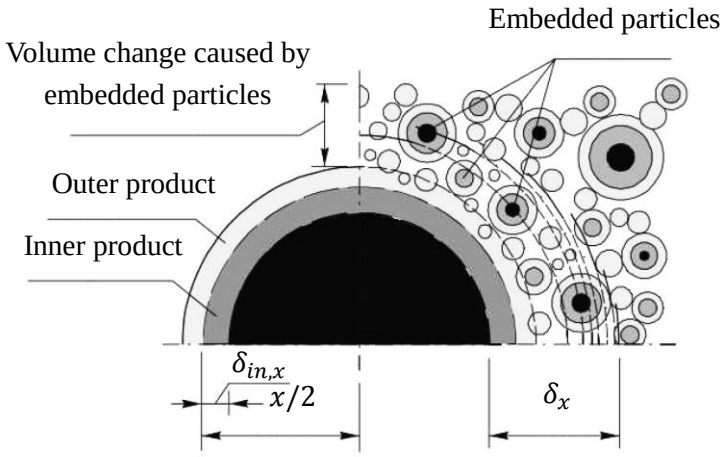

Fig. 4.16 Basic principles of HYMOSTRUC3D and formation of hydration products (by van Breugel [8]).

In HYMOSTRUC3D model, only capillary water is considered freely available for cement hydration. During the hydration process, the capillary water is gradually consumed. It is believed that an adsorbed water layer of some thickness will remain at the capillary pore wall (Fig. 4.17). This layer is assumed to be less easy to mobilize for further hydration. In the model, pore wall area $A_{wat}(\alpha)$ that is in contact with free water is introduced to address the influence of water on the rate of hydration of cement paste. This effect is quantified with a reduction factor $\Omega_2(\alpha)$:

$$\Omega_2(\alpha) = \frac{A_{wat}(\alpha)}{A_{por}(\alpha)} \tag{4.17}$$

where $A_{wat}(\alpha)$ is the surface area of water-filled capillary pores at DOH α, and $A_{por}(\alpha)$ is the total surface area of all capillary pores (for details, see [8]).

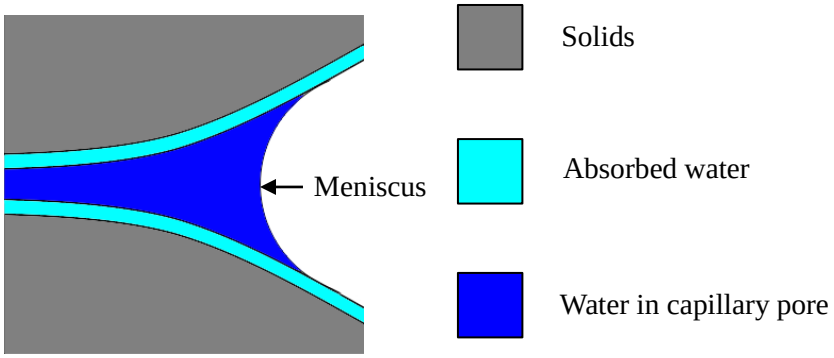

Fig. 4.17 Schematic illustration of water in a capillary pore of a cement paste.

Besides the surface area of water-filled capillary pores, the amount of residual water in capillary pores is also significant to cement hydration. It is relevant for the amount of dissolved Ca^{2+}, which is important for the reaction. To account for the amount of the capillary water, a reduction factor $\Omega_3(\alpha)$ was defined as [8]:

$$\Omega_3(\alpha) = \frac{\omega - 0.4 \cdot \alpha}{\omega} \tag{4.18}$$

where ω is the w/c ratio.

For determining $\Omega_3(\alpha)$ in this study, a schematic cement paste is depicted in Fig. 4.18. Fig. 4.18a shows the initial state of a cement paste, where only cement and water are present. As the hydration proceeds, hydration products form in the matrix, while the large capillary pores are gradually emptied (Fig. 4.18b). In Eq. (4.18), the term $(\omega - 0.4 \cdot \alpha)$ refers to the volume of water remaining in the capillary pores (Fig. 4.18c).

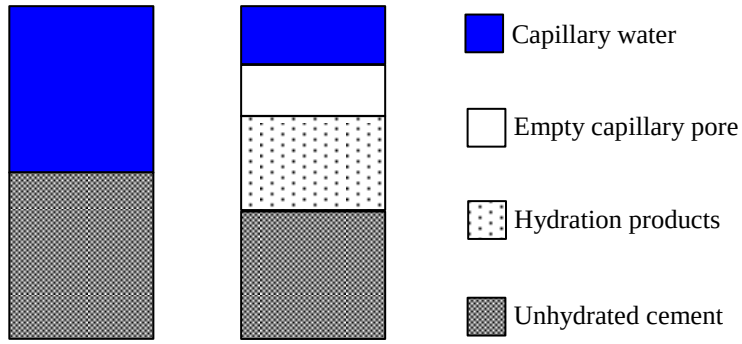

(a) Initial state (b) Hydrated cement paste

Fig. 4.18 Schematic illustration of the composition of a cement paste.

The modified version of the HYMOSTRUC3D model aims to deal with cement hydration under arbitrary degree of water saturation in capillary pores s_{cap} (see Eq. (3.18)). In the modified model, the water saturation level in capillary pores ranges from 0 to 100%. Accordingly, the values of $\Omega_2(\alpha, s_{cap})$ and $\Omega_3(\alpha, s_{cap})$ are changed.

With the specified degree of water saturation in capillary pores s_{cap}, the rate of hydration $\dot{\alpha}$ of a cement paste with arbitrary water content can be calculated with Eq. (4.16), provided that the values of $\Omega_2(\alpha, s_{cap})$ and $\Omega_3(\alpha, s_{cap})$ are adjusted for the prevailing value of s_{cap}. The hydration process of a non-sealed cement paste will be simulated and discussed in section 4.4.2.

4.4.2 Example calculation of rate of hydration $\dot{\alpha}(\alpha, s_{cap})$ of a cement paste

In this chapter, the HYMOSTRUC3D model was modified for calculating the rate of hydration $\dot{\alpha}$ of a cement paste (w/c = 0.3) that has arbitrary water content. To demonstrate the performance of the modified HYMOSTRC 3D, cement hydration process either under a sealed curing condition or under a saturated curing condition is simulated. The curing temperature is 20 °C. The simulation results are plotted in Fig. 4.19, and compared with experimental results from [147], a good agreement can be found from the figure. Note that, in [147] a ASTM type I Portland cement was used, with a similar mineral composition to the cement used in this study (see Table 4.2.).

The purpose of the extended HYMOSTRUC3D is to give the rate of hydration for cement pastes at arbitrary DOH with various capillary water contents, since the rate of hydration (Eq. (3.17)) is an important parameter in the Moisture-Hydration model. In cementitious materials, the capillary water contents are the result of hydration, external drying or external water supply (moist curing). As presented above, by specifying various capillary water saturations s_{cap}, the rate of hydration $\dot{\alpha}$ is calculated. Fig. 4.20 shows the α and s_{cap} dependency of $\dot{\alpha}$. It can be seen from the figure that, for a cement paste with a particular degree of hydration α, the rate of hydration $\dot{\alpha}$ increases with the capillary water saturation s_{cap}. As can be expected, with a particular capillary water saturation s_{cap}, the cement paste has a higher rate of hydration $\dot{\alpha}$ when the degree of hydration α is lower. To facilitate the implementation of Moisture-Hydration model, a lookup table is created. From the lookup table, the rate of hydration $\dot{\alpha}$ can be determined for a given degree of hydration α and a given capillary water saturation s_{cap}.

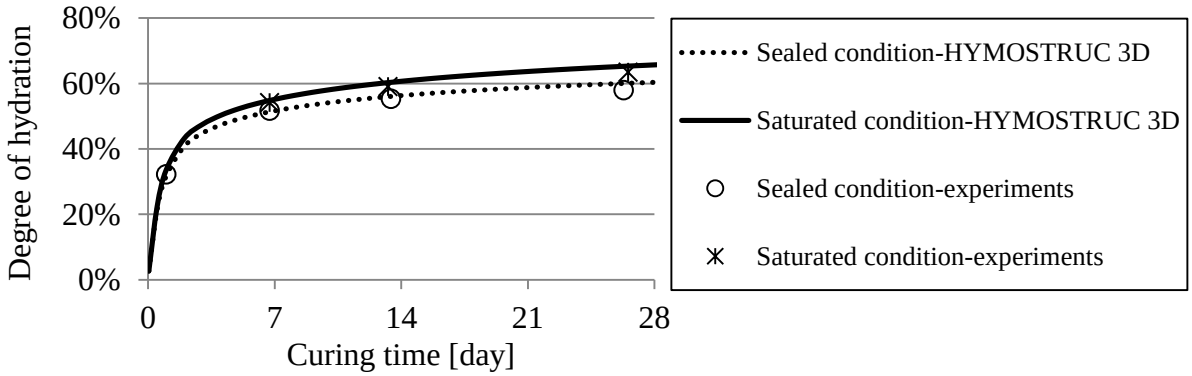

Fig. 4.19 DOH of cement pastes (w/c = 0.3). Hydration takes place under a sealed or a saturated condition. Experimental data were derived from [147].

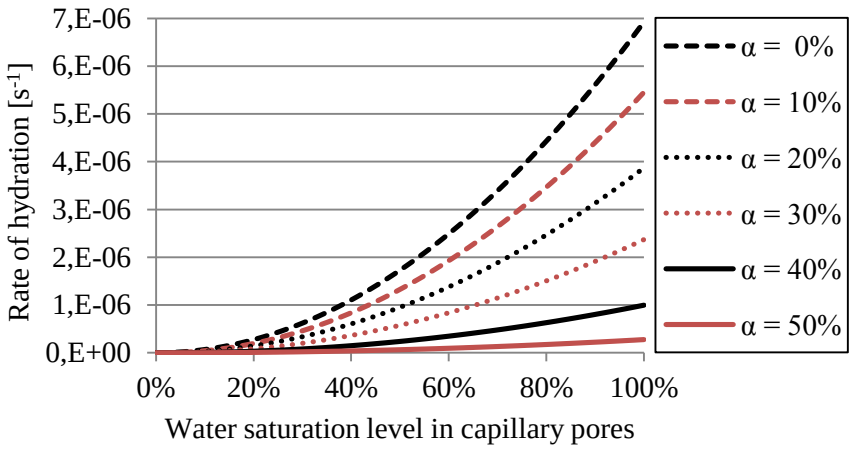

Fig. 4.20 Influence of water saturation level in capillary pores on the rate of hydration $\dot{\alpha}$ of the cement particles in a cement paste with w/c = 0.3.

4.5 Capillary porosity ϕ_{cap}, gel porosity ϕ_{gel} and total porosity ϕ

In cement pastes, capillary pores are the residual unfilled space between cement particles. Gel porosity, as a first approximation, is entirely contained within C-S-H [148]. As mentioned in section 3.3.3, the capillary porosity and the gel porosity of the coating have to be determined for the calculation of the rate of hydration of the coating with arbitrary water content. The capillary porosity ϕ_{cap}, the gel porosity ϕ_{gel} and the total porosity ϕ will be calculated based on the composition and the degree of hydration α of the cement paste (i.e. coating material).

4.5.1 Method to determine capillary porosity ϕ_{cap}

Fresh cement paste consists of cement particles and water filled pores. During hydration, water is gradually consumed by the reaction of cement with water and transferred into hydration products. The volume of initially water filled pores becomes smaller due to the formation of hydration products. The capillary porosity ϕ_{cap} of a cement paste can be calculated with [8]:

$$\phi_{cap} = \frac{\rho_{cem}}{\rho_w + \rho_{cem} \cdot \frac{w}{c}} \cdot \left(\frac{w}{c} - 0.3375 \cdot \alpha\right) \tag{4.19}$$

where ρ_{cem} and ρ_w are the densities of cement particles and water, w/c is water/cement (w/c) ratio and α is the degree of hydration (DOH).

4.5.2 Method to determine gel porosity ϕ_{gel}

The finest pores, ranging from approximately 10 nm to 0.5nm, are called gel pores, which are pores of the C-S-H gels. When calculating the gel porosity, different structures of C-S-H (i.e. low density (LD) C-S-H and high density (HD) C-S-H) are considered according to the model proposed by Jennings et al. [145].

In cement pastes, C-S-H gel is the main hydration product of C_3S and C_2S. The amounts of LD and HD C-S-H gel change with the hydration. The following reactions hold [149]:

$$2C_3S + 10.6H \rightarrow C_{3.4}S_2H_8 + 2.6CH \tag{4.20}$$

$$2C_2S + 8.6H \rightarrow C_{3.4}S_2H_8 + 0.6H \tag{4.21}$$

In order to determine the amount of C-S-H, the hydration of individual clinker component needs to be calculated. During hydration, the reaction of four major clinkers develops differently. A parameter k_i is introduced to describe the relation between the degree of hydration α_i of clinker i and the total degree of hydration α:

$$k_i = \frac{\alpha_i}{\alpha} = \frac{\alpha_i}{\sum_{i=1}^{4} \alpha_i} \tag{4.22}$$

The degree of hydration α_i of clinker i can be approximated by [150]:

$$\alpha_i = 1 - e^{-(k_2 \cdot (t-k_3)^{k_1})} \tag{4.23}$$

where k_1, k_2 and k_3 are empirical constants given in Table 4.3, t is the time (in days).

Note that Eq. (4.23) is only used to determine the parameter k_i in Eq. (4.22), and not for determining the exact value of α_i. In practice, the hydration of the clinker depends on water content in cement paste, which will be considered in the Moisture-Hydration model. From the total degree of hydration α of cement, the degree of hydration α_i of clinker i can be determined:

$$\alpha_i = k_i \cdot \alpha \tag{4.24}$$

Then the amount of C-S-H gel can be calculated with Eq. (4.20) and Eq. (4.21). Parameters needed for the calculation are listed Table 4.4, including parameters of Alite, Belite and C-S-H.

Table 4.3 Values of constants in Eq. (4.23) for the hydration of individual clincker in cement pastes [150].

	k1	k2	k3
Alite (C_3S[1])	0.25	0.70	0.90
Belite (C_2S)	0.46	0.12	0
Aluminate (C_3A)	0.28	0.77	0.90
Ferrite(C_4AF)	0.26	0.55	0.90

Note that the constants in Table 4.3 have been determined empirically for a specific Portland cement with a mineral composition C_3S : C_2S : C_3A : C_4AF = 60% : 15% : 8% : 10%. The constants will be used as an approximation for ordinary Portland cement used in this thesis.

Table 4.4 Parameters for determining the mass of C-S-H gel in a cement paste [149].

	Nominal formula	Molecular weight (kg/mol)	Density (kg/m^3)	Porosity
LD C-S-H, dry	$C_{3.4}S_2H_3$	0.365	1440 (ρ_{LD})	49% (ϕ_{LD})
HD C-S-H, dry	$C_{3.4}S_2H_3$	0.365	1750 (ρ_{HD})	38% (ϕ_{HD})
Alite	C_3S	0.228	–	–
Belite	C_2S	0.172	–	–
Water	H	0.018	–	–

According to Tennis et al. [151], M_r is defined as the ratio of the mass of LD C-S-H (M_{LD}) to the total mass of C-S-H (M_{CSH}), which can be obtained by using multiple linear regression:

$$M_r = 3.017 \cdot \frac{w}{c} \cdot \alpha - 1.347 \cdot \alpha + 0.538 \tag{4.25}$$

The mass of LD C-S-H (M_{LD}) and the mass of HD C-S-H (M_{HD}) in a unit volume of cement paste can be calculated:

$$M_{LD} = M_{CSH} \cdot M_r, \qquad M_{HD} = M_{CSH} - M_{LD} \tag{4.26}$$

Gel pores exist in both LD C-S-H and HD C-S-H. Gel porosity ϕ_{gel} can be calculated as:

$$\phi_{gel} = \frac{M_{LD}}{\rho_{LD}} \cdot \phi_{LD} + \frac{M_{HD}}{\rho_{HD}} \cdot \phi_{HD} \tag{4.27}$$

The total porosity of cement paste reads:

$$\phi = \phi_{cap} + \phi_{gel} \tag{4.28}$$

[1] Cement chemists' notation is used throughout this study; C = CaO; S = SiO_2; A = Al_2O_3; F = Fe_2O_3; $\bar{S}$= SO_3; H = H_2O. Thus, C_3S = $3CaO{\cdot}SiO_2$.

4.5.3 Example calculation of capillary porosity ϕ_{cap}, gel porosity ϕ_{gel} and total porosity ϕ of a hydrating cement paste

Porosities of an example cement paste (w/c = 0.3) are calculated using above methods. The mineral composition of the cement used was previously listed in Table 4.2. In Fig. 4.21, the evolution of porosities of the example cement paste is plotted against the degree of hydration α. As the hydration of the cement paste proceeds, the gel porosity ϕ_{gel} increases with the degree of hydration α, while the capillary porosity ϕ_{cap} decrease drastically with the increase of α. As a result, total porosity ϕ decreases with the increase of the degree of hydration α. All porosities (i.e. ϕ, ϕ_{gel} and ϕ_{cap}) together with the water saturation s in Eq. (3.18) will determine how much water is available for further hydration and for moisture transport.

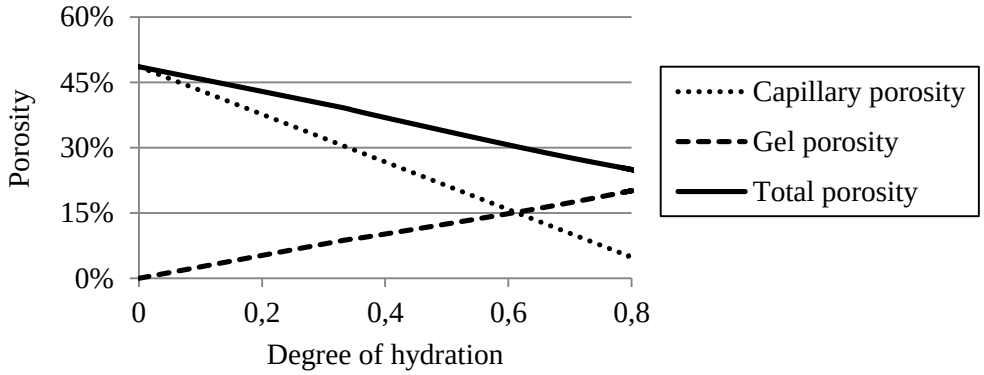

Fig. 4.21 Evolution of capillary, gel and total porosity of a cement paste (w/c = 0.3).

4.6 Summary

For simulating moisture transport in a hydrating cementitious coating system, transport properties of the coating and sink term accounting for hydration of the coating need to be known. This chapter quantified the parameters needed for determining the transport properties and the sink term for the coating. The parameters include intrinsic permeability, Van Genuchten parameters (obtained from the moisture isotherm), porosity and rate of hydration.

– The intrinsic permeability of early-age cement pastes is determined by simulating the water flow through the pastes. The simulation is conducted using a Lattice Boltzmann Method (LBM). For hardened cement pastes, the intrinsic permeability is determined according to an empirical equation. The empirical equation relates the permeability of cement pastes to the 28-day permeability value. The permeability is described as a function of the degree of hydration of the pastes.

- The desorption isotherms of early-age cement pastes are determined using a Level Set Method. For hardened cement pastes, an empirical model is used to determine the adsorption isotherms. Based on the moisture isotherms, two parameters (a and m) in the Van Genuchten model are determined and described as a function of the degree of hydration of the pastes.
- The rate of hydration of cement pastes with various water contents is studied, by modifying the numerical cement hydration model HYMOSTRUC3D.
- The porosities (capillary porosity, gel porosity and total porosity) of cement pastes are parameterized with respect to the w/c ratio and the degree of hydration.

Example calculations of above parameters of a hydrating cement paste (w/c = 0.3) are presented. This cement paste will be used as a coating material and applied on concrete substrates. Simulation of moisture transport in the coating systems will be presented in chapter 5.

Chapter 5

Simulation of moisture transport in hydrating cementitious coating systems and evaluation of drying shrinkage-induced cracking of coatings

5.1 Introduction

When a cementitious coating is applied on a concrete substrate, moist curing is normally required for a certain period of time to ensure a proper hydration of the coating material. Moist curing is also beneficial to prevent plastic shrinkage-induced cracking at early ages due to rapid water loss from the material [102]. After a period of moist curing the coating system can become subjected to drying. Moisture starts to evaporate from the coating to the environment. Meanwhile, moisture exchange takes place between the coating and the substrate. Consequently, differential drying shrinkage of the coating and the substrate develops over time, which increases the probability of cracking and/or debonding of the coating material [70].

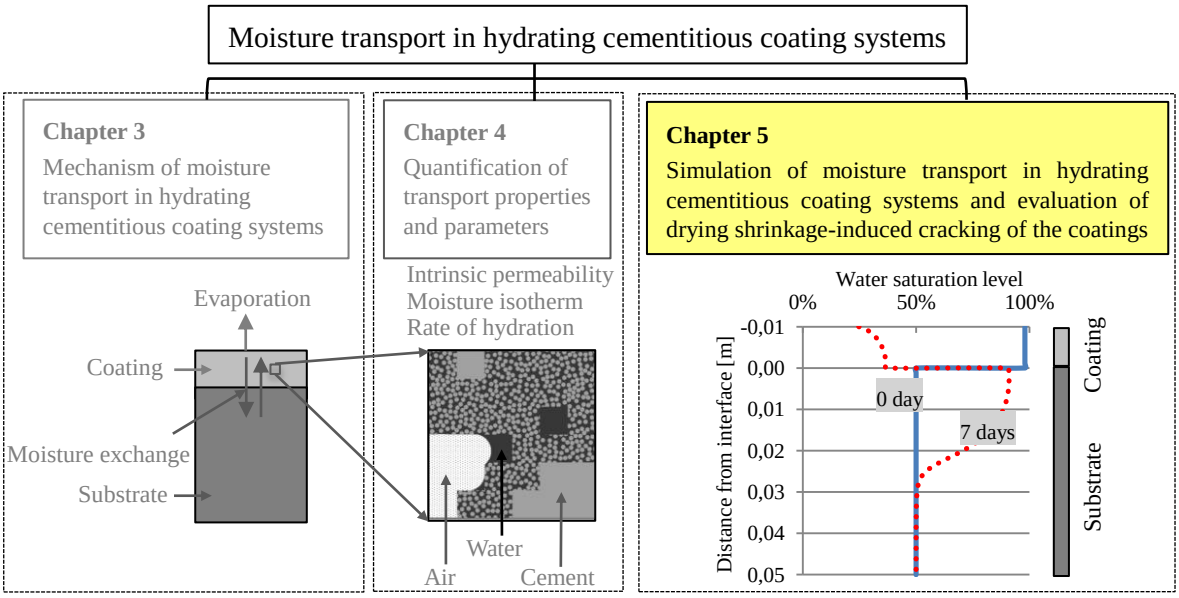

Fig. 5.1 Structure of the study of moisture transport in hydrating cementitious coating systems.

In this chapter moisture transport in hydrating coating systems is simulated with the Moisture-Hydration model discussed in chapter 3 (Fig. 5.1). The Moisture-Hydration model is implemented in Matlab, and the results of simulation are mesh and time discretization independent. One-dimensional (1D) simulation of moisture transport in the coating system is considered. The top surface of the coating system is subjected to various curing conditions, while the bottom surface of the substrate is always sealed (Fig. 5.2). The moisture profiles in the coating systems and the degree of hydration of the coating material are determined. The influence of several parameters on the moisture transport is evaluated, viz., the coating thickness, the duration of different curing conditions, the initial water content of the substrate and the type of substrate (i.e. ordinary concrete or high performance concrete). Based on the evaluation of the influencing parameters (e.g., various curing regimes), measures are recommended to ensure a proper hydration of the coating material.

From the simulated degree of hydration (DOH), the mechanical properties (e.g. elastic modulus and tensile strength) are determined. The drying shrinkage-induced stress is calculated based on the moisture content in the coating material. Then the probability of drying shrinkage-induced cracking of the coating is evaluated.

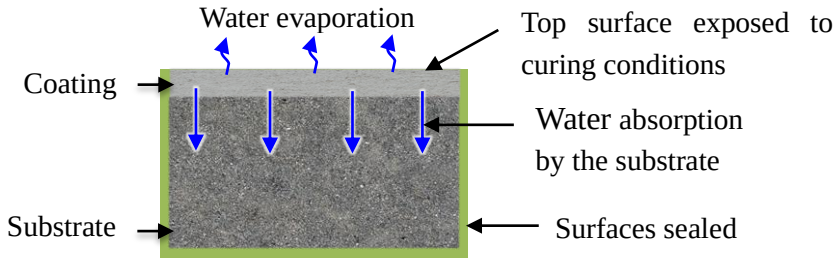

Fig. 5.2 A typical scenario of moisture transport in a coating system.

5.2 Moisture change and hydration of a reference cement paste (sealed curing)

Before simulating the moisture transport and its interaction with the hydration process in the coating materials, the hydration process of a reference coating material (i.e. cement paste) is simulated by using HYMOSTRUC3D. The simulated evolution of the DOH and the changes of the water content of the reference cement paste in case of standard sealed curing will be compared with those of the coatings applied on the substrates.

5.2.1 Materials of the reference cement paste

The reference cement paste is made of Portland cement CEM I 42.5N and has a w/c of 0.3. The mineral composition of the cement was previously given in Table 4.2. Sealed curing condition (20 °C) is considered.

5.2.2 Moisture content and degree of hydration of the reference cement paste

The evolution of the DOH and the total porosity of the reference cement paste are presented in Fig. 5.3a and Fig. 5.3b, respectively. The hydration process takes place mainly within 14 days. At 28 days the cement paste has a DOH of 60%, and a total porosity of 31% (Eq. (4.28)). Fig. 5.3c shows the water content in the reference cement paste. The mixing water of the cement paste is 0.467 g/cm^3. After casting, the water in the cement paste is gradually consumed by hydration. At 28 days, the water content decreases to 0.256 g/cm^3.

The water is assumed to be uniformly distributed in the reference cement paste. The water saturation level s in the cement paste is calculated from the water content and the total porosity ϕ:

$$s = \theta/(\rho_w \cdot \phi) \tag{5.1}$$

Fig. 5.3d presents the evolution of the water saturation level in the reference cement paste. At 28 days the water saturation level is still above 80%. The results presented in Fig. 5.3 are used as a reference for those of the coating materials presented in the following section (5.5).

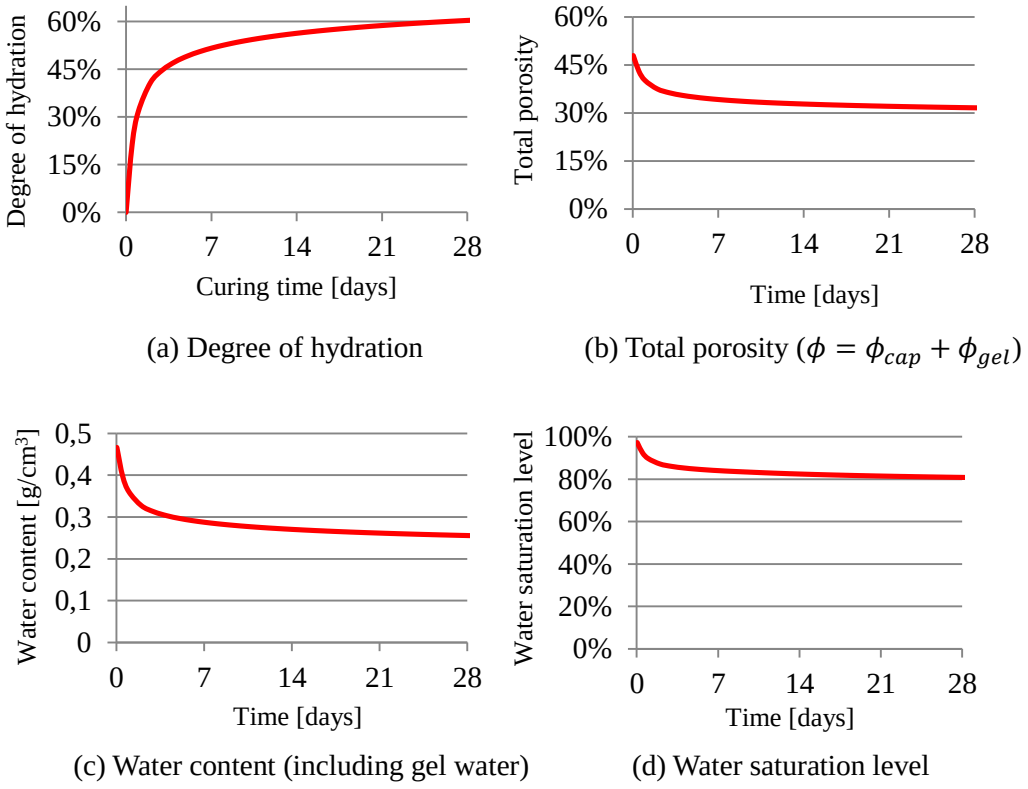

(a) Degree of hydration

(b) Total porosity ($\phi = \phi_{cap} + \phi_{gel}$)

(c) Water content (including gel water)

(d) Water saturation level

Fig. 5.3 Evolution of calculated degree of hydration, porosity, water saturation level and water content of a reference cement paste (w/c = 0.3, Portland cement CEM I 42.5N is used). The reference cement paste is cured under sealed curing condition (20 °C).

5.3 Materials of coating systems for the simulation of moisture transport

5.3.1 Coating-mixture composition

The coatings are made of Portland cement CEM I 42.5N and have a w/c of 0.3. The mineral composition of the cement was previously given in Table 4.2.

5.3.2 Substrate

Two types of concrete substrates are used, i.e. ordinary concrete (OC) and high performance concrete (HPC). The substrates are characterized by their porosity and permeability. The characteristics of the substrates (1 year-old) are taken arbitrarily from Baroghel-Bouny et al. [60] and listed in Table 5.1. Further hydration of concrete substrate after application of the coating is neglected. The thickness of the substrates is 50 mm. Note that, in practice the thickness of concrete elements will be larger than 50 mm. This thickness is chosen for a fast numerical computation and is considered large enough for the parameter study of moisture transport in the coating system.

Table 5.1 Water-to-cement ratios and properties of the concrete substrates [60].

	OC (Ordinary concrete)	HPC (High performance concrete)
Water/cement (by mass)	0.48	0.26
Total porosity	12.2%	8.2%
Intrinsic permeability [m^2/s]	3×10^{-21}	5×10^{-22}

5.4 Exposure scenarios of the coating systems and parameters to be evaluated

After the coating has been applied on the substrate, moisture exchange takes place between the coating and the substrate, and/or between the coating and the environment. The water loss to the substrate and/or to the environment will affect the hydration process of the coating material. Consequently, the properties of the coating material will change. Moisture transport in different coating systems (Table 5.2) is simulated for different coating thicknesses, duration of the moist curing, type and initial water content of the substrate. The values of each parameter is given below:

a) Coating thickness: 6, 10 and 20 mm.
b) Duration of the various curing conditions applied on top surface of the coating (Fig. 5.4):
   - 1, 3 and 7 days moist curing (Moist1d, Moist3d and Moist7d)
   - 1, 3 and 7 days sealed curing (Sealed1d, Sealed3d and Sealed7d)
   - wet-dry cycles (WetDry)
c) Initial water content of the substrate OC: standard (s = 50%) and saturated (s = 100%)
d) Type of the substrate (Table 5.1): substrate OC (s = 50%) and substrate HPC (s = 77%)

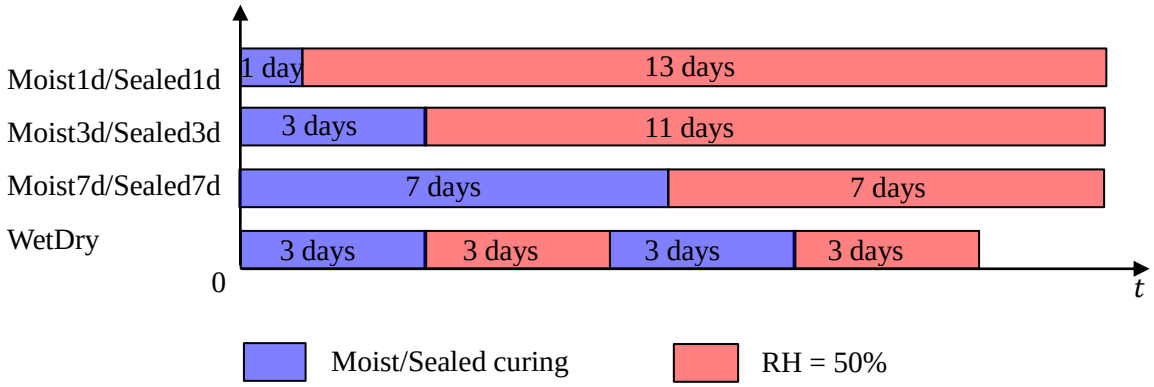

Fig. 5.4 Illustration of different curing regimes (T = 20 °C). The coating is applied on the substrate at $t = 0$. In the 1D simulation, the top surface of the coating system is subjected to various curing regimes, while the bottom surface of the substrate is always sealed (Fig. 5.2). One wet-dry cycle consists of 3 days moist curing and 3 days curing at 50% RH.

Table 5.2 Description of the reference cement paste and the coating-substrate systems.

	Coating thickness	Substrate and its initial water saturation level	Curing regime ($T = 20$°C)
Reference cement paste			Sealed condition
C06-OC(s=50%)-Moist1d	6 mm	OC, $s = 50\%^{*}$	1 d moist + 13 d 50% RH
C20-OC(s=50%)-Moist1d	20 mm	OC, $s = 50\%$	1 d moist + 13 d 50% RH
C10-OC(s=50%)-Moist1d	10 mm	OC, $s = 50\%$	1 d moist + 13 d 50% RH
C10-OC(s=100%)-Moist1d	10 mm	OC, $s = 100\%$	1 d moist + 13 d 50% RH
C10-HPC(s=77%)-Moist1d	10 mm	HPC, $s = 77\%^{*}$	1 d moist + 13 d 50% RH
C10-OC(s=50%)-Moist3d	10 mm	OC, $s = 50\%$	3 d moist + 11 d 50% RH
C10-OC(s=100%)-Moist3d	10 mm	OC, $s = 100\%$	3 d moist + 11 d 50% RH
C10-HPC(s=77%)-Moist3d	10 mm	HPC, $s = 77\%$	3 d moist + 11 d 50% RH
C10-OC(s=50%)-Moist7d	10 mm	OC, $s = 50\%$	7 d moist + 7 d 50% RH
C10-OC(s=100%)-Moist7d	10 mm	OC, $s = 100\%$	7 d moist + 7 d 50% RH
C10-HPC(s=77%)-Moist7d	10 mm	HPC, $s = 77\%$	7 d moist + 7 d 50% RH
C10-OC(s=50%)-Sealed1d	10 mm	OC, $s = 50\%$	1 d sealed +13 d 50% RH
C10-HPC(s=77%)-Sealed1d	10 mm	HPC, $s = 77\%$	1 d sealed +13 d 50% RH
C10-OC(s=50%)-Sealed3d	10 mm	OC, $s = 50\%$	3 d sealed +11 d 50% RH
C10-HPC(s=77%)-Sealed3d	10 mm	HPC, $s = 77\%$	3 d sealed +11 d 50% RH
C10-OC(s=50%)-Sealed7d	10 mm	OC, $s = 50\%$	7 d sealed +7 d 50% RH
C10-HPC(s=77%)-Sealed7d	10 mm	HPC, $s = 77\%$	7 d sealed +7 d 50% RH
C10-OC(s=50%)-WetDry	10 mm	OC, $s = 50\%$	2 wet-dry cycles (see Fig. 5.4)

* The internal relative humidity of substrate OC and substrate HPC is 75%.

5.5 Simulation results and discussion

In this section moisture transport in hydrating coating systems (Table 5.2) is simulated. The simulated moisture profiles in the coating systems and the evolution of the DOH of the coatings are presented and discussed. The simulated water content (in g per cm^3 of the coating) and degree of hydration of the coating materials are compared to those of the reference cement paste (w/c = 0.3, cured under sealed condition) presented in section 5.2.

5.5.1 Effect of coating thickness (6, 10 and 20 mm) on moisture transport in the coating system and on the hydration of the coatings

5.5.1.1 Moisture profile in the coating system with a 10 mm-thick coating

Fig. 5.5 presents the moisture profiles in the coating system with a 10 mm-thick coating. After application of the coating, the substrate immediately starts absorbing water from the coating. During 1 day moist curing, the coating still remains saturated with water. After 1 day, the coating is exposed to a RH of 50%. The water saturation level in the coating decreases drastically, due to the continuing water absorption by the substrate and the water evaporation to the environment. Meanwhile, hydration of the coating consumes some amount of water. An almost uniform moisture distribution is observed over the thickness of the coating. This phenomenon can be explained by the fact that the moisture moves rapidly in a young coating material with a highly connected pore system. Similar results regarding the uniform moisture distribution in young cement-based materials subjected to drying have been reported by Selih et al. [152] and Bentz et al. [75].

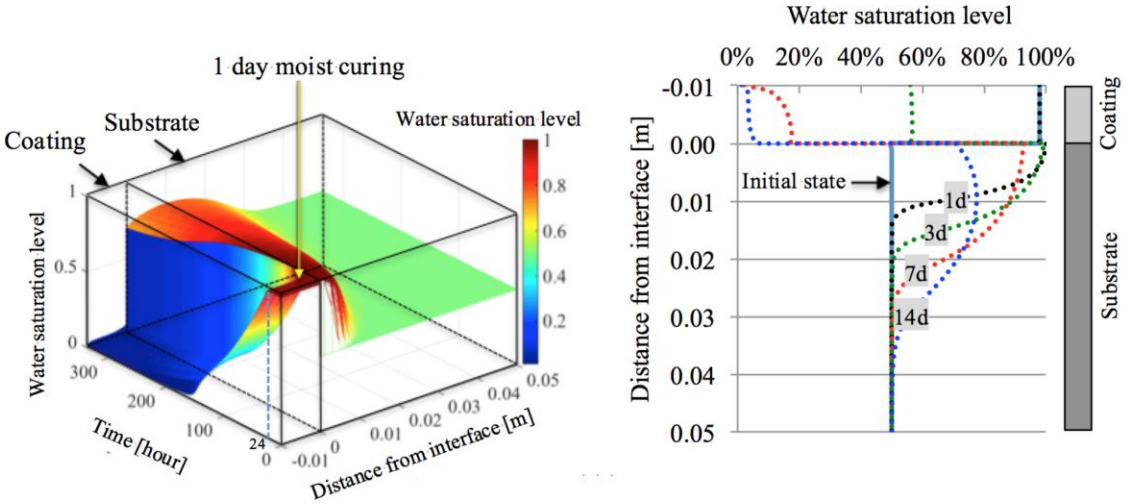

(a) 3D plot (b) 2D plot

Fig. 5.5 Calculated moisture profiles in the coating system C10-OC(s=50%)-Moist1d (Table 5.2). A 10 mm-thick coating (w/c = 0.3) is applied on substrate OC. One day moist curing is applied, followed by exposure to 50% RH until 14 days.

After 3 days, the water saturation level in the 10 mm-thick coating has dropped below 60% (Fig. 5.5b), which is lower than that in the reference cement paste (> 80%, see Fig. 5.3d). Distinct difference in water saturation level can be clearly seen from the coating-substrate interface (Fig. 5.5b). The water saturation level of the substrate at the interface remains higher than 70% at 14 days. At 14 days the water saturation level in the coating reached a value as low as 5%. It can be explained by the difference in the microstructures of the coating and the substrate. Distinct moisture contents of overlay material and substrate at the interface have also been reported by Brocken et al. [50] and Qiu et al. [153].The decrease of the water saturation level in the coating will affect the hydration process of the coating, which will be discussed below.

5.5.1.2 Evolution of water content and degree of hydration of the coatings with different thicknesses (6, 10 and 20 mm)

Fig. 5.6a presents the evolution of the water content θ in coatings with different thicknesses (i.e. 6, 10 and 20 mm). After 1 day moist curing, the water content θ in the thicker coating (e.g. 20 mm) is higher than that in thinner coatings (6 or 10 mm).

Average values of DOH of the coatings at discretized nodes are calculated. The evolution of the DOH of the coatings is depicted in Fig. 5.6b. There is no difference of the DOH between the coatings during 1 day moist curing. After the coatings are exposed to a RH of 50%, the DOH curves of the coatings start to diverge. An earlier cease of hydration is seen for a thinner coating (i.e. 6 mm-thick coating).

By comparing the DOH of the coatings with that of the reference cement paste, the combined effect of the water evaporation and the water absorption by the substrates on the hydration of coatings is evaluated. The hydration process of the coatings has almost ceased after 4 days due to drying, while the sealed cured reference coating material continues to hydrate. Fig. 5.7 shows the DOH of the coatings with different thicknesses at 14 days. The coating with a larger thickness has a higher DOH at 14 days. As expected, the coating thickness has a noticeable influence on the hydration process of a coating. A thinner coating is more susceptible to lose its water when it is applied on the absorptive substrate and exposed to a dry environment (e.g., RH = 50%). The greater water loss results in a lower DOH and will result in a higher permeability of the coating materials.

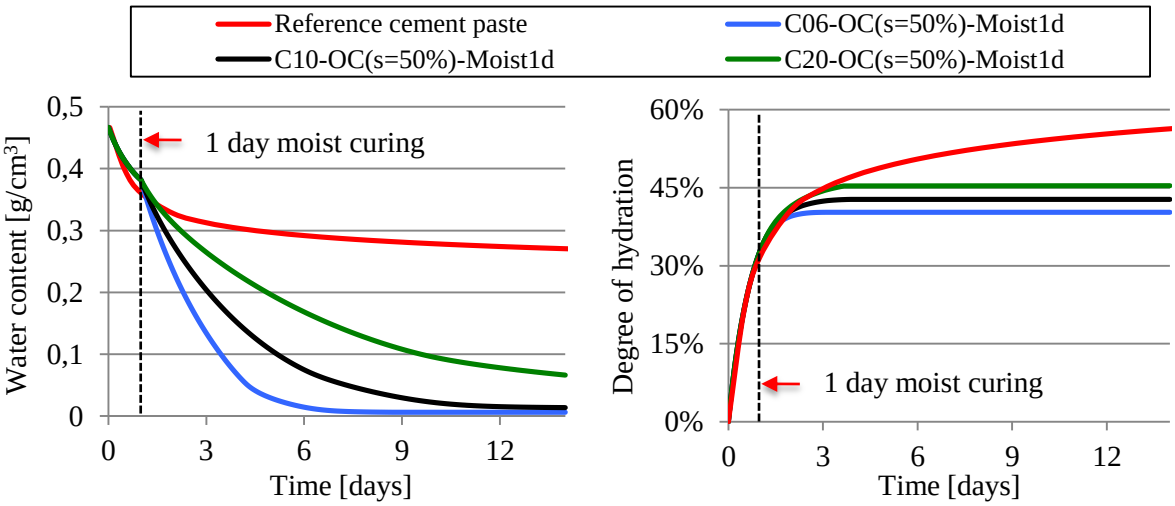

(a) Water content (b) Degree of hydration

Fig. 5.6 Calculated water content and calculated average degree of hydration of the coatings (w/c = 0.3) with different thicknesses (6, 10 and 20 mm). The coatings are applied on substrate OC (s = 50%). One day moist curing is applied, followed by exposure to 50% RH until 14 days. The reference cement paste (w/c = 0.3, no substrate) is cured under sealed condition.

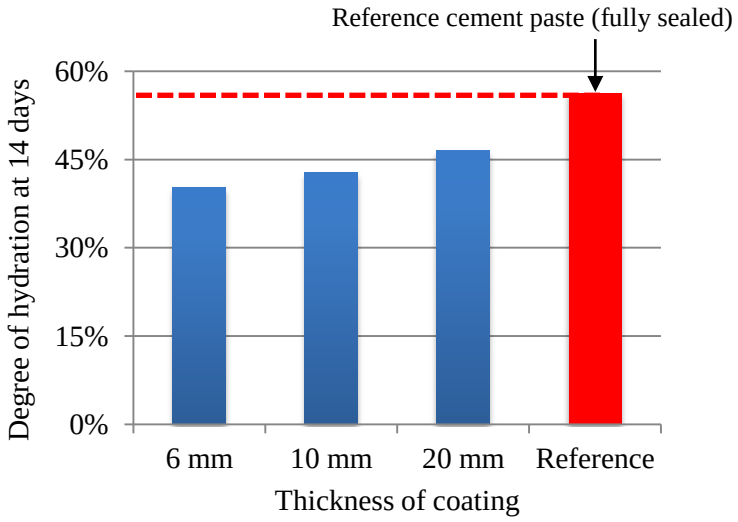

Fig. 5.7 Calculated average degree of hydration at 14 days of the coatings (w/c = 0.3) with different thicknesses (6, 10 and 20 mm). The coatings are applied on substrate OC (s = 50%). One day moist curing is applied, followed by exposure to 50% RH until 14 days. The reference cement paste (w/c = 0.3) is cured under sealed condition.

5.5.2 Effect of curing regime on moist transport in the coating system and on the hydration of the 10 mm-thick coatings

In order to investigate the role of the curing regime on the moisture distribution in the coating systems and the degree of hydration of the coatings, different curing regimes were applied to the coating systems (Table 5.2). A 10-mm thick coating (w/c = 0.3) is applied on substrate OC ($s = 50\%$). The curing regimes that will be studied are:

- 1, 3 or 7 days moist curing, followed by exposure to RH = 50% until 14 days
- 1, 3 or 7 days sealed curing, followed by exposure to RH = 50% until 14 days
- 2 wet-dry cycles, each cycle consists of 3 days moist curing and 3 days sealed curing

5.5.2.1 Moisture profiles in coating systems under various curing regimes (water saturation level of substrate: 50%)

Moisture profiles in 3 typical coating systems are presented. Various curing regimes are applied, including 3 days sealed curing, 3 days moist curing and 2 wet-dry cycles.

3 days moist curing: C10-OC(s=50%)-Moist3d

In C10-OC(s=50%)-Moist3d, 3 days moist curing is applied to the coating system after application of the coating. Fig. 5.8 presents the moisture profile in the coating system. After 14 days the water saturation level of the coating becomes low ($s < 20\%$), but is higher than that in the coating with 1 day moist curing ($s < 5\%$) (Fig. 5.5b). Longer moist curing means that more water remains available for the hydration of the coating material.

3 days sealed curing: C10-OC(s=50%)-Sealed3d

The sealed curing simulates the situation that a curing compound is applied on the surface of the coating material. Fig. 5.9 presents the moisture profiles in the coating system. Immediately after application of the coating, the water saturation level in the coating material starts to decrease because of water consumption due to hydration of the coating and water absorption by the substrate.

After 3 days sealed curing and exposure to an ambient RH of 50%, water starts to evaporate from the surface of the coating, causing a drastic decrease of the water saturation level in the coating. The water saturation level in the coating with 3 days sealed curing (Fig. 5.9) is much lower compared to the coating with 3 days moist curing (Fig. 5.8). It indicates that 3 days sealed curing is less efficient for a coating to retain water than 3 days moist curing.

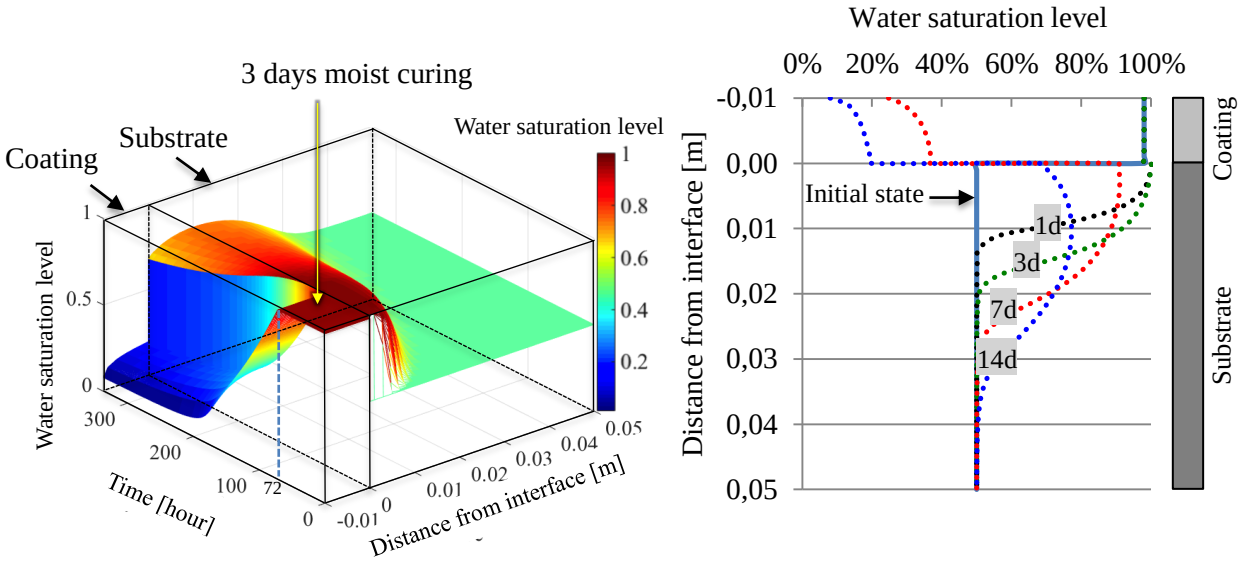

(a) 3D plot (b) 2D plot

Fig. 5.8 Calculated moisture profiles in the coating system C10-OC(s=50%)-Moist3d (Table 5.2). A 10 mm-thick coating (w/c = 0.3) is applied on substrate OC (s = 50%). Three days moist curing is applied, followed by exposure to 50% RH until 14 days.

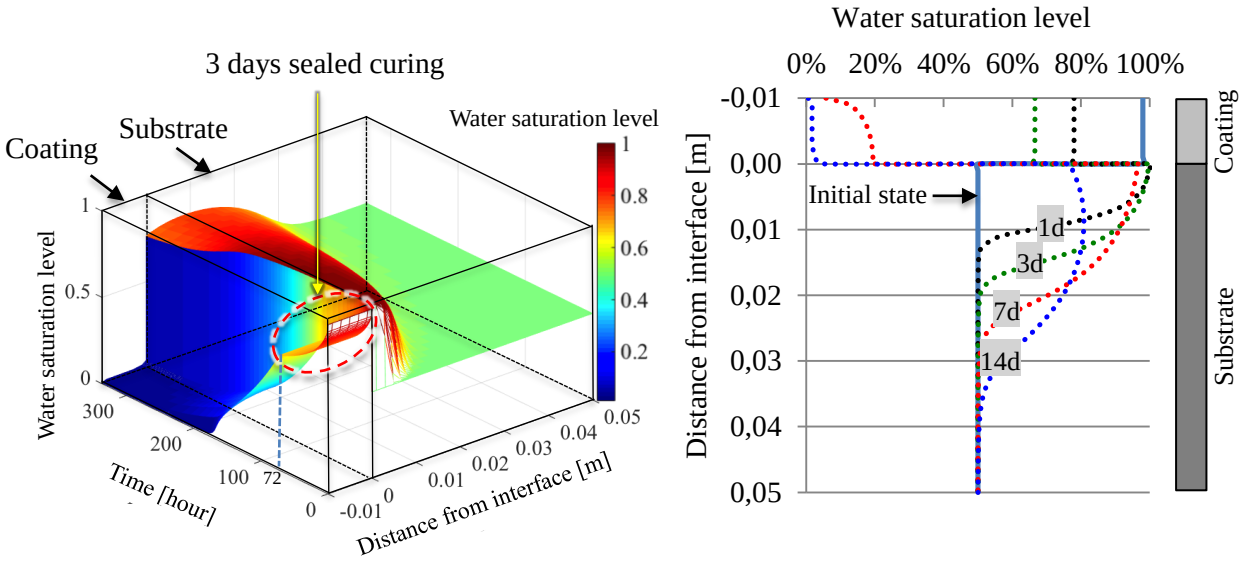

(a) 3D plot (b) 2D plot

Fig. 5.9 Calculated moisture profiles in the coating system C10-OC(s=50%)-Sealed3d (Table 5.2). A 10 mm-thick coating (w/c = 0.3) is applied on substrate OC (s = 50%). Three days sealed curing is applied, followed by exposure to 50% RH until 14 days.

2 wet-dry cycles: C10-OC(s=50%)-WetDry

In practice, alternating rainy and sunny days cause the condition of wet-dry cycles. To simulate this condition, the coating system is subjected to 2 wet-dry cycles after application of the coating. Fig. 5.10 shows the moisture profiles in the coating system. During the first wet-dry cycle, 3 days moist curing is applied to the coating system, followed by 3 days exposure to a RH of 50%. The coating remains saturated during the first 3 days. When exposed to RH = 50%, the water saturation level in the coating starts to decrease drastically. After 6 days, the water saturation level in the coating is lower than 50%, with a slight gradient over the thickness of the coating (Fig. 5.10b).

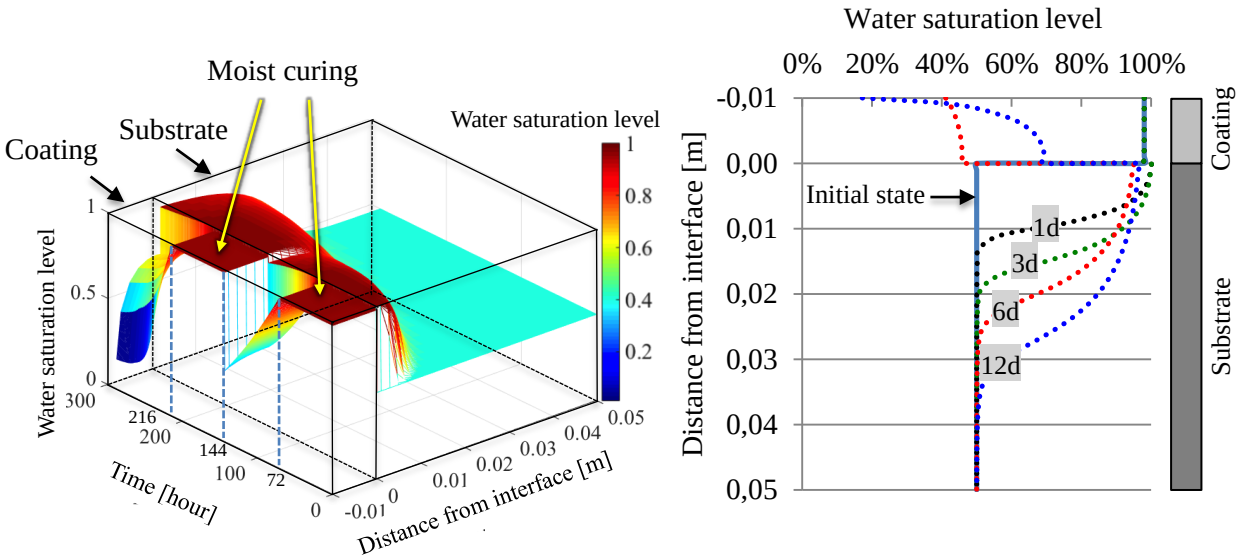

(a) 3D plot (b) 2D plot

Fig. 5.10 Calculated moisture profiles in the coating system C10-OC(s=50%)-WetDry (Table 5.2). A 10 mm-thick coating (w/c = 0.3) is applied on substrate OC ($s = 50\%$). Two wet-dry cycles are applied, followed by exposure to RH = 50% until 14 days. One wet-dry cycle consists of 3 days moist curing and 3 days curing at 50% RH.

After 6 days, the second wet-dry cycle starts (from 7-12 days). The coating becomes saturated in the wetting process (moist curing from 7-9 days, 144-216 hours). After 10 days the second drying period (10 -12 days) starts. During the second period of drying, water loss from the coating exhibits a different pattern from the first drying. A clear gradient of the water saturation level over the thickness of the coating is observed. The lowest water saturation level in the coating exists in the exposed surface of the coating (mainly due to water evaporation). The non-uniform drying of the coating can be explained by the denser microstructure that develops in the hydration process. In a denser microstructure, moisture transport becomes slower. Therefore, water loss from the exposed surface of the coating cannot be easily compensated by water from inner parts of the coating. This leads to a gradient of the water saturation level in the coating. It can be seen

from Fig. 5.10 that the water saturation level of the coating is significantly influenced by the varying curing condition (i.e., wet-dry cycle). The response of the hydration process to the wet-dry cycles will be discussed in the following section.

5.5.2.2 Evolution of water content and degree of hydration of 10 mm-thick coatings under various curing regimes (water saturation level of substrate: s = 50%)

Coatings moist-cured for 1, 3 or 7 days, followed by exposure to RH = 50%

Fig. 5.11a presents the evolution of the water content in the coatings with moist curing. The water content in a 10 mm-thick coating highly depends on the period of moist curing. With a longer period of moist curing, the water content in the coating is much higher. During the moist curing (1, 3 or 7 days), the water content in the coating is higher than that in the reference cement paste. After the coatings are exposed to RH = 50%, the water content in the coatings decreases drastically due to the water evaporation to the environment and the water absorption by the substrate, and becomes lower than that in the reference cement paste.

Fig. 5.11b presents the evolution of the DOH of coatings under moist curing. With a longer moist curing, the DOH of the coating is noticeably higher than that with a shorter moist curing.

Coatings sealed-cured for 1, 3 or 7 days, followed by exposure to RH = 50%

Fig. 5.12 presents the evolution of the water content and the DOH of various coatings. After application of the coatings, the top surfaces of the coatings were sealed. From the figure it can be seen that the coatings have lower water content than the reference cement paste. This is caused by the water absorption by the substrates. Coatings with longer sealed curing exhibit higher water content and higher DOH. Moreover, the coatings with sealed curing have lower water content and lower DOH than those with moist curing (Fig. 5.11). It shows that moist curing is essential for the hydration of coatings at early age.

Coating cured under 2 wet-dry cycles (1 cycle consists of 3 days moist curing and 3 days exposure to RH = 50%)

Fig. 5.13 presents the water content and the degree of hydration of the coating cured under wet-dry cycles. It can be seen from Fig. 5.13a that the water content of the coating is very sensitive to the wet-dry cycles. The evolution of the DOH is presented in Fig. 5.13b. The DOH of the coating material develops fast during the first period of moist curing (0-3 days). After that, the coating system is exposed to a RH of 50% (4-6 days), and the hydration process proceeds at a lower rate. When the second moist curing (7-9 days) is applied, the rate of hydration slightly increases until the second exposure to a RH of 50% (10-12 days). At 12 days, the coating cured under 2 wet-dry cycles has a similar DOH with the reference cement paste. For coatings applied on unsheltered concrete structures, moist curing is less important since the rainfall supplies water for the hydration. A short moist curing may be sufficient as long as the plastic shrinkage-induced cracking can be avoided.

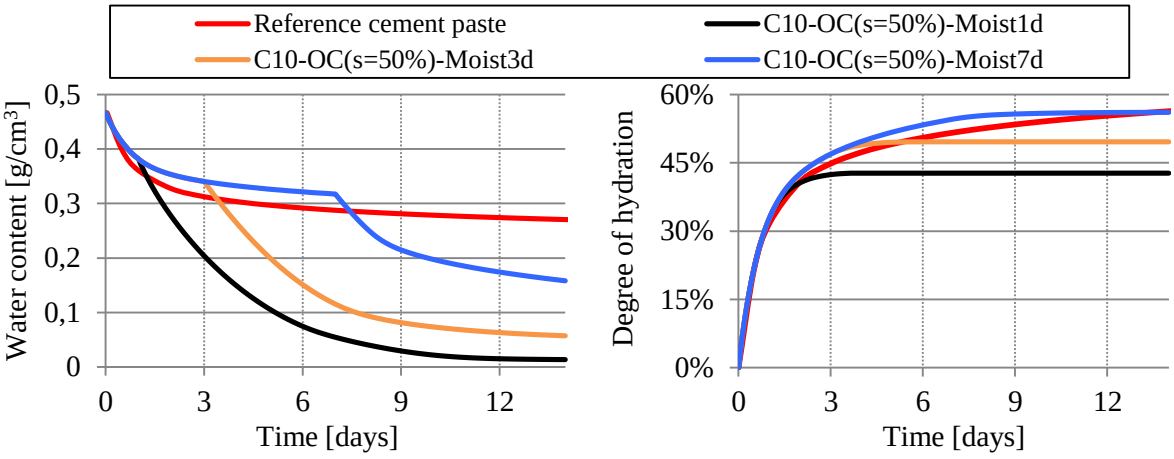

(a) Water content (b) Degree of hydration

Fig. 5.11 Calculated water content and calculated degree of hydration of the 10 mm-thick coatings (w/c = 0.3) applied on substrate OC (s = 50%), and exposed to different curing regimes (1, 3 or 7 days moist curing, followed by exposure to RH = 50% until 14 days). The reference cement paste (w/c = 0.3) is cured under sealed condition.

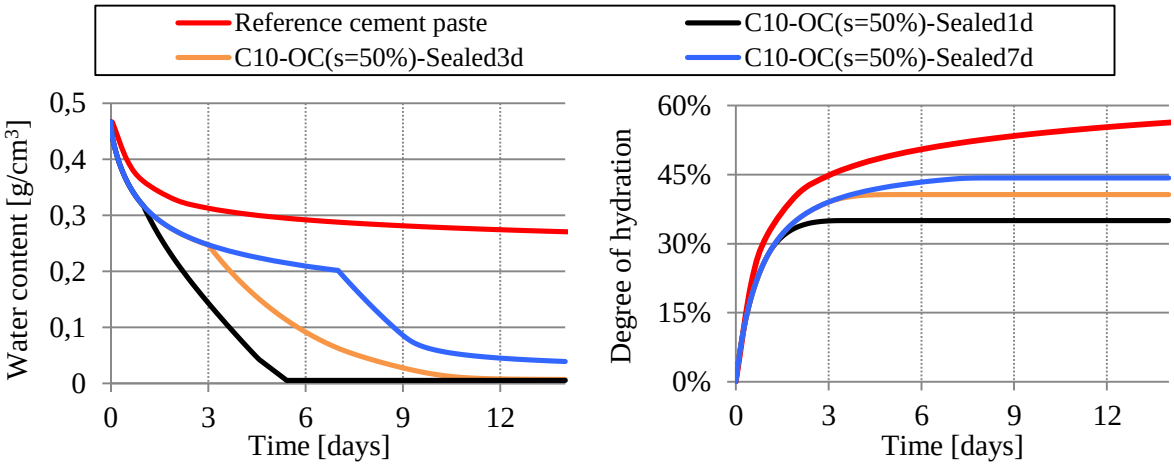

(a) Water content (b) Degree of hydration

Fig. 5.12 Calculated water content and calculated degree of hydration of the 10 mm-thick coatings (w/c = 0.3) applied on substrate OC (s = 50%), and exposed to different curing regimes (1, 3 or 7 days sealed curing, followed by exposure to RH = 50% until 14 days). The reference cement paste (w/c = 0.3) is cured under sealed condition.

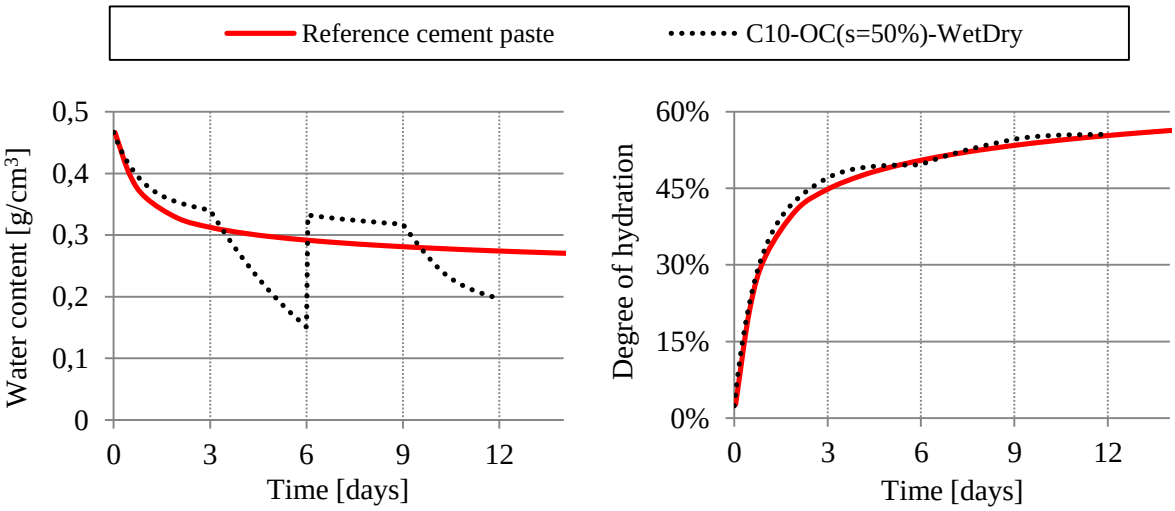

(a) Water content (b) Degree of hydration

Fig. 5.13 Calculated water content and calculated degree of hydration of the 10 mm-thick coating (w/c = 0.3) applied on substrate OC (s = 50%), and cured under 2 wet-dry cycles. One wet-dry cycle consists of 3 days moist curing and 3 days curing at 50% RH. The reference cement paste (w/c = 0.3) is cured under sealed condition.

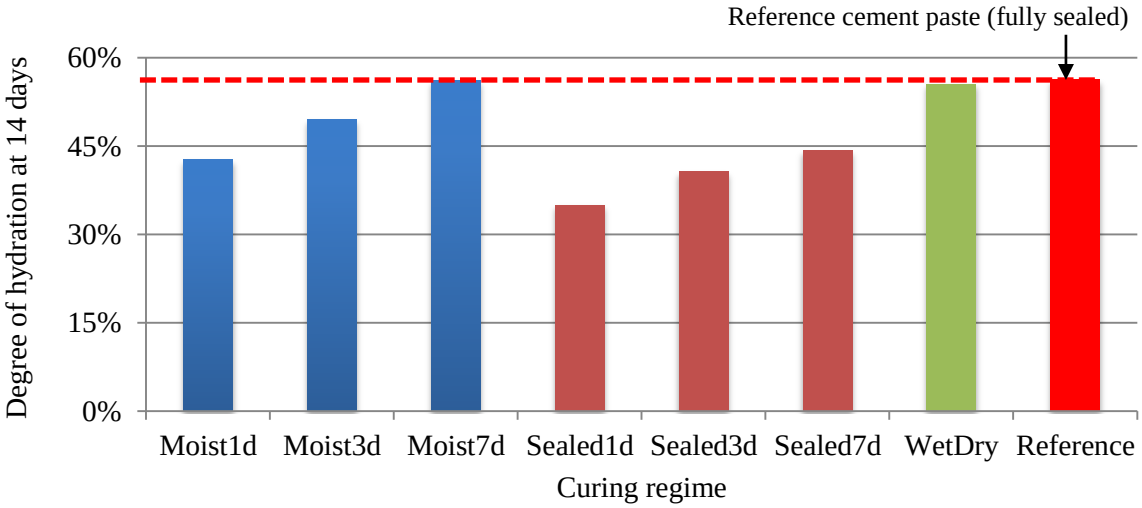

Fig. 5.14 Calculated average degree of hydration of the 10 mm-thick coatings (w/c = 0.3) at 14 days. The coatings are applied on substrate OC (s = 50%). The top surfaces of the coatings are sealed or subjected to moist curing for 1, 3 or 7 days, followed by exposure to RH = 50% until 14 days. In addition, the DOH of a coating cured under 2 wet-dry cycles is also presented (green column). The reference cement paste (w/c = 0.3) is cured under sealed condition all the time.

Fig. 5.14 presents the overview of DOH of the coatings at 14 days. The curing regime plays a critical role in the hydration of the coatings. To reach the DOH of the reference cement paste at 14 days, at least 7 days moist curing is needed. For coatings exposed to alternating rainy and sunny days (or subjected to wet-dry cycles), the hydration is less dependent on moist curing.

5.5.3 Effect of substrate type (substrate OC and substrate HPC) on moisture transport in coating systems and on the hydration of 10 mm-thick coatings

In previous sections (5.5.1 and 5.5.2), ordinary concrete (standard substrate OC, s = 50%) is used. To investigate the influence of initial water content of the substrates on the hydration of the coating material, moisture transport in coating systems with a saturated concrete (substrate OC, s = 100%) is simulated. Moreover, the influence of the absorptivity of the substrates on the hydration of the coating material is also investigated. Moisture transport in coating systems with a high performance concrete (substrate HPC, s = 77%) is simulated.

5.5.3.1 Evolution of water content and degree of hydration of the coatings applied on substrate OC (s = 50% or s = 100%)

Fig. 5.15 presents the evolution of the water content and the DOH of the coatings applied on ordinary concrete (standard substrate OC with s = 50%, or saturated substrate OC with s = 100%). The curves of the water content (Fig. 5.15a) and the DOH (Fig. 5.15b) of the coatings applied on standard substrate OC or saturated substrate OC are close to each other. It indicates that the initial water content of the substrates only plays a minor role in the water content and the DOH of the coatings if moist curing is applied. Obviously, the water loss of the coating at early ages due to water absorption by the substrates is almost completely compensated by the moist curing. The influence of water absorption by the substrate on hydration of coatings under sealed curing will be studied in section 5.5.3.2.

5.5.3.2 Evolution of water content and degree of hydration of the coatings applied on substrate OC (s = 50%) or substrate HPC (s = 77%)

In this section, the influence of the type of substrates on the change of water content and on the DOH of the coatings is studied. The 10 mm-thick coatings (w/c = 0.3) are applied on ordinary concrete (substrate OC, s = 50%) or high performance concrete (substrate HPC, s = 77%). Moist or sealed curing (1, 3 or 7 days) is applied to the coatings, followed by exposure to RH = 50% until 14 days.

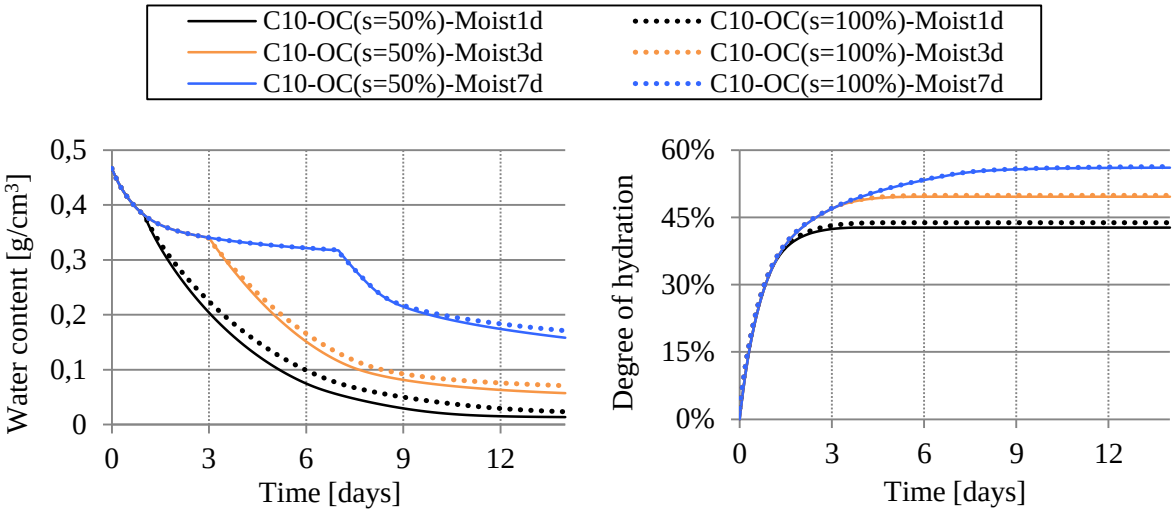

(a) Water content (b) Degree of hydration

Fig. 5.15 Calculated evolution of water content (a) and degree of hydration (b) of the 10 mm-thick coatings (w/c = 0.3). The coatings are applied on substrate OC (s = 50%, or s = 100%). Moist curing (1, 3 or 7 days) is applied, followed by exposure to RH = 50% until 14 days. The reference cement paste (w/c = 0.3, no substrate) is cured under sealed condition.

Top surfaces of the coatings, moist-cured for 1, 3 or 7 days, followed by exposure to RH = 50%
Fig. 5.16 presents the evolution of the water content and the DOH of the coatings applied on substrate OC or substrate HPC. The top surfaces of the coatings are subjected to moist curing for 1, 3 or 7 days, followed by exposure to RH = 50%. The simulated curves of water content and DOH of the coating materials applied on different substrates almost coincide, indicating that the type of the substrates play only a minor role in the evolution of water content and the DOH of the coatings, even through substrate OC and substrate HPC have different characteristics (Table 5.1). Explanation will be given in section 5.5.4.

Top surfaces of the coatings, sealed for 1, 3 or 7 days, followed by exposure to RH = 50%
Fig. 5.17a presents the evolution of the change of water content of the coatings applied on substrate OC or substrate HPC. The top surfaces of the coatings are sealed for 1, 3 or 7 days, followed by exposure to RH = 50%. The coatings applied on substrate OC have higher water content compared to those applied on substrate HPC. The difference is attributed to the water absorption by different substrates. When sealed curing is applied, the water loss of the coatings due to absorption by the substrate cannot be compensated and has a noticeable influence on water content in the coatings. As seen from Fig. 5.17b, the coatings applied on substrate OC have a lower DOH compared to those applied on substrate HPC, because substrate OC absorbs higher amounts of water from the coatings compared to substrate HPC.

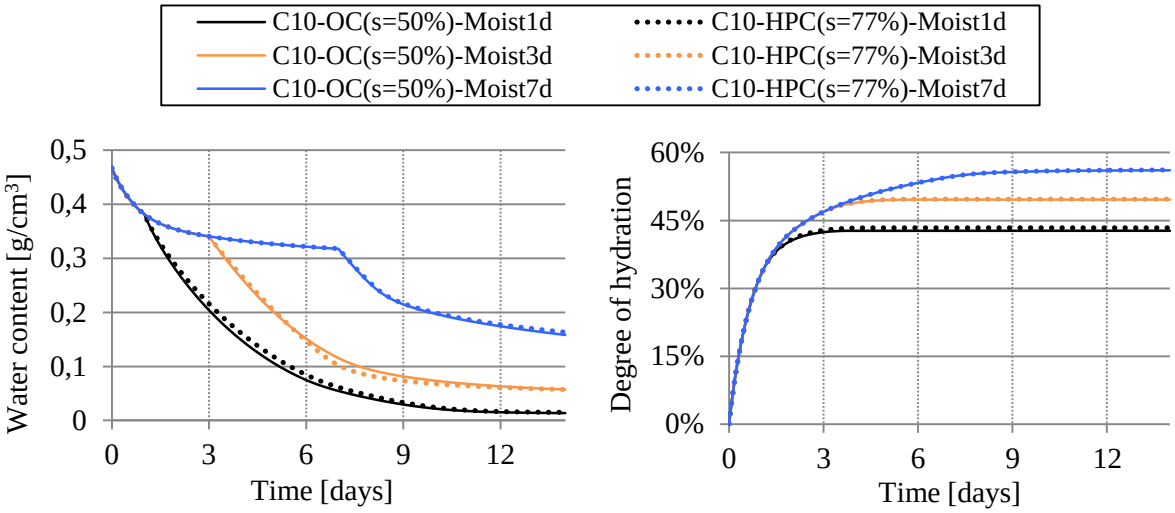

(a) Water content (b) Degree of hydration

Fig. 5.16 Calculated evolution of water content (a) and degree of hydration (b) of the coatings. The coatings (10 mm-thick, w/c = 0.3) are applied on substrate OC (s = 50%) or substrate HPC (s = 77%). The coatings are moist-cured for 1, 3 or 7 days, followed by exposure to RH = 50% until 14 days.

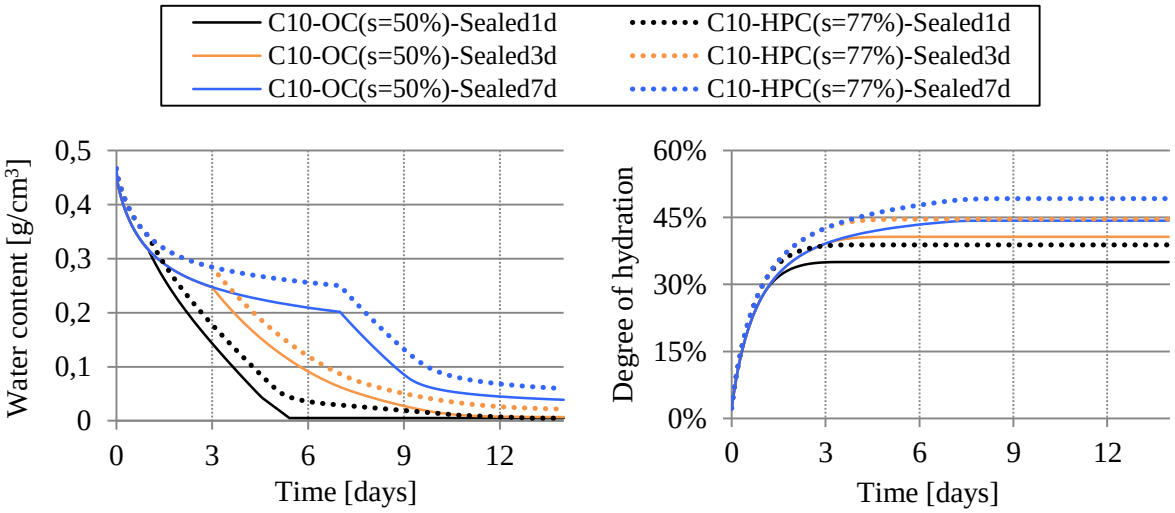

(a) Water content (b) Degree of hydration

Fig. 5.17 Calculated evolution of water content (a) and degree of hydration (b) of the coatings. The coatings (10 mm-thick, w/c = 0.3) are applied on substrate OC (s = 50%) or substrate HPC (s = 77%). The coatings are sealed-cured for 1, 3 or 7 days, followed by exposure to RH = 50% until 14 days.

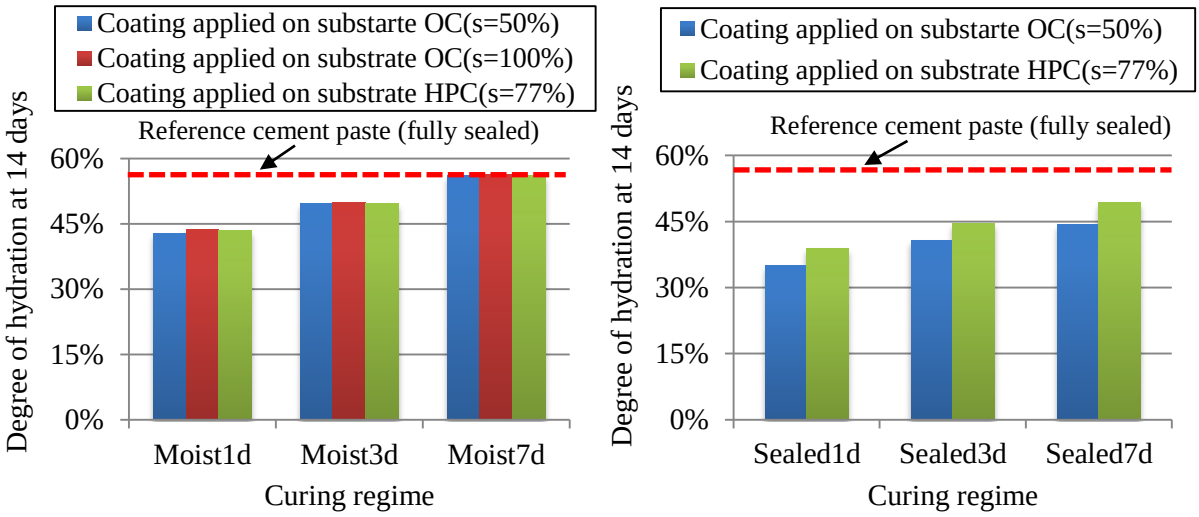

(a) Moist curing for 1, 3 or 7 days (b) Sealed curing for 1, 3 or 7 days

Fig. 5.18 Calculated average degree of hydration at 14 days of the 10 mm-thick coatings (w/c = 0.3) applied on different substrates (OC with s = 50%, OC with s = 100% and HPC with s = 77%). The coatings are moist/sealed cured for 1, 3 or 7 days, followed by exposure to RH = 50% until 14 days. The reference cement paste (w/c = 0.3, no substrate) is cured under sealed condition.

Fig. 5.18 shows the DOH of the coatings at 14 days. The coatings are applied on different substrates (substrate OC with s = 50% or s = 100%, substrate HPC with s = 77%) and cured under different regimes (1, 3 or 7 days moist/sealed curing). It can be seen from Fig. 5.18a that the hydration of the coatings is very sensitive to the period of moist curing (1, 3 or 7 days), but not sensitive to the initial water content of the substrates or to the type of the substrates. As shown in Fig. 5.18b, in case of sealed curing the hydration of the coating is sensitive to both the type of the substrate and the period of sealed curing.

5.5.4 Investigation of water loss of the coating materials

To further investigate the role of the substrates on the hydration of the coatings, water loss of the coatings applied on different substrates (OC with s = 50% and HPC with s = 77%) is calculated and discussed. The water loss of the coating includes the amounts of evaporated water, water absorbed by the substrate and water consumed by hydration. The remaining water in the coating material available for hydration is also calculated and discussed.

5.5.4.1 Water loss of the 10 mm-thick coatings applied on different substrates (OC and HPC) - 3 days moist curing, followed by exposure to RH = 50%

The water loss of the 10 mm-thick coating applied on an ordinary concrete substrate (substrate OC) is elaborated first. After application of the coating, 3 days moist curing is

applied. Fig. 5.19 shows the average water saturation level s of the coating. During 3 days moist curing, the coating remains saturated. After the coating system is exposed to the 50% RH, the water saturation level of the coating gradually drops due to evaporation of water to the environment.

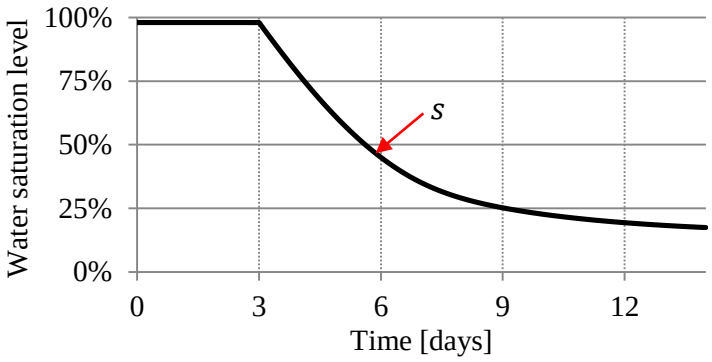

Fig. 5.19 Calculated average water saturation level of the coating material in C10-OC(s=50%)-Moist3d. A 10 mm-thick coating (w/c = 0.3) is applied on substrate OC(s=50%). Three days moist curing is applied, followed by exposure to RH = 50% until 14 days.

In the coating material, the water content θ is calculated as the sum of capillary water and gel water. As described in section 4.5, only capillary water is available for the hydration of cement, while water in gel pores of C-S-H doesn't contribute to hydration. Description of the mechanism is given in section 3.3.3. The amount of capillary water $\theta_{cap}(t)$ changes during the hydration process and can be calculated with:

$$\theta_{cap}(t) = \rho_w \cdot \left(\phi(t) \cdot s(t) - \phi_{gel}(t)\right) \tag{5.2}$$

where ρ_w is the density of water, $\phi(t)$ is the porosity of the coating (calculated with Eq. (4.28)), $s(t)$ is the water saturation level and $\phi_{gel}(t)$ is the gel porosity (calculated with Eq. (4.27)).

The evolution of the porosity of the coating material is plotted in Fig. 5.20a. As the hydration proceeds, the total porosity and the capillary porosity decrease over time (mainly within 3 days), while the gel porosity increases.

Fig. 5.20b shows the total water content and the capillary water content of the coating material. As the hydration proceeds, pores become gradually filled up with hydration products. Accordingly, the amount of capillary water available for the hydration decreases. The coating has lost all the capillary water after 6.5 days, and no capillary water is left for further hydration. Water in large gel pores hardly contributes to the hydration. However, drying of the coating still proceeds, by losing part of its gel water from larger gel pores. The drying of the coating in the coating system is indicated by the decrease of total water content θ.

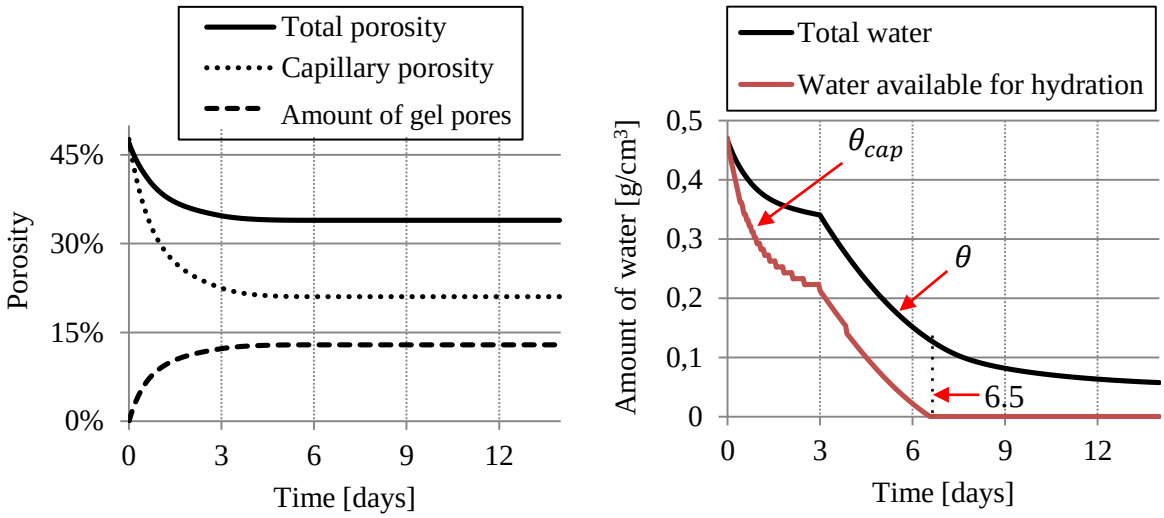

(a) Porosity of coating material

(b) Water content in coating material

Fig. 5.20 Calculated evolution of porosity and water content of the coating in C10-OC(s=50%)-Moist3d. A 10 mm-thick coating (w/c = 0.3) is applied on substrate OC. Three days moist curing is applied, followed by exposure to RH = 50% until 14 days.

5.5.4.2 Comparison of water loss of the 10 mm-thick coatings applied on different substrates (OC and HPC) - 3 days moist curing

As presented in Fig. 5.18a, when moist curing is applied, the coatings on different substrates (OC with s = 50% and HPC with s = 77%) exhibit a similar DOH, when moist curing (1, 3 or 7 days) is applied. To explain this phenomenon, the water loss from the coatings are categorized, viz. water evaporation to the environment and water absorption by the substrate. The coatings are applied on substrate OC (s = 50%) or substrate HPC (s = 77%), and moist-cured for 3 days. Fig. 5.21 shows the water loss from the coatings, together with the amount of water consumed by hydration.

After application of the coating, the substrates immediately absorb water from the coatings (red lines). Substrate OC absorbs a much higher amount of water (Fig. 5.21a) compared to substrate HPC (Fig. 5.21b). After 3 days moist curing, the coating systems are exposed to 50% RH. Water starts to evaporate from the coatings to the environment (blue lines). After 6 days, the substrates stop absorbing water from the coating and start losing water. The water loss of the substrates is caused by water extraction by the coatings (see Fig. 5.8).

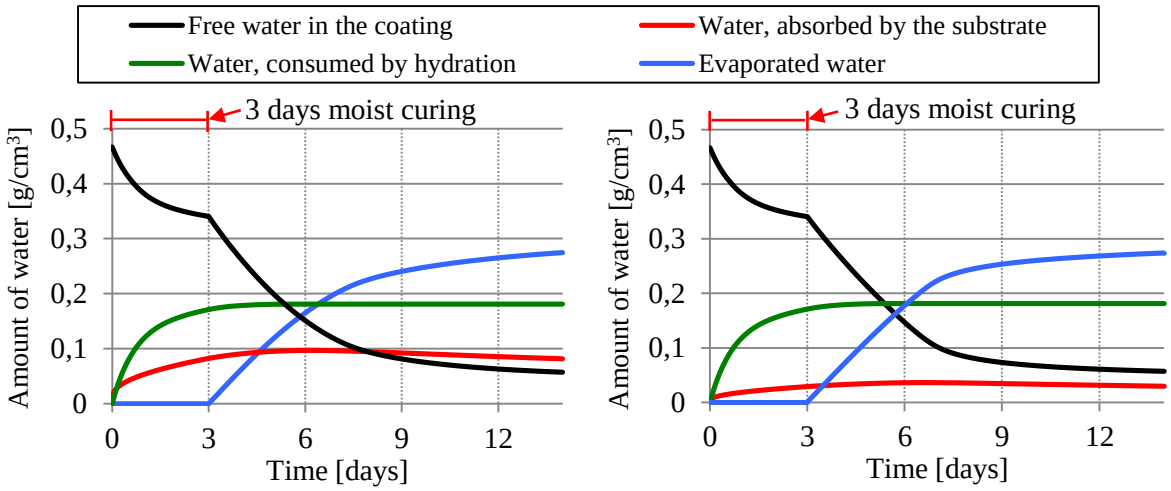

(a) C10-OC(s=50%)-Moist3d (b) C10-HPC(s=77%)-Moist3d

Fig. 5.21 Calculated water loss of the coatings applied on different substrates. The 10 mm-thick coatings are applied on ordinary concrete (substrate OC) or a high performance concrete (substrate HPC). Three days moist curing is applied, followed by an exposure to RH = 50% until 14 days.

Both the water absorption by the substrates and the evaporation of capillary water may affect the hydration process of the coatings. It can be seen from Fig. 5.21 that the curves for the free water of the two coatings are similar to each other and almost identical. It also applies for the curves for the water consumed by hydration as well as the curves for the evaporated water. Clear difference can be seen from the curves for the amount of water absorbed by the substrates. The absorption by the substrate mostly takes place during 3 days moist curing. However, the water absorption by the substrate can hardly affect the hydration of the coatings, because the coatings remain saturated during moist curing. After 3 days moist curing the dominant factor of water loss of the coatings is water evaporation, while the water absorption by the substrates plays only a minor role. It explains why the coatings applied on different substrates (i.e. OC and HPC) have a similar DOH when 3 days moist curing is applied.

5.5.5 Overview of the simulated DOH of the coatings at 14 days

Table 5.3 presents an overview of the DOH of the coating materials in various coating systems. It can be seen that the initial water content of the substrates and the type of the substrate have only a marginal effect on the DOH of the coatings. The most influencing factor of the DOH of the coatings appears to be the curing regime. Moist curing is much more efficient than sealed curing. With longer moist curing (e.g. 7 days), the DOH of the coating at 14 days is close to that of the reference cement paste cured under sealed condition. Therefore, a long moist curing is essential for the hydration of the coatings.

Table 5.3 Calculated degree of hydration and calculated capillary porosity of the coating materials at 14 days after application.

	Coating thickness	Substrate and water saturation level	Curing regime ($T = 20$°C)	Degree of hydration
Reference cement paste			Sealed condition	56.3%
C06-OC(s=50%)-Moist1d	6 mm	OC, s = 50%	1 day moist + 13 days 50% RH	40.3%
C20-OC(s=50%)-Moist1d	20 mm	OC, s = 50%	1 day moist + 13 days 50% RH	46.6%
C10-OC(s=50%)-Moist1d	10 mm	OC, s = 50%	1 day moist + 13 days 50% RH	42.8%
C10-OC(s=100%)-Moist1d	10 mm	OC, s = 100%	1 day moist + 13 days 50% RH	43.8%
C10-HPC(s=77%)-Moist1d	10 mm	HPC, s = 77%	1 day moist + 13 days 50% RH	43.4%
C10-OC(s=50%)-Moist3d	10 mm	OC, s = 50%	3 days moist + 11 days 50% RH	49.6%
C10-OC(s=100%)-Moist3d	10 mm	OC, s = 100%	3 days moist + 11 days 50% RH	49.9%
C10-HPC(s=77%)-Moist3d	10 mm	HPC, s = 77%	3 days moist + 11 days 50% RH	49.7%
C10-OC(s=50%)-Moist7d	**10 mm**	**OC, s = 50%**	**7 days moist + 7 days 50% RH**	**56.1%**
C10-OC(s=100%)-Moist7d	**10 mm**	**OC, s = 100%**	**7 days moist + 7 days 50% RH**	**56.3%**
C10-HPC(s=77%)-Moist7d	**10 mm**	**HPC, s = 77%**	**7 days moist + 7 days 50% RH**	**56.2%**
C10-OC(s=50%)-Sealed1d	**10 mm**	**OC, s = 50%**	**3 days sealed +11 days 50% RH**	**35.0%**
C10-HPC(s=77%)-Sealed1d	**10 mm**	**HPC, s = 77%**	**3 days sealed +11 days 50% RH**	**38.9%**
C10-OC(s=50%)-Sealed3d	10 mm	OC, s = 50%	3 days sealed +11 days 50% RH	40.7%
C10-HPC(s=77%)-Sealed3d	10 mm	HPC, s = 77%	3 days sealed +11 days 50% RH	44.6%
C10-OC(s=50%)-Sealed7d	10 mm	OC, s = 50%	3 days sealed +11 days 50% RH	44.3%
C10-HPC(s=77%)-Sealed7d	10 mm	HPC, s = 77%	3 days sealed +11 days 50% RH	49.2%
C10-OC(s=50%)-WetDry	10 mm	OC, s = 50%	2 wet-dry cycles (see Fig. 5.4)	55.6%

Note: The bold texts show the coating material with the highest and the lowest values of the DOH. A long moist curing (e.g. 7 days) appears to be very important for the hydration of the coating material. One day sealed curing cannot ensure a proper hydration of the coating material.

5.6 Probability of drying shrinkage-induced cracking

After moist curing, the coating system is usually subjected to drying. Water starts to evaporate from the coating to the environment. Meanwhile, moisture exchange takes place between the coating and the substrate. Consequently, differential drying shrinkage of the coating and the substrate develops over time, which increases the probability of cracking of the coating material. A preliminary study is conducted to calculate the drying shrinkage-induced stress in the coating material, and to evaluate the probability of cracking of the coating. Some assumptions are made below:

– The coating materials are fully restrained (the coating is much thinner than the substrate).
– The moisture distributes uniformly across the thickness of the coatings.
– Only elastic deformation of the coating is considered; relaxation of stress is ignored.

Fig. 5.22 schematically shows the development of tensile strength $f_t(t)$ and drying shrinkage-induced stress $\sigma(t)$ of the coating material. In this figure the Gaussian distributions of $f_t(t)$ and $\sigma(t)$ are also shown.

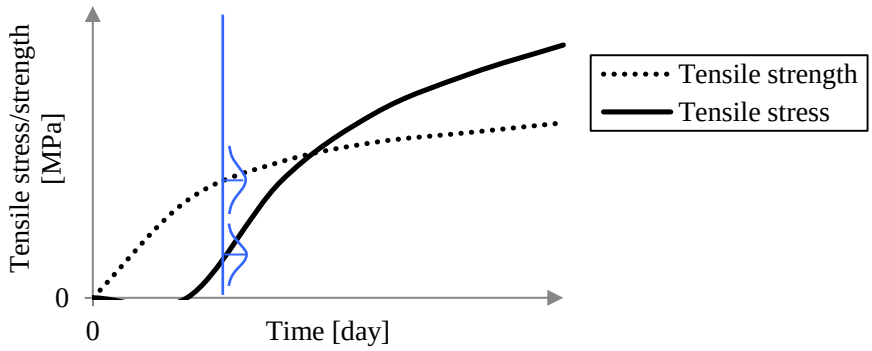

Fig. 5.22 Schematic illustration of the development of tensile strength $f_t(t)$ and drying shrinkage-induced stress $\sigma(t)$ of the coating material. $f_t(t)$ and $\sigma(t)$ have a Gaussian distribution with a standard deviation of $0.08 \cdot f_t(t)$ and $0.08 \cdot \sigma_t(t)$, respectively.

Cracking of the coating occurs when the shrinkage-induced stress $\sigma(t)$ exceeds the tensile strength $f_t(t)$. Assuming that the tensile strength $f_t(t)$ follows a Gaussian distribution, the probability of cracking of the coating, $\Phi(t)$, is calculated as [154]:

$$\Phi(t) = \frac{1}{s_{sd}(t) \cdot \sqrt{2\pi}} \cdot \int_{-\infty}^{X(t)} e^{-\frac{(X(t))^2}{2 \cdot (s_{sd}(t))^2}} d(X(t)) \tag{5.3}$$

where $X(t) = \sigma(t) - f_t(t)$, $s_{sd}(t)$ is the standard deviation of $X(t)$. $s_{sd}(t)$ is calculated with $s_{sd}(t) = 0.08 \cdot \sigma_t(t) + 0.08 \cdot f_t(t)$.

5.6.1 Calculation of mechanical properties of the coating

5.6.1.1 Development of tensile strength of the coating

To calculate the probability of drying shrinkage-induced cracking, the evolution of the tensile strength of the coating and the shrinkage-induced stress in the coating need to be calculated.

According to Neville [155], the tensile strength $f_t(t)$ of cementitious material can be calculated from the compressive strength $f_c(t)$ at time t:

$$f_t(t) = 0.23 \cdot f_c(t)^{0.67} \tag{5.4}$$

The compressive strength $f_c(t)$ of the coating is determined by the microstructure of cementitious materials, and has been calculated using HYMOSTRUC3D model [8, 156]. The methodology to determine the compressive strength is also adopted in this thesis.

5.6.1.2 Drying shrinkage-induced tensile stress in the fully restrained coating

According to Mindess et al. [102], capillary tension is an effective mechanism of drying shrinkage when the internal relative humidity of the material is higher than 45%. The free drying shrinkage strain $\varepsilon(t)$ of the coating can be calculated with [157]:

$$\varepsilon(t) = \frac{s(t) \cdot p(t)}{3} \cdot \left(\frac{1}{K_p(t)} - \frac{1}{K_s} \right) \tag{5.5}$$

where $\mathrm{s}(t)$ is the water saturation level, $p(t)$ [MPa] is the capillary tension in pore water. $p(t)$ is calculated with Eq. (3.12) based on the water saturation level $\mathrm{s}(t)$. K_p [MPa] is the bulk modulus of coating material, and K_s [MPa] is the bulk modulus of the solid material in the coating (taken as 44,000 MPa [158]).

The bulk modulus $K_p(t)$ of the coating material is described as:

$$K_p(t) = \frac{E_p(t)}{3 \cdot (1 - 2\upsilon_p)} \tag{5.6}$$

where $E_p(t)$ is the elastic modulus of coating material at time t, υ_p the Poisson's ratio (taken as 0.2 [159]).

The elastic modulus $E_p(t)$ of coating material is determined by the capillary porosity ϕ_{cap} (calculated with Eq. (4.19)) [160]:

$$E_p(t) = 46.03 \cdot \left(1 - \phi_{cap}(t)\right)^{3.16} \tag{5.7}$$

The drying shrinkage (elastic deformation) induced-stress $\sigma(t)$ can be calculated:

$$\sigma(t) = E(t) \cdot \varepsilon(t) \tag{5.8}$$

5.6.2 Case study of drying shrinkage-induced cracking

5.6.2.1 Evaluation of the probability of shrinkage-induced cracking using simulation results of this study

Two coating systems are chosen to study the probability of drying shrinkage-induced cracking of the coating materials. The 10 mm-thick coatings (w/c = 0.3) are applied on substrate OC (s = 50%). The two coatings are moist-cured for 3 and 7 days, respectively. After the moist curing, the coatings are exposed to 50% = RH until 56 days. The evolution of the DOH and the water saturation level of the coatings are presented in Fig. 5.23.

Based on the simulated DOH and water saturation level, the shrinkage-induced stress in the coatings is calculated using Eq. (5.5)-(5.8). Fig. 5.24 shows the evolution of calculated shrinkage-induced stress in the coatings, together with the evolution of the tensile strength (calculated with Eq. (5.4)). The tensile strength develops fast at early ages, and remains constant at later ages due to the ceased hydration process. The drying shrinkage-induced stress increases continuously until 56 days. In the two coating systems shown in Fig. 5.24, the shrinkage-induced stress exceeds the tensile strength at 25 days and 29 days for the coating materials with 3 days and 7 days moist curing, respectively.

The probability of cracking of the coating $\Phi(t)$ is presented in Fig. 5.25. It can be seen that the coating with longer moist curing has lower probability of cracking $\Phi(t)$ at early ages (e.g. before 30 days) and higher probability at later ages (e.g. after 30 days). The higher probability of cracking for the coating material with a longer moist curing is in accordance with the experimental work on concrete by Samouh et al. [161]. They reported a higher drying shrinkage of the concrete with a longer sealed curing. The case study suggests that long moist curing is beneficial to reduce the probability of early-age cracking induced by drying shrinkage. However, measures should be taken to deal with the shrinkage-induced cracking of the coatings at later age, e.g. by using polymeric fibers [19]. It has to be pointed out that in the case study only elastic deformation is considered. In practice, relaxation of shrinkage-induced stress will reduce the stress in the coating material. The relaxation of tensile stress is substantial for cement-based materials at early ages [162]. Therefore, the drying shrinkage-induced stress in the coating calculated with Eq. (5.8) is an overestimation. For a detailed analysis of the probability of cracking relaxation should be taken into account. This section presents preliminary study of the sensitivity of the probability of cracking for coatings cured under different conditions.

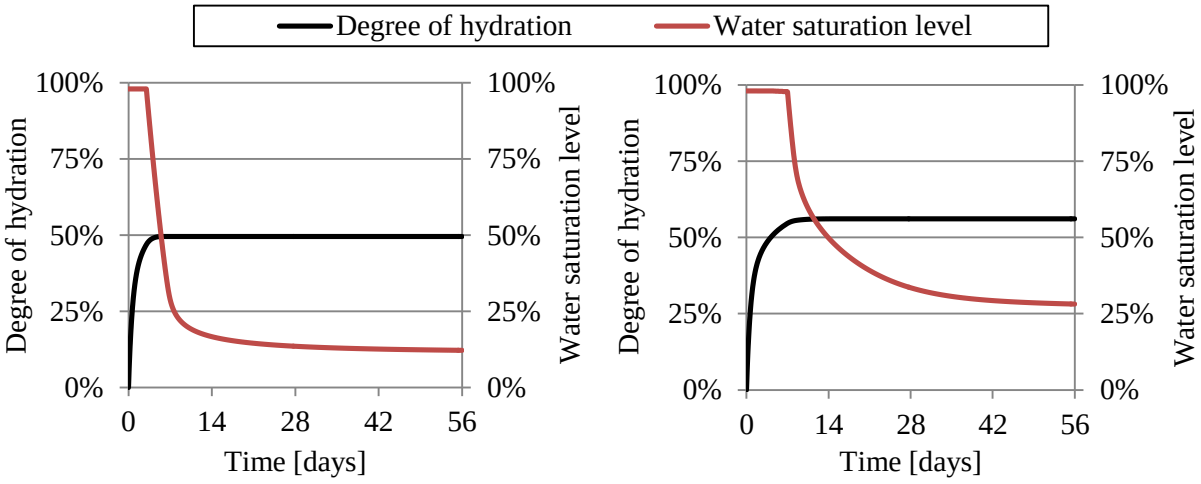

(a) C10-OC(s=50%)-Moist3d (b) C10-OC(s=50%)-Moist7d

Fig. 5.23 Evolution of the calculated DOH and the calculated water saturation level of the coatings. The 10 mm-thick coatings (w/c = 0.3) are applied on substrate OC (s = 50%), and moist-cured for 3 or 7 days, followed by exposure to 50% RH until 56 days.

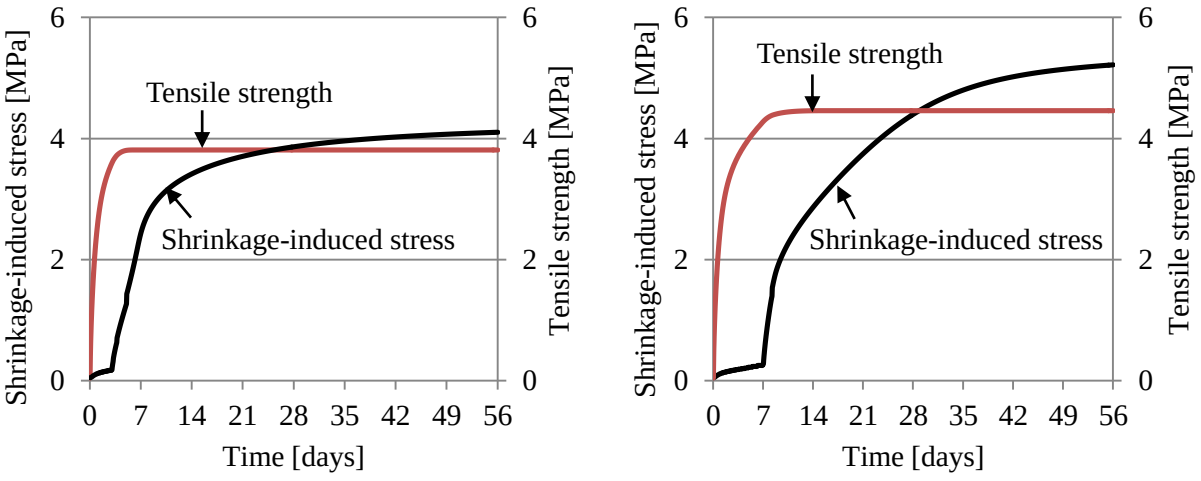

(a) C10-OC(s=50%)-Moist3d (b) C10-OC(s=50%)-Moist7d

Fig. 5.24 Calculated shrinkage-induced stress in the coatings. The 10 mm-thick coatings (w/c = 0.3) are applied on substrate OC (s = 50%), and moist-cured for 3 or 7 days, followed by exposure to 50% RH until 56 days.

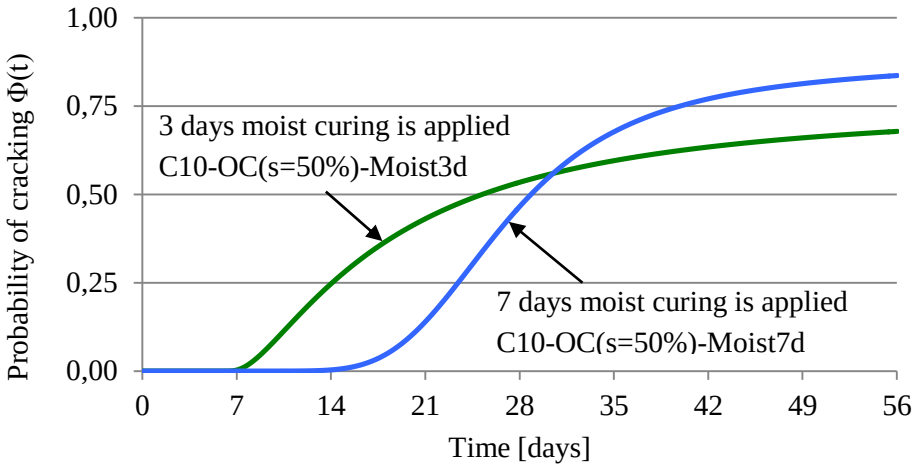

Fig. 5.25 Calculated index of drying shrinkage-induced cracking of the coatings. The 10 mm-thick coatings (w/c = 0.3) are applied on substrate OC (s = 50%), and moist-cured for 3 or 7 days, followed by exposure to 50% RH until 14 days. The probability of cracking is caculated based on the curves presented in Fig. 5.24.

5.6.2.2 Comparison between development of drying-shrinkage induced stress and development of strength with simplified current procedure

For the design of a coating, the evolution of tensile strength of the coating material may be calculated assuming that the coating material is fully sealed or saturated, as shown in Fig. 5.26. This figure indicates that the shrinkage-induced stress in the coating material will not exceed the calculated tensile strength, contrary to the information presented in Fig. 5.24. In this chapter, the evolution of tensile strength of the coating material is calculated considering the water absorption by the substrate and water evaporation to the environment, and is therefore more practical.

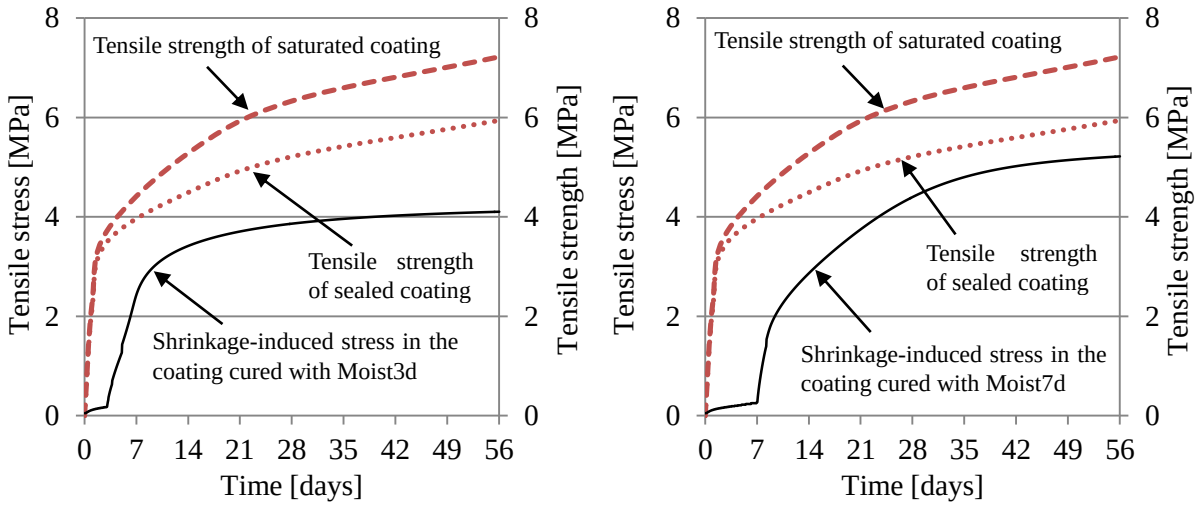

(a) C10-OC(s=50%)-Moist3d (b) C10-OC(s=50%)-Moist7d

Fig. 5.26 Calculated shrinkage-induced stress in the coatings. The 10 mm-thick coatings (w/c = 0.3) are applied on substrate OC (s = 50%), and moist-cured for 3 or 7 days, followed by exposure to 50% RH until 56 days. This figure shows a comparison of the tensile stress induced by drying with the tensile strength. The tensile strength is calculated assuming that the coating material is fully sealed or saturated.

5.7 Conclusion

By implementing the Moisture-Hydration model proposed in chapter 3, moisture transport in various coating systems is simulated in this chapter. During the moisture transport, the hydration process of the coating is explicitly taken into account, which is influenced by the water absorption of the substrates or the curing regimes. The evolution of the degree of hydration and the evolution of the water content of the coatings are determined. Based on the simulation results, the probability of drying shrinkage-induced cracking is studied. The following conclusions can be drawn:

- Among the effects of the evaluated parameters (i.e. the coating thickness, the duration of moist/sealed curing conditions, the initial water content of the substrates and the type of the substrates), the duration of moist curing is the parameter that affects the hydration of the coating materials the most.
- If moist curing is applied, the influence of initial water content of the substrates and the type of the substrates on the hydration of the coating is relatively low. The influence of the type of the substrate on the hydration of the coating becomes noticeable when sealed curing is applied.

– Longer moist curing is essential to compensate for water absorption by the substrates, and for ensuring a proper hydration process of the coating. With 7 days moist curing, the DOH of the coating at 14 days is comparable with or higher than the DOH of a reference cement paste cured under sealed condition. Longer moist curing is also beneficial for reducing the probability of early-age cracking induced by drying shrinkage. However, the probability of cracking is increased for coating materials at later ages. Measures should be taken to deal with the shrinkage-induced cracking of coatings at later ages, e.g. by using polymeric fibers. Note that the calculation of the probability of cracking of the coating is preliminary. Relaxation of the drying shrinkage-induced stress is not considered in the calculation. This will lead to an overestimation of the probability of shrinkage-induced cracking of the coating. Further study of the effect of relaxation on the probability of drying shrinkage-induced cracking is recommended.

Chapter 6

Numerical study on chloride ingress in cementitious coating systems and evaluation of effectiveness of coatings

6.1 Introduction

Transport of moisture and chemical substances (e.g. Cl^- and SO_4^{2-}) in cementitious materials are critical for the durability of the materials. Chloride ingress in a porous material is highly dependent on the microstructure of the material and the moisture content [163]. In chapter 5 we have seen that the curing condition is the most important factor for the continuation of hydration process of the coating materials. In this chapter, coatings are cured under saturated condition. The substrate is also considered saturated. The chloride transport in hydrating cementitious coating systems (Fig. 6.1) is simulated, taking into account the time-dependent properties, viz. porosity, chloride diffusivity and chloride binding capacity of the hydrating coating and the hydrating substrate.

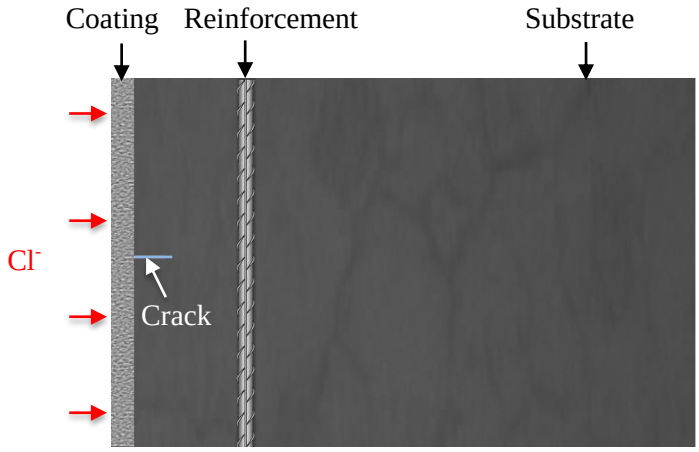

Fig. 6.1 Schematic illustration of chloride ingress into a cementitious coating system. The coating is applied on a cracked concrete substrate.

To determine the time-dependent chloride binding capacity of the coating and the substrate, the degree of hydration and the porosity of the coating and the substrate are calculated according to the procedures presented in chapter 4. Besides, the porosity of both the coating and the substrate also plays an important role in the chloride flux through the

coating-substrate interface. In the simulation, attention is paid to the mass conservation of the chloride ions in the coating-substrate interface.

The coatings are made of cement pastes and applied on different concrete substrates (i.e. substrates with different ages, with or without surface crack). Factors considered in the simulation of the chloride transport are the composition of the coating, the thickness of the coating, early or late application of the coating, time of failure of the coating, and presence of surface crack in the substrate. Compared to the crack-free substrates, cracked substrates may have a more urgent need of a coating, because the cracks allow a rapid penetration of the chloride ions into the concrete structure [164, 165]. A coating can be applied to bridge the crack and to prevent the cracked substrate against rapid chloride ingress. Therefore, chloride transport in coating systems with cracked substrate structures is also studied (the coatings are crack-free). Description of the parameters is listed in Table 6.1.

Table 6.1 Factors considered in the numerical simulation.

Parameters	Description
w/c of the coating	Cement paste with a w/c of 0.3, 0.4 or 0.5
Thickness of the coating	The coating thickness is 3, 6 or 10 mm
Early or late application of the coating	The coatings are applied on young substrates, or on old substrates that have been exposed to chloride environment for 5, 10 or 20 years
Time of failure of the coating	The coating fails at 5, 10 or 20 years after application
Crack depth of the concrete substrate	The substrate is crack-free, or has a surface crack with a size of 0.4×10 mm^2 0.4×15 mm^2 or 0.4×20 mm^2

A commercial FEM software COMSOL Multiphysics [166] is used to perform the simulation of chloride transport in uncoated and coated concrete structures. Based on the simulated profiles of free chloride, the time needed for reaching a critical chloride concentration at the steel reinforcement is determined. This time, $T_{corrosion}$, also corresponds to the time until initiation of reinforcement corrosion in the concrete structures. According to the published data, the critical chloride concentration for the initiation of reinforcement corrosion falls within a broad range (0.045 to 3.22 moles of free chloride per liter of pore solution) [91]. In this chapter the critical chloride concentration in the pore solution is chosen to be 0.2 mol/L. The study of chloride transport in the coating systems gives guidance for the design and the application of coatings for concrete structures that have an unsatisfactory resistance to chloride ingress.

6.2 Mechanisms of chloride ingress in hydrating coating systems

6.2.1 Chloride transport in hydrating cementitious materials

The total chloride content in cementitious materials consists of free chloride and bound chloride. The total chloride content is commonly expressed relative to the weight of cement, mortar or concrete [167, 168]. Insofar chloride penetration is determined by diffusion, Fick's 2nd law is commonly used to describe the diffusion process of free chloride ions in saturated cementitious materials:

$$\frac{\partial C_c}{\partial t} = div(D_{Cl} \cdot grad\ C_c) \tag{6.1}$$

where C_c is the free chloride content in concrete (in kg/m^3 of cementitious material), D_{Cl} is the chloride diffusivity [m^2/s], t is time [s].

In a saturated coating system chloride is only transported by diffusion. The chloride diffusion is driven by the concentration gradient of free chloride in the pore solution of the material. The concentration of free chloride C_f (in mole of Cl^- per liter of pore solution) needs to be calculated from the free chloride content C_c [169]:

$$C_f = \frac{C_c}{M_{Cl} \cdot \phi} \tag{6.2}$$

In Eq. (6.2) M_{Cl} is the molar mass of chloride [g/mol], ϕ is the total porosity of the material. To account for the chloride binding effect, the term $\partial C_f / \partial C_t$ is introduced:

$$\frac{\partial C_f}{\partial C_t} = \frac{\partial C_f}{\partial C_f + \partial C_b} \tag{6.3}$$

where C_t is the total chloride content in the material and consists of the free chloride C_f and the bound chloride C_b. The unit of C_t is usually expressed as kg/m^3 of the material. In numerical calculations, the unit of C_t is preferably transformed into mole of Cl^- per liter of pore solution.

$\partial C_f / \partial C_t$ can be determined from the chloride binding isotherm which describes the relationship between the amount of bound chloride C_b and total chloride C_t [170]. By substituting Eq. (6.2) in Eq. (6.1) and introducing $\partial C_f / \partial C_t$, a new form reads:

$$\frac{\partial(\phi \cdot C_f)}{\partial t} = \frac{\partial C_f}{\partial C_t} \cdot div\left(D_{Cl} \cdot grad\left(\phi \cdot C_f\right)\right) \tag{6.4}$$

Applying the product rule to the left term of Eq. (6.4) gives:

$$\phi \cdot \frac{\partial C_f}{\partial t} + C_f \cdot \frac{\partial \phi}{\partial t} = \frac{\partial C_f}{\partial C_t} \cdot div\left(\phi \cdot D_{Cl} \cdot grad\ C_f\right) \tag{6.5}$$

After rearrangement, Eq. (6.5) becomes:

$$\phi \cdot \frac{\partial C_t}{\partial C_f} \cdot \frac{\partial C_f}{\partial t} = div\left(\phi \cdot D_{Cl} \cdot grad\ C_f\right) - C_f \cdot \frac{\partial \phi}{\partial t} \cdot \frac{\partial C_t}{\partial C_f} \tag{6.6}$$

The initial concentration of free chloride $C_f(t = 0, x)$ in cementitious materials and the surface (i.e. exposed surface) chloride concentration $C_f(t, x = x_s)$ are described as:

$$C_f(t = 0, x) = C_o \tag{6.7}$$

$$C_f(t, x = x_s) = C_s \tag{6.8}$$

where C_o and C_s are the values of the initial concentration of free chloride in the materials and the surface chloride concentration, respectively. x_s is the coordinate of the exposed surface of the materials (see Fig. 6.2).

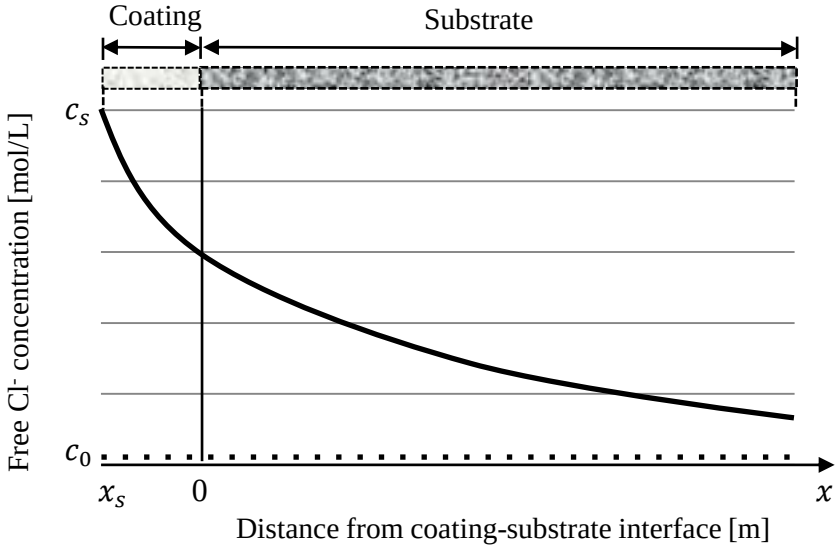

Fig. 6.2 Schematic illustration of chloride profiles in a coating-substrate system.

6.2.2 Chloride transport in the crack of the materials

In a cracked concrete structure, the cracks provide a free path for chloride transport. The chloride transport in the cracks should be considered separately from the transport through the bulk concrete, and can be described as [171]

$$\frac{\partial C_f}{\partial t} = div\left(D_{Cl-cr} \cdot grad\ C_f\right) \tag{6.9}$$

where D_{Cl-cr} is the chloride diffusivity in the solution in the cracks.

The crack width is an important parameter in chloride transport in cementitious materials [171-173]. For very small cracks (e.g. crack width < 0.03 mm), the cracks are believed to close due to the self-healing and don't contribute to the chloride transport process. For larger cracks (e.g. crack width > 0.1 mm), the chloride diffusivity in the solution in cracks, D_{Cl-cr}, is assumed to be the same as the one in water [174]. In this study, the value of D_{Cl-cr} for water in large cracks (e.g. crack width > 0.1 mm) is taken as $1.8 \times 10^{-9}\ m^2/s$ at 20 °C [175].

6.2.3 Chloride transport across the coating-substrate interface

When simulating chloride transport in a coating system, attention has to be paid to the coating-substrate interface (Fig. 6.3). The flux of free chloride across the interface is determined by several parameters: viz. the gradient of free chloride in the coating system, the chloride diffusivity and the porosities of the coating material and the substrate.

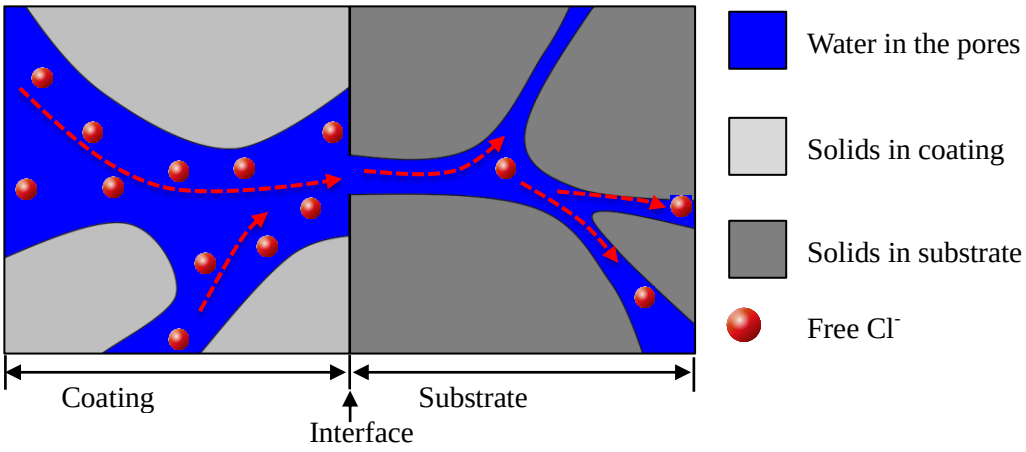

Fig. 6.3 Schematic illustration of chloride diffusion through the interface between two materials.

In order to conserve the mass of chloride in the coating system, two criteria should be fulfilled. One criterion is the continuity in concentration of free chloride at the coating-substrate interface (Eq. (6.10)):

$$C_{f_{c0}} = C_{f_{s0}} \tag{6.10}$$

where $C_{f_{c0}}$ and $C_{f_{s0}}$ are concentration of free chlorides of the coating and of the substrate at the interface, respectively (Fig. 6.4)

Another criterion is the continuity in the flux of chloride at the coating-substrate interface. The flux of concentration of free chloride across the coating-substrate interface J_{Cl-int} is described by Fick's 1st Law (Eq. (6.11)):

$$J_{Cl-int} = -\phi_c \cdot D_{Cl-c} \cdot grad\ C_f = -\phi_s \cdot D_{Cl-s} \cdot grad\ C_f \tag{6.11}$$

where ϕ_c and ϕ_s are the porosities of the coating and the substrate, respectively. D_{Cl-c} and D_{Cl-s} are the chloride diffusivity of the coating and the substrate, respectively.

Eq. (6.6)-(6.11) govern the chloride transport in coating systems. By specifying the boundary conditions (i.e. a surface chloride concentration in Eq. (6.8)), the evolution of the profile of concentration of free chloride in the coating system can be simulated.

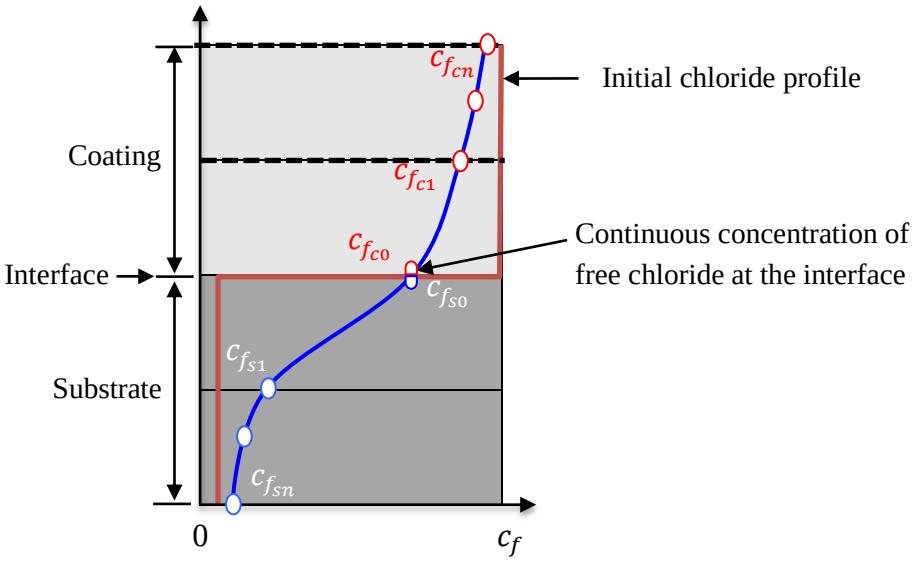

Fig. 6.4 1D schematic illustration of the free chloride profile in a coating system. The red lines show the initial state. The nodes are numbered incrementally from $c0$ to cn in the coating, and $s0$ to sn in the substrate. $c0$ and $s0$ represent the interface nodes in the coating and the substrate, respectively.

6.3 Quantification of material properties for the simulation

To implement the "Diffusion-Binding model", the porosity, the chloride diffusivity and the chloride binding isotherm of the materials should be quantified. The total porosity ϕ of a hydrating cement paste can be quantified according to the methodology presented earlier in section 4.5. The quantification of the chloride diffusivity and the binding isotherm is presented below.

6.3.1 Chloride diffusivity

The chloride diffusivity (i.e. chloride diffusion coefficient) depends on the microstructure and the water saturation of cementitious materials [95]. For a hydrating cementitious material cured under saturated condition, the chloride diffusivity changes with increasing degree of hydration [92]. Gaboczi et al. [96] proposed an equation (Eq. (6.12)) to predict the chloride diffusivity $D_{Cl-c}(t)$ of a hydrating ordinary Portland cement paste as function of time:

$$\frac{D_{Cl-c}(t)}{D_0} = 0.001 + 0.07 \cdot \phi_{cap}(t)^2 + H\left(\phi_{cap}(t) - \phi'_{cap}\right) \cdot 1.8 \cdot \left(\phi_{cap}(t) - \phi'_{cap}\right)^2 \quad (6.12)$$

where D_0 (m^2/s) is the chloride diffusivity in free water, $\phi_{cap}(t)$ is the capillary porosity at time t (calculated with Eq. (4.19)). ϕ'_{cap} is the percolation threshold of capillary pores (taken as 0.18 [96]), $H(X)$ is the Heaviside function. $H(X) = 0$ for $X \leq 0$, and 1 for $X > 0$.

Eq. (6.12) is based on the time-dependent capillary porosity $\phi_{cap}(t)$ of cementitious material. When the capillary pores percolate through the materials (i.e. $\phi_{cap}(t) > \phi_c$), the capillary pores dominate the diffusion process. When the capillary pores become disconnected (i.e. $\phi_{cap}(t) \leq \phi_c$), chloride ions have to diffuse through gel pores, in which case a lower chloride diffusivity applies

The diffusivity of concrete depends on the pore structure of the cement matrix, the aggregates and the interfacial transition zone (ITZ) [176]. For simplicity, only the cement matrix and the aggregates are considered for determining the chloride diffusivity of the concrete. The diffusivity of concrete $D_{Cl-s}(\alpha)$ can be determined based on a composite model developed by Christensen [177]:

$$D_{Cl-s}(t) = D_{Cl-c}(t) \cdot \left(1 + \frac{g_{agg}}{\left(1 - g_{agg}\right)/3 + D_{Cl-c}(t)/\left(D_{agg} - D_{Cl-c}(t)\right)}\right) \quad (6.13)$$

where g_{agg} is the volume fraction of the aggregates. D_{agg} is the diffusivity of aggregate. When the type of aggregate is unknown, the value of D_{agg} can be simply taken as 1×10^{-12} cm^2/s [169].

6.3.2 Chloride binding isotherm

The binding isotherm highly depends on the chemical composition of the materials. Hirao et al. [98] investigated chloride binding isotherms of C-S-H and AFm hydrates. They found that the chloride binding isotherm of AFm follows a Freundlich-type adsorption [98]:

$$C_{b-AFm} = 0.86 \cdot C_f{}^{0.58} \quad \text{[mol/mol]} \tag{6.14}$$

where C_{b-AFm} is the bound chloride, in moles of chloride per mole of AFm. The chloride binding isotherm of C-S-H follows a Langmuir-type adsorption [98]:

$$C_{b-CSH} = 0.61 \cdot \frac{2.65 \cdot C_f}{1+2.65 \cdot C_f} \quad \text{[mmol/g]} \tag{6.15}$$

where C_{b-CSH} is the bound chloride in milli-moles of chloride per gram C-S-H, and C_f is free chloride in moles of free chloride per liter pore solution. In order to combine them and incorporate them in Eq. (6.6), the same unit has to be used for free and bound chloride concentrations. For this reason, bound chloride C'_{b-AFm} and C'_{b-CSH} are introduced in Eq. (6.16) and Eq. (6.17), with the unit in moles of chloride per gram of hydration products:

$$C'_{b-AFm} = 0.0014 \cdot C_f{}^{0.58} \quad \text{[mol/g]} \tag{6.16}$$

$$C'_{b-CSH} = 0.0017 \cdot C_f/(1 + 2.65C_f) \quad \text{[mol/g]} \tag{6.17}$$

The mass of monosulphate M_{AFm}, the mass of C-S-H gel M_{CSH}, and the total porosity ϕ are needed for the calculation of the total amount of bound chloride C_b [mol/L] (Eq. (6.18)). The unit of M_{AFm} and M_{CSH} is in kilograms of hydrates per cubic meter of cementitious material (kg/m^3).

$$\begin{aligned} C_b &= (M_{CSH} \cdot C'_{b-CSH} + M_{AFm} \cdot C'_{b-AFm})/\phi \\ &= \left(M_{CSH} \cdot 0.0017 \cdot C_f/(1 + 2.65C_f) + M_{AFm} \cdot 0.0014 \cdot C_f{}^{0.58}\right)/\phi \quad \text{[mol/L]} \end{aligned} \tag{6.18}$$

The term $\partial C_f/\partial C_t$ in Eq. (6.6) can be calculated:

$$\frac{\partial C_f}{\partial C_t} = \frac{\partial C_f}{\partial C_f + \partial C_b} = \left(1 + \frac{\partial C_b}{\partial C_f}\right)^{-1} = \left(1 + \frac{0.0017 \cdot M_{CSH}}{\phi \cdot (1 + 2.65 \cdot C_f)^2} + \frac{M_{AFm}}{\phi} \cdot \left(0.0008 \cdot C_f{}^{-0.42}\right)\right)^{-1} \tag{6.19}$$

A schematic presentation of chemical reactions in cement pastes is shown in Fig. 6.5 regarding the formation of C-S-H and the AFm.

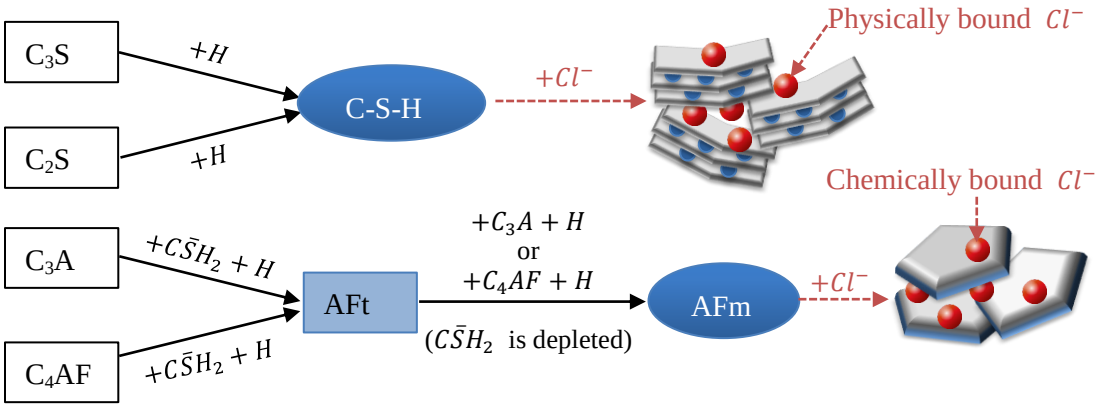

Fig. 6.5 Schematic presentation of chemical reactions in a Portland cement paste. The hydration products of interest are C-S-H and AFm, which bind the chlorides. Schematic chloride binding of each product is shown.

The C-S-H gel is the hydration product of C_3S and C_2S. In a hydrating cement paste, the amount of C-S-H (M_{CSH}) can be determined by the procedure presented in section 4.5.

C_3A and C_4AF are two sources for the formation of AFm. At the beginning of the hydration process these two sources hydrate with $C\bar{S}H_2$ and water to form $C_6A\bar{S}_3H_{32}$ (AFt).

$$C_3A + 3C\bar{S}H_2 + 26H \rightarrow C_6A\bar{S}_3H_{32} \tag{6.20}$$

$$C_4AF + 3C\bar{S}H_2 + 30H \rightarrow C_6A\bar{S}_3H_{32} + CH + FH_3 \tag{6.21}$$

After the depletion of $C\bar{S}H_2$, the residual C_3A and C_4AF gradually transfer AFt into $C_4A\bar{S}H_{12}$ (AFm):

$$2C_3A + C_6A\bar{S}_3H_{32} + 4H \rightarrow 3C_4A\bar{S}H_{12} \tag{6.22}$$

$$2C_4AF + C_6A\bar{S}_3H_{32} + 12H \rightarrow 3C_4A\bar{S}H_{12} + 2CH + 2FH_3 \tag{6.23}$$

Given the degree of hydration of individual clinker component (e.g. C_3A and C_4AF, see section 4.5), the amount of AFm (M_{AFm}) can be calculated with Eq. (6.20) - (6.23). Parameters needed for the calculation are listed in Table 4.3, Table 4.4 and Table 6.2.

Table 6.2 Parameters for determining the mass of AFm in a cement paste [149].

	Nominal formula	Molecular weight (kg/mol)
Aluminate	C_3A	0.270
Ferrite	C_4AF	0.477
Gypsum	$C\bar{S}H_2$	0.172
AFt	$C_6A\bar{S}H_{32}$	0.715
AFm	$C_4A\bar{S}H_{12}$	0.623

6.4 Validation of the simulation of chloride ingress in the coating system

The chloride profile in a two-layer sample as experimentally obtained by Yu et al. [6] is used to validate the model proposed in section 6.2. In the experiments two cement paste specimens (ordinary Portland cement, w/c = 0.5) were prepared. In one specimen, 2% chloride (as $NaCl$) by weight of cement was added. In another specimen no chloride was added. After 90-day sealed curing at 25 ± 2 ℃, the two cement paste samples (49 mm in diameter and 65 mm in length) were cemented together by a thin layer of fresh cement slurry (w/c = 0.5) (Fig. 6.6). The cemented samples were sealed for 225 days. Then the concentration of free chloride in the samples was measured by extracting the pore solution (Fig. 6.7). The best-fit chloride diffusivity of the 90-day old cement paste was calculated to be $D_{Cl} = 3.93 \times 10^{-12}$ (m^2/s), and considered constant throughout the test [6].

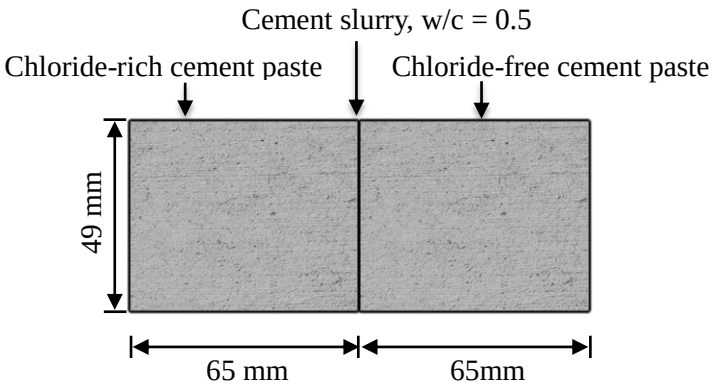

Fig. 6.6 Schematic illustration of two hardened cement pastes that are cemented by a cement slurry.

Chloride transport in the two-layer cement paste sample is simulated using the model proposed in section 6.2. The simulated free chloride profile in the specimens 225 days after the two specimens are cemented together is presented together with experimental data in Fig. 6.7. The simulated profile agrees well with the experimental data. The comparison of the experimental and simulation results in this figure indicates that the simulation tool proposed in this chapter is able to appropriately consider the chloride diffusion in two-layer cementitious system with consideration of chloride binding. Therefore, the use of the simulation tool for simulating chloride transport in cementitious coating systems is considered justified.

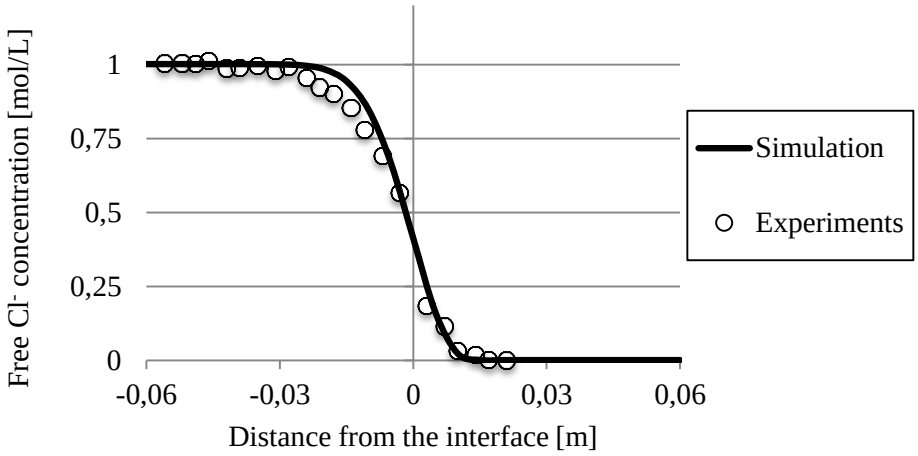

Fig. 6.7 Comparison of simulated and measured ([6]) profiles of free chloride in two specimens. The two specimens (90 days old) are cemented together by a fresh cement slurry. After another 225 days, free chloride profile is determined. In the experiments ([6]), the solutions expressed from the discs of specimens were analysed for the Cl^- content by means of a spectrophotometric technique.

6.5 Simulation of chloride transport in coating systems

This section presents numerical simulations of chloride transport in hydrating cementitious coating systems. The simulation results are mesh and time discretization independent. Based on the simulated profiles of free chloride, the time until initiation of reinforcement corrosion in the concrete substrates, $T_{corrosion}$, is predicted (i.e. time for reaching a critical chloride concentration at the steel reinforcement). The effectiveness of the coatings to extend the $T_{corrosion}$ for the substrates is evaluated.

6.5.1 Materials of coating systems

6.5.1.1 Materials of coating and substrate

The coatings are made of cement pastes. Ordinary Portland cement is used (previously listed in Table 4.4). Different w/c ratios (0.3, 0.4 and 0.5) are considered for the coatings. The concrete substrate has a cement content of 350 kg/m^3 (ordinary Portland cement) and a w/c ratio of 0.48. The volume fraction of the aggregates in the substrate is 70%. These parameters are needed for determining chloride diffusivity (Eq. (6.12)-(6.13)) and chloride binding isotherms (see section 6.3.2) of the coatings and the substrate. The materials used in the coating systems are summarized in Table 6.3.

Table 6.3 Materials used in the coating systems.

	Type	w/c	Content of cement [kg/m^3]
Coating	Cement paste	0.3, 0.4 or 0.5	–
Substrate	Concrete	0.48	350

6.5.1.2 Hydration and chloride binding of the coating and the substrate

The hydration processes of the coating (w/c = 0.3) and the substrate (w/c = 0.48) under saturated condition are simulated by HYMOSTRUC3D. Fig. 6.8 shows the evolution of degree of hydration of the coating and the substrate. Time "0" in Fig. 6.8 refers to the time when the raw materials of the coating or the substrate are mixed. The hydration process of both materials takes place quickly in the first 7 days. After 7 days, the rate of hydration becomes slow. The amounts of C-S-H and AFm in the coating and the substrate are also presented in Fig. 6.8 and used for determining chloride binding ($\partial C_f/\partial C_t$).

The term accounting for chloride binding of the coating and the substrate, $\partial C_f/\partial C_t$, is calculated with Eq. (6.14)-(6.18) and presented in Fig. 6.9. The ratio of free chloride to total chloride, $\partial C_f/\partial C_t$, decreases with increasing degree of hydration, indicating an increasing chloride binding capacity. At the same degree of hydration, the substrate (w/c = 0.48) has a higher ratio of free chloride to total chloride (i.e. a higher value of $\partial C_f/\partial C_t$ or lower chloride binding capacity) than the coating (w/c = 0.3). This can be explained by the fact that the substrate has higher water-to-cement ratio than the coating. The higher water-to-cement ratio of the substrate leads to lower amounts of C-S-H and AFm (C-S-H and AFm are two hydrates that bind chlorides).

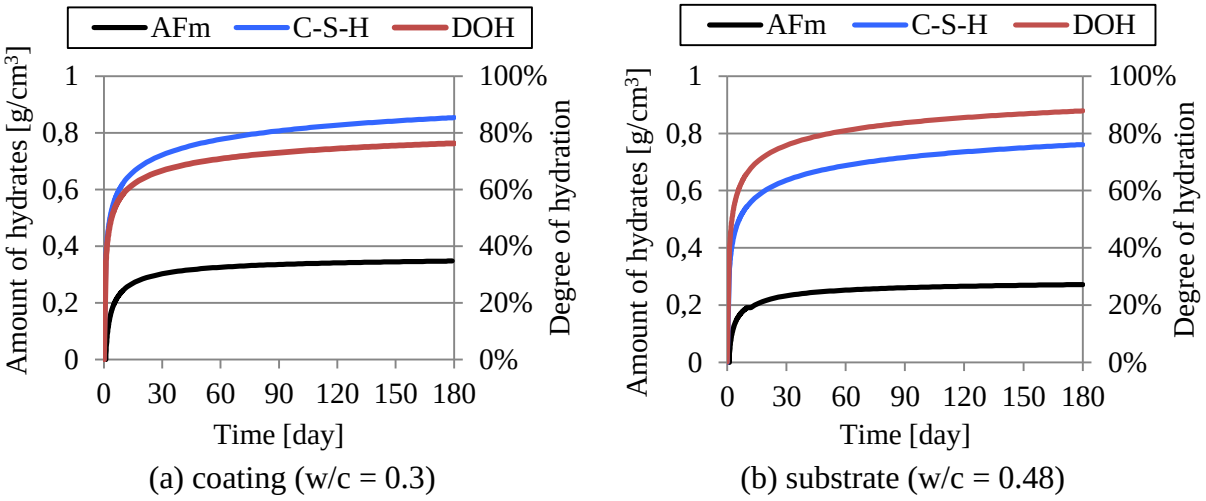

Fig. 6.8 Evolution of degree of hydration and the amounts of hydrates ([g per cm^3 of cement paste]). (a) coating (w/c = 0.3), (b) substrate (w/c = 0.48). The coating and the substrate are cured under saturated condition.

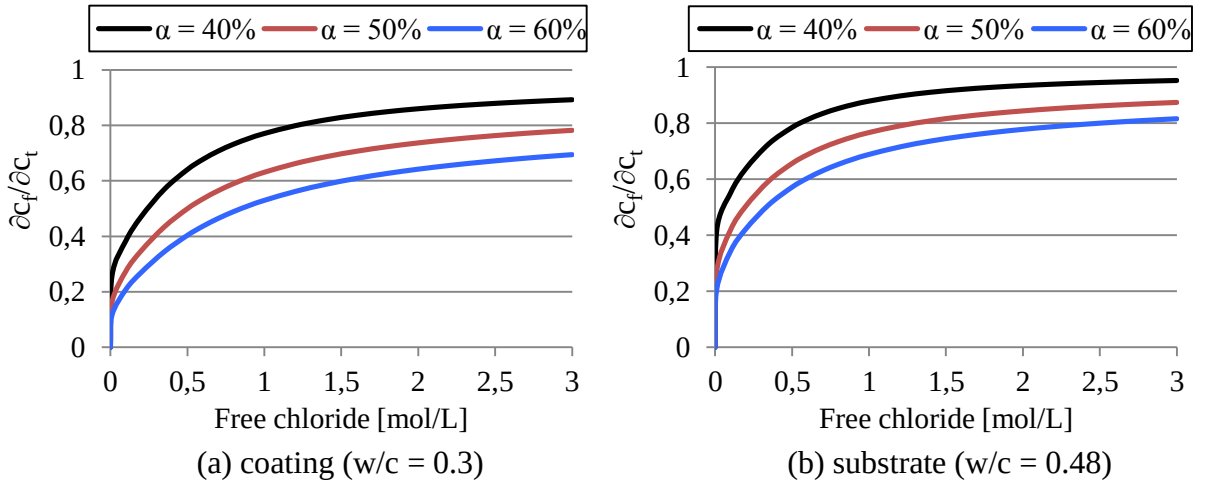

Fig. 6.9 Chloride binding capacity ($\partial C_f/\partial C_t$) of the coating (w/c = 0.3) and the substrate (w/c = 0.48) at different degree of hydration. $\partial C_f/\partial C_t$ is calculated with Eq. (6.14)-(6.18).

6.5.1.3 Dimension of the substrate and size of the surface crack

Both a crack-free substrate (Sub) and a cracked concrete substrate (Sub-Crack) are considered. One-dimensional (1D) and two-dimensional (2D) simulations are conducted on crack-free and cracked substrates, respectively. The dimensions of the substrates and the sizes of the cracks in the substrates are listed in Table 6.5. Illustration of the dimension of the substrate is shown in Fig. 6.10.

Table 6.4 Dimension of the substrates and size of the cracks.

	Thickness	Height	Length	Size of the surface crack [width × depth]
Sub	150 mm	Infinite	Infinite	–
S(Crack10mm)	150 mm	200 mm	Infinite	0.4×10 mm^2
S(Crack15mm)	150 mm	200 mm	Infinite	0.4×15 mm^2
S(Crack20mm)	150 mm	200 mm	Infinite	0.4×20 mm^2

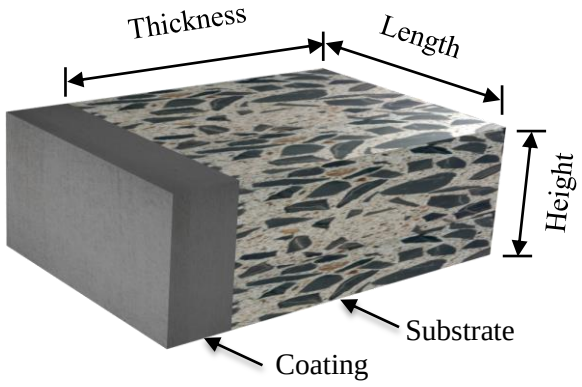

Fig. 6.10 Illustration of the dimension of the coating system (coating and substrate).

6.5.2 Exposure scenario for the coating systems and parameters to be evaluated

6.5.2.1 Exposure scenario

The coating system is schematically shown in Fig. 6.11. The coating is applied on a cracked substrate. The surface with the coating is exposed to chloride environment (splash and tidal zone); the other surface of the substrate is sealed. Steel reinforcement is placed at a 30 mm from the exposed surface. The concrete structure is located in the tidal and splash zone. Note that the cover thickness of marine concrete structures is usually larger than 30 mm [178]. This chapter considers a relatively small thickness of concrete cover and investigates the effectiveness of cementitious coatings to retard the chloride ingress into reinforced concrete structures. In the simulation, the coating system is considered saturated.

Note that the hydration of the substrate may cause internal desiccation under sealed condition. According to Persson [179], the internal relative humidity (RH) of a 1 m-thick concrete (w/c = 0.465) was 88% after 450 days sealed curing. The internal RH in the concrete (w/c = 0.465, at 150 mm depth) remained above 94% when water curing was applied. Therefore, the saturated condition for the substrate (w/c = 0.48, thickness = 150 mm) considered in this simulation is only an approximation.

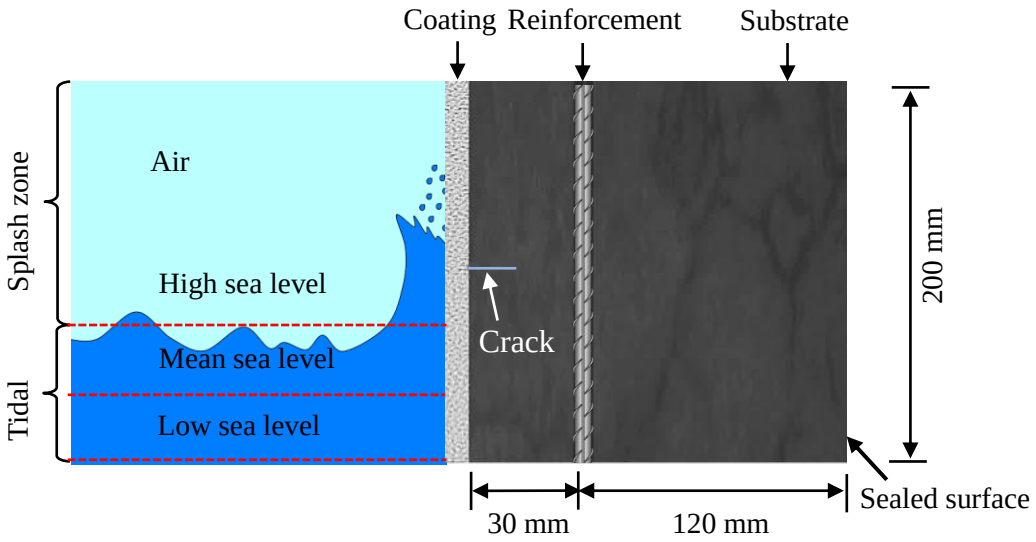

Fig. 6.11 Schematic illustration of a coating system exposed in a tidal and splash zone (modified based on [180]).

6.5.2.2 Parameters to be evaluated

Coatings with different compositions (w/c ratios)
Chloride transport in the uncoated substrate (Sub) (Fig. 6.12a) is taken as a reference for evaluating the effectiveness of the coatings. To investigate the influence of the coating composition on chloride transport in the coating systems, coatings with different w/c ratios (i.e. 0.3, 0.4 and 0.5) are applied on the substrates (Fig. 6.12b).

Coatings with different thicknesses
The influence of the coating thickness is also studied. Different thicknesses (i.e. 3, 6 and 10 mm) are considered for the coatings with a w/c of 0.3 (Fig. 6.12b).

Time of failure of the coating
As mentioned in section 1.1, only 10% of the repairs remain intact for 25 years after application [3]. To investigate the effect of coating failure on chloride ingress in the coating systems, an early failure of the coating is considered in the simulation (Fig. 6.13). In the coating system, a 10 mm-thick coating is applied on a young substrate. The coating fails due to cracking or debonding after a certain period of time (e.g. 5, 10 or 20 years). No protection of the substrate is considered after the failure of the coating. In the simulation, the domain of coating after failure is removed from the coating system.

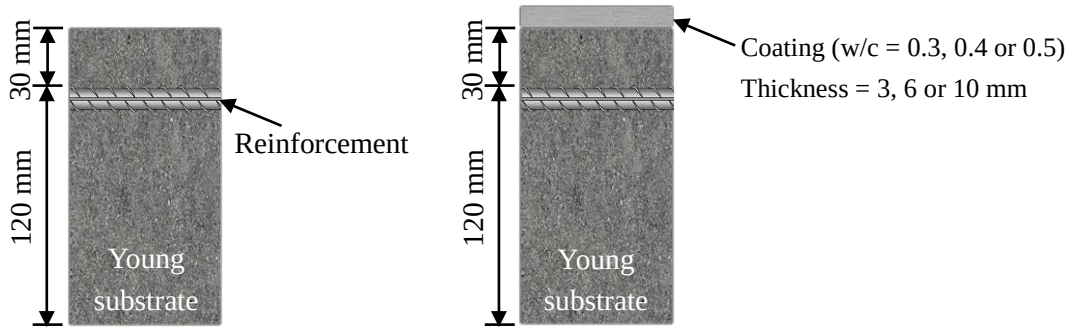

(a) substrate (b) coating system

Fig. 6.12 Substrate and coating systems. Coatings with different w/c ratios and thicknesses are applied on young substrates.

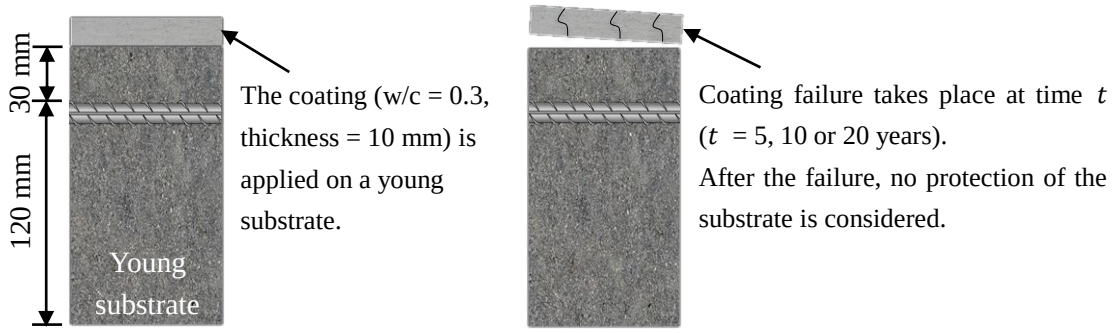

(a) coating system (t = 0 year) (b) coating failure at t = 5, 10 or 20 years

Fig. 6.13 Coating failure in the coating system. Coatings are applied on young substrates. After t (5, 10 or 20) years, the coating fails due to cracking or de-bonding.

Early or late application of the coating

In practice, before applying the coating material, the substrate may have been exposed to the chloride environment. To simulate this scenario, 10 mm-thick coatings (w/c = 0.3) are applied on old concrete substrates (Fig. 6.14). Before applying the coating, the concrete substrates have been exposed to the chloride environment for 5, 10 or 20 years. The profiles of free chloride in the old substrates will be presented in section 6.6.4.

Crack in the concrete substrate

To evaluate the effectiveness of the coating on cracked substrates (Fig. 6.15a), chloride transport in the coating system with cracked substrates (Fig. 6.15b) is simulated. A 10 mm-thick coating material (w/c = 0.3) is applied on the cracked substrate after the substrate has been exposed to the chloride environment for 10 years.

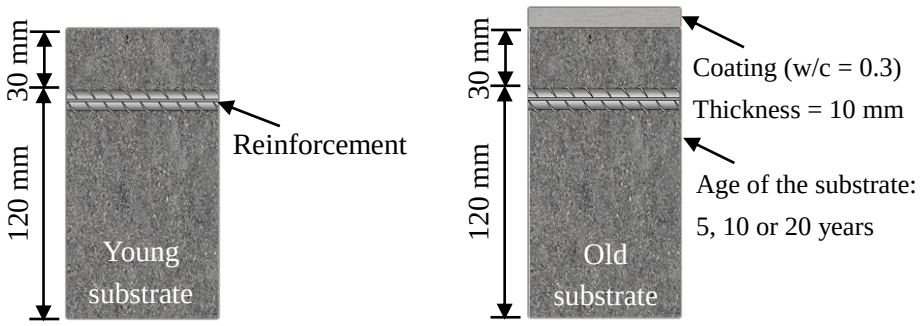

(a) substrate (b) substrate with a coating (late application)

Fig. 6.14 Concrete substrate with a late application of the coating. Before applying the coatings, the substrates have been exposed to the chloride environment for 5, 10 or 20 years.

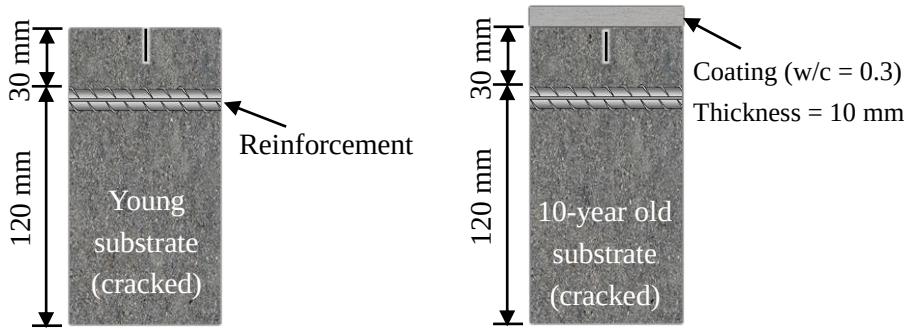

(a) cracked substrate (b) cracked substrate with a coating

Fig. 6.15 Cracked substrates with coatings. The surface crack has a size of 0.4×10 mm^2, 0.4×15 mm^2 or 0.4×20 mm^2. Before applying the coatings, the cracked substrates have been exposed to the chloride environment for 10 years.

Abbreviations and descriptions of the coating systems are presented in Table 6.5. The coating systems are classified based on the w/c ratio of the coating, the thickness of the coating, the time of coating failure, early or late application of the coating and the depth of the surface crack in the substrate.

Table 6.5 Abbreviated designations of the concrete substrate and the coating systems (the coatings and the substrates are saturated).

Designation	Coating[1] (Thickness and w/c)	Substrate (Age and crack)	Coating failure at t years[2]
Sub[6]		Young Substrate[3]	
C10(wc0.5)-S	10 mm (w/c = 0.3)	Young Substrate	−
C10(wc0.4)-S	10 mm (w/c = 0.4)	Young Substrate	−
C10(wc0.3)-S	10 mm (w/c = 0.5)	Young Substrate	−
C06(wc0.3)-S	6 mm (w/c = 0.4)	Young Substrate	−
C03(wc0.3)-S	3 mm (w/c = 0.5)	Young Substrate	−
C10(wc0.3-Fail05y)-S	10 mm (w/c = 0.3)	Young Substrate	5 years
C10(wc0.3-Fail10y)-S	10 mm (w/c = 0.3)	Young Substrate	10 years
C10(wc0.3-Fail20y)-S	10 mm (w/c = 0.3)	Young Substrate	20 years
C10(wc0.3)-S05y	10 mm (w/c = 0.3)	5-year old Substrate[4]	−
C10(wc0.3)-S10y	10 mm (w/c = 0.3)	10-year old Substrate	−
C10(wc0.3)-S20y	10 mm (w/c = 0.3)	20-year old Substrate	−
S(Crack10mm)	−	Young S(Crack10mm) [5]	−
S(Crack15mm)	−	Young S(Crack15mm)	−
S(Crack20mm)	−	Young S(Crack20mm)	−
C10(wc0.3)-S(Crack10mm)10y	10 mm (w/c = 0.3)	10-year old S(Crack10mm)	−
C10(wc0.3)-S(Crack15mm)10y	10 mm (w/c = 0.3)	10-year old S(Crack15mm)	−
C10(wc0.3)-S(Crack20mm)10y	10 mm (w/c = 0.3)	10-year old S(Crack20mm)	−

(1) After application of the coating, 0.5 days moist curing is applied to the coating system, followed by an exposure to the chloride environment.

(2) The coating fails due to cracking or de-bonding within a certain period of time (t = 5, 10 or 20 years) after application. After t years, no protection of the substrate is considered.

(3) A young crack-free concrete refers to the substrate cured under a saturated condition for 7 days. It simulates the situation that the substrate is diagnosed unsatisfactory 7 days after casting, and then a coating is needed.

(4) The 5-year old concrete substrate refers to that cured under a saturated condition for 7 days, followed by an exposure to chloride environment until 5 years.

(5) Description of the cracked substrate is given in Table 6.5.

(6) Chloride binding of the coating and the substrate are considered throughout the simulation. To investigate the effect of chloride binding, chloride transport in the uncoated substrate (Sub) is simulated with/without consideration of the chloride binding. When chloride binding is not considered, the value of $\partial C_f/\partial C_t$ in Eq. (6.3) is set equal to 1.

6.5.3 Surface chloride and initial chloride

The surface chloride content is usually expressed by its mass percentage to cement paste. The surface chloride content may vary with time due to the accumulation of chloride [181]. In this study, a constant concentration of free chloride is specified on the exposed surface of the concrete structures. The input parameters are listed in Table 6.6.

Table 6.6 Parameters for simulating chloride transport in the coating systems.

Parameters	Symbol	Values
Initial concentration of free chloride in coating and substrate	C_0	0.01 mol/L
Surface chloride concentration	C_s	0.5 mol/L*
Exposure time	t	60 years

* The chosen surface chloride concentration of 0.5 mol/L is close to that in seawater with salinity of 3.5%.

6.5.4 Critical chloride concentration and cover thickness

Based on the simulation results, the time until initiation of reinforcement corrosion in concrete structures with different coatings (see section 6.5.2) is predicted with the parameters listed in Table 6.7.

Table 6.7 Parameters for predicting the time until initiation of reinforcement corrosion in concrete structures.

Parameters	Symbol	Values
Critical concentration of free chloride at rebar surface	C_r	0.2 mol/L
Concrete cover	L_c	30 mm

6.6 Simulation results and discussion

6.6.1 Effect of chloride binding on chloride transport in the substrate

Profiles of free chloride in concrete structures - reference profiles

Fig. 6.16 shows the simulated profiles of free chloride in the uncoated substrate (Sub). The chloride profile in the substrate after 50-year exposure in the chloride environment is chosen for illustration. The simulation of chloride transport is performed with and without considering chloride binding of the substrate. In case of chloride binding is considered, the concentration of free chloride is much lower than that when chloride binding is not considered.

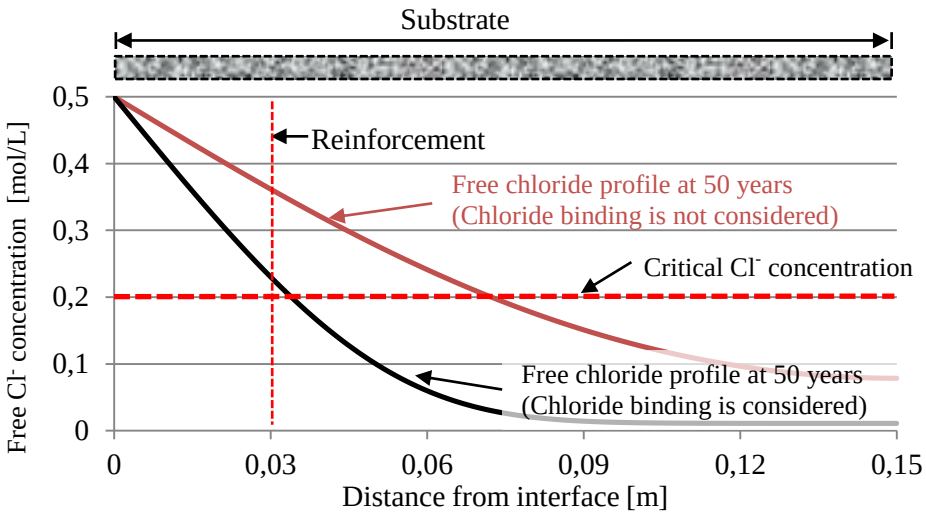

Fig. 6.16 Profiles of free chloride in the uncoated substrate (Sub in Table 6.5) after 50-year exposure to the chloride environment. Chloride transport is simulated with and without considering chloride binding of the substrate.

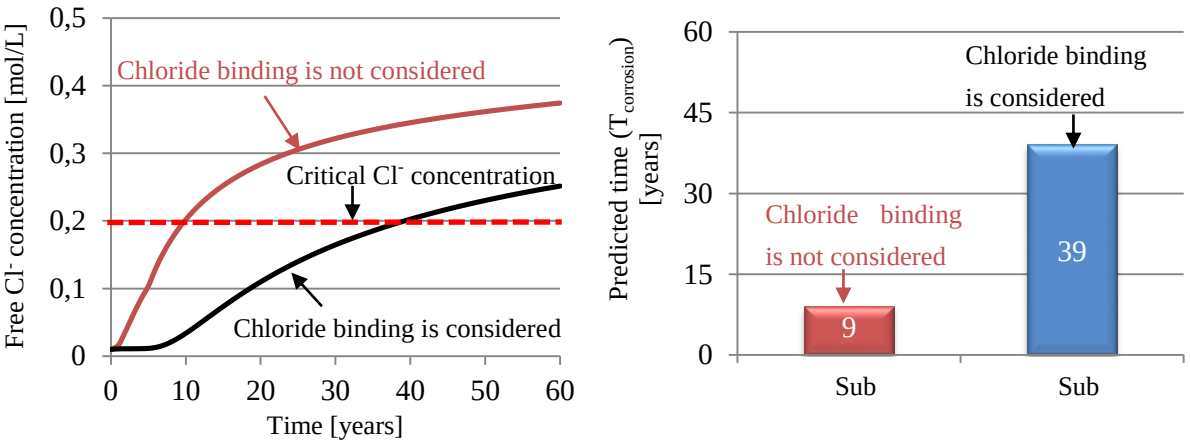

(a) Concentration of free chloride at steel surface in the uncoated substrate

(b) Predicted time until initiation of reinforcement corrosion in the uncoated substrate (concrete cover = 30 mm)

Fig. 6.17 Evolution of concentration of free chloride at the steel surface and predicted time until initiation of reinforcement corrosion in the uncoated substrates (Sub in Table 6.5). Chloride transport is simulated with and without considering chloride binding of the substrate.

Evolution of concentration of free chloride at steel surface and predicted time until initiation of reinforcement corrosion in the substrate

The significance of chloride binding of the substrate can also be seen from the concentration of free chloride at the steel surface (Fig. 6.17a). The concentration of free chloride at the steel surface increases with time and reaches the critical chloride concentration after 9 years (without chloride binding) or after 39 years (with chloride binding) (Fig. 6.17b). The significant impact of chloride binding of the substrate on chloride profiles is in accordance with that reported by Perez et al. [99]. Therefore, the chloride binding of the coating and the substrate will be considered in the simulations of chloride ingress in coated substrates. Note that the prediction of the time until initiation of reinforcement corrosion in concrete structures, $T_{corrosion}$, is only based on the critical chloride content at the surface of the steel reinforcement. However, other parameters should also be considered for a better prediction of $T_{corrosion}$, including the pH of pore solution and electrochemical potential of steel [91].

6.6.2 Coatings with different w/c ratios (0.3, 0.4 and 0.5)

Profiles of free chloride in concrete structures

Fig. 6.18 shows the profiles of free chloride in the uncoated substrate (Sub) and the coating-substrate system with 10 mm-thick coating after 50 years exposure to the chloride environment. In the coating systems, 10 mm-thick coatings with different w/c ratios (i.e. 0.3, 0.4 and 0.5) are applied on young substrates (w/c = 0.48, age = 7 days). The coatings with a w/c of 0.3 or 0.4 can effectively reduce the chloride ingress in the substrates. However, the coating with a w/c of 0.5 has a very limited effectiveness to reduce the chloride ingress.

Evolution of free chloride concentration at the reinforcement

The evolution of the concentration of free chloride at the steel surface in the substrates is presented in Fig. 6.19a. The coatings with low w/c ratios (i.e. 0.3 and 0.4) significantly increase the period needed for the concentration of free chloride at the steel surface (thickness of concrete cover = 30 mm) to reach the critical value (0.2 mol/L). When a coating with a w/c of 0.5 is applied on the substrate, the evolution of the concentration of free chloride at the steel surface in the coated substrate (dotted red line) almost coincides with that in the uncoated substrate (black line).

Predicted time until initiation of reinforcement corrosion in the concrete structures

Fig. 6.19b shows the effect of the coatings with different w/c ratios on the predicted time until initiation of reinforcement corrosion in the concrete structures, $T_{corrosion}$. The extra time of $T_{corrosion}$ for the concrete structures is 17 years (from 39 to 56 years), 5 years (from 39 to 44 years) and 1 year (from 39 to 40 years), when the coatings with a w/c of 0.3, 0.4 and 0.5 are applied, respectively. It can be concluded that the w/c ratio of the coatings plays an important role in the chloride ingress in the coating systems. To effectively protect the concrete substrate against the chloride ingress, a proper w/c ratio should be chosen for the coating material.

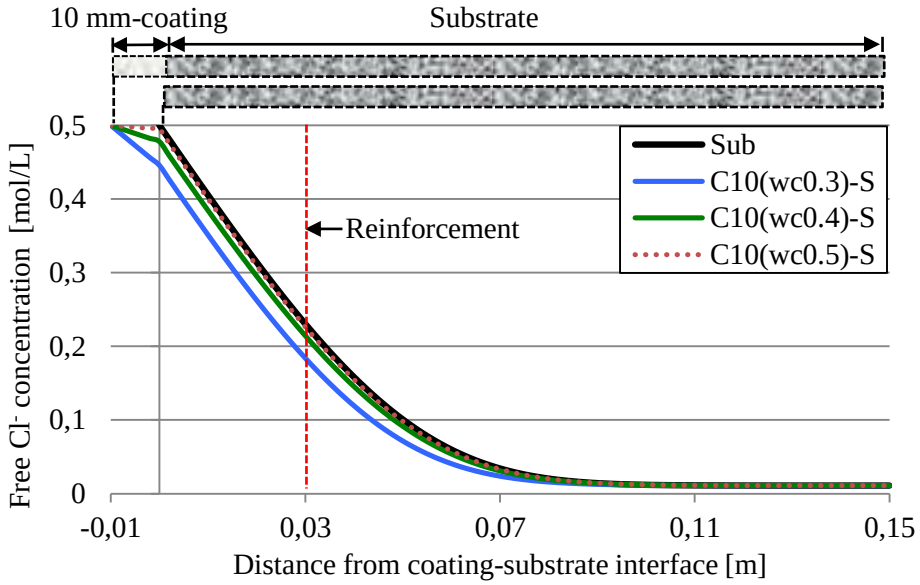

Fig. 6.18 Profiles of free chloride in the uncoated substrate and the coating systems with 10 mm-thick coatings after 50-year exposure to the chloride environment. The 10 mm-thick coatings with different w/c ratios (i.e. 0.3, 0.4 or 0.5) are applied on young substrates (age = 7 days).

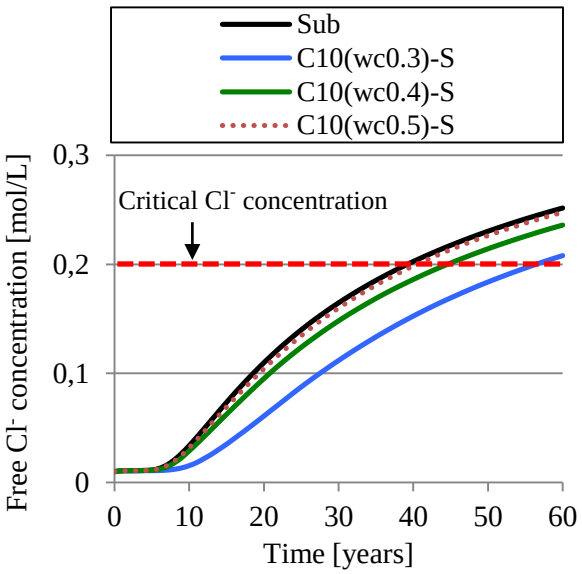

(a) Concentration of free chloride at steel surface

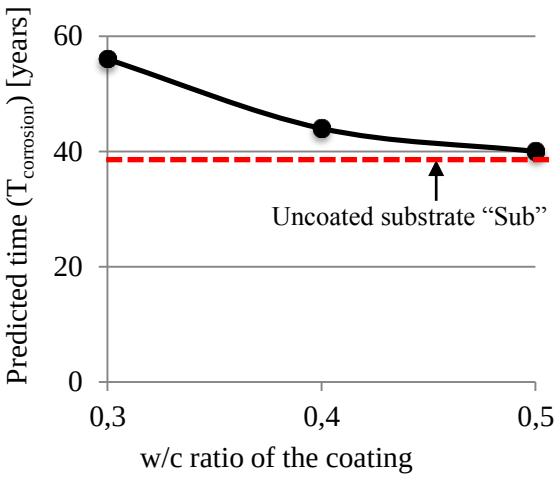

(b) Predicted time until initiation of reinforcement corrosion in the substrate (concrete cover = 30 mm)

Fig. 6.19 Evolution of concentration of free chloride at the steel surface (a) and predicted time until initiation of reinforcement corrosion in the concrete substrates (b). The 10 mm-thick coatings with different w/c ratios are applied on young substrates (age = 7 days).

6.6.3 Coatings with different thicknesses (3, 6 and 10 mm)

Profiles of free chloride in concrete structures

Fig. 6.20 shows the profiles of free chloride in the uncoated substrate (Sub) and the coating systems after 50-year exposure. In the coating systems, 3, 6 or 10 mm-thick coatings (w/c = 0.3) are applied on young substrates (age = 7 days). Not surprising, a thicker coating has a more pronounced effect on protecting the concrete substrate against chloride ingress.

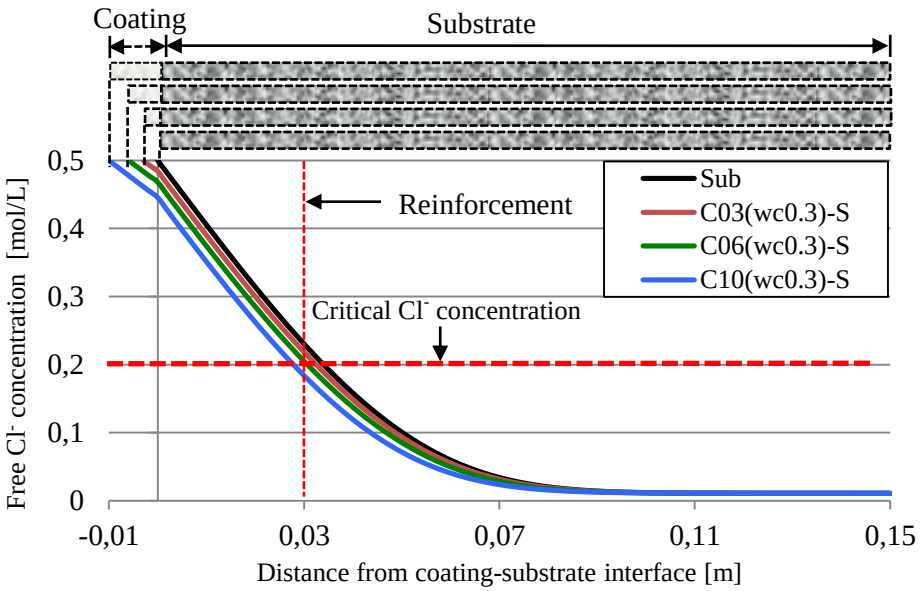

Fig. 6.20 Profiles of free chloride in the uncoated substrate and the coating systems after 50-year exposure to the chloride environment. The coatings (w/c = 0.3) with different thicknesses (i.e. 3, 6 or 10 mm) are applied on young substrates (age = 7 days).

Evolution of free chloride concentration at the reinforcement

Fig. 6.21a presents the evolution of the concentration of free chloride at the steel surface in the substrates. The coatings with different thicknesses cause a noticeable difference in the concentration of free chloride. The concentration of free chloride at the steel surface is clearly affected by a 3 mm-thick coating. A thicker coating (e.g. 10 mm-thick) results in a lower concentration of free chloride at the reinforcement.

Predicted time until initiation of reinforcement corrosion in the concrete structures

Fig. 6.21b shows the effect of the coatings with different thicknesses on the predicted time until initiation of reinforcement corrosion in the concrete structures, $T_{corrosion}$. $T_{corrosion}$ for the concrete structures increases from 39 years to 43, 48 and 56 years by a coating (w/c = 0.3) with a thickness of 3, 6 and 10 mm, respectively. It indicates that the coating thickness has a great effect on the effectiveness of the coatings to reduce the chloride ingress in the substrates.

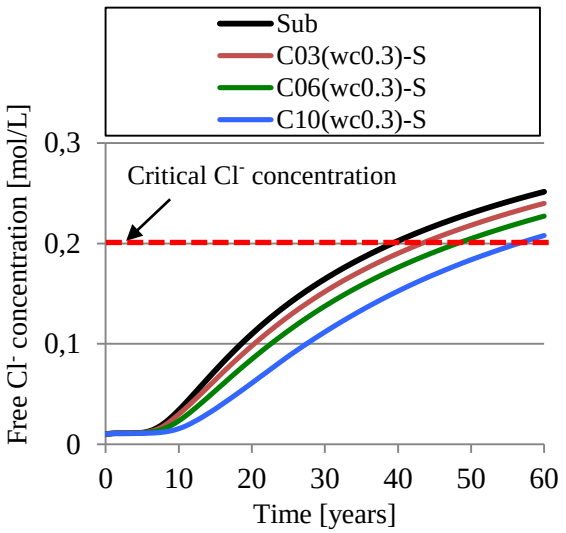

(a) Concentration of free chloride at steel surface

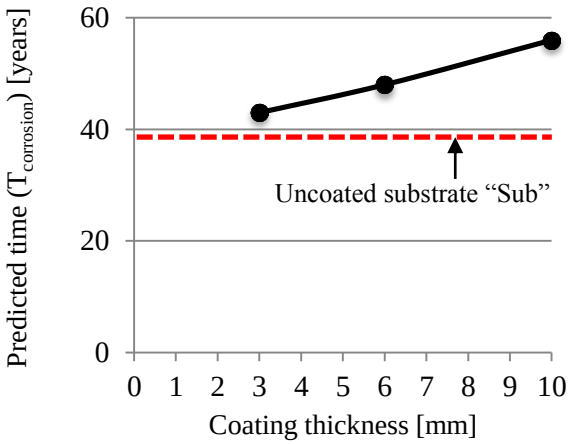

(b) Predicted time until initiation of reinforcement corrosion in the substrate (concrete cover = 30 mm)

Fig. 6.21 Evolution of concentration of free chloride at the steel surface (a) and predicted time until initiation of reinforcement corrosion in the concrete substrates (b). The coatings (w/c = 0.3) with different thicknesses (i.e. 3, 6 or 10 mm) are applied on young substrates (age = 7 days).

6.6.4 Coating systems with a late application of the coating (at 5, 10 and 20 years)

Profiles of free chloride in concrete structures

Fig. 6.22 presents the profiles of free chloride in a substrate before and after application of the coating. The uncoated substrate has been exposed to chloride environment for 10 years (the curve "10y"). After 10 years, a 10 mm-thick coating (w/c = 0.3) is applied on the substrate. Immediately after application of the coating, the concentration of free chloride in the coating material increases (see the curve "10.1y"). This increase is caused by the chloride diffusion from both the exposed surface and the substrate to the coating. After 10.1 years, more and more chloride ions are taken up from the substrate by the coating (e.g. at 11 years). In 5 years after applying the coating, the redistribution process of the chloride ions has more or less finished. As seen from the curve "15y", the chloride profile in the coating system shows a monotonic trend, and is lower than that in the uncoated substrate (Sub).

Fig. 6.23 presents the chloride profiles in the uncoated substrate (Sub) and in 4 coating systems after 50 years exposure to chloride environment. In the coating system C10(wc0.3)-S, a 10 mm-thick coating (w/c = 0.3) is applied on a young substrate (7-day old). In other coating systems, the 10 mm-thick coatings (w/c = 0.3) are applied on old substrates that have been exposed to chloride environment for 5, 10 or 20 years.

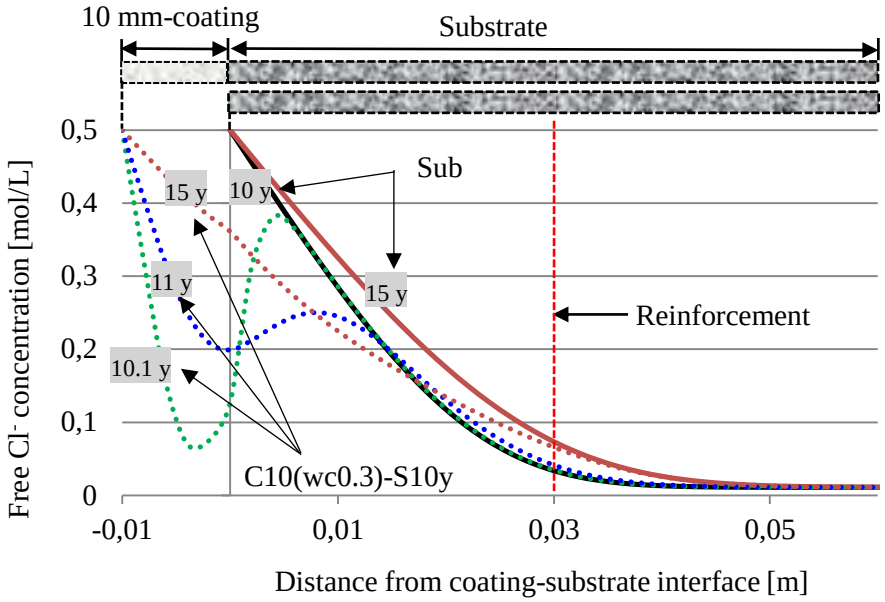

Fig. 6.22 Chloride profiles in the uncoated substrate and the coating system. This figure shows the chloride profile in the uncoated substrate after 10-year exposure to the chloride environment. Then a 10 mm-thick coating (w/c = 0.3) is applied on the 10-year old substrate. The chloride profiles in the coating system (C10(wc0.3)-S10y) at 10.1, 11 and 15 years are presented.

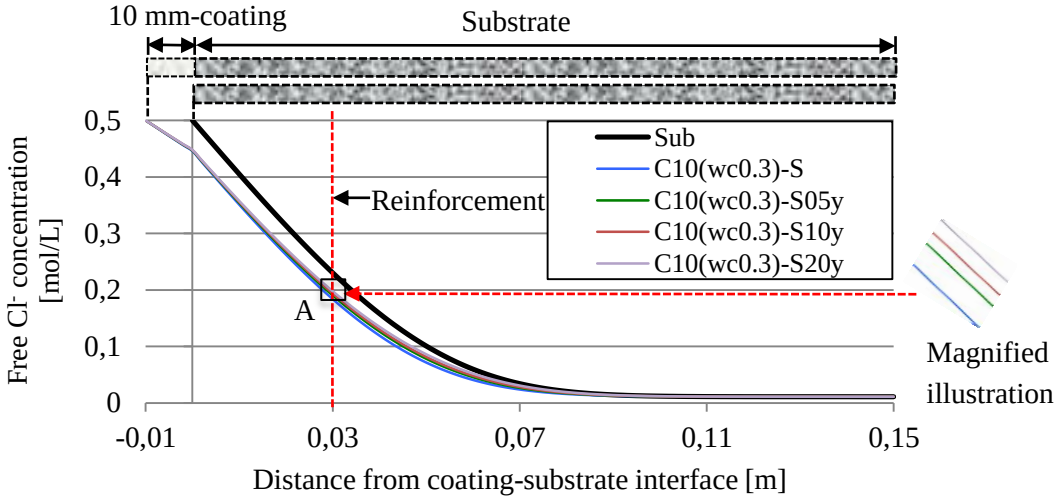

Fig. 6.23 Chloride profiles in the uncoated substrate and the coating systems after 50-year exposure to the chloride environment. The 10 mm-thick coatings (w/c = 0.3) are applied on old substrates. Before application of the coatings, the substrates have been exposed to chloride environment for 0, 5, 10 or 20 years. Magnified illustration of the chloride profiles at the steel surface is also shown.

Fig. 6.23 shows that the chloride profiles in all coated substrates are lower than that of the uncoated substrate (Sub). As can be seen from the magnified illustration of chloride profiles at the steel surface (area indicated by A in Fig. 6.23), a late application of the coating at 20 years (C10(wc0.3)-S20y) results in a slightly higher chloride concentration in the substrate compared to the early application of the coating (C10(wc0.3)-S). Therefore, for the coatings applied on the young substrate (age = 7 days) and the old substrates (age = 5, 10, or 20 years), the application of the coatings makes only marginal difference in the free chloride profile in the substrate after 50 years exposure to the chloride environment. The marginal difference can be explained as follows: before the application of coating the chloride has penetrated at only a limited depth of the substrate (e.g. about 40 mm at 15 years for the uncoated substrate "Sub", see Fig. 6.22), while the free chloride profile in the substrate at 50 years should be largely determined by the chloride ingress during the period from 20 to 50 years (note that the coatings were applied at 5, 10 or 20 years).

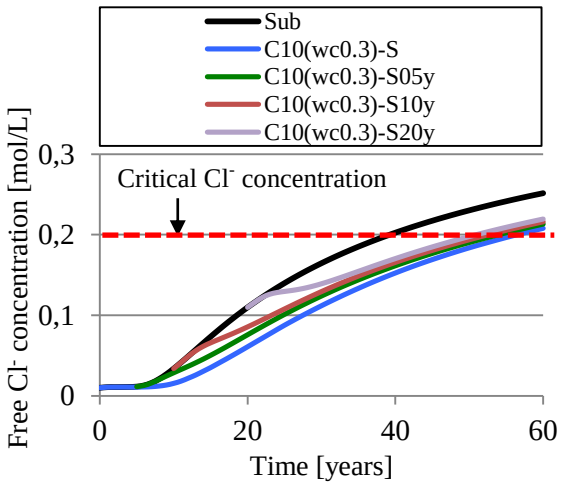

(a) Concentration of free chloride at steel surface

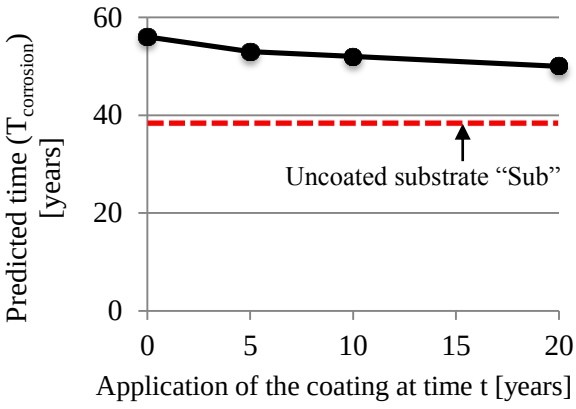

(b) Predicted time until initiation of reinforcement corrosion in the substrate (concrete cover = 30 mm)

Fig. 6.24 Evolution of concentration of free chloride at the steel surface (a) and predicted time until initiation of reinforcement corrosion in the concrete substrates (b). The 10 mm-thick coatings (w/c = 0.3) are applied on old substrates. Before application of the coatings, the substrates have been exposed to chloride environment for 0, 5, 10 or 20 years.

Evolution of free chloride concentration at the reinforcement

Fig. 6.24a presents the evolution of the concentration of free chloride at the steel surface. With an earlier application of the coating, the concentration of free chloride at the steel surface is evidently lower. The curves showing the evolution of the concentration of free chloride tend to converge over time.

Predicted time until initiation of reinforcement corrosion in the concrete structures
Fig. 6.24b shows the predicted time until initiation of reinforcement corrosion, $T_{corrosion}$, for the substrates with coatings applied at different ages of substrates. $T_{corrosion}$ for the substrates is extended from 39 years to 56 years by an early application (i.e. at 7 days) of the coating, and to 50, 52 and 53 years by a late application of the coating at 5, 10 and 20 years, respectively. It means that a late application of the coating can still reduce the chloride ingress from the environment, but the effectiveness is lower compared to an early application. For a higher effectiveness of the coating to extend the time until initiation of reinforcement corrosion in the substrate, the coating is preferably applied as early as possible to the substrate.

6.6.5 Coating systems with failure of the coating at 5, 10 20 years

Profiles of free chloride in concrete structures
Fig. 6.25 presents the profiles of free chloride in the uncoated substrate (Sub) and the coating system. In the coating system, a 10 mm-thick coating (w/c = 0.3) is applied on a young concrete substrate (age = 7 days). After application of the coating, the coating system is exposed to the chloride environment. The chloride profile in the coating system after 20-year exposure to the chloride environment is shown in Fig. 6.25. After 20 years, the coating is assumed to fail and no protection of the substrate is considered. After 50 years exposure the effect of the coating on the chloride distribution is still noticeable, despite that the coating has failed 20 years after application.

Evolution of free chloride concentration at the reinforcement
Fig. 6.26a shows the evolution of the concentration of free chloride at the steel surface in several coating systems. In these coating systems, the 10 mm-thick coatings with a w/c of 0.3 are applied on a young substrate (age = 7 days). In C10(wc0.3)-S, it is assumed that the coating does not fail. In the other 3 coating systems the coating is assumed to fail 5, 10 and 20 years after application, respectively. After failure of the coatings, the curves of the evolution of the concentration of free chloride for the substrates start to deviate from that for substrate in C10(wc0.3)-S (no coating failure is considered in this coating system). The concentration of free chloride in the coated substrates is always lower than that in the uncoated substrate (Sub), even though the coatings fail after a certain period of time (e.g. 5, 10 or 20 years). The lower Cl^- concentration in the coated substrates is due to the protection of the substrates before the failure of the coatings.

Predicted time until initiation of reinforcement corrosion in the concrete structures
Fig. 6.26b shows the predicted time until initiation of reinforcement corrosion, $T_{corrosion}$, for the uncoated substrate and the coated substrates. $T_{corrosion}$ for the substrate is extended from 39 years to 42, 44 or 46 years by application of the coatings, if the coatings fail at 5, 10 or 20 years after application, respectively. It suggests that the robustness of the coating, i.e. a good bond to the substrate, is crucial for the effectiveness of the coating to extend the time until initiation of reinforcement corrosion in the substrate.

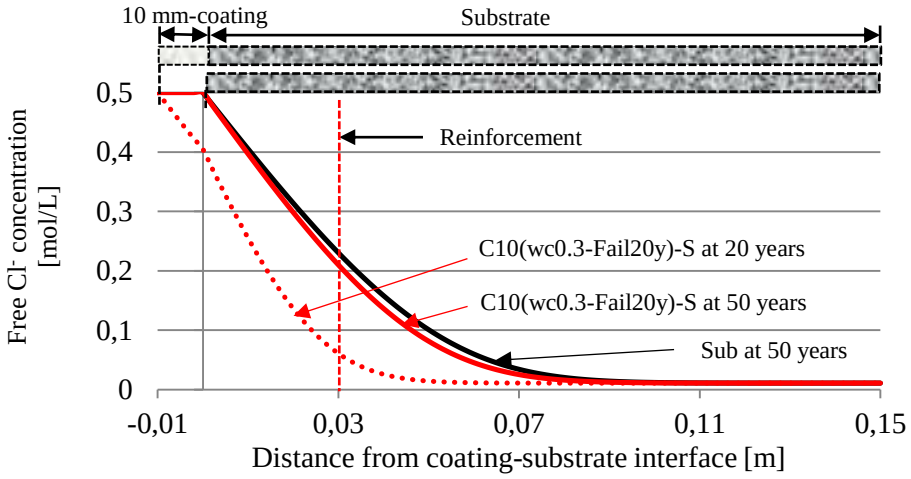

Fig. 6.25 Profiles of free chloride in the uncoated substrate and the coating system. In the coating system, a 10-mm thick coating (w/c = 0.3) is applied on a young substrate (age = 7 days). The free chloride profile in the coating system at 20 years (dotted red line) is presented. After 20 years, the coating fails and no protection of the substrate is considered. The chloride profile in the coating system at 50 years (red line) is compared to that in the uncoated substrate (black line).

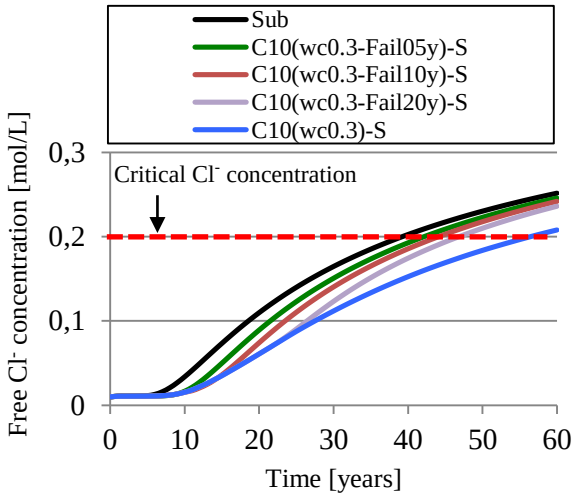

(a) Concentration of free chloride at steel surface

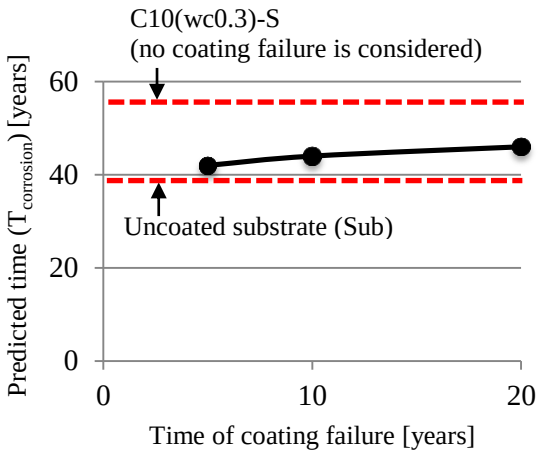

(b) Predicted time until initiation of reinforcement corrosion in the substrate (concrete cover = 30 mm)

Fig. 6.26 Evolution of concentration of free chloride at the steel surface (a) and predicted time until initiation of reinforcement corrosion in the concrete substrates (b). The 10 mm-thick coatings (w/c = 0.3) are applied on young substrates (age = 7 days). The time of coating failure is assumed to be 5, 10 or 20 years, respectively.

6.6.6 Coatings applied on cracked substrates

Profiles of free chloride in concrete structures

In addition to chloride penetration in crack-free concrete structures, also chloride transport in cracked concrete structures is simulated. A substrate with a crack (Sub-Crack15) is schematically shown in Fig. 6.27. The crack in the substrate has a width of 0.4 mm and a depth of 15 mm. Fig. 6.27b and c show the chloride profile in the cracked substrate after 10 and 50-year exposure to the chloride environment. Higher chloride concentration is seen in the areas around the crack, because the crack provides a free path for chloride diffusion.

Fig. 6.28 shows the chloride ingress in the coating system C10-Old Sub-Crack15mm. A 10 mm-thick coating material is applied on a cracked concrete substrate that has been exposed to the chloride environment for 10 years (Fig. 6.28a). The chloride profile in the coating system at 10.1 years is shown in Fig. 6.28b. The chloride concentration around the crack was decreased due to the chloride diffusion from the surface area of the substrate to both the coating material and the inner part of the substrate. The chloride profile around the crack in the coating system after 50-year exposure to the chloride environment (Fig. 6.28c) is more blunt than that in the uncoated substrate (Fig. 6.27c). It indicates that the coating reduces the influence of the crack on the chloride ingress in the substrate.

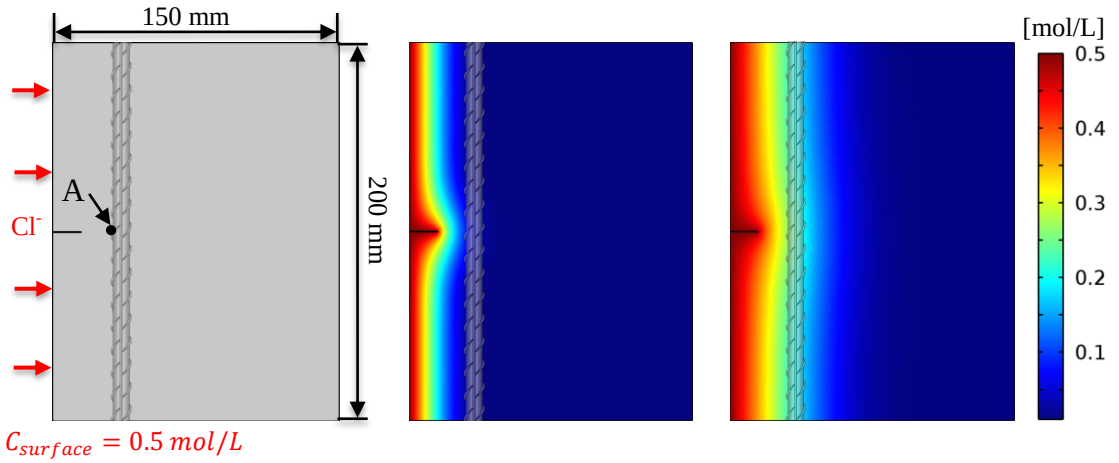

Fig. 6.27 Chloride transport in the substrate (Sub-Crack15mm). A surface crack is located at half height of the substrate. The crack has a size of $0.4 \times 15\ mm^2$. (a) cracked concrete structure (b) free chloride profile after 10 years exposure (c) free chloride profile after 50 years exposure.

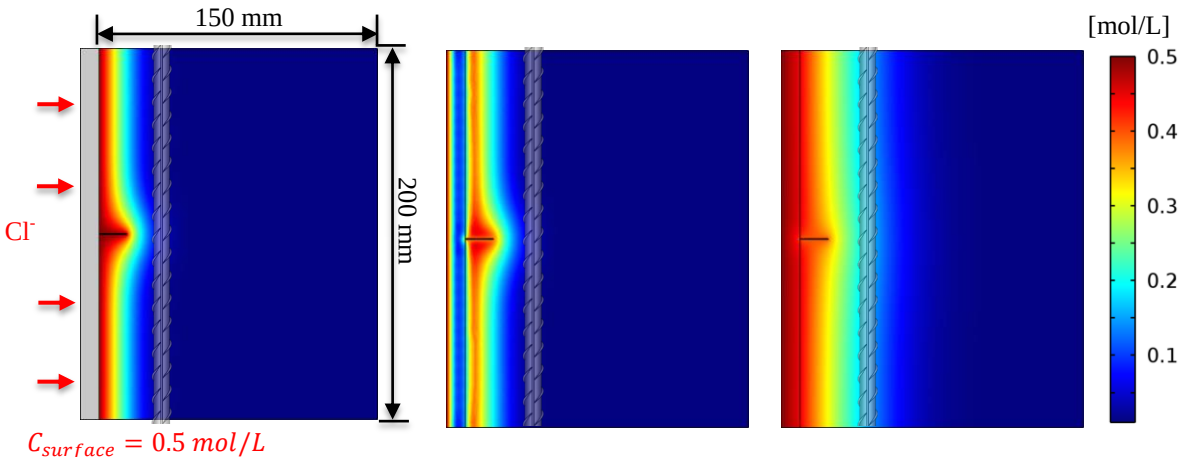

(a) $t = 10\ years$ (b) $t = 10.1\ years$ (c) $t = 50\ years$

Fig. 6.28 Chloride transport in the coating system ("C10-Old Sub-Crack15mm"). The crack has a size of $0.4 \times 15\ mm^2$. (a) a 10 mm-thick coating is applied on a cracked concrete substrate that has been exposed to chloride environment for 10 years (b) free chloride profile after 10.1 years exposure (c) free chloride profile after 50 years exposure.

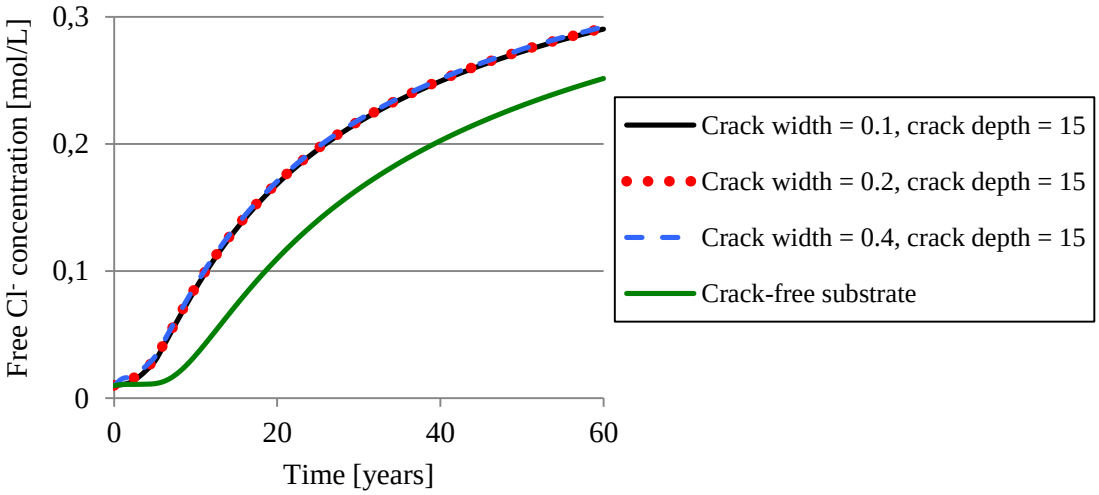

Fig. 6.29 Evolution of concentration of free chloride at the steel surface in the uncoated substrates (see Fig. 6.27a). The substrates have a surface crack with a depth of 15 mm and different widths (i.e. 0.1, 0.2 and 0.4 mm). The thickness of concrete cover is 30 mm.

Effect of crack width on free chloride concentration at the reinforcement

Fig. 6.29 shows the evolution of the concentration of free chloride at the steel surface in several uncoated substrates. Both the crack-free substrate and cracked substrates are considered in the simulation. The cracked substrates have a transverse surface crack (crack depth = 15 mm) with different widths (i.e. 0.1, 0.2 and 0.4 mm) (see Fig. 6.27a). The surface cracks clearly cause an increase of the concentration of free chloride at the steel surface compared to that in a crack-free substrate. For cracks with different widths, the curves of the evolution of the concentration of free chloride at the steel surface almost coincide. Therefore, the surface cracks with different widths considered in the simulations have similar influence on the chloride ingress. This is in accordance to the findings reported in [174]. Note that, for transverse surface cracks with a width < 0.1 mm, the influence of the surface crack on chloride ingress in concrete is dependent on the crack width [174].

Effect of crack depth on free chloride concentration at the reinforcement

The evolution of the concentration of free chloride at the steel surface (point A in Fig. 6.27a) in cracked substrates and the coated cracked substrates is depicted in Fig. 6.30a. The cracks in the substrates have a width of 0.4 mm, and a depth of 10, 15 or 20 mm. The concentration of free chloride at the steel surface is higher for a substrate with a larger crack depth.

In the coating systems, the 10 mm-thick coatings (w/c = 0.3) are applied on the cracked substrates. Before applying the coating, the cracked substrates have been exposed to the chloride environment for 10 years. It can be seen from Fig. 6.30a that the concentration of free chloride at the reinforcement in the coated cracked substrate is much lower than that in the uncoated cracked substrate. Therefore, the 10 mm-thick coatings are efficient to enhance the chloride resistance of the cracked substrates.

Predicted time until initiation of reinforcement corrosion in the concrete structures

The time until initiation of reinforcement corrosion, $T_{corrosion}$, for the uncoated and coated substrates is depicted in Fig. 6.30b. $T_{corrosion}$ for the cracked substrates is 32, 25 and 17 years for crack depths of 10, 15 and 20mm, respectively. Due to the presence of the surface crack, $T_{corrosion}$ for the cracked substrates is significantly shorter than that for the crack-free substrate (39 years).

With a 10-mm thick coating, $T_{corrosion}$ for the cracked substrates is extended from 32 to 47 years, from 25 to 41 years and from 17 to 33 years for the substrates with a crack depth of 10, 15 and 20 mm, respectively.

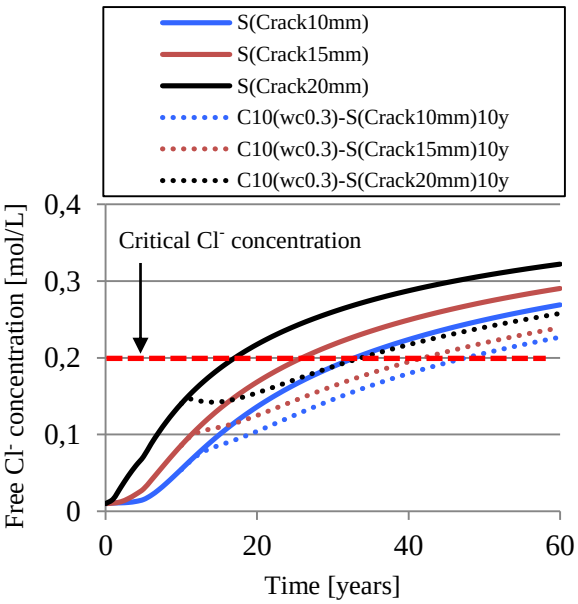

(a) Concentration of free chloride at steel surface

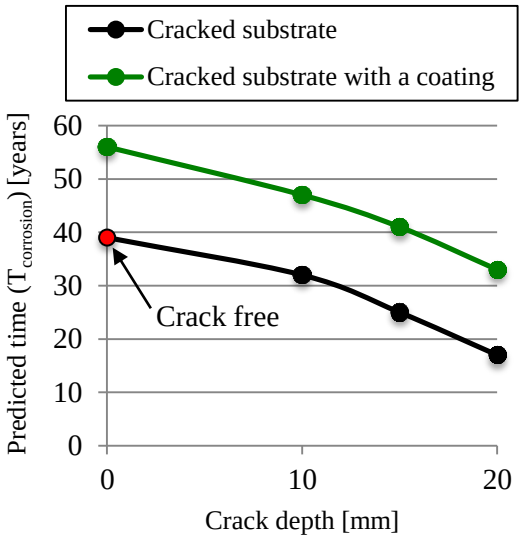

(b) Predicted time until initiation of reinforcement corrosion in the substrate (concrete cover = 30 mm)

Fig. 6.30 Evolution of concentration of free chloride at the steel surface (a) and the predicted time until initiation of reinforcement corrosion in the cracked substrates (b). The coatings (10 mm-thick, w/c = 0.3) are applied on 10 year-old cracked substrates. Before application of the coating, the cracked substrates have been exposed to chloride environment for 10 years. The surface crack in the substrate has a width of 0.4 mm, and a depth of 10, 15 or 20 mm. The original thickness of concrete cover is 30 mm.

6.6.7 Overview of the predicted time until initiation of reinforcement corrosion in the concrete structures

To summarize, the predicted time until initiation of reinforcement corrosion, $T_{corrosion}$, for concrete structures foreseen with different coatings is listed in Table 6.8. From the table the influence of various coating/substrate parameters can be seen. The results indicate that the surface cracks significantly reduce $T_{corrosion}$ for the concrete structures. However, with a 10 mm-thick cementitious coating (w/c = 0.3), $T_{corrosion}$ for both crack-free and cracked substrates can be extended significantly.

The water-to-cement ratio of the coating and the thickness of the coating have a great effect on the effectiveness of the coating. $T_{corrosion}$ for the substrate can be only slightly extended by a coating with a high w/c (e.g. 0.5) or a small thickness (e.g. 3 mm). Moreover, late application of the coating has little influence on the effectiveness of the coating to extend the $T_{corrosion}$ for the substrate.

Table 6.8 Overview of the predicted time until initiation of reinforcement corrosion in the concrete structures [years].

Parameter to be evaluated	Designation	Coating (Thickness, w/c)	Substrate (Age, crack)	Coating fails at t years	Predicted time until initiation of reinforcement corrosion		Extra time
					Uncoated substrate	Coated substrate	
	Sub		Young Substrate		39		
w/c ratios of the coating	C10(wc0.5)-S	10 mm (w/c = 0.5)	Young Substrate		39	40	1
	C10(wc0.4)-S	10 mm (w/c = 0.4)	Young Substrate		39	44	5
	C10(wc0.3)-S	10 mm (w/c = 0.3)	Young Substrate		39	56	17
Coating thickness	C06(wc0.3)-S	6 mm (w/c = 0.3)	Young Substrate		39	48	9
	C03(wc0.3)-S	3 mm (w/c = 0.3)	Young Substrate		39	43	4
Time of failure of the coating	C10(wc0.3-Fail05y)-S	10 mm (w/c = 0.3)	Young Substrate	5	39	42	3
	C10(wc0.3-Fail10y)-S	10 mm (w/c = 0.3)	Young Substrate	10	39	44	5
	C10(wc0.3-Fail20y)-S	10 mm (w/c = 0.3)	Young Substrate	20	39	46	7
Time of application of the coating	C10(wc0.3)-S05y	10 mm (w/c = 0.3)	5-year old Substrate		39	53	16
	C10(wc0.3)-S10y	10 mm (w/c = 0.3)	10-year old Substrate		39	52	13
	C10(wc0.3)-S20y	10 mm (w/c = 0.3)	20-year old Substrate		39	50	11
Depth of surface crack in the substrate	S(Crack10mm)		Young S(Crack10mm)		32		
	S(Crack15mm)		Young S(Crack15mm)		25		
	S(Crack20mm)		Young S(Crack20mm)		17		
	C10(wc0.3)-S(Crack10mm)10y	10 mm (w/c = 0.3)	10-year old S(Crack10mm)		32	47	15
	C10(wc0.3)-S(Crack15mm)10y	10 mm (w/c = 0.3)	10-year old S(Crack15mm)		25	41	16
	C10(wc0.3)-S(Crack20mm)10y	10 mm (w/c = 0.3)	10-year old S(Crack20mm)		17	33	16

C = Coating, S = Substrate.

6.7 Conclusion

In this chapter, the effectiveness of cementitious coatings to retard chloride ingress into concrete substrates was studied by simulation. The coatings are applied either on crack-free or on cracked substrates. The uncoated substrates (w/c = 0.48, cover thickness = 30 mm) and the coated substrates are considered saturated and exposed to marine environment (chloride concentration = 0.5 mol/L). In the simulation both diffusion and chloride binding were taken into account.

The simulation results included the free chloride profile in the coating systems and the evolution of the free chloride concentration at the reinforcement. Assuming a critical chloride concentration of 0.2 mol/L at the reinforcement, the effect of coatings on the time until initiation of reinforcement corrosion in concrete structures, $T_{corrosion}$, was investigated. Based on the simulation results, the influence of several parameters was evaluated, viz. the coating composition (i.e. w/c), coating thickness, time of application of the coating and premature failure of the coating. The following conclusions can be drawn:

- The chloride binding of the substrate has a significant effect on the chloride ingress. For the chosen example, $T_{corrosion}$ for the substrate is 39 years. The time for $T_{corrosion}$ will be underestimated by 30 years when the chloride binding is not considered in the simulation of chloride ingress.
- The w/c ratio of the coating plays an important role in the chloride ingress into the coating system. $T_{corrosion}$ for the substrates is extended by 5 or 17 years, when a 10 mm-coating with a w/c of 0.4 or 0.3 is applied. However, a coating with a w/c of 0.5 will extend the $T_{corrosion}$ for the substrate by only 1 year.
- The coating thickness is also an important parameter in chloride ingress into coated substrates. $T_{corrosion}$ for the substrates differs a lot when coatings with different thicknesses are applied. With a 3, 6 and 10 mm-thick coating (w/c = 0.3), $T_{corrosion}$ for the substrate can be extended by 4, 9 and 17 years, respectively. For a proper protection of the substrate, the w/c ratio and the thickness of the coating should be carefully designed.
- The exposure regime of the substrate before applying the coating has an influence on the effectiveness of the coating. With a 10 mm-thick coating (w/c = 0.3), $T_{corrosion}$ for the 5, 10 and 20-year old substrates that are exposed to chloride environment can be extended by 16, 13 and 11 years, respectively. In case a coating is needed for the substrate to provide extra resistance against chloride ingress, it is preferable to apply a coating as early as possible, since the effectiveness of the coating is reduced by a late application.
- When a coating undergoes an early failure due to cracking or debonding, the effectiveness of the coating is significantly reduced compared to the coating that doesn't fail. The predicted $T_{corrosion}$ for the coated substrates (coating is applied on 7-day old substrate) can be extended by 3, 5 and 7 years if the coating fails at 5, 10 and 20 years after application respectively.
- Chloride ingress into cracked substrate (crack width = 0.4 mm) is promoted by the

presence of the surface crack. The influence of the crack depth is more important than that of the crack width. The substrate with a deeper surface crack has a shorter $T_{corrosion}$ (e.g. 32, 25 and 17 years for crack depth = 10, 15 and 20 mm, respectively). $T_{corrosion}$ for the cracked substrates can be significantly extended by about 15-16 years when a 10 mm-thick coating (w/c = 0.3) is applied.

– In this chapter the chloride diffusivity of the substrate is determined by the capillary porosity of cement matrix (section 6.3.1). Further study is needed for a more precise determination of the chloride diffusivity, i.e. taking into account the microstructure of cement matrix and the interface transition zones of the substrate.

Chapter 7

Retrospection, Conclusions, Recommendations and Future work

7.1 Retrospection

Concrete is widely used in the construction field. Long-term performance of concrete has to be guaranteed for concrete structures to reach the designed service life. However, the initial scatter in the quality of concrete is unavoidable in practice, possibly resulting from improper design, poor execution and improper curing. Areas of concrete with poor quality may become a path for aggressive substances, like chloride ions and CO_2, to penetrate into the concrete, resulting in premature deterioration of the concrete and/or corrosion of the reinforcing steel.

The original idea of this project was to develop a self-healing cementitious coating to protect the low quality concrete structures against ingress of aggressive substances. A durable coating system requires great care, right from its design phase to the total life span. It entails a number of requirements, including a good mix design and a proper curing regime, etc. A type of self-healing agent (i.e. sodium silicate particles encapsulated in epoxy resin) was prepared and incorporated in the coating material in previous study, and promising results regarding self-healing were obtained [182]. For a thin coating material, drying shrinkage-induced cracking of the coating is a great concern, because the coating is vulnerable to water loss due to water absorption by the substrate and/or water evaporation to the environment. In order to achieve a good performance of the coating system, the probability of drying shrinkage induced-cracking of the coating has to be reduced. Moisture transport in a hydrating cementitious coating system and the effect of moisture transport on the hydration process of the coating material are investigated in this thesis (chapter 3 to chapter 5).

Long-term performance (e.g. chloride resistance) of the coating of a concrete structure determines the service life of the coated concrete structure. Chloride ingress in cementitious coating systems and the influencing factors of the effectiveness of the coating are investigated in chapter 6.

In Chapter 3, the mechanism of moisture transport in a hydrating cementitious coating system was studied. A Moisture-Hydration model was proposed to simulate moisture transport in hydrating cementitious coating systems.

In Chapter 4, the properties and parameters of the coating and the substrate were characterized for running the Moisture-Hydration model. The relevant parameters were: porosity, intrinsic permeability, moisture isotherm, and rate of hydration of the coating material with arbitrary water saturation level that determines moisture sink.

In Chapter 5, moisture transport in hydrating cementitious coating systems was simulated.

The moisture profiles in the coating systems and the DOH of the coating were determined. Based on the simulation results, the probability of drying shrinkage-induced cracking was calculated. Some influencing parameters of moisture transport are evaluated:

a) Coating thickness (6, 10 and 20 mm)
b) Duration of sealed/moist curing applied on the top surface of the coating (1, 3 and 7 days)
c) Type of the substrate (ordinary concrete OC with water saturation level s = 50% and high performance concrete HPC with s = 77%)
d) Initial water content of the substrate (standard OC with s = 50% and saturated OC with s = 100%)

In Chapter 6, chloride transport in cementitious coating systems was studied, taking into consideration chloride diffusion and chloride binding. Both the coating and the substrate were considered saturated. The surface chloride concentration was 0.5 mol/L. The profiles of free chloride in the uncoated substrates and coated substrates were determined. With the calculated chloride profiles, the time needed for free chloride to reach a critical concentration (assumed to be 0.2 mol/L) at the reinforcing steel of concrete structures was determined. This time, $T_{corrosion}$, corresponds to the initiation of reinforcement corrosion in concrete structures. The effectiveness of the coatings was indicated by $T_{corrosion}$ for the concrete structures. Some influencing parameters were studied:

a) Water-to-cement ratio of the coating (0.3, 0.4 and 0.5). The coatings were applied on young substrates (age = 7 days).
b) Thickness of the coatings (3, 6 and 10 mm). The coatings were applied on young substrates (age = 7 days).
c) Exposure regime of the substrate before application of the coating. The coatings were applied on old substrates that had been exposed to chloride environment for 5, 10 and 20 years.
d) Time of failure of the coating (at 5, 10 and 20 years after application of the coating). The coatings were applied on young substrates (age = 7 days).
e) Presence of surface crack in the substrate (crack width: 0.2 and 0.4, crack depth: 10, 15 and 20 mm). The coatings were applied on old substrates that had been exposed to chloride environment for 10 years.

7.2 Conclusions

This study deals with the simulation of transport processes in hydrating cementitious coating systems. Based on the parameter study on moisture transport (chapter 5) and chloride transport (chapter 6), the following conclusions can be drawn:

Moisture transport in hydrating coating systems

- Among the evaluated parameters (i.e. the coating thickness, the duration of moist/sealed curing conditions, the initial water content of the substrates and the type of substrates), the duration of moist curing is the most influencing parameter that affects the hydration of the coating materials.
- The influence of the initial water content of the substrates on the hydration of the coating is small when moist curing is applied. This also applies for the influence of the type of substrates. In this sense, pre-saturation of concrete substrates is not crucial. However, the influence of the type of the substrate on the hydration of the coating becomes noticeable when sealed curing of the coating is applied.
- Moist curing is essential to compensate for water absorption by the substrates, and to ensure a proper hydration process of the coating. Longer moist curing is also beneficial for reducing the probability of drying shrinkage-induced cracking of the coating at early ages. However, at later ages the probability of cracking of the coating with longer moist curing is higher than that of the coating with short moist curing. These findings are in accordance with experimental results in literature.

Chloride transport in hydrating coating systems under saturated condition

- The chloride binding of the substrate has a significant effect on the chloride ingress. The time until initiation of reinforcement corrosion, $T_{corrosion}$, is 39 years for the uncoated substrate in this study. $T_{corrosion}$ is underestimated by 30 years when the chloride binding is not considered in the simulation of chloride ingress.
- The w/c ratio of the coating plays an important role in the chloride ingress into the coating system. $T_{corrosion}$ for the substrates is extended by 5 and 17 years, when a 10 mm-coating with a w/c of 0.4 and 0.3 is applied, respectively. However, the chloride ingress in the substrate can hardly be affected by applying a coating with a w/c of 0.5. With this coating (i.e. w/c = 0.5), $T_{corrosion}$ for the substrate can be extended by only 1 year.
- The coating thickness is also an important parameter in chloride ingress into coated substrates. With a 3, 6 and 10 mm-thick coating, $T_{corrosion}$ for the substrate can be extended by 4, 9 and 17 years, respectively.
- The exposure regime of the substrate before applying the coating has an influence on the effectiveness of the coating. With a 10 mm-thick coating (w/c = 0.3), $T_{corrosion}$ for old substrates that have been exposed to chloride environment for 5, 10 and 20 years can be extended by 16, 13 and 11 years, respectively.

- When a coating undergoes an early failure due to cracking or debonding, the effectiveness of the coating is significantly reduced. The predicted $T_{corrosion}$ for the substrates (coating applied on 7-day old substrate) can be extended by 3, 5 and 7 years, if a 10 mm-thick coating fails after 5, 10 and 20 years, respectively.
- Chloride ingress into cracked substrate (crack width = 0.4 mm) is much faster than that into crack-free substrate. The substrate with a deeper surface crack has a shorter $T_{corrosion}$ (e.g. 32, 25 and 17 years for crack depth = 10, 15 and 20 mm, respectively). A cementitious coating can also extend $T_{corrosion}$ for cracked substrate. For a cracked substrate that has been exposed to chloride environment for 10 years, $T_{corrosion}$ for the cracked substrates can be extended by about 15 years if a 10 mm-thick coating (w/c = 0.3) is applied.

7.3 Recommendations for the design and the application of cementitious coating material

Moisture transport in hydrating coating systems

- The hydration process of the coating material is significantly influenced by water evaporation. After application of a coating, 7 days moist curing is recommended for a proper hydration of the coating. The 7 days moist curing is also beneficial for eliminating the negative effect of water absorption by the substrate on hydration of the coating.
- The probability of cracking is high for the coatings subjected by drying. Measures should be taken to deal with the shrinkage-induced cracking of coatings, e.g. using polymeric fibers and proposing self-healing cement-based coatings.

Chloride transport in hydrating coating systems under saturated condition

- To protect a concrete structure against chloride ingress, a sufficiently low w/c ratio and a sufficiently large thickness of the coating should be used, because chloride ingress in the substrate can be hardly affected when the coating has a high w/c ratio or a small thickness. For instance, a 10 mm-thick coating with w/c = 0.3 is recommended for the concrete structure (w/c = 0.48, cover thickness = 30 mm) in this study.
- To protect a concrete structure against chloride ingress, it is preferable to apply a coating as early as possible, since the effectiveness of the coating decreases with a late application.
- The effectiveness of the coating is reduced by an early failure (e.g. cracking or debonding). Mixtures containing polymeric fibers are recommended to prevent the early failure of the coating, and to ensure the effectiveness of the cementitious coatings.
- Chloride ingress into concrete is greatly promoted by surface cracks. A cementitious coating is recommended for protecting the cracked substrates against chloride ingress. For the design of the coating material, the effectiveness of the coating needs to be evaluated by simulating chloride ingress in the coated cracked substrate. The crack depth should be inspected for the simulation of chloride ingress.

7.4 Contributions of this study

In fact all aspects from this study have been under investigation by researchers for decades. This thesis highlights a few aspects that have been given less attention in previous studies:

Moisture transport in hydrating coating systems

- Moisture transport in hydrating coating systems is studied in detail. The interaction between moisture transport and hydration process in the coating are explicitly considered in the Moisture-Hydration model, making it possible to determine the development of the degree of hydration of the coating material as a function of time.
- For a coating system exposed to an environment with RH = 50%, the evaporation of water from the coating surface is simulated, taking into account the characteristics of the coating, instead of applying an empirical convection coefficient. Note that the commonly used convection coefficient for studying water evaporation from hardened cementitious materials cannot easily be applied to a hydrating cementitious material. The convection coefficient for hardened material corresponds to a fine pore structure in comparison to the relatively coarse pore structure of a hardening material. When the convection coefficient for hardened material is used to account for the evaporation process of hardening material, the rate of water evaporation from the hardening material will be underestimated.
- The combined effect of environment and substrate on hydration process of the coating is evaluated. It is found that the influence of the water saturation level of the substrate on the hydration process of the coating will be eliminated by when at least 1-day moist curing is applied to the coating. It indicates that the combined effect of environment and substrate should be considered when evaluating the influence of the substrates on the hydration process of the coating.
- For a broader application, the Moisture-Hydration model can also be used for investigating the interaction between moisture transport and hydration process in uncoated concrete structures, and for evaluating the quality of concrete cover.

Chloride transport in hydrating coating systems under saturated condition

- The chloride ingress in hydrating cementitous coating systems is simulated. Two important points have been considered explicitly in view of a proper simulation of chloride transport, viz.:
  1. Mass conservation of chlorides at the coating-substrate interface;
  2. Chloride diffusivity and chloride binding capacity of hardening coating and hardening substrate.
- Time until initiation of reinforcement corrosion, $T_{corrosion}$, for the coated concrete structures (i.e. corrosion of steel reinforcement) is assessed based on chloride ingress. Parameter studies are performed to evaluate the influencing factors of chloride ingress in the coating systems. The parameter studies provide information for a proper design and application of the coating, in terms of the sensitivity of w/c ratio of the coating, thickness of the coating and early or late application of the coating on chloride ingress in coated concrete structures.

7.5 Future work

This thesis presents a parameter study of the transport processes in hydrating cementitious coating systems, and gives guidance to the design and the application of the coatings. For a durable cementitious coating, further study is still recommended. This study needs to be continued with the following aspects:

Moisture transport in hydrating coating systems

- In this study moisture transport in the coating systems is limited to cement paste-concrete substrate system. From a practical point of view, coatings made of various types of cements (e.g. cement, fly ash and slag) should be considered for simulation. The greatest difficulty lies in the determination of the parameters of the Moisture-Hydration model, including time-dependent porosity, intrinsic permeability and Van Genuchten parameters (derived from moisture isotherm curves). In addition, a perfect interface between the coating and substrate was assumed in this study. However, practically, an interface transition zone exists between the coating and the substrate. The microstructure and the transport properties of the interfacial transition zone are different from that of the coating or the substrate. Therefore, the interfacial transition zone between the coating and the substrate needs to be considered in the simulation of moisture transport.
- The Moisture-Hydration model has been validated in different modeling steps (e.g. simulation of moisture transport in hydrating cement pastes, see appendix B). For an extensive validation of the model, the evolution of moisture profile in the coating system and the development of degree of hydration of the coating need to be determined experimentally, e.g. by using NMR.
- To determine the probability of drying shrinkage-induced cracking of the coating material, the scatter in material properties should be considered. Moreover, relaxation behavior of the coating and the substrate need to be taken into account.

Chloride transport in hydrating coating systems under saturated condition

- In the simulation of chloride ingress into cementitious coating systems, the chloride diffusivity of the substrate is determined by the capillary porosity. Further study is needed for a more precise determination of the chloride diffusivity, i.e. taking into account the microstructure of cement matrix as well as the cement matrix-aggregate interface.
- In chapter 6, chloride ingress in saturated cementitious coating system was investigated. In practice, the coating system can be partially saturated due to drying. On one hand, the drying of the coating system leads to an unsaturated coating system for chloride transport. On the other hand, the drying of the coating system affects the hydration processes of the coating and the substrate. Further investigation of chloride ingress in hydrating coating systems subjected to drying is needed.
- Cracks in cementitious coatings and self-healing of the cracks are commonly seen in practice. The influence of occurrence and self-healing of cracks of the coatings on chloride ingress in the coating systems needs to be evaluated in future studies.

Summary

Concrete is currently the most widely used material in construction field. A good performance of concrete structures is required for reaching the designed service life. However, the initial scatter in the quality of concrete is unavoidable in practice, possibly resulting from improper design, poor execution, or deterioration due to stresses during the service life of concrete structures (e.g. external load, stress induced by temperature, drying shrinkage or ingress of chemical substances, etc.). A cementitious coating can be used to protect low quality concrete structures against the ingress of aggressive substances, like CO_2 and chloride ions, and to extend the service life of the reinforced concrete structures.

A durable cementitious coating system entails a number of requirements, including a good mix design of the coating as well as a proper curing regime. A small thickness of the coating material suggests that the coating is susceptible to water loss when the coating is applied on a dry substrate, or subjected to drying condition while hardening. The effectiveness of the coating will be impaired when differential drying shrinkage-induced cracking or debonding of the coating takes place. In this thesis moisture transport in hydrating coating systems and the probability of drying shrinkage-induced cracking of the coating are studied. To evaluate the effectiveness of the coating, chloride ingress in concrete with various coatings is simulated. The effectiveness of the coating is indicated by the time needed for free chloride to reach a critical concentration at the reinforcing steel of concrete structures. This time, $T_{corrosion}$, also corresponds to the initiation of reinforcement corrosion in concrete structures.

In chapter 3, mechanisms of moisture transport in a hydrating cementitious coating system were studied. A Moisture-Hydration model was proposed to simulate moisture transport in hydrating cementitious coating systems.

In chapter 4, parameters needed for determination of moisture transport properties of the coating and the substrate were quantified, i.e. porosity, intrinsic permeability, moisture isotherm. The rate of hydration of the coating material with arbitrary water saturation level was calculated.

In chapter 5, moisture transport in hydrating cementitious coating systems was simulated. The moisture profiles in the coating systems and the degree of hydration of the coatings were determined. Based on the simulation results, the probability of drying shrinkage-induced cracking was calculated. Some influencing parameters of moisture transport were evaluated: coating thickness, duration of sealed/moist curing applied on top surface of the coating, type of the substrate and initial water content of the substrate. Among the evaluated parameters, the duration of moist curing is the most influencing parameter that affects the hydration of the coating materials. Moist curing is essential to compensate for water absorption by the substrates, and to ensure a proper hydration process of the coating. The longer moist curing is also beneficial to reduce the probability of early-age cracking induced by drying shrinkage. However, the probability of cracking is increased for coating materials at later ages when

longer moist curing is applied. Polymeric fibers are recommended to reduce the probability of the shrinkage-induced cracking of coatings. Note that the calculation of the probability of cracking of the coating is preliminary, further study is needed for more accurate predictions of the probability of cracking, e.g. taking into account the relaxation process.

If moist curing is applied, the influence of initial water content of the substrates and the type of the substrates on hydration process of the coating is relatively low. In this sense, pre-saturation of concrete substrates is not necessary. However, the influence of the type of the substrate on the hydration of the coating becomes noticeable when sealed curing is applied. This influence can be minimized by pre-treatment of the substrates, e.g. pre-wetting.

In chapter 6, mechanisms of chloride transport in cementitious coating systems were studied, taking into consideration chloride diffusion and chloride binding. The chloride profiles in the coating systems were determined by simulation. With the calculated chloride profiles, the time until initiation of reinforcement corrosion, $T_{corrosion}$, for the uncoated (w/c = 0.48) and coated concrete structures was determined. Some influencing parameters were evaluated: water-to-cement (w/c) ratio of the coating, thickness of the coating, early or later application of the coating, time of failure of the coating and presence of surface crack in the substrate. The w/c ratio of the coating plays an important role in the chloride ingress into the coating system. $T_{corrosion}$ for the substrate can be substantially extended by applying a coating with a low w/c ratio (e.g. w/c = 0.3). However, the chloride ingress in the substrate can hardly be affected by applying a coating with a high w/c ratio (e.g. w/c = 0.5). $T_{corrosion}$ for the substrates differs a lot when coatings with different thicknesses are applied. For a proper protection of the substrate, the w/c ratio and the thickness of the coating should be carefully designed. The exposure regime of the substrate before applying the coating has an influence on the effectiveness of the coating. In order to protect a concrete structure exposed to the chloride environment, it is preferable to apply a coating as early as possible, since the effectiveness of the coating is reduced by a late application. When a coating undergoes an early failure due to cracking or debonding, the effectiveness of the coating is also reduced. Polymeric fibers are again recommended to prevent the early failure, and to ensure the effectiveness of the cementitious coatings. Chloride ingress into the substrate is promoted by cracks. In comparison with crack width, crack depth has a great influence on chloride ingress in concrete structures. Substrate with a deeper surface crack has a shorter $T_{corrosion}$. $T_{corrosion}$ for the cracked substrates can be significantly extended by application of a cementitious coating.

To summarize, this thesis investigated the transport processes (moisture transport and chloride transport) in hydrating cementitious coating systems. Based on this study of influencing parameters of moisture transport, suggestions regarding curing condition have been given for a proper hydration of the coating. Parameter studies were performed to investigate effectiveness of coatings for extending the time until initiation of reinforcement corrosion in concrete structures, $T_{corrosion}$. These parameter studies give guidance for the design of coating materials with regard to water-to-cement ratio of the coatings and thickness of the coatings.

Samenvatting

Beton is momenteel het meest gebruikte materiaal in de bouwsector. Om een vereiste levensduur te bereiken moet het beton van een betonconstructie aan minimale eisen voldoen. De spreiding in de kwaliteit van beton is echter in de praktijk onvermijdelijk, bijvoorbeeld als gevolg van onjuist ontwerp, slechte uitvoering of degradatie door (hoge) spanningen tijdens de levensduur van de constructies (bijv. door externe belasting, door temperatuur veroorzaakte spanningen, krimp tijdens het uitdrogen of binnendringen van chemische stoffen, enz.). Een cementgebonden coating kan worden toegepast om constructies van (onverwacht) lage kwaliteit te beschermen tegen het binnendringen van agressieve stoffen, zoals CO_2 en chloride-ionen, en om de levensduur van de constructies van gewapend beton te verlengen.

Een duurzaam cementgebonden coatingsysteem (systeem = coating + substraat) moet aan een aantal eisen voldoen, waaronder een goed mensgelontwerp van de coating en een goed uithardingsregime. Een geringe dikte van het coatingmateriaal maakt de coating gevoelig voor waterverlies wanneer de coating wordt aangebracht op een droog substraat of wordt onderworpen aan uitdroging tijdens het verharden. De effectiviteit van de coating zal verminderen wanneer krimp resulteert in scheuren of onthechting van de coating. In dit proefschrift worden vochttransport in verhardende coatingsystemen en de kans op het optreden van krimpscheuren van de coating bestudeerd. Om de effectiviteit van de coating te evalueren, wordt chloride-indringing in beton met verschillende coatings gesimuleerd. De effectiviteit van de coating wordt beoordeeld aan de hand van de tijd die nodig is om een kritische chloride concentratie te bereiken aan het oppervlak van het wapeningsstaal. Deze tijd, $T_{corrosion}$, wordt beschouwd als het begin van wapeningscorrosie in betonconstructies.

In hoofdstuk 3 worden mechanismen van vochttransport in een hydraterend cementgebonden coatingsysteem bestudeerd. Een Moisture-Hydration-model wordt voorgesteld om vochttransport in hydraterende cementgebonden coatingsystemen te simuleren.

In hoofdstuk 4 worden de parameters die nodig zijn voor de bepaling van vochttransporteigenschappen van de coating en het substraat gekwantificeerd, d.w.z. porositeit, intrinsieke permeabiliteit en vochtgehalte. De snelheid van hydratatie van het coatingmateriaal met willekeurig watergehalte wordt berekend.

In hoofdstuk 5 wordt vochttransport in hydraterende cementgebonden coatingsystemen gesimuleerd. De vochtprofielen in de coatingsystemen en de graad van hydratatie van het coatingmateriaal worden bepaald. Op basis van de simulatieresultaten wordt de kans op krimpscheuren berekend. Een aantal parameters die het vochttransport beïnvloeden wordt geëvalueerd: coatingdikte, duur van nabehandeling van de aangebrachte coating, type substraat en initieel watergehalte van het substraat. Van de geëvalueerde parameters is de duur van de nabehandeling de meest invloedrijke parameter die de hydratatie van het coatingmateriaal bepaalt. Nabehandeling met veel vocht is essentieel om de waterabsorptie door het substraat te compenseren en om een goed hydratatieproces van de coating te verzekeren.

Een langere nabehandeling (onder vochtige condities) is gunstig voor het verminderen van vroegtijdige scheurvorming door uitdrogingskrimp. Bij (te) lange nabehandeling (met vocht) neemt de kans op scheurvorming in de coating neemt echter weer toe. Polymeervezels worden aanbevolen om de kans op krimpscheuren van de coating te verminderen. Benadrukt wordt dat dit het resultaat is van een voorlopige berekening. Verder onderzoek is nodig voor nauwkeuriger voorspellingen te kunnen doen van de kans op scheuren, o.a. rekening houdend met relaxatie van materiaalspanningen.

Bij uitharding in vochtige omgeving (moist curing) is de invloed van het initiële watergehalte van het substraat en het type substraat op het hydratatieproces van de coating relatief laag. In deze situatie is voorverzadiging van het betonsubstraat niet noodzakelijk. De invloed van het type substraat op de hydratatie van de coating wordt echter merkbaar wanneer de coating gedurende het verharden aan het oppervlak wordt afgedekt (sealed curing). In dat geval is voorbevochtiging van het substraat nuttig om de kans op scheurvorming van de coating te verminderen.

In hoofdstuk 6 worden mechanismen van chloridetransport in cementgebonden coatingsystemen bestudeerd, rekening houdend met chloridediffusie en chloride-binding. De chlorideprofielen in de coatingsystemen zijn numeriek gesimuleerd. Met de berekende chlorideprofielen is de tijd tot initiatie van wapeningscorrosie bepaald in betonconstructies (w/c = 0,48) met en zonder coating. Het effect van verschillende invloedsfactoren is geëvalueerd: water-cement (w/c) factor van de coating, dikte van de coating, vroeg of laat aanbrengen van de coating, moment van falen van de coating en aanwezigheid van oppervlakscheuren in het substraat. De w/c-factor van de coating speelt een belangrijke rol bij de indringing van chloride in het coatingsysteem. De tijd tot het initiëren van wapeningscorrosie in betonconstructies kan aanzienlijk worden verlengd door het aanbrengen van een coating met een lage w/c-factor, bijvoorbeeld w/c = 0,3. Het indringen van chloride in het substraat wordt nauwelijks beïnvloed door het aanbrengen van een coating met een hoge w/c-factor, bijvoorbeeld w/c = 0,5. De tijd tot het begin van wapeningscorrosie verschilt sterk wanneer coatings met verschillende diktes worden aangebracht. Voor een goede bescherming van het substraat moeten de w/c-factor en de dikte van de coating zorgvuldig worden gekozen. De klimaatcondities waaraan het substraat is blootgesteld vóór het aanbrengen van de coating heeft invloed op de effectiviteit van de coating. Om een betonconstructie te beschermen tegen chloride-indringing, is het aan te raden om de coating zo vroeg mogelijk aan te brengen. Later aanbrengen vermindert de effectiviteit van de coating. Wanneer een coating vroegtijdig faalt door scheuren of onthechting wordt de effectiviteit van de coating eveneens verminderd. Toepassen van een coating met polymeervezels wordt aanbevolen om vroegtijdig falen te voorkomen en om de effectiviteit van cementgebonden coatings te verzekeren. Scheuren bevorderen het binnendringen van chloride in het substraat. Bij het indringen van chloride in betonconstructies heeft de *diepte* van de scheur een grotere invloed dan de *breedte* hiervan. Substraat met een diepere oppervlaktescheur leidt tot versnelde corrosie. De tijd tot corrosie in een gescheurd substraat kan aanzienlijk worden verlengd door een cementgebonden coating aan te brengen.

Samengevat: in dit proefschrift is onderzoek gedaan naar transportprocessen (vocht- en chloridetransport) in hydraterende cementgebonden coatingsystemen. Gebaseerd op deze studie worden suggesties gedaan met betrekking tot de verhardingscondities voor een goede hydratatie van de coating. Parameterstudies zijn uitgevoerd om de effectiviteit van coatings voor het verlengen van de tijd tot wapeningscorrosie vast te stellen. Deze parameterstudies geven aanwijzingen voor het ontwerp van het coatingmateriaal, met betrekking tot de water-cement-factor en de dikte van de coatings.

Appendix A

Evaluation of equations commonly used for simulating moisture transport in partially saturated cementitious materials

A.1 Introduction

Moisture transport process in cementitious materials is usually described with nonlinear diffusion equations [50, 63-71]. Either relative humidity or water content is used as a variable in the equations. When simulating moisture transport in coating systems, the principle of mass conservation of moisture should be fulfilled. However, attention with respect to mass conservation is still needed when using these equations. In this appendix a brief review on the equations describing moisture transport process in porous materials is presented, followed by a case study of moisture transport for evaluating the equations regarding mass conservation.

A.2 Equations describing moisture transport in partially saturated cementitious materials

A.2.1 Relative humidity as a variable

Moisture transport process in cementitious materials can be described by [63] (see also section 3.2.3):

$$\frac{\partial \theta}{\partial RH} \cdot \frac{\partial RH}{\partial t} = div(D_{RH} \cdot grad\ RH) \tag{A.1}$$

where RH is the relative humidity, $\partial\theta/\partial RH$ the moisture capacity and D_{RH} the effective diffusivity.

Based on Eq. (A.1), a simplified equation for simulating moisture transport in cementitious materials is [64-70]:

$$\frac{\partial RH}{\partial t} = div(D'_{RH} \cdot grad\ RH) \tag{A.2}$$

where D'_{RH} is the effective diffusivity, D'_{RH} depends on relative humidity, compressive strength of the material, as well as moisture diffusivity at RH = 100% and RH = 0% [76].

A.2.2 Water content as a variable

For simulating the moisture transport in unsaturated cementitious materials, a formula based on Fick's law is adopted [50, 71]:

$$\frac{\partial \theta}{\partial t} = div(D_\theta \cdot grad\ \theta) \tag{A.3}$$

In Eq. (A.3), θ is the volumetric water content, expressed in m^3 of water per m^3 of material. D_θ is hydraulic diffusivity m^2/s.

The term D_θ can be approximated by an exponential function $D_\theta = D_0 \cdot e^{n \cdot s}$, or a power function $D_\theta = D_0 \cdot s^n$, in which D_0 is a empirically fitted constant, n is a shape term, and s is water saturation level of porous material with the form $s = (\theta - \theta_r)/(\theta_s - \theta_r)$, defined by the value of water filled pores divided by the total pore volume. θ_s is water content in saturated condition (here taken as total porosity of the material), θ_r is the residual water content (here taken as 0). Determination of D_0 requires experimental water sorption test on cementitious materials [71]. However, for hydrating cementitious materials, no straightforward test can be done to determine D_0.

A.3 Case study of moisture transport in cementitious materials for evaluating the equations

From a physical point of view, Eq. (A.1) and Eq. (A.3) fulfill the principle of mass conservation, while Eq. (A.2) may not. However, a lot of studies have been conducted based on Eq. (A.2) [64-70]. A case study is conducted to show the discrepancy between the results calculated by Eq. (A.2) and Eq. (A.3).

Two identical concrete samples (1-year old, w/c = 0.48 [60]) are bonded together (Fig. A.1a). Then the surfaces of the bonded samples are sealed. The concrete samples have different initial water contents (Table A.1). The initial moisture distribution in the samples is shown in Fig. A.1b. Moisture tends to transfer from sample A (saturated) to sample B (partially saturated).

Table A.1 Water saturation level and relative humidtity in two identical concrete samples (w/c = 0.48, the relation between s and RH is described by the desorption isotherm derived from [60]).

Sample	A (Saturated)	B (Partially-saturated)
Water saturation level (s)	100%	27%
Relatieve humidity (RH)	100%	50%

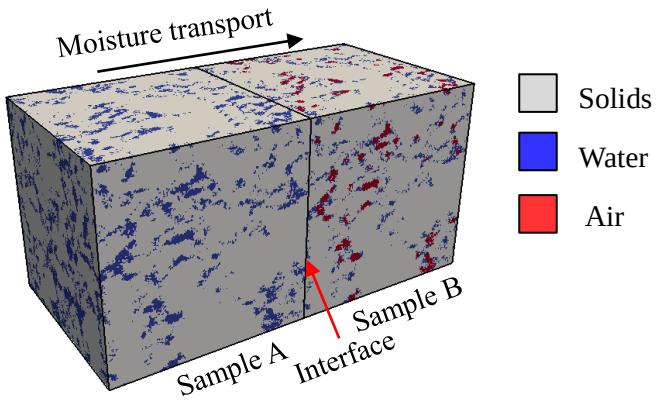

(a) Initial moisture distribution in sample A and sample B

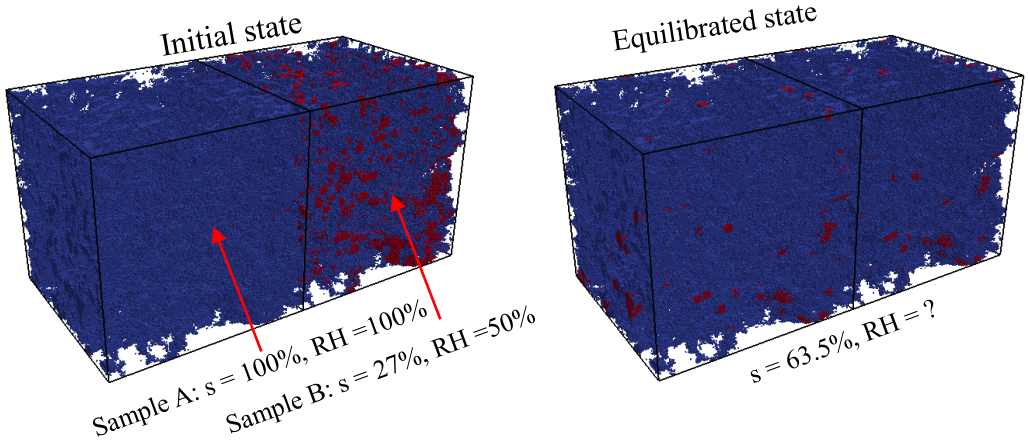

(b) Initial distribution of water and air phases (c) Distribution of water and air phases in equilibrated state

Fig. A.1 Schematic illustration of moisture transport in two identical concrete samples. Sample A is water saturated, and sample B is partially saturated. The surfaces of the bonded samples are sealed. Moisture is only allowed to transfer within the two samples.

According to Eq. (A.2), the equilibrated relative humidity in the bonded samples is 75% (the average value of 100% for sample A and 50% for sample B). According to Eq. (A.3), the equilibrated water saturation level in the bonded samples is 63.5% (Fig. A.1c), which is the average value of the initial values (100% for sample A, and 27% for sample B). Moisture profiles of the bonded samples are plotted in Fig. A.2. Initial and equilibrated states of water saturation level and relative humidity are shown is Fig. A.2a and Fig. A.2b, respectively. Significant discrepancy in water saturation level and relative humidity can be observed when a simplified equation (Eq. (A.2)) is used.

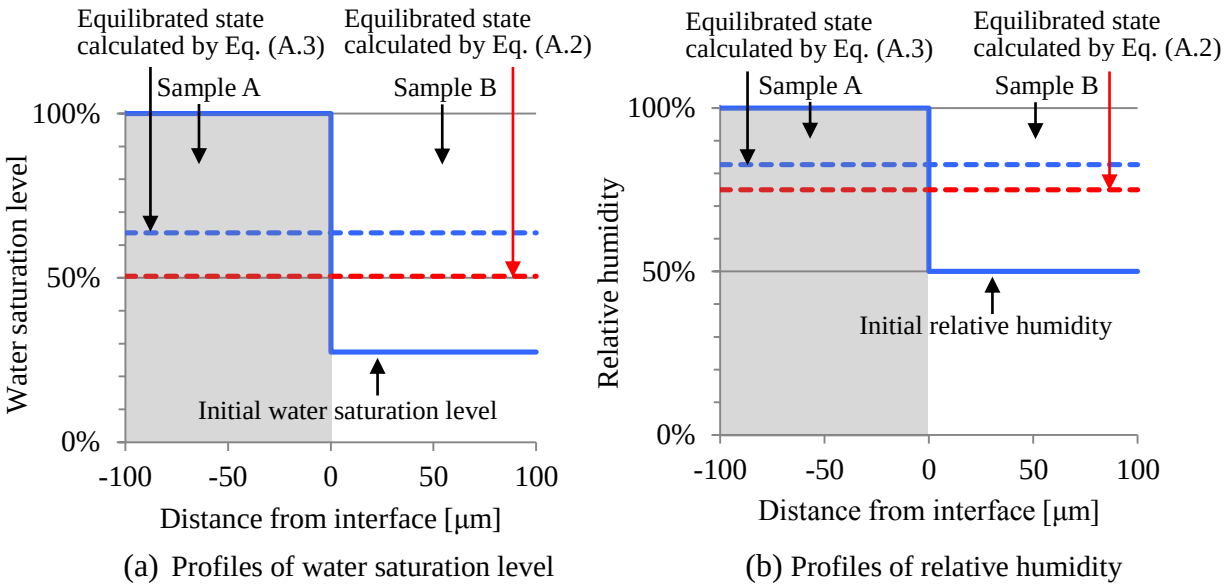

(a) Profiles of water saturation level (b) Profiles of relative humidity

Fig. A.2 Moisture profiles in the bonded concrete samples (A and B). Sample A and B have an initial water saturation level of 100% and 27%, respectively. The samples are bonded together (Fig. A.1a). Moisture is allowed to transfer within the samples. The moisture profiles in the bonded concretes in equlibrated state are calculated by Eq. (A.3) and Eq. (A.2), respectively. Note that Eq. (A.3) gives a proper description of moisture transport process in concrete, while Eq. (A.2) does not.

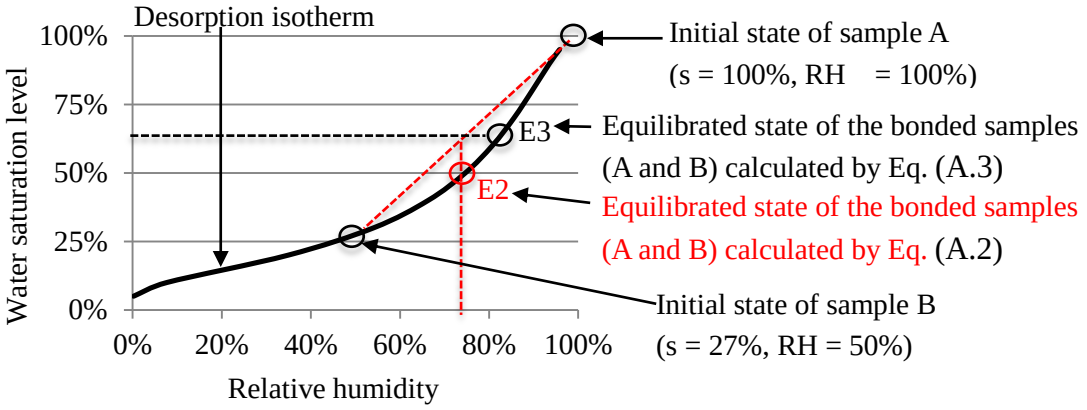

Fig. A.3 Water saturation level versus relative humidity of the concrete samples. The desorption isotherm of the concrete (1-year old, w/c = 0.48) is derived from [60]. The initial moisture state of sample A and sample B are shown in this figure. The two sample s are bonded together and sealed. Moisture is only allowed to transfer within in the samples. E2 and E3 show the moisture states of the bonded samples (A and B) in equilibrated state, calculated by Eq. (A.2) and Eq. (A.3), respectively. Note that Eq. (A.3) gives a proper description of moisture transport process in concrete, while Eq. (A.2) does not.

The relation between the water saturation level and the relative humidity can be described by the water-vapour desorption isotherm of the concrete. The desorption isotherm is derived from [60] and shown in Fig. A.3. Point "E2" on the curve of desorption isotherm corresponds to the relative humidity of 75% calculated by Eq. (A.2), while point "E3" corresponds to the water saturation level of 63.7% calculated by Eq. (A.3). Note that, Eq. (A.3) gives the correct water saturation level (point "E3") in the bonded samples in equilibrated state, because this equation, in principle, conserves the mass of water, while Eq. (A.2) does not. The discrepancy between point "E2" and point "E3" can be even bigger for fresh or early-age cementitious materials, because the curve in Fig. A.3 will be more nonlinear for younger cementitious materials when $RH > 50\%$ [63].

It suggests that the moisture capacity $\partial\theta/\partial RH$ in Eq. (A.1) is essential for conserving the mass of moisture in porous materials when relative humidity is used as a variable. A simplified equation (e.g. Eq. (A.2)) that ignores the moisture capacity will lead to discrepancy between the realistic and the calculated moisture profiles.

A.4 Summary

A brief review of the equations commonly used for studying moisture transport in cementitious materials is given. The validity of the equations regarding the principle of mass conservation is evaluated. The evaluation suggests that the moisture capacity cannot be ignored in the equation when relative humidity is used as a variable, because the moisture capacity is essential for conserving the mass of moisture in the material.

Appendix B

Boundary conditions for simulating moisture transport in cementitious materials

B.1 Introduction

Specification of the boundary conditions at the exposed surface of cementitious materials is a critical issue in the simulation of moisture transport. As stated in section 3.3.7, a convection coefficient is commonly used to describe the moisture exchange between the exposed surface of the material and the environment. The convection coefficient is empirical and depends mainly on the ambient temperature, the wind speed and the characteristics of the porous material. However, a proper determination of the convection coefficient for a hydrating cementitious material is still lacking. In this thesis, instead of using a convection coefficient, a fundamental moisture flux across the exposed surface of cementitious material is simulated. It allows for conserving the mass of moisture at the exposed surface of the material. Boundary condition is applied at a distance from the exposed surface to account for different curing conditions.

Li et al. [183] found that there was a significant moisture gradient above the surface of drying concrete during first day of exposure. In their work, 50 mm-thick concrete specimens with a w/c ratio of 0.5 were prepared. After 28 days saturated curing, the concrete specimen was put in a glass container (Fig. B.1). The depth of the container was around 110 mm. The top surface of the container was open to the environment (RH = 33%). A significant moisture gradient was found within 35 mm from the exposed surface. In order to match the experimental results, they calibrated their moisture transport model by adjusting the distance from the surface of the material for applying the boundary condition (i.e. RH = 33%). They found that a distance of 25 mm from the concrete surface was appropriate for applying the boundary condition. It should be noted that this distance was only justified for 28-day old concrete specimens used in their study. It is believed that the distance would be higher for younger specimens subjected to drying. For newly cast coating, this distance should be longer, because moisture in a fresh coating can evaporate much easier and cause higher relative humidity in the ambient air than that in a hardened coating.

For a proper simulation of moisture transport in a coating system with a hydrating coating material, the distance above the exposed surface of the material for applying the boundary condition (i.e. relative humidity) is calibrated for the case of a hydrating cement paste. Moisture transport in a matured concrete subjected to drying is simulated with the same boundary condition. The simulated moisture content in the concrete is compared to experimental results.

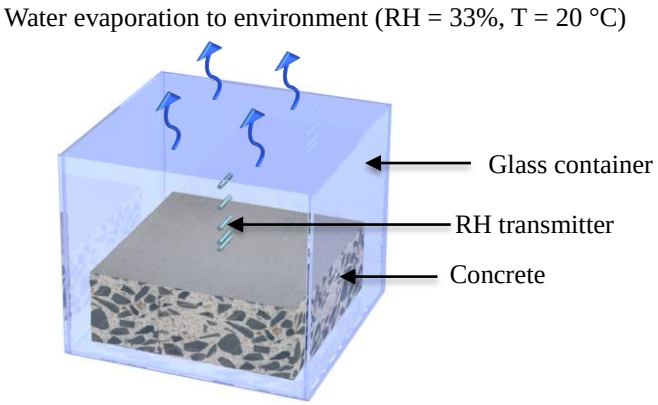

Fig. B.1 Schematic illustration of a setup for relative humidity measurement above the concrete surface, reproduced based on [183]. The concrete specimen is placed in a glass container. Only the top surface of the container is open. The top surface of the specimen is exposed, and other surfaces are sealed.

B.2 Calibration of the boundary condition - cement paste hydrating under 90% RH

Cement pastes are used to calibrate the boundary condition of the Moisture-Hydration model. Snyder et al. [184] studied the hydration of the cement pastes (w/c = 0.3) that were cured under various conditions. 1.6 mm-thick cement pastes (150 mm wide and 160 mm long) were first moist cured for a certain period of time. A moist curing period of 6 hours is chosen to calibrate the model. In [184], after the moist curing, the cement pastes were placed in a glove box for further hydration (Fig. B.2), the glove box was equipped with a fan for circulation (RH = 90%, T = 25 °C). However, it was noted that the RH in the glove box first increased and subsequently returned to 90% RH during a few hours after the cement pastes were put inside. Therefore, the calibration is somewhat difficult and cannot be rigorous. The correlation of the measured and the simulated DOH of the cement pastes will still be estimated.

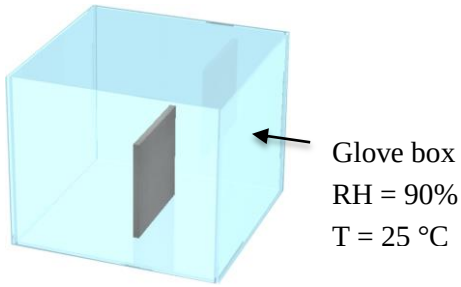

Fig. B.2 Schematic illustration of a cement paste (w/c = 0.3) hydrating in a glove box [184].

In the simulation, the thickness of the cement paste is 1.6 mm. The length and width of the specimens (w/c = 0.3) are infinite. The top and bottom surfaces are subjected to a moist curing for 6 hours, followed by exposure to RH = 90% at 20 °C. The boundary condition is specified at a distance of x from the surfaces (Fig. B.3). Three distances are adopted for calibration, i.e., $x = 30$ mm, $x = 60$ mm and $x = 100$ mm.

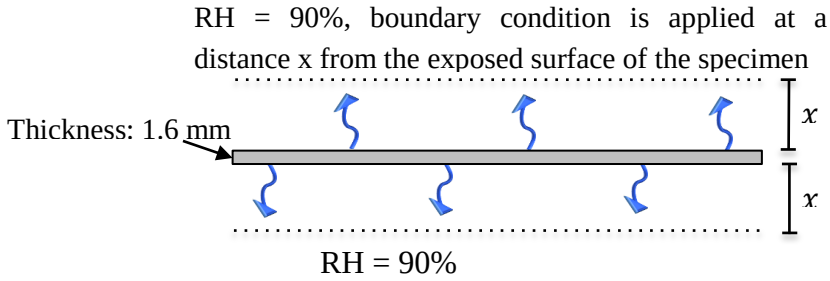

Fig. B.3 Schematic illustration of a cement paste (w/c = 0.3) hydrating under RH = 90%. The boundary condition is applied at a distance x (x = 30, 60 or 100 mm) from the surfaces of the specimen.

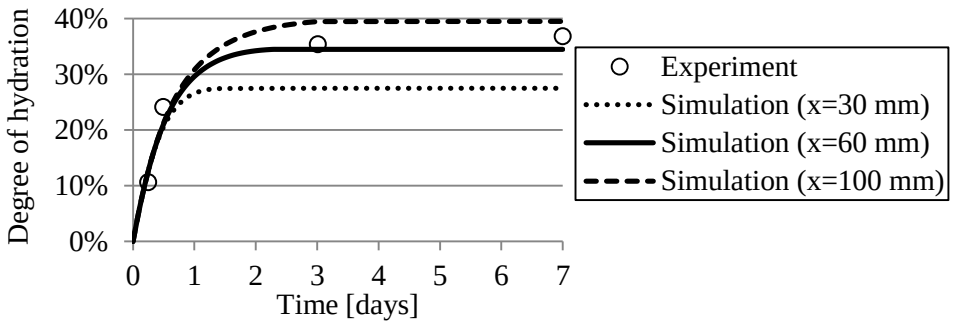

Fig. B.4 Comparison of experimental ([184]) and simulation results of the DOH of a 1.6 mm-thick cement paste. The cement paste is moist-cured for 6 hours, followed by exposure to RH = 50% at 25 °C. In the simulation, the boundary condition ($RH = 90\%, T = 20$ °C) is applied at a distance x (x = 30, 60 or 100 mm) from the exposed surfaces of the cement paste.

The hydration process of cement pastes is known to be highly dependent on their moisture content. The DOH of the cement pastes is depicted in Fig. B.4. With a distance $x = 60$ mm, the simulated DOH of cement pastes is close to the experimental results [184]. It indicates that $x = 60$ mm is a proper distance for specifying the boundary condition above a hydrating cement paste. Note that the temperature has an effect on the hydration process of cement pastes. For cement pastes (w/c = 0.3) cured under sealed condition at 20 °C and 25 °C respectively, the difference of DOH is about 2.5% (calculated by HYMOSTRUC3D [8]). In this appendix the influence of the temperature (i.e. 20 °C and 25 °C) on cement hydration is neglected.

B.3 Validation of the boundary condition - drying of hardened concrete substrate

Validation of the distance for specifying the boundary condition is conducted based on moisture transport in a 50 mm-thick 1-year old concrete (ordinary concrete OC in Table. 5.1). The water saturation level of the sealed cured concrete at the age of 1 year was 89% (corresponding to a relative humidity of 94%) [60]. The top surface of the concrete is exposed to RH = 50% at 20 °C, other surfaces remain sealed (Fig. B.5).

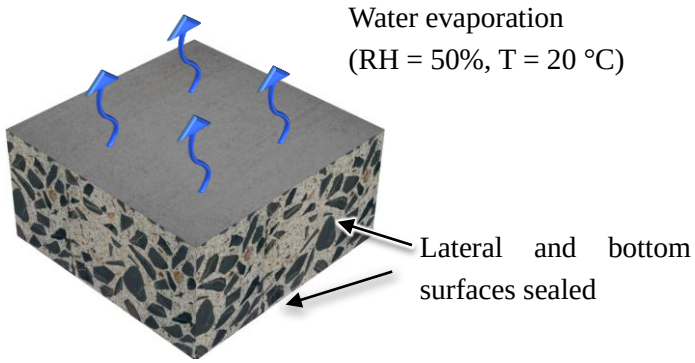

Fig. B.5 Schematic illustration of the concrete substrate under drying.

The simulated water saturation profile in the concrete is shown in Fig. B.6, and compared with the experimental results from [60]. This figure shows a good agreement between the experimental and the simulation results. Therefore, the distance of $x = 60\ mm$ can be used for specifying the boundary condition (i.e. relative humidity) when simulating moisture transport in hardening materials.

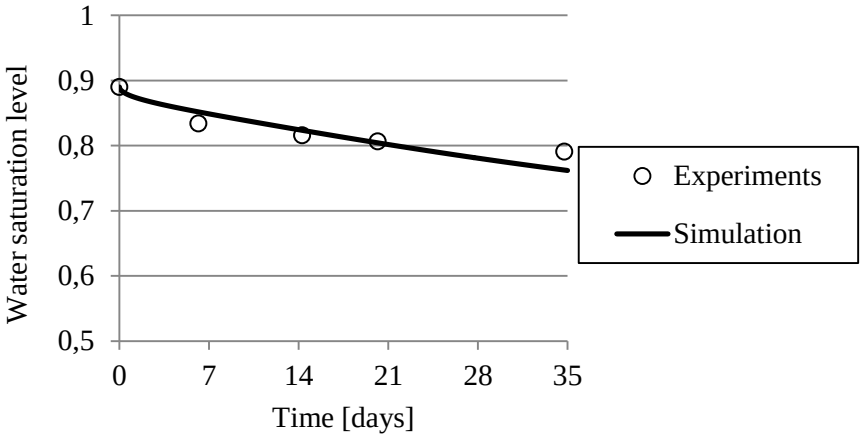

Fig. B.6 Drying of 1-year old concrete. The concrete has a w/c of 0.48 (see Table. 5.1). The top surface of the concrete is exposed to a 50% relative humidity at 20 °C, with other surfaces sealed. Experimental results are derived from [60]. In the simulation, the boundary condition ($RH = 50\%$) is applied at a distance x = 60 mm from the exposed surface of the concrete.

B.4 Summary

This appendix presented the study of boundary conditions for simulating moisture transport in cementitious materials. The top surfaces of the materials were exposed to RH = 90% or RH = 50%. The boundary condition (i.e. relative humidity) is applied at a certain distance x above the exposed surface of the materials. Moisture transport in a cement paste that hydrates under RH =90% is simulated to determine the distance x. By comparing the simulated DOH of the cement paste to experimental results. A distance of 60 mm from the exposed surface of the materials turned out to be an appropriate distance for applying the boundary condition. This distance is also proved reasonable for a hardened concrete drying at RH = 50%. Therefore, for simulating the moisture transport in hydrating cementitious materials, the boundary condition (e.g. RH = 50%) will be applied at a distance of 60 mm from the exposed surface of the materials.

Appendix C

Methodology of Lattice Boltzmann Method

C.1 Introduction

The lattice Boltzmann method (LBM) is a class of computational fluid dynamics methods for the computational modeling of fluid flow problems. Based upon the Boltzmann equation [127], LBM discretizes a physical space with lattice nodes and a velocity space by a set of microscopic velocity vectors. It considers a typical volume element of fluid to be composed of a collection of particles that are represented by a particle velocity distribution function for each fluid component at each lattice node. By performing consecutive propagation and collision steps over a discrete lattice mesh, the fluid flow can be simulated.

C.2 Basic equations of Lattice Boltzmann Method

In LBM, the distribution function is introduced to define the density and velocity at each lattice node. Specific particle interaction rules are set to satisfy Navier-Stokes equations. The movement of fluid particles at each lattice node follows:

$$f_i(x + e_i \cdot \delta t, t + \delta t) = f_i(x, t) - \frac{f_i(x, t) - f_i^{eq}(x, t)}{\tau} + F_i \tag{C.1}$$

where f_i is the non-equilibrium distribution function, f_i^{eq} is the equilibrium distribution function, and e_i is the microscopic velocity vector at lattice node x at time t, respectively, and τ is the relaxation time. The subscript i represents the lattice directions around the node. F_i is the external forcing term describing, e.g. pressure gradients, gravity, or interfacial tension in multi-fluid/phase applications.

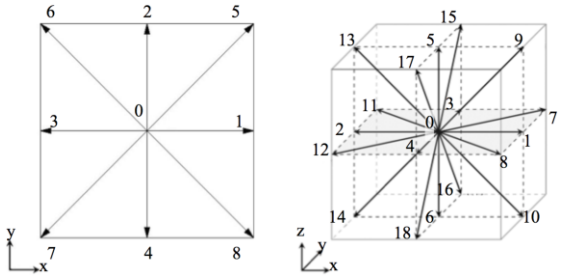

(a) D2Q9 model (b) D3Q19 model

Fig. C.1. Lattice velocity directions of two Lattice Boltzmann models.

Equilibrium distribution function is given in the following form for n-dimensional model with b microscopic velocity vectors ($DnQb$ models are described in Fig. C.1):

$$f_i^{eq} = w_i \cdot \rho \cdot \left[1 + \frac{e_i \cdot u}{c_s^2} + \frac{(e_i \cdot u)^2}{2 \cdot c_s^4} - \frac{u \cdot u}{2 \cdot c_s^2}\right] \tag{C.2}$$

where ρ and u are the macroscopic density and velocity, respectively. w_i is the weight factor in the ith direction, c_s^2 is the lattice speed of sound, with a value of 1/3.

Weight factors ($D2Q9$ by Eq. (C.3) and $D3Q19$ by Eq. (C.4)) are defined as:

$$w_i = \begin{cases} 4/9, & i = 0 \\ 1/9, & i = 1,2,\dots,4 \\ 1/36, & i = 5,6,\dots 8 \end{cases} \tag{C.3}$$

$$w_i = \begin{cases} 1/3, & i = 0 \\ 1/18, & i = 1,2,\dots,6 \\ 1/36, & i = 7,6,\dots 18 \end{cases} \tag{C.4}$$

Lattice velocity vectors ($D2Q9$ 2D with Eq. (C.5) and $D3Q19$ with Eq. (C.6)) are given as:

$$e_i = \begin{bmatrix} 0 & 1 & 0 & -1 & 0 & 1 & -1 & -1 & 1 \\ 0 & 0 & 1 & 0 & -1 & 1 & 1 & -1 & -1 \end{bmatrix} \tag{C.5}$$

$$e_i = \begin{bmatrix} 0 & 1 & -1 & 0 & 0 & 0 & 0 & 1 & 1 & 1 & 1 & 0 & 0 & -1 & -1 & -1 & -1 & 0 & 0 \\ 0 & 0 & 0 & -1 & 0 & 0 & 0 & 1 & -1 & 0 & 0 & 1 & 1 & 1 & -1 & 0 & 0 & -1 & -1 \\ 0 & 0 & 0 & 0 & 0 & 1 & -1 & 0 & 0 & 1 & -1 & 1 & -1 & 0 & 0 & 1 & -1 & 1 & 1 \end{bmatrix} \tag{C.6}$$

The macroscopic properties, density (ρ), and velocity (u) of the nodes are calculated using the following relations:

$$\rho = \sum_{i=1}^{Q} f_i \tag{C.7}$$

$$u = \frac{\sum_{i=1}^{Q} f_i \cdot e_i}{\rho} \tag{C.8}$$

where Q is the number of microscopic velocity vectors connected to node i.

The lattice kinematic shear viscosity of the fluid υ is given by:

$$\upsilon = c_s^2 \cdot \left(\tau - \frac{1}{2}\right) \cdot \delta t = \frac{1}{3} \cdot \left(\tau - \frac{1}{2}\right) \tag{C.9}$$

The pressure p can be obtained according to the equation of state (EOS) of an ideal gas:

$$p = c_s^2 \cdot \rho = \frac{1}{3} \cdot \rho \tag{C.10}$$

To specify pressure gradient, a constant density at the inlet, and a lower density at the outlet are imposed to simulate a stationary pressure-driven flow through the cement paste [185].

The permeability of porous material (2D with Eq. (C.11) and 3D with Eq. (4.9)), k_{lb}, can be calculated according to Darcy's law and expressed in terms of LB parameters:

$$k_{lb} = \frac{\upsilon \langle u_y \rangle}{\nabla p} = \upsilon \cdot \frac{N_y}{c_s^2 \cdot \Delta\rho} \cdot \frac{1}{N_x \cdot N_y \cdot \delta x^2} \cdot \sum_{i=1}^{N_x} \sum_{i=1}^{N_y} u_y\,(i,j) \tag{C.11}$$

$$k_{lb} = \frac{\upsilon \langle u_z \rangle}{\nabla p} = \upsilon \cdot \frac{N_z}{c_s^2 \cdot \Delta\rho} \cdot \frac{1}{N_x \cdot N_y \cdot N_z \cdot \delta x^3} \cdot \sum_{i=1}^{N_x} \sum_{i=1}^{N_y} \sum_{i=1}^{N_z} u_z\,(i,j,k) \tag{C.12}$$

In the simulation, all physical quantities (velocity, pressure, and viscosity) are, for convenience, expressed in a system of lattice units. The final quantity of interest, the permeability, has dimensions of length squared. The physical intrinsic permeability, K, is calculated as:

$$K = k_{lb} \cdot \left(\frac{\delta_{x-phy}}{\delta_x}\right)^2 \tag{C.13}$$

where δ_x is the length of lattice and δ_{x-phy} is the corresponding length in physical field. In this study, $\delta_x = 1$ and $\delta_{x-phy} = 0.5 \times 10^{-6}$ m.

References

[1] Saricimen, H., Maslehuddin, M., Iob, A., Eid, O. A., 'Evaluation of a surface coating in retarding reinforcement corrosion', Constr Build Mater, 10 (1996) 507-513.

[2] Al-Dulaijan, S., Maslehuddin, M., Al-Zahrani, M., Al-Juraifani, E., Alidi, S., Al-Mehthel, M., 'Performance evaluation of cement-based surface coatings', ACI Special Publication, 193 (2000).

[3] Moon, H. Y., Shin, D. G., Choi, D. S., 'Evaluation of the durability of mortar and concrete applied with inorganic coating material and surface treatment system', Constr Build Mater, 21 (2007) 362-369.

[4] Grantham, M. G., 'Concrete Repair: A Practical Guide', CRC Press, 2011.

[5] Song, H. W., Shim, H.-B., Petcherdchoo, A., Park, S.-K., 'Service life prediction of repaired concrete structures under chloride environment using finite difference method', Cem Concr Compos, 31 (2009) 120-127.

[6] Yu, S., Sergi, G., Page, C., 'Ionic diffusion across an interface between chloride-free and chloride-containing cementitious materials', Mag Concrete Res, 45 (1993) 257-261.

[7] Zhang, J. Z., McLoughlin, I. M., Buenfeld, N. R., 'Modelling of chloride diffusion into surface-treated concrete', Cem Concr Compos, 20 (1998) 253-261.

[8] Van Breugel, K., 'Simulation of hydration and formation of structure in hardening cement-based materials', TU Delft, Delft University of Technology, 1991.

[9] Koenders, E. A. B., 'Simulation of volume changes in hardening cement-based materials', TU Delft, Delft University of Technology, 1997.

[10] Ye, G., 'Experimental study and numerical simulation of the development of the microstructure and permeability of cementitious materials', TU Delft, Delft University of Technology, 2003.

[11] Kirby, R. S., 'Engineering in history', Courier Corporation, 1990.

[12] Aïtcin, P. C., 'The durability characteristics of high performance concrete: A review', Cem Concr Compos, 25 (2003) 409-420.

[13] Shi, X., Xie, N., Fortune, K., Gong, J., 'Durability of steel reinforced concrete in chloride environments: An overview', Constr Build Mater, 30 (2012) 125-138.

[14] Swamy, R. N., Tanikawa, S., 'An External Surface Coating to Protect Concrete and Steel from Aggressive Environments', Mater Struct, 26 (1993) 465-478.

[15] Buenfeld, N. R., Zhang, J. Z., 'Chloride diffusion through surface-treated mortar specimens', Cement Concrete Res, 28 (1998) 665-674.

[16] Diamanti, M. V., Brenna, A., Bolzoni, F., Berra, M., Pastore, T., Ormellese, M., 'Effect of polymer modified cementitious coatings on water and chloride permeability in concrete', Constr Build Mater, 49 (2013) 720-728.

[17] Swamy, R. N., 'Corrosion and corrosion protection of steel in concrete', Sheffield Academic Press, Sheffield, 1994.

[18] Zhou, J., 'Performance of engineered cementitious composites for concrete repairs', TU Delft, Delft University of Technology, 2011.

[19] Li, M., Li, V. C., 'Behavior of ECC/concrete layer repair system under drying shrinkage conditions', Proceedings of ConMat, 5 (2006) 22-24.

[20] Li, V. C., Herbert, E., 'Robust self-healing concrete for sustainable infrastructure', J Adv Concr Technol, 10 (2012) 207-218.

[21] DIN, E., '1504-2: 2005-01 Products and systems for the protection and repair of concrete structures–Definitions, requirements, quality control and evaluation of conformity–Part 2: Surface protection systems for concrete', German version EN, (2004) 1504-1502.

[22] Ababneh, A., Benboudjema, F., Xi, Y., 'Chloride penetration in nonsaturated concrete', J Mater Civil Eng, 15 (2003) 183-191.

[23] Sobolev, K., Shah, S. P., 'Nanotechnology of concrete: recent developments and future perspectives', American Concrete Institute, 2008.

[24] Flores-Vivian, I., Hejazi, V., Kozhukhova, M. I., Nosonovsky, M., Sobolev, K., 'Self-Assembling Particle-Siloxane Coatings for Superhydrophobic Concrete', Acs Appl Mater Inter, 5 (2013) 13284-13294.

[25] Kevern, J., Sparks, J., 'Low-cost techniques for improving the surface durability of pervious concrete', Transportation Research Record, 2342 (2013) 83-89.

[26] Almusallam, A. A., Khan, F. M., Dulaijan, S. U., Al-Amoudi, O. S. B., 'Effectiveness of surface coatings in improving concrete durability', Cement Concrete Comp, 25 (2003) 473-481.

[27] Al-Zahrani, M. M., Al-Dulaijan, S. U., Ibrahim, M., Saricimen, H., Sharif, F. M., 'Effect of waterproofing coatings on steel reinforcement corrosion and physical properties of concrete', Cem Concr Compos, 24 (2002) 127-137.

[28] Aguiar, J. B., Camoes, A., Moreira, P. M., 'Coatings for concrete protection against aggressive environments', J Adv Concr Technol, 6 (2008) 243-250.

[29] Saraswathy, V., Rengaswamy, N. S., 'Adhesion of an acrylic paint coating to a concrete substrate - Some observations', Journal of Adhesion Science and Technology, 12 (1998) 681-694.

[30] Seneviratne, A. M. G., Sergi, G., Page, C. L., 'Performance characteristics of surface coatings applied to concrete for control of reinforcement corrosion', Constr Build Mater, 14 (2000) 55-59.

[31] Beushausen, H., Burmeister, N., 'The use of surface coatings to increase the service life of reinforced concrete structures for durability class XC', Mater Struct, 48.4 (2015) 1243-1252.

[32] Moraes, C. A. M., Kieling, A. G., Caetano, M. O., Gomes, L. P., 'Life cycle analysis (LCA) for the incorporation of rice husk ash in mortar coating', Resour Conserv Recy, 54 (2010) 1170-1176.

[33] Nieuwoudt, P., Zaffaroni, P., Pistolesi, C., 'Case history of polymer-modified cementitious membrane used to protect new and repair concrete', Concrete Repair, Rehabilitation and Retrofitting III, CRC Press, (2012) 932-937.

[34] Bedi, R., Chandra, R., Singh, S., 'Mechanical properties of polymer concrete', Journal of Composites, 2013 (2013).

[35] Bolzoni, F., Ormellese, M., Brenna, A., 'Efficiency of concrete coatings on chloride-induced corrosion of reinforced concrete structures', NACE - International Corrosion Conference Series, 2011.

[36] Ignoul, S., Van Rickstal, F., Van Gemert, D., 'Blistering of Epoxy Industrial Floors on concrete substrate: phenomena and case study', International Conference on Polymers in Concrete, 2004.

[37] Dhir, R., Green, J., 'Protection of Concrete: Proceedings of the International Conference, University of Dundee, September 1990', CRC Press, 2003.

[38] Safiuddin, M., Soudki, K., 'Sealer and coating systems for the protection of concrete bridge structures', International Journal of the Physical Sciences, 6 (2011) 8188-8199.

[39] Harwood, P., 'Surface coating - specification criteria', Protection of Concrete: Proceedings of the International Conference, University of Dundee, September 1990, CRC Press, (2003) 176.

[40] Emmons, P., Vaysburd, A., 'Compatibility considerations for durable concrete repairs', Transportation Research Record, 1382 (1993) 13.

[41] Emmons, P., McDonald, J., Vaysburd, A., 'Some compatibility problems in repair of concrete structures–fresh look', International Colloquium Materials Science and Restoration, Esslingen, 1992 836-848.

[42] Hassan, K., Brooks, J., Al-Alawi, L., 'Compatibility of repair mortars with concrete in a hot-dry environment', Cem Concr Compos, 23 (2001) 93-101.

[43] Decter, M., 'Durable concrete repair—Importance of compatibility and low shrinkage', Constr Build Mater, 11 (1997) 267-273.

[44] Vaysburd, A. M., Bissonnette, B., von Fay, K. F., Engineering, M., Laboratory, R., Center, U. S. B. o. R. D. O. T. S., 'Compatibility Issues in Design and Implementation of Concrete Repairs and Overlays', 2014.

[45] Morgan, D. R., 'Compatibility of concrete repair materials and systems', Constr Build Mater, 10 (1996) 57-67.

[46] Emmons, P. H., Emmons, B. W., 'Concrete repair and maintenance illustrated: problem analysis, repair strategy, techniques', (1993).

[47] Weldon, D. G., 'Failure analysis of paints and coatings', John Wiley & Sons, 2009.

[48] Taffesea, W. Z., Sistonen, E., 'Service life prediction of repaired structures using concrete recasting method: state-of-the-art', Procedia Engineering, 57 (2013) 1138-1144.

[49] Martinola, G., Sadouki, H., Wittman, F. H., 'Numerical model for minimizing risk of damage in repair system', J Mater Civil Eng, 13 (2001) 121-129.

[50] Brocken, H. J. P., Spiekman, M. E., Pel, L., Kopinga, K., Larbi, J. A., 'Water extraction out of mortar during brick laying: A NMR study', Mater Struct, 31 (1998) 49-57.

[51] Faure, P., Caré, S., Po, C., Rodts, S., 'An MRI-SPI and NMR relaxation study of drying–hydration coupling effect on microstructure of cement-based materials at early age', Magnetic Resonance Imaging, 23 (2005) 311-314.

[52] Kazemi Kamyab, M., Denarié, E., Brühwiler, E., Wang, B., Thiéry, M., Faure, P. F., Baroghel-Bouny, V., 'Characterization of moisture transfer in UHPFRC-concrete composite systems at early age', Proceedings of the 2nd International Conference on Microstructural-related Durability of Cementitious Composites, 2012 163.

[53] Bentz, D. P., Hansen, K. K., 'Preliminary observations of water movement in cement pastes during curing using X-ray absorption', Cement Concrete Res, 30 (2000) 1157-1168.

[54] Lukovic, M., Ye, G., 'Effect of Moisture Exchange on Interface Formation in the Repair System Studied by X-ray Absorption', Materials, 9.1 (2015) 2.

[55] Júlio, E. N. B. S., Branco, F. A. B., Silva, V. t. D., 'Concrete-to-concrete bond strength. Influence of the roughness of the substrate surface', Constr Build Mater, 18 (2004) 675-681.

[56] Ong, K., Chandra, L., 'The effect of substrate preparation on early age shrinkage and crack developements of composite cementitious materials', 35th Conference on OUR WORLD IN CONCRETE & STRUCTURESSingapore, 2010.

[57] Courard, L., Degeimbre, R., 'A capillary action test for the investigation of adhesion in repair technology', Canadian Journal of Civil Engineering, 30 (2003) 1101-1110.

[58] Courard, L., Lenaers, J.-F., Michel, F., Garbacz, A., 'Saturation level of the superficial zone of concrete and adhesion of repair systems', Constr Build Mater, 25 (2011) 2488-2494.

[59] Daian, J. F., 'Condensation and isothermal water transfer in cement mortar Part I—Pore size distribution, equilibrium water condensation and imbibition', Transport Porous Med, 3 (1988) 563-589.

[60] Baroghel-Bouny, V., Mainguy, M., Lassabatere, T., Coussy, O., 'Characterization and identification of equilibrium and transfer moisture properties for ordinary and high-performance cementitious materials', Cement Concrete Res, 29 (1999) 1225-1238.

[61] Bakhshi, M., Mobasher, B., Soranakom, C., 'Moisture loss characteristics of cement-based materials under early-age drying and shrinkage conditions', Constr Build Mater, 30 (2012) 413-425.

[62] Samson, E., Marchand, J., Snyder, K. A., Beaudoin, J. J., 'Modeling ion and fluid transport in unsaturated cement systems in isothermal conditions', Cement Concrete Res, 35 (2005) 141-153.

[63] Xi, Y. P., Bazant, Z. P., Jennings, H. M., 'Moisture Diffusion in Cementitious Materials - Adsorption-Isotherms', Adv Cem Based Mater, 1 (1994) 248-257.

[64] Kim, J. K., Lee, C. S., 'Prediction of differential drying shrinkage in concrete', Cement Concrete Res, 28 (1998) 985-994.

[65] Kim, J. K., Lee, C. S., 'Moisture diffusion of concrete considering self-desiccation at early ages', Cement Concrete Res, 29 (1999) 1921-1927.

[66] West, R. P., Holmes, N., 'Predicting moisture movement during the drying of concrete floors using finite elements', Constr Build Mater, 19 (2005) 674-681.

[67] Zhang, J., Qi, K., Huang, Y., 'Calculation of moisture distribution in early-age concrete', Journal of engineering mechanics, 135 (2009) 871-880.

[68] Ba, M. F., Qian, C. X., Wang, H., 'Effects of specimen shape and size on water loss and drying shrinkage of cement-based materials', J Wuhan Univ Technol, 28 (2013) 733-740.

[69] Ali, W., Urgessa, G., 'Computational Model for Internal Relative Humidity Distributions in Concrete', Journal of Computational Engineering, 2014 (2014).

[70] Lukovic, M., Savija, B., Schlangen, E., Ye, G., van Breugel, K., 'A modelling study of drying shrinkage damage in concrete repair systems', Structural faults and repair conference 2014, 8–10 July 2014, London, UK, The Electrochemical Society, 2014.

[71] Leech, C., Lockington, D., Dux, P., 'Unsaturated diffusivity functions for concrete derived from NMR images', Mater Struct, 36 (2003) 413-418.

[72] Zhang, J., Wang, J., Gao, Y., 'Moisture movement in early-age concrete under cement hydration and environmental drying', Mag Concrete Res, 68 (2016) 391-408.

[73] Oh, B. H., Cha, S. W., 'Nonlinear analysis of temperature and moisture distributions in early-age concrete structures based on degree of hydration', Aci Mater J, 5 (2003) 361-370.

[74] Oh, B., Cha, S., 'Realistic models for degree of hydration and moisture distribution in concrete at early age', Fourth International Conference on Fracture Mechanics of Concrete and Concrete Structures, (2001) 279-286.

[75] Bentz, D. P., Hansen, K. K., Madsen, H. D., Vallee, F., Griesel, E. J., 'Drying/hydration in cement pastes during curing', Mater Struct, 34 (2001) 557-565.

[76] Bažant, Z., Najjar, L., 'Nonlinear water diffusion in nonsaturated concrete', Matériaux et Construction, 5 (1972) 3-20.

[77] Wong, S., Wee, T., Swaddiwudhipong, S., Lee, S., 'Study of water movement in concrete', Mag Concrete Res, 53 (2001) 205-220.

[78] Akita, H., Fujiwara, T., Ozaka, Y., 'A practical procedure for the analysis of moisture transfer within concrete due to drying', Mag Concrete Res, 49 (1997) 129-137.

[79] Åhs, M., 'Moisture redistribution in screeded concrete slabs', Report TVBM 3136, (2007).

[80] Martinola, G., Sadouki, H., Wittmann, F. H., 'Numerical model for minimizing risk of damage in repair system', J Mater Civil Eng, 13 (2001) 121-129.

[81] Martinola, G., Sadouki, H., 'Combined experimental and numerical study to assess shrinkage cracking of cement-based materials', International Journal for Restoration of Buildings and Monuments, 4 (1998) 479-506.

[82] Ahmad, S., 'Reinforcement corrosion in concrete structures, its monitoring and service life prediction—a review', Cem Concr Compos, 25 (2003) 459-471.

[83] Cusson, D., Lounis, Z., Daigle, L., 'Benefits of internal curing on service life and life-cycle cost of high-performance concrete bridge decks – A case study', Cem Concr Compos, 32 (2010) 339-350.

[84] Matthews, S., 'CONREPNET: performance-based approach to the remediation of reinforced concrete structures: achieving durable repaired concrete structures', Journal of Building Appraisal, 3 (2007) 6-20.

[85] Alonso, C., Andrade, C., Castellote, M., Castro, P., 'Chloride threshold values to depassivate reinforcing bars embedded in a standardized OPC mortar', Cement Concrete Res, 30 (2000) 1047-1055.

[86] Gulikers, J., 'Considerations on the reliability of service life predictions using a probabilistic approach', Journal de Physique IV (Proceedings), EDP sciences, 136 (2006) 233-241.

[87] ASTMC1152, 'Standard Test Method for Acid-soluble Chloride in Mortar and. Concrete', American Society for Testing and Materials and Structures.

[88] Castellote, M., Andrade, C., Alonso, C., 'Accelerated simultaneous determination of the chloride depassivation threshold and of the non-stationary diffusion coefficient values', Corrosion Science, 44 (2002) 2409-2424.

[89] Trejo, D., Pillai, R. G., 'Accelerated chloride threshold testing: part I-ASTM A 615 and A 706 reinforcement', Materials Journal, 100 (2003) 519-527.

[90] Tuutti, K., 'Corrosion of steel in concrete', Swedish Cement and Concrete Research Institute, Stockholm, 1982.

[91] Angst, U., Elsener, B., Larsen, C. K., Vennesland, Ø., 'Critical chloride content in reinforced concrete — A review', Cement Concrete Res, 39 (2009) 1122-1138.

[92] Tang, L., Lars-Olof, N., 'Chloride diffusivity in high strength concrete at different ages', NORDIC CONCRETE RESEARCH. PUBLICATION NO 11, (1992).

[93] Tang, L. P., Joost, G., 'On the mathematics of time-dependent apparent chloride diffusion coefficient in concrete', Cement Concrete Res, 37 (2007) 589-595.

[94] Thomas, M. D., Bamforth, P. B., 'Modelling chloride diffusion in concrete: effect of fly ash and slag', Cement Concrete Res, 29 (1999) 487-495.

[95] Nielsen, E. P., Geiker, M. R., 'Chloride diffusion in partially saturated cementitious material', Cement Concrete Res, 33 (2003) 133-138.

[96] Garboczi, E., Bentz, D., 'Computer simulation of the diffusivity of cement-based materials', Journal of Materials Science, 27 (1992) 2083-2092.

[97] Tang, L. P., Nilsson, L. O., 'Chloride Binding-Capacity and Binding Isotherms of Opc Pastes and Mortars', Cement Concrete Res, 23 (1993) 247-253.

[98] Hirao, H., Yamada, K., Takahashi, H., Zibara, H., 'Chloride binding of cement estimated by binding isotherms of hydrates', J Adv Concr Technol, 3 (2005) 77-84.

[99] Martin-Perez, B., Zibara, H., Hooton, R. D., Thomas, M. D. A., 'A study of the effect of chloride binding on service life predictions', Cement Concrete Res, 30 (2000) 1215-1223.

[100] Nurge, M. A., Youngquist, R. C., Starr, S. O., 'Mass conservation in modeling moisture diffusion in multi-layer composite and sandwich structures', Journal of Sandwich Structures and Materials, 12.6 (2010) 755-763.

[101] Klopfer, H., 'Lehrbuch der Bauphysik', Teubner, Stuttgart, 1985.

[102] Mindess, S., Young, J. F., Darwin, D., 'Concrete', Prentice Hall, 2003.

[103] Winkler, E., 'Stone in architecture: properties, durability', Springer Science & Business Media, 2013.

[104] Welty, J. R., Wicks, C. E., Rorrer, G., Wilson, R. E., 'Fundamentals of momentum, heat, and mass transfer', John Wiley & Sons, 2009.

[105] ISO, E., '12572', Hygrothermal performance of building materials and products—Determination of water vapour transmission properties, 2001.

[106] Ranaivomanana, H., Verdier, J., Sellier, A., Bourbon, X., 'Prediction of relative permeabilities and water vapor diffusion reduction factor for cement-based materials', Cement Concrete Res, 48 (2013) 53-63.

[107] Xi, Y. P., Bazant, Z. P., Molina, L., Jennings, H. M., 'Moisture Diffusion in Cementitious Materials - Moisture Capacity and Diffusivity', Adv Cem Based Mater, 1 (1994) 258-266.

[108] Münch, B., Holzer, L., 'Contradicting Geometrical Concepts in Pore Size Analysis Attained with Electron Microscopy and Mercury Intrusion', J Am Ceram Soc, 91 (2008) 4059-4067.

[109] Sant, G., Bentz, D., Weiss, J., 'Capillary porosity depercolation in cement-based materials: measurement techniques and factors which influence their interpretation', Cement Concrete Res, 41 (2011) 854-864.

[110] Gregg, S., Sing, K., 'Adsorption, surface area and porosity', Academic Press, New York, 1982.

[111] Richards, L. A., 'Capillary conduction of liquids through porous mediums', Physics-J Gen Appl P, 1 (1931) 318-333.

[112] Cerny, R., Rovnaníková, P., 'Transport processes in concrete', CRC Press, 2002.

[113] Hall, C., 'Anomalous diffusion in unsaturated flow: Fact or fiction?', Cement Concrete Res, 37 (2007) 378-385.

[114] Baroghel-Bouny, V., 'Water vapour sorption experiments on hardened cementitious materials. Part II: Essential tool for assessment of transport properties and for durability prediction', Cement Concrete Res, 37 (2007) 438-454.

[115] Baroghel-Bouny, V., 'Water vapour sorption experiments on hardened cementitious materials - Part I: Essential tool for analysis of hygral behaviour and its relation to pore structure', Cement Concrete Res, 37 (2007) 414-437.

[116] Van Genuchten, M. T., 'A closed-form equation for predicting the hydraulic conductivity of unsaturated soils', Soil science society of America journal, 44 (1980) 892-898.

[117] Jensen, O. M., Hansen, P. F., 'Water-entrained cement-based materials: I. Principles and theoretical background', Cement Concrete Res, 31 (2001) 647-654.

[118] Ho, C. K., Webb, S. W., 'Gas transport in porous media', Springer, 2006.

[119] Millington, R., Quirk, J., 'Permeability of porous solids', Transactions of the Faraday Society, 57 (1961) 1200-1207.

[120] Shimomurat, T., Maekawa, K., 'Analysis of the drying shrinkage behaviour of concrete using a micromechanical model based on the micropore structure of concrete', Mag Concrete Res, 49 (1997) 303-322.

[121] Szymkiewicz, A., 'Modelling water flow in unsaturated porous media: accounting for nonlinear permeability and material heterogeneity', Springer Science & Business Media, 2012.

[122] Wiederhold, P. R., 'Water vapor measurement: methods and instrumentation', CRC Press, 1997.

[123] Powers, T. C., Copeland, L., Hayes, J., Mann, H., 'Permeablity of Portland Cement Paste', ACI Journal proceedings, ACI, 1954.

[124] Nyame, B. K., 'Permeability and Pore Structure of Hardened Cement Paste and Mortar', King's College London, 1979.

[125] Banthia, N., Mindess, S., 'Water permeability of cement paste', Cement Concrete Res, 19 (1989) 727-736.

[126] McNamara, G. R., Zanetti, G., 'Use of the Boltzmann equation to simulate lattice-gas automata', Physical Review Letters, 61 (1988) 2332.

[127] He, X., Luo, L.-S., 'Theory of the lattice Boltzmann method: From the Boltzmann equation to the lattice Boltzmann equation', Physical Review E, 56 (1997) 6811.

[128] Zhang, M., 'Multiscale lattice Boltzmann-finite element modelling of transport properties in cement-based materials', TU Delft, Delft University of Technology, 2013.

[129] Zalzale, M., 'Water dynamics in cement paste: insights from lattice Boltzmann modelling', École Polytechnique Fédérale de Lausanne, 2014.

[130] Gallucci, E., Scrivener, K., Groso, A., Stampanoni, M., Margaritondo, G., '3D experimental investigation of the microstructure of cement pastes using synchrotron X-ray microtomography (μCT)', Cement Concrete Res, 37 (2007) 360-368.

[131] Bentz, D. P., 'CEMHYD3D: A three-dimensional cement hydration and microstructure development modelling package. Version 2.0', National Institute of Standards and Technology Interagency Report, 7232 (2000).

[132] Bishnoi, S., Scrivener, K. L., 'μic: A new platform for modelling the hydration of cements', Cement Concrete Res, 39 (2009) 266-274.

[133] Zalzale, M., McDonald, P., 'Lattice Boltzmann simulations of the permeability and capillary adsorption of cement model microstructures', Cement Concrete Res, 42 (2012) 1601-1610.

[134] Picandet, V., Rangeard, D., Perrot, A., Lecompte, T., 'Permeability measurement of fresh cement paste', Cement Concrete Res, 41 (2011) 330-338.

[135] Ye, G., 'Percolation of capillary pores in hardening cement pastes', Cement Concrete Res, 35 (2005) 167-176.

[136] Grasley, Z. C., Scherer, G. W., Lange, D. A., Valenza, J. J., 'Dynamic pressurization method for measuring permeability and modulus: II. cementitious materials', Mater Struct, 40 (2007) 711-721.

[137] Nyame, B., Illston, J., 'Relationships between permeability and pore structure of hardened cement paste', Mag Concrete Res, 33 (1981) 139-146.

[138] Powers, T. C., Copeland, L. E., Mann, H., 'Capillary continuity or discontinuity in cement pastes', 1959.

[139] Mehta, P. K., 'Durability of Concrete in Marine Environment--A Review', ACI Special Publication, 65 (1980).

[140] Aligizaki, K. K., 'Pore structure of cement-based materials: testing, interpretation and requirements', CRC Press, 2005.

[141] Saeidpour, M., Wadsö, L., 'Moisture equilibrium of cement based materials containing slag or silica fume and exposed to repeated sorption cycles', Cement Concrete Res, 69 (2015) 88-95.

[142] Powers, T. C., Brownyard, T. L., 'Studies of the physical properties of hardened Portland cement paste', ACI Journal Proceedings, ACI, 1946.

[143] Prodanović, M., Bryant, S. L., 'A level set method for determining critical curvatures for drainage and imbibition', Journal of Colloid and Interface Science, 304 (2006) 442-458.

[144] Shabro, V., Prodanovic, M., Arns, C. H., Bryant, S. L., Torres-Verdin, C., Knackstedt, M. A., 'Pore-scale modeling of two-phase flow', XVIII International Conference on Computational Methods in Water Resources, Barcelona, 2010.

[145] Jennings, H. M., 'A model for the microstructure of calcium silicate hydrate in cement paste', Cement Concrete Res, 30 (2000) 101-116.

[146] Jennings, H. M., Thomas, J. J., Gevrenov, J. S., Constantinides, G., Ulm, F.-J., 'A multi-technique investigation of the nanoporosity of cement paste', Cement Concrete Res, 37 (2007) 329-336.

[147] Bentz, D. P., Snyder, K. A., Stutzman, P. E., 'Hydration of portland cement: The effects of curing conditions', Proceedings of the 10th International Congress on the Chemistry of Cement, 1997.

[148] Jennings, H. M., Tennis, P. D., 'Model for the Developing Microstructure in Portland-Cement Pastes', J Am Ceram Soc, 77 (1994) 3161-3172.

[149] Jennings, H. M., Bullard, J. W., Thomas, J. J., Andrade, J. E., Chen, J. J., Scherer, G. W., 'Characterization and modeling of pores and surfaces in cement paste: correlations to processing and properties', J Adv Concr Technol, 6 (2008) 5-29.

[150] Taylor, H. F., 'A method for predicting alkazi ion concentrations in cement pore solutions', Advances in Cement Research, 1 (1987) 5-17.

[151] Tennis, P.D., Jennings, H.M., 'A model for two types of calcium silicate hydrate in the microstructure of Portland cement pastes', Cement Concrete Res, 30 (2000) 855-863.

[152] Šelih, J., Sousa, A. C., Bremner, T. W., 'Moisture transport in initially fully saturated concrete during drying', Transport Porous Med, 24 (1996) 81-106.

[153] Qiu, F., Haghighat, X., Kumaran, M.K., 'Moisture transport across interfaces between autoclaved aerated concrete and mortar', Journal of Thermal Envelope and Building Science, 26 (2003) 213-236.

[154] Simon, M. K., 'Probability distributions involving Gaussian random variables: A handbook for engineers and scientists', Springer Science & Business Media, 2007.

[155] Neville, A., 'Properties of Concrete, Fourth and Final Edition Standards', Pearson, Prentice Hall. ISBN 0-582-23070-5. OCLC, 1996.

[156] Sun, Z., Ye, G., Shah, S. P., 'Microstructure and early-age properties of Portland cement paste–effects of connectivity of solid phases', Aci Mater J, 102 (2005) 122-129.

[157] Bentz, D. P., Garboczi, E. J., Quenard, D. A., 'Modelling drying shrinkage in reconstructed porous materials: application to porous Vycor glass', Model Simul Mater Sc, 6 (1998) 211.

[158] Lura, P., 'Autogenous deformation and internal curing of concrete', TU Delft, Delft University of Technology, 2003.

[159] Nielsen, L. F., 'A research note on sorption, pore size distribution, and shrinkage of porous materials', Danmarks Tekniske Højskole. Laboratoriet for Bygningsmaterialer, 1991.

[160] Kamali, S., Moranville, M., Garboczi, E., Prené, S., Gérard, B., 'Hydrate dissolution influence on the young's modulus of cement paste', 5th International Conference of Fracture Mechanics of Concrete Structures, Vail, CO, April, 2004 12-16.

[161] Samouh, H., Rozière, E., Wisniewski, V., Loukili, A., 'Consequences of longer sealed curing on drying shrinkage, cracking and carbonation of concrete', Cement Concrete Res, 95 (2017) 117-131.

[162] Altoubat, S., Lange, D., "Creep, shrinkage and cracking of restrained concrete at early age." Urbana, 51 (2001): 61801.

[163] Basheer, L., Kropp, J., Cleland, D. J., 'Assessment of the durability of concrete from its permeation properties: a review', Constr Build Mater, 15 (2001) 93-103.

[164] Win, P. P., Watanabe, M., Machida, A., 'Penetration profile of chloride ion in cracked reinforced concrete', Cement Concrete Res, 34 (2004) 1073-1079.

[165] Šavija, B., Pacheco, J., Schlangen, E., 'Lattice modeling of chloride diffusion in sound and cracked concrete', Cem Concr Compos, 42 (2013) 30-40.

[166] Multiphysics, C., '4.3 User's Guide', Comsol, 2012.

[167] Mangat, P. S., Limbachiya, M. C., 'Effect of initial curing on chloride diffusion in concrete repair materials', Cement Concrete Res, 29 (1999) 1475-1485.

[168] Bentz, D. P., Garboczi, E. J., Lu, Y., Martys, N., Sakulich, A. R., Weiss, W. J., 'Modeling of the influence of transverse cracking on chloride penetration into concrete', Cement Concrete Comp, 38 (2013) 65-74.

[169] Xi, Y. P., Bazant, Z. P., 'Modeling chloride penetration in saturated concrete', J Mater Civil Eng, 11 (1999) 58-65.

[170] Midgley, H., Illston, J., 'The penetration of chlorides into hardened cement pastes', Cement Concrete Res, 14 (1984) 546-558.

[171] Wang, X., Zhang, L., 'Simulation of Chloride Diffusion in Cracked Concrete with Different Crack Patterns', Adv. Mater. Sci. Eng, 2016 (2016) 11.

[172] Şahmaran, M., 'Effect of flexure induced transverse crack and self-healing on chloride diffusivity of reinforced mortar', J. Mater. Sci, 42 (2007) 9131.

[173] Ismail, M., Toumi, A., François, R., Gagné, R., 'Effect of crack opening on the local diffusion of chloride in cracked mortar samples', Cement Concrete Res, 38 (2008) 1106-1111.

[174] Jin, W., Yan, Y., Wang, H., 'Chloride diffusion in the cracked concrete', Fracture Mechanics of Concrete and Concrete Structures—Assessment, Durability, Monitoring and Retrofitting of Concrete Structures. Korea Concrete Institute, Seoul, (2010) 880-886.

[175] Jensen, O. M., 'Chloride ingress in cement paste and mortar measured by Electron Probe Micro Analysis', Department of Structural Engineering, Technical University of Denmark, 1999.

[176] Caré, S., 'Influence of aggregates on chloride diffusion coefficient into mortar', Cement Concrete Res, 33 (2003) 1021-1028.

[177] Christensen, R. M., 'Mechanics of composite materials', Courier Corporation, 2012.

[178] Polder, R. B., De Rooij, M.R., 'Durability of marine concrete structures-field investigations and modelling', HERON-ENGLISH EDITION, 50 (2005) 133.

[179] Persson, B., 'Moisture in concrete subjected to different kinds of curing', Mater Struct, 30 (1997) 533-544.

[180] Bertolini, L., Elsener, B., Pedeferri, P., Redaelli, E., Polder, R. B., 'Corrosion of steel in concrete: prevention, diagnosis, repair', John Wiley & Sons, 2013.

[181] Ann, K. Y., Ahn, J. H., Ryou, J. S., 'The importance of chloride content at the concrete surface in assessing the time to corrosion of steel in concrete structures', Constr Build Mater, 23 (2009) 239-245.

[182] Dong, H., Lukovic, M., Yu, Z., Ye, G., 'Smart superabsorbent polymers for self-sealing and-healing of mortar.' 5th International conference on Self-Healing Materials (ICSHM 2015). Duke University, 2015.

[183] Li, C., Li, K., Chen, Z., 'On the boundary condition of moisture transport in concrete', Engineering Mechanics, 8 (2009) 16.

[184] Snyder, K., Bentz, D., 'Suspended hydration and loss of freezable water in cement pastes exposed to 90% relative humidity', Cement Concrete Res, 11(2004) 2045-56.

[185] Narváez A., Harting J., 'Evaluation of pressure boundary conditions for permeability calculations using the lattice-Boltzmann method', Adv Appl Math Mech 2(2010), 685-700.

Curriculum Vitae

Hua Dong

Date of birth: 08 October, 1983
Nationality: China

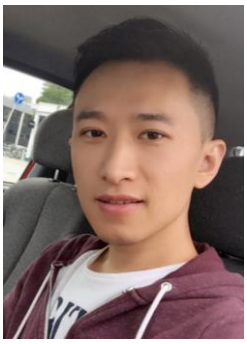

2011.06 ~ 2018.06

PhD candidate in TU Delft, Delft, The Netherlands

2008.04 ~ 2011.03

BASF Construction Chemicals (China) Co., Ltd., Nanjing, China

2005.09 ~ 2008.03

Master study on material science in Southeast University, Nanjing, China

2001.09 ~ 2005.07

Bachelor study on civil engineering in Jiangnan University, Wuxi, China

List of publications

1. M. Luković, **H. Dong**, B. Šavija, E. Schlangen, G. Ye and K. van Breugel. Tailoring strain-hardening cementitious composite repair systems through numerical experimentation. Cement and Concrete Composites, 2014, 53: 200-213.
2. M. Lukovic, B. Savija, **H. Dong**, E. Schalangen and G. Ye. Micromechanical study of the interface properties in concrete repair systems. Journal of Advanced Concrete Technology, 2014, 12(9): 320-339.
3. **H. Dong**, P. Gao and G. Ye. Characterization and comparison of capillary pore structures of digital cement pastes. Materials and structures, 2017, 50(2):154.
4. **H. Dong**, H. Zhang, Y. Zuo, P. Gao, and G. Ye. Relationship between the size of the samples and the interpretation of the mercury intrusion results of an artificial sandstone. Materials, 2018, 11.2: 201.
5. **H. Dong**, P. Gao and G. Ye. Chloride transport in cement-based overlay systems and service life assessment of concrete structures. Accepted by Journal of Materials in Civil Engineering.
6. **H. Dong**, H. Huang and G.Ye. Inorganic powder encapsulated in brittle polymer particles for self-healing cement-based materials. 4th international conference on self-healing materials, 2013, Ghent, Belgium.
7. **H. Dong** and G.Ye. Freezing and thawing resistance of high performance concrete incorporating superabsorbent polymer. International conference on application of superabsorbent polymers and other new admixtures in concrete construction, 2014, Dresden, Germany.
8. **H. Dong**, G.Ye. Influence of pore refinement on chloride transport in cement-based material. 3rd international conference on service life design for infrastructure, 2014, Zhuhai, China.
9. **H. Dong**, M. Lukovic, Z. Yu and G.Ye. Sodium silicate particles encapsulated in epoxy resin for self-healing cement-based materials. 5th international conference on self-healing materials, 2015, Durham, USA.
10. **H. Dong** and G.Ye. Service life prediction of a cementitious coating system based on chloride-induced corrosion. International RILEM conference on Materials, Systems and Structures in Civil Engineering, 2016, Lyngby, Denmark.
11. **H. Dong**, P. Gao, and G.Ye. Simulation of drying processes in early age cement pastes. 9th international symposium on cement and concrete, 2017, Wuhan, China.